Keele University

Design and fabrication of hydrogel scaffolds for osteochondral tissue regeneration

Zaid Muwafaq Younus

Thesis submitted for the degree of Doctor of Philosophy

June 2019

Keele University

Abstract

Osteochondral defects are serious clinical problems relating to damaged articular cartilage within joints, usually resulting from acute traumatic injury or an underlying bone disorder. A variety of therapeutic options have been investigated, with several commercial products addressing this problem, but with limitations in the technology used in terms of biomaterials and construct presentation. Many of the current devices used to 'plug' the osteochondral defect presents a laminated structure which will interact with bone and cartilage layers within the damaged site. These devices do not offer reconstruction of normal tissue architecture and may delaminate in worse cases resulting in pain and repeated surgical intervention.

Advances in biomaterial design and tissue engineering offer promise for the development of new approaches to direct cell architecture and tissue formation. The current work focuses on testing the impact of biomaterial chemistry and presentation in 3D, using a poly (N-isopropylacrylamide) (pNIPAM), and slightly less wettable poly (N-tert-butylacrylamide) (pNTBAM) to support spatial control of osteogenic and chondrogenic growth. Both materials were demonstrated as single component hydrogel, and presented in gradient form, in order to steer attachment of these two cell types.

Both materials were prepared using ion transfer radical polymerization. FTIR spectroscopy and water droplet angle measurements used to describe main chemical variations and the wettability profile. Mechanical testing determines materials strength and stiffness, while scanning electron microscopy (SEM) defines architectural and pore differences. Bio-glass (BG) fibres were embedded within hydrogels to support mineral environment and aid in cellular transportation. Histological staining using H&E stain together with confocal imaging used to configure cell attachment upon each hydrogel. Cell survival was examined using live/dead staining of hydrogel samples for immortalized cell lines (MG63, OK3H) and primary cell lines including human osteoblasts (hOBs) and human chondrocytes (hCHs).

Osteogenic and chondrogenic potential of cells were investigated with alizarin red staining and calcium assay. Alcian blue and dimethyl methylene blue were used to assess glycosaminoglycan (GAG) production. Protein assessment was performed using immunostaining and ELISA assay for collagens I, and II as a marker for cell function in addition to collagen X and ELISA quantification of annexin A2 as a markers for mineralization.

Results indicated more hydrophobic stiffer mass for pNTBAM compared to pNIPAM. Internal architecture revealed larger pore diameter measured for pNIPAM hydrogel. Viability of all cell types was found to be good on both gel types, although proliferation was higher on pNTBAM compared to pNIPAM, and the latter gave rise to greater number of cell aggregates. Both hydrogels supported mineralization and GAG production, with pNTBAM presenting higher amounts mostly for GAGs. Higher levels of mineralization were obtained with BG embedded samples. These results were confirmed by detecting collagens and annexin A2 levels.

In conclusion, the various characteristics for pNIPAM and pNTBAM impacted the biological observations in terms of survival and cell function. This was useful in establishing a combined multi-regional scaffold which revealed the development of mineral and cell functional gradient between the scaffold's sides.

Keywords: osteochondral, biomaterials, hydrogel, polymer, scaffold, tissue engineering, mineralization, osteoblasts, chondrocytes, gradient, bio-glass fibres, calcium, alizarin, GAGs, collagen, annexin A2.

Table of contents

List of figures

List of tables

Abbreviations

µCT	Micro computed tomography
ACI	Autologous chondrocyte transplantation
ALP	Alkaline phosphatase
BG	Bio-glass
CAD	Computer aided design
CPC	Cetylpyridenium chloride
dH_2O	De-ionized water
DMMB	Dimethyl methylene Blue
ECM	Extra cellular matrix
ELISA	Enzyme linked immunosorbent assay
FDM	Fused deposition modelling
FTIR	Fourier transform infra-red
GAG	Glycosaminoglycan
HA	Hydroxyapatite
hCHs	Human chondrocytes
hOBs	Human osteoblasts
ICRS	International cartilage repair society
Kpa	Kilo pascal
Mg	Magnesium
MSCs	Mesenchymal stem cells
NICE	National institute for health and care excellence

PBS	Phosphate buffer saline
PGA	Poly (glycolic acid)
PLA	Poly (lactic acid)
pNIPAM	Poly (N-isopropylacrylamide)
*p*NPP	Poly-nitro phenyl phosphate
pNTBAM	Poly (N-tert-butylacrylamide)
Pt	Platinum
SBF	Simulated body fluid
SEM	Scanning electron microscope
SFF	Solid free form
SLS	Selective Laser Sintering

Presentations and conferences

Talk presentations

- Zaid Younus, Paul Roach, Nicholas Forsyth Hydrogel scaffold engineering for osteochondral tissue regeneration. Keele University postgraduate symposium / keele University 2016.
- Zaid Younus, Paul Roach. Hydrogel scaffold engineering for osteochondral tissue regeneration. Future investigators of regenerative medicine (FIRM) conference / Girona –Spain September 2016

Poster presentations

- Zaid Younus, Paul Roach, Nicholas Forsyth. 3D scaffolds for osteochondral tissue engineering. Royal society of biomaterials (RSC) Biomaterials conference / Birmingham January 2016
- Zaid Younus, Paul Roach, Nicholas Forsyth. Hydrogel scaffold engineering for osteochondral tissue regeneration. United Kingdom society of biomaterials (UKSB) conference/ London June 2016.
- Zaid Younus, Paul Roach, Nicholas Forsyth. Hydrogel scaffold engineering for osteochondral tissue regeneration. United Kingdom society of biomaterials (UKSB) conference/ Loughborough University, Loughborough June 2017.
- Zaid Younus, Paul Roach, Nicholas Forsyth. Hydrogel scaffold engineering for osteochondral tissue regeneration. Tissue and cell engineering society (TCES) conference / Manchester metropolitan University, Manchester July 2017
- Zaid Younus, Paul Roach, Nicholas Forsyth. Tuning of pNIPAM-based scaffolds to regenerate the osteochondral region. Royal society of biomaterials (RSC) Biomaterials conference/ Bradford January 2018

Acknowledgement

Firstly, I would like to express my sincere gratitude to my supervisor Prof. Nicholas Forsyth for the optimum support of my Ph.D study and research, for his patience, encouragement, and immense knowledge and for giving me the freedom to work in the lab but continuously inspiring me with his feedback throughout my study. His guidance helped me all the time of research and writing of this thesis.

My sincere thanks also goes to my second supervisor Dr. Paul Roach for his support and care in establishing the bases of this project. His insightful thoughts enlighten me in every aspects of materials science during my PhD. His continued help and feedback supported me throughout my lab work and thesis writing.

I would like to present my special thanks and appreciation to the Higher Committee for Education Development (HCED) in Iraq. This work would not have been possible without the continued financial support from the HCED Iraq. Thanks and gratitude also goes to the Iraqi Cultural Attache for the premium support to Iraqi students throughout their study in the UK.

To Keele University, I would like to present my thanks and appreciation for providing all the resources and facilities from the beginning to the end of my study.

Special thanks to Dr. Ahmed Ifty / University of Nottingham for kindly donating the bio glass fibres and Ann Canning for her contribution in the 3D printing design to support this project.

I would like to thank Prof. Ying Yang and her group members for help and advice throughout my experimental work.

I would like to present my deep gratefulness to Dr. Joshua Price, Dr. Michael Rotherham and Dr. Abigail Rutter for their help, advice and support in experimental lab training.

My sincere thanks and gratitude to my colleagues and friends in the ISTM specially to mention my dear friend Dr Mohammed Najim and his family for the help and care they provided and for their kind hospitality for me and my family the first time when we arrived at the UK. Special thanks and appreciations to my friends Dr Hamza Abu Owida and Dr Marwan Merkhan for their enormous support and advice during my experimental work. I would like also to thank my wonderful group members Dr Tina Dale, Dr Rakad Al-Jumaily, Jessica Bratt, Emily Borg D'Anastas, Ana Kyoseva, Michelle Chen, and Idowu Fadayomi. Their help and advice supported me a lot in the most difficult moments of my study.

I would also present my deep gratitude to the people who supported me to join this scholarship Mr Gazanfer Kanna, Mr Nizar Al-Dabbagh, Dr Nabhan Al-Saadoon, and Dr Suheir Muayed. I would never reach this position without their kind attitude and help.

Last but not least, nobody has been more important to me in the pursuit of this project than the members of my family. I would like to thank my parents, whose love and guidance are with me in whatever I pursue. They are the ultimate role models. Most importantly, I wish to thank my loving and supportive wife, Hala, for her stand to me throughout the difficult times of my study, she made countless sacrifices to help me get to this point. My two wonderful children, Yahya and Jannah, seeing you every day provide unending inspiration for me to keep going and not to give up. I consider myself the luckiest in the world to have such a lovely and caring family, standing beside me with their love and unconditional support.

Chapter 1

General introduction

1.1. Introduction

Articular cartilage is a hyaline cartilage that covers the ends of long bones where joints are formed and, together with the underlying bone, constitute one functional unit. In words, both tissues contribute so that any deterioration in cartilage tissues will be directly reflected on sub-chondral bone and vice versa (Chiang & Jiang 2009; Qui et al. 2003). Osteochondral lesions comprise a group of defects that usually affects both the sub-chondral bone and the overlaying cartilage (Qui et al. 2003; Nukavarapu & Dorcemus 2013a). These disorders may be related to a pathological illness such as osteoarthritis or caused by traumatic injury to the joint (Johnna S. Temenoff & Mikos 2000). Serious pain and disability may arise from such conditions, with difficulties in the healing process due to the lack of blood or lymphatic vessels within cartilage, reducing the chance for tissue regeneration (Getgood et al. 2009; Da Cunha Cavalcanti Filho et al. 2012). Sub-chondral bone involvement, however, results in tissue response to fill the defect. This process is mostly insufficient for accurate repair of the tissue, as it leads to the production of fibrous cartilage which is inefficient in load-bearing tissues and will degenerate within months (Shahgaldi 1998; Getgood et al. 2009).

Current therapeutic techniques range from surgical attempts to stimulate tissue repair and regeneration by abrasion chondroplasty, drilling and micro-fracture of sub-chondral bone (Chiang & Jiang 2009), to the use of osteochondral auto-grafts and allograft techniques as a substitute for damaged tissues (Kheir & Shaw 2009b; Zengerink et al. 2010). These current treatment strategies have proved to be successful to some extent in dealing with such defects. However, clinical outcomes still show the production of fibrous cartilage tissues which are unable to resist high compressive forces compared to normal cartilage. Consequently there is often a recurrence of symptoms with time and the situation deteriorates to osteoarthritis (Chiang & Jiang 2009; Falah et al. 2010).

Tissue engineering and regenerative medicine has emerged, since the mid-1980s, as one of the future trends towards defining new therapeutic approaches for managing certain forms of tissue damage including osteochondral defects, which possibly provide a solution for a

healthier and natural tissue restoration of defective human organs (Panseri et al. 2012; Filardo et al. 2013). The basic principle for establishing tissue engineering techniques necessitate the use of biomaterials for designing and fabrication of scaffolds that mimic the three dimensional tissue environment and extracellular matrix (ECM), and then to seed these scaffolds with the specific cells intended to build-up these tissues (Castro et al. 2012). It is particularly important to investigate materials' culturing in 3D rather than 2D environment. Cells on 3D cultures are more prone to sense their spatial orientation and to act in a manner that closely related the natural tissue construct. In contrast, culturing on 2D surfaces promote cells to spread on as a monolayer which could impacted some aspects of their functions as per cell signalling and gene expression compared to 3D based culture (Edmondson et al. 2014).

Restoring complex tissue interfaces constitute one of the challenges facing tissue engineering approaches. This is basically attributed to the fact that these are hosting different types of tissues and in many times different types of cells forming an integrated tissue transformation (Leong et al. 2008; Karimi et al. 2015). Regenerating osteochondral interface was directed to restore the complex bone to cartilage transformation that involves gradients of minerals, tissues, and different architectural composites (Liu et al. 2011; Bian et al. 2016). In such a case, the choice of biomaterials is critical to ensure the proper functioning of bone and cartilage cells in addition to the proper design of an integrated multilayer scaffold that will guide the process of tissue regeneration (Swieszkowski et al. 2007).

Tissue engineering has evolved over the past decade, giving promising results for an osteochondral tissue repair according to both *in vitro* and *in vivo* studies (Swieszkowski et al. 2007; Ando et al. 2007; Camarero-Espinosa & Cooper-White 2017); scaffolds have been designed with multi-phasic compositions to present complex templates to address the bone–cartilage interface (Kon et al. 2014; Sola et al. 2016). In addition, tuning materials characteristics' such as surface chemical treatments have proved effective in dealing with issues such as cell attachment and migration, thus enabling improved tissue growth and development (Van der Kraan et al. 2002; Roach et al. 2010). In the current work, certain

materials characteristics were investigated, presented in 3D hydrogels, to address their suitability for bone and cartilage tissue regeneration. The plan was to target the osteochondral interface with focus on the sub-chondral bone plate and calcified cartilage zone. The materials should then be joined together to produce an integrated scaffold with the hope of mimicking the targeted regions. The normal osteochondral interface composed from the sub-chondral bone plate which is a compact layer with less porosity compared to the underlying cancellous bone but highly mineralized. This bone layer is followed by a calcified cartilage mass which involve hypertrophic chondrocytes embedded in calcified matrix. The thickness of these layers in the healthy joint was assessed according to certain studies at a mean of 1 mm for the sub-chondral bone plate and about 143 µm for the calcified cartilage zone which could be variable according to location (Müller-Gerbl et al. 1987; Koszyca et al. 1996; Patel & Buckland-Wright 1999). The sub-chondral bone plate is infiltrated by small channels (~ 40-50 µm) that allow for vascular penetration up to the calcified cartilage zone (Burr 2004; Lyons et al. 2006). As such, the current design focuses on replicating this region by producing a multiregional scaffold vertically threaded with bio-glass (BG) fibres (~ 60-70 µm). The degradation of these fibres will leave channels that will reassemble the original osteochondral interface.

1.2. Natural bone structure

Bone provides mechanical support for the body; it also acts as a source of blood cells, and as a reservoir of minerals. Bone in general is formed from an outer dense cortical bone mainly containing osteocytes embedded in a solid matrix, and an inner trabecular; spongy bone network immersed in bone marrow (Figure 1-1). Bone matrix is composed of an inorganic component, of which calcium is the main constituent, usually existing in combination with phosphate to form hydroxyapatite ($Ca_5(PO_4CO_3)_3(OH)$). Other inorganic constituents include carbonates, citrates, and traces of minerals and ions such as Mg, Na, Cl, F, K^+, Sr_2^+, Pb_2^+,Zn_2^+, Cu_2^+, Fe_2^{3+} The organic components include collagen type I in addition to small amounts of glycoproteins, proteoglycans, peptides, carbohydrates and lipids (Weiner & Wagner 1998;

Gaharwar et al. 2011). Within bone tissues collagen forms a network of fibres that is arranged in a 3D shape. Further mineralization and crystal formation, as part of bone mass growth, takes place within this 3D network of collagen (Weiner & Traub 1992; Lopes et al. 2018).

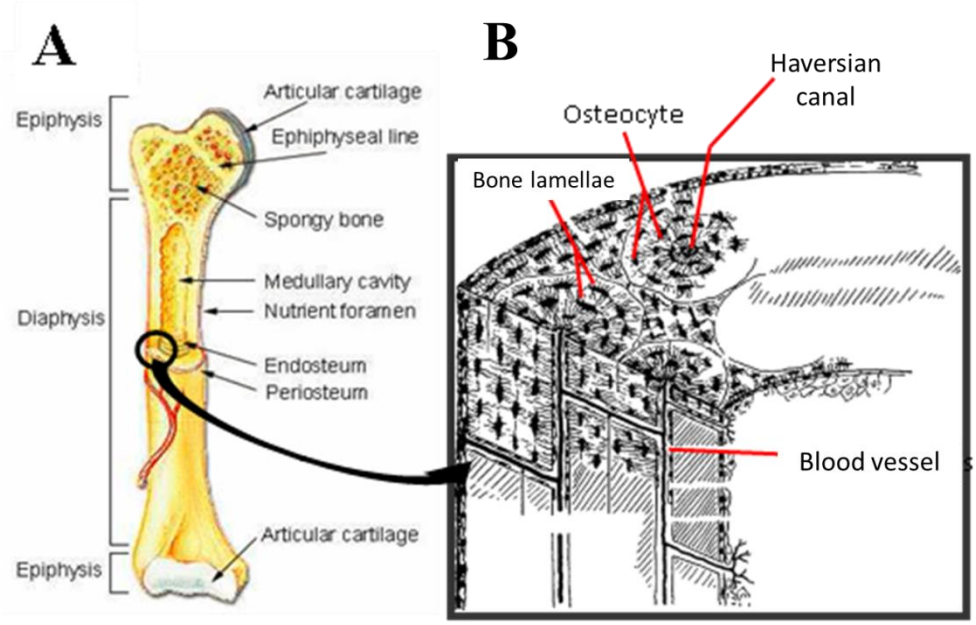

Figure 1-1. Bone structure and microstructure. *(A) normal bone morphology and compartments, with the spongy bone and articular cartilage location, (B) enlarged section showing the compact bone microstructures with solid matrix shape, canaliculi, and osteocyte distribution (Wojnar 2010).*

1.3. Natural structure of cartilage

Cartilage is a specialized connective tissue in the body with a single cell type, it is divided into three different types based on their location and specific function. The three major types of cartilage are the elastic, fibrous, and hyaline cartilage (Mow VC, Huiskes R, Stokes IA 2005). These are mostly distinguished according to ECM composition. Elastic cartilage composed of large amounts of elastic fibres and mainly exists in epiglottis and ear (Mow VC, Huiskes R, Stokes IA 2005). Fibrocartilage and hyaline cartilage are mainly associated with the skeletal system (Benjamin & Ralphs 2004; Kheir & Shaw 2009a). The fibrocartilage is characterized by higher percentage of collagen I compared to other types of cartilage and is found in regions like the meniscus and the intervertebral discs (Benjamin & Ralphs 2004). The hyaline cartilage is the most abundant type in the body and is exist in skeletal sites such

as the articular cartilage, it also found in other sites such as the trachea and nose (Mow VC, Huiskes R, Stokes IA 2005; Kheir & Shaw 2009a; Carballo et al. 2017a).

Articular cartilage supports the low friction motion of joints. It differs from bone in that it composed from only a single type of cell, the chondrocyte, surrounded (Gaharwar et al. 2011). Cartilage also lacks vascular and nerve tissue supply, which explains the low healing ability of cartilage tissues (Kheir & Shaw 2009a). Although chondrocytes comprise about 1% of the total cartilage volume, they are necessary for the replacement of degraded ECM in order to preserve cartilage size and mechanical characteristics. During embryogenesis chondrocytes are actively proliferative cells, however, mature chondrocytes are unable to proliferate, appears as a rounded shape cells completely embedded in ECM. (Johnna S. Temenoff & Mikos 2000). The ECM within cartilage is a mixture of collagen fibres (mainly type II), proteoglycans, and water, being arranged to efficiently provide tensile sheer force resistance (Melero-Martin & Al-Rubeai 2007). The overall structure is divided into 3 differential zones; the superficial, middle, and deep zones, followed by a calcified layer that separates bone from cartilage (calcified zone). Each of these divisions has characteristic composition and orientation (Figure 1-2) (Melero-Martin & Al-Rubeai 2007; Sophia Fox et al. 2009; Carballo et al. 2017b).

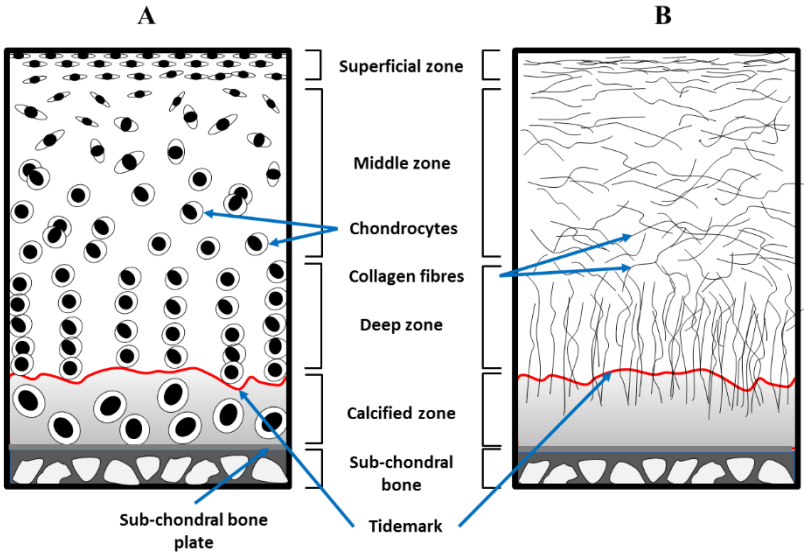

Figure 1-2. Microstructure of articular cartilage*. (A) showing arrangement of chondrocytes within the matrix and across cartilage zones, (B) collagen fibres orientation along the cartilage zones.*

The organization of collagen fibres along the three zones of cartilage is of major interest (Figure 2), being arranged parallel to the surface of cartilage in the superficial zone, variably distributed in the middle zone, and perpendicular to the surface of cartilage at the deep zone (Sophia Fox et al. 2009). Such arrangement provides an ability of cartilage to withstand certain kinds of force from the tensile and sheer forces to compression and overloaded pressure (Kheir & Shaw 2009a).

The concentration of matrix components differs notably between cartilage zones with the superficial zone containing the lowest concentration of proteoglycans, compared with the highest concentration in the deep zone of the cartilage. The calcified zone represents a transitional layer between articular cartilage and the sub-chondral bone beneath (Cohen et al. 1998; Sophia Fox et al. 2009).

1.4. Architecture of bone cartilage interface

The bone-cartilage interface describes the region where the different tissue compositions of bone and cartilage are connected together in a manner that ensures optimization of their mechanical properties and weight-bearing capability (Figure 1-3) (Zizak et al. 2003; Madry 2010). The calcified zone of cartilage is the deeper layer of articular cartilage where underneath lies the sub-chondral bone (Nukavarapu & Dorcemus 2013a). The sub-chondral bone is composed of a sub-chondral plate and an underlying bony spongiosa, both vary in thickness depending upon the joint, and are separated from the calcified zone by "the cement line" (Madry et al. 2010; Nukavarapu & Dorcemus 2013a). The osteochondral interface is characterized by higher mineralization and calcium percentage compared to the adjacent bone (Bullough & Jagannath 1983; Carballo et al. 2017b). It has been shown that the calcification process in this layer is an active process involving the production of substances that promote mineralization and matrix calcification in this cartilage layer. At the osteochondral interface, there is a continuous process of mineral growth and vascular invasion originated from the underlying bone towards calcification and forming new bone tissues. This process is regulated through a complex and balanced tissue transformation between cartilage and bone forming a

stable reserve zone at the epiphyseal bone interface (Bullough & Jagannath 1983; Hoemann et al. 2012a). The '*tidemark*', which separates the calcified zone from the rest of articular cartilage, represents a barrier that involves active enzymatic processes preventing further vascular invasion and continuous cartilage calcification (Bullough & Jagannath 1983; Huber et al. 2000).

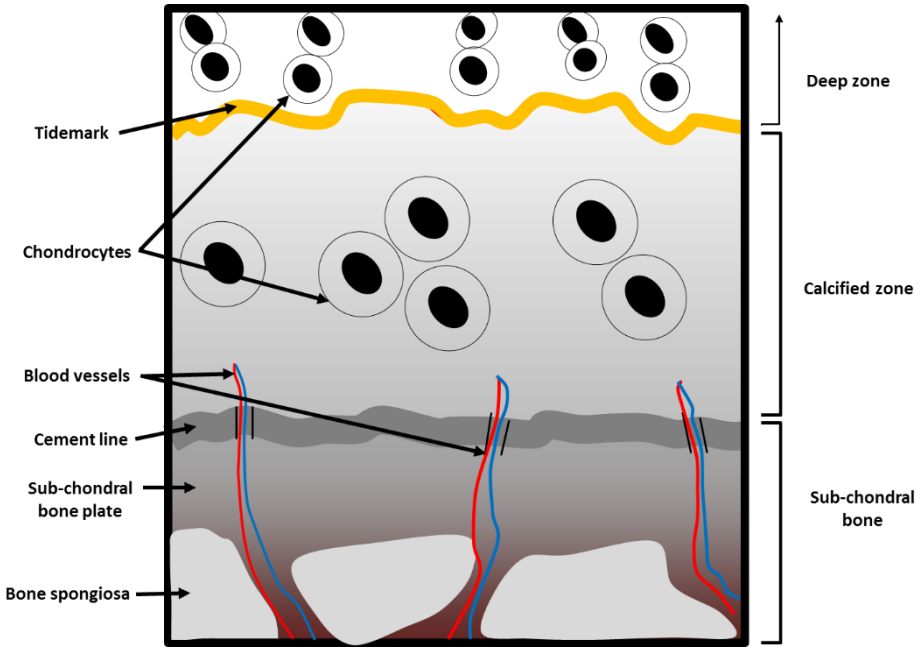

Figure 1-3. Schematic representation of the Osteochondral interface. *The figure is showing the bone-cartilage interface with vascular infiltration (blue and red thick lines) towards the calcified cartilage layer and the tidemark (orange) which supresses further mineralization towards cartilage.*

1.5. Pathology of osteochondral defects

Lesions to articular cartilage are usually categorised as either partial injury, where the defect occurs in the upper layers of articular cartilage without the involvement of the calcified layer or the sub-chondral bone, or full thickness injury, where the defect penetrates deeply along the whole cartilage reaching the sub-chondral bone (Figure 1-4) (Hunziker 1999; Hunziker 2002; Redman et al. 2005).

Articular cartilage injuries can be classified into several grades according to certain specifications of the damaged area. This classification has been adapted by different systems (Table 1), the most popular is the Outerbridge system which relies mostly on the location, size, depth, shape and boundaries of the lesion, in order to confirm the type of injury (Figure 1-5) (Kheir & Shaw 2009; Falah et al. 2010). Other classification systems have also been introduced including those by the international cartilage repair society (ICRS) and the Bauer-Jackson Descriptive systems (Falah et al. 2010). As a common measure, osteochondral damage is attributed to traumatic or accidental injury, where a potential stress fracture is generated along the cartilage thickness to the sub-chondral bone leading to serious damage. As a result of the limited ability for chondrocytes to migrate and their poor capacity to regenerative the ECM, the lesion will usually progress to a more complicated defect (Getgood et al. 2009; Da Cunha Cavalcanti Filho et al. 2012; Katagiri et al. 2017).

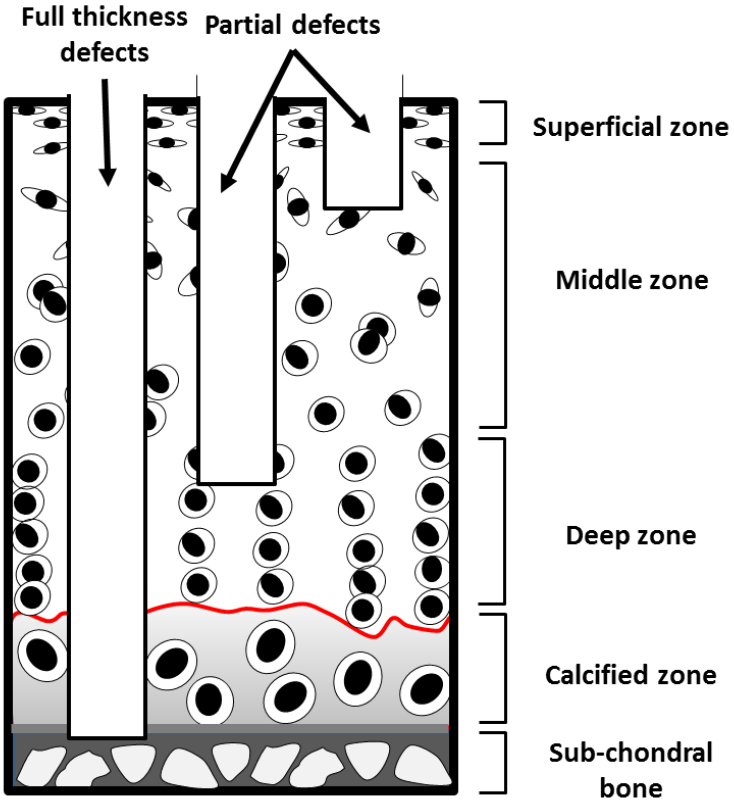

Figure 1-4. Schematic figure of articular cartilage defects, *showing the difference between partial defects (affecting upper layers) and full thickness defects (reaching the calcified zone down to sub-chondral bone).*

Table 1-1. Classification of articular cartilage damage. *The main grades established to describe the level of articular cartilage defect (Kheir & Shaw 2009; Falah et al. 2010)*

Classification System		Grades	Specifications
Outerbridge		0	Normal cartilage
		I	Softening and swelling of the cartilage
		II	Partial thickness defects not exceeding 1-1.5 cm of diameter
		III	Defects and fissures reaching the sub-chondral bone (more than 1-1.5 cm)
		IV	Exposed sub-chondral bone
ICRS		I	Superficial defect or fissure (nearly normal)
		II	Fissures with less than 50% depth
		III	Severe damage with osteochondral region involvement (50% or more)
		IV	Extending beyond osteochondral region through underlying bone
Bauer-Jackson Descriptie	Traumatic	I	Linear defect
		II	Stellate
		III	Chondral flat
			Chondral crater
		IV	
	Degenerative	V	Fibrillation
		VI	Exposed sub-chondral bone

The normal mechanism of cartilage to resist ordinary compressive force arises from the entrapment of interstitial fluid within the cartilage matrix (Suh et al. 1997).Upon increasing stress there is a parallel increase in the hydrostatic pressure within the joint so preserving more fluid in the cartilage matrix creating a strong resistance against damage (Suh et al. 1997). It is evident that degenerative changes to articular cartilage, whether related to injury, pathologic loading, or aging, will progressively lead to loss of the structural integration of cartilage layers starting from reducing cartilage volume with impaired function tailed by defects which will

increase the contact pressure within the joint surfaces and eventually developing osteoarthritis (Freemont 1996; Mithoefer et al. 2009).

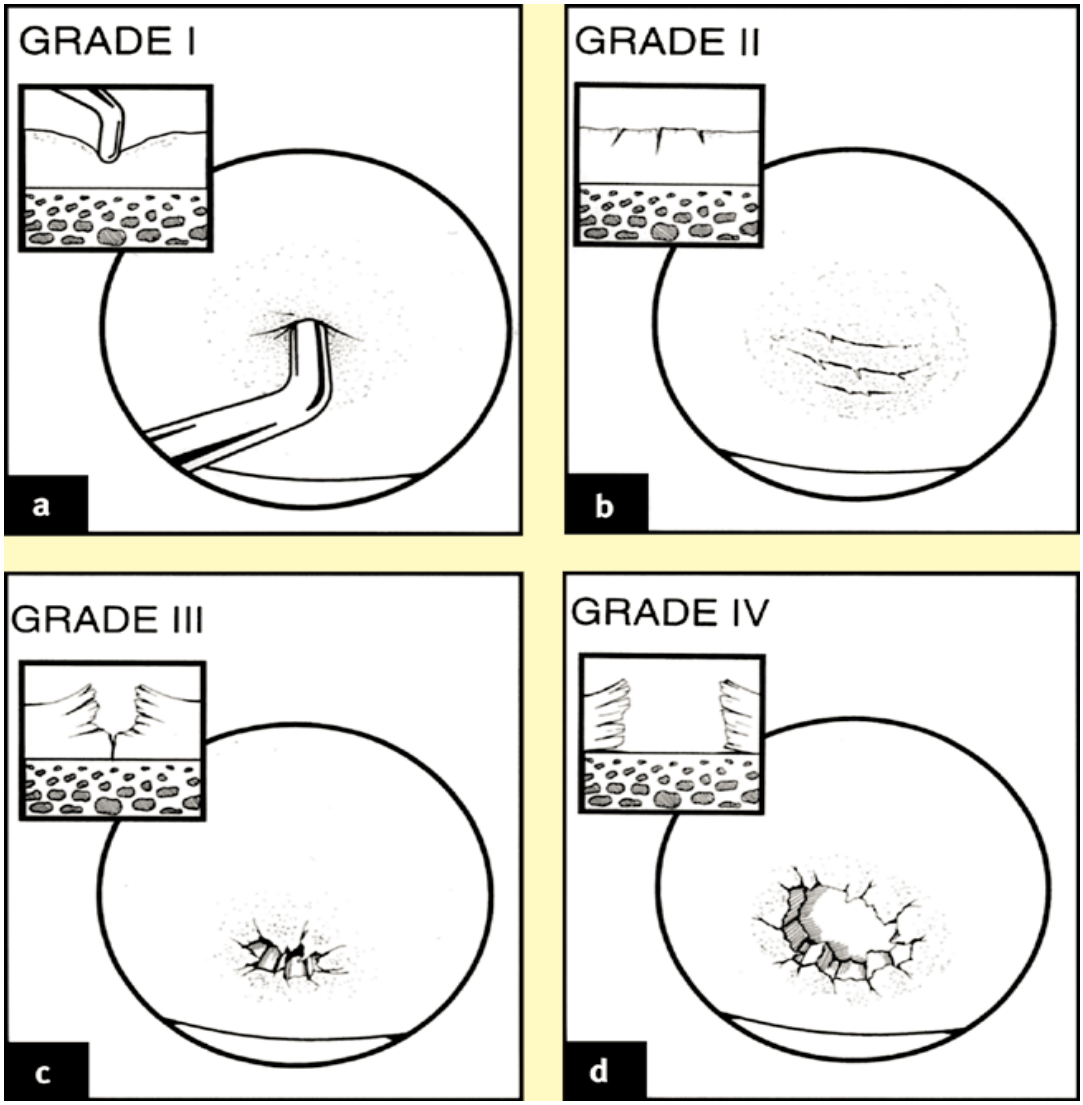

Figure 1-5. Schematic drawing of cartilage defect classification according to Outbridge system*. Grades of cartilage involvement are explained serially from (a) to (d) (Kheir & Shaw 2009a).*

Such structural damage usually begins with the loss of the matrix proteoglycans accompanied by destruction of the collagen grid; this is followed by metaplasia and cell damage (Hunziker 2002). Healing of these lesions are markedly poor, however when the sub-chondral bone is

involved in the progressive degenerative damage, bleeding will happened and blood clot formation triggers spontaneous healing to start over (Hunziker 2002).

1.6. Current treatment strategies

The applicable therapeutic preferences involve various options ranging from conservative and symptomatic treatment with specific anti-inflammatory medications and nutritional supplements (Fox et al. 2012; Detterline et al. 2005), to a number of therapeutic surgical procedures aimed at correcting osteochondral lesions and restoring normal function depending on certain techniques (Johnna S. Temenoff & Mikos 2000).

1.6.1. Stimulation of tissue regeneration

Several procedures were intended to stimulate the natural healing of damaged osteochondral tissue including drilling and micro-fracture (Figure 1-6), both examples of a predominant technique of articular cartilage restoration that depends on stimulation of blood flow to a specific lesion of cartilage with the resultant clot formation and migration of marrow cells to start correcting the damage area (Chen et al. 2009a). The process involves the debridement of all the injured and affected cartilage tissues until reaching the sub-chondral bone (Smith 2005). Multiple 3-4 mm holes are then drilled into the bone to stimulate bleeding, allowing marrow elements including MSCs to cover and begin to regenerate the area. This will resemble a blood clot which fills the defect.

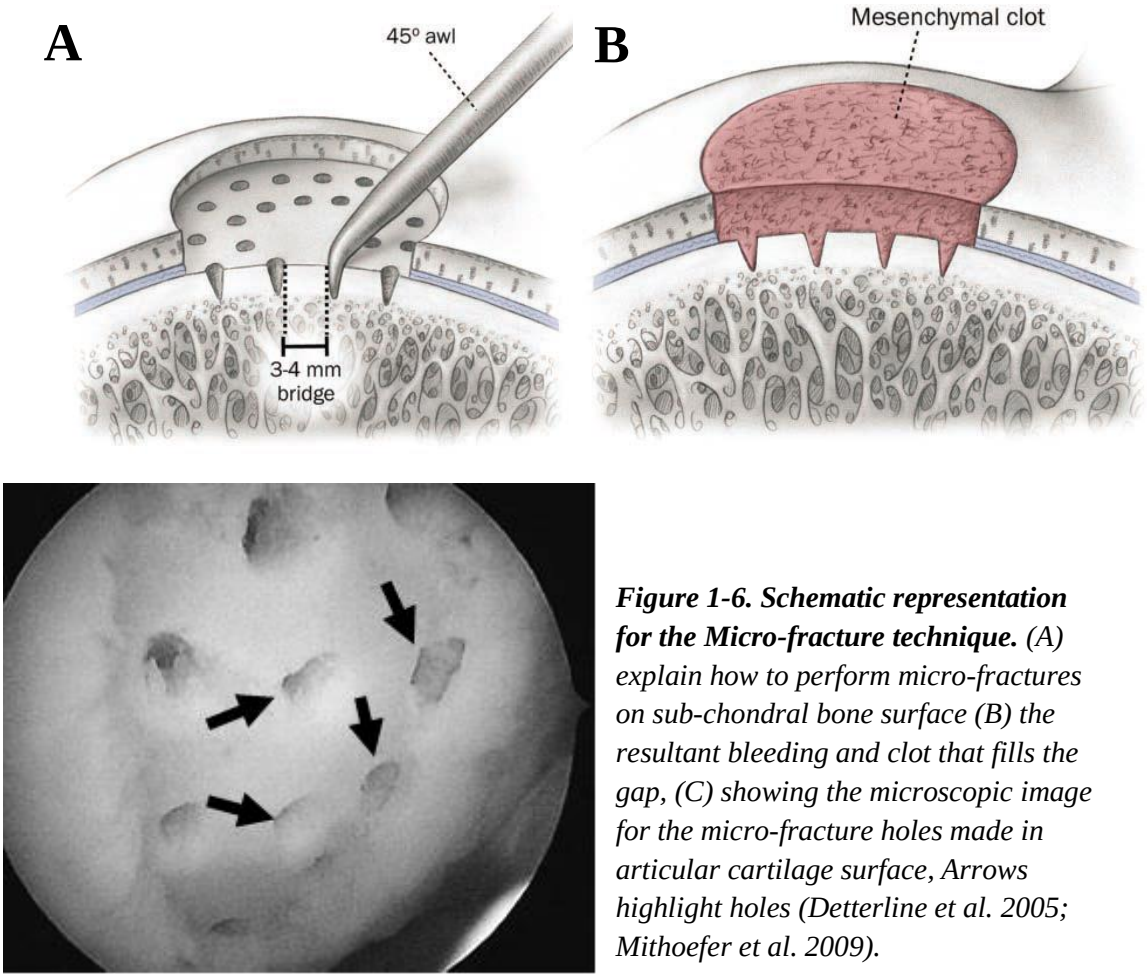

Figure 1-6. Schematic representation for the Micro-fracture technique. *(A) explain how to perform micro-fractures on sub-chondral bone surface (B) the resultant bleeding and clot that fills the gap, (C) showing the microscopic image for the micro-fracture holes made in articular cartilage surface, Arrows highlight holes (Detterline et al. 2005; Mithoefer et al. 2009).*

1.6.2. Replacement of injured tissues

Grafting of autogenic or allogenic osteochondral tissues is another technique used most often for correcting medium size to large osteochondral lesions (Redman et al. 2005). Osteochondral auto-graft gives the advantage that the tissues are autologous normal living tissues, to ensure chondrocyte viability, and usually results in production of similar cartilage to the injured one. This technique involves the debridement of a cartilage lesion, including a small portion of the underlying bone, and then to be fitted with osteochondral autograft of the same size and thickness, it results in the formation of mosaic or patch work and so are called mosaicplasty; usually the grafts are cylinders of normal full length cartilage which is taken

from a non-weight bearing regions of the joint (Detterline et al. 2005; Crist et al. 2016; Gelber et al. 2018).

Osteochondral allografts are frequently used to correct cartilage defects of intermediate to large scale (Chu 2001). This technique has shown good osteochondral tissue survival within a reasonable period of follow up, however, it requires a fresh tissue transplant to ensure the viability of the osteochondral graft. A frozen osteochondral tissue grafts may be used to reduce the immune response usually encountered from the fresh ones, although this is often at the expense of reduced tissue viability (Hunziker 1999; Johnna S. Temenoff & Mikos 2000).

1.6.3. Cell Transplantation

This technique Involve the transplantation of chondrocytes or soft tissues containing progenitor cells into the defective area with the hope of restoring the lost tissues (Aston, Bentley 1986). Periosteum and perichondrium (a delicate cellular layer located adjacent to bone and around the ribs respectively) were observed to have a chondrogenic potential due to the presence of chondrocyte precursor cells (Jobanputra et al. 2001; Redman et al. 2005). Grafts of these tissues were transplanted in full thickness cartilage defect (after debridement of the area exposing sub-chondral bone) and fixed in the area by fibrin glue. Results have indicated successful production of hyaline-like cartilage in most of the cases (Roberts et al. 2003; Redman et al. 2005; Bhosale et al. 2007). A study conducted by Homminga for perichondral grafting of cartilage damage using autogenic tissue graft showed very good results concerning cartilage growth in most cases (Homminga et al. 1990).

Autologous chondrocyte implantation (ACI) was introduced in the late 1990s as a new surgical approach for the treatment of full-thickness articular cartilage defects, it involves taking autografts or biopsies of cartilage from a non-weight bearing areas of the same joint, extracting chondrocytes from these grafts in the laboratory (Jobanputra et al. 2001), expanding their number by tissue culturing, and then returning them back to the damaged region (Figure 1-7). A periosteal tissue flap was placed by surgical suturing to seal around the defect,

then the cultured cells suspension was returned back into the region by injection through the flap. The technique revealed promising results in repairing osteochondral defects and restoring joint function as revealed by long-term monitoring studies (Brittberg et al. 1994; Johnna S. Temenoff & Mikos 2000; Roberts et al. 2003; Marlovits et al. 2005). The ACI method was modified by using a biomaterial like collagen (type I and III were implicated) to seal the damaged area instead of using periosteal flap (Jobanputra et al. 2001).the technique has recently approved by the National institute for health and care excellence (NICE 2017) and is now recommended as an option for treating symptomatic articular cartilage defects of the femoral condyle and patella of the knee . An updated research on ACI suggested the implication of collagenous matrix seeded by the previously expanded chondrocytes. The technique showed an improvement in the quality of results (mostly for the top cartilage layers) but does not address deep lesions of sub-chondral bone involvement (Buchmann et al. 2012; Erickson et al. 2018).

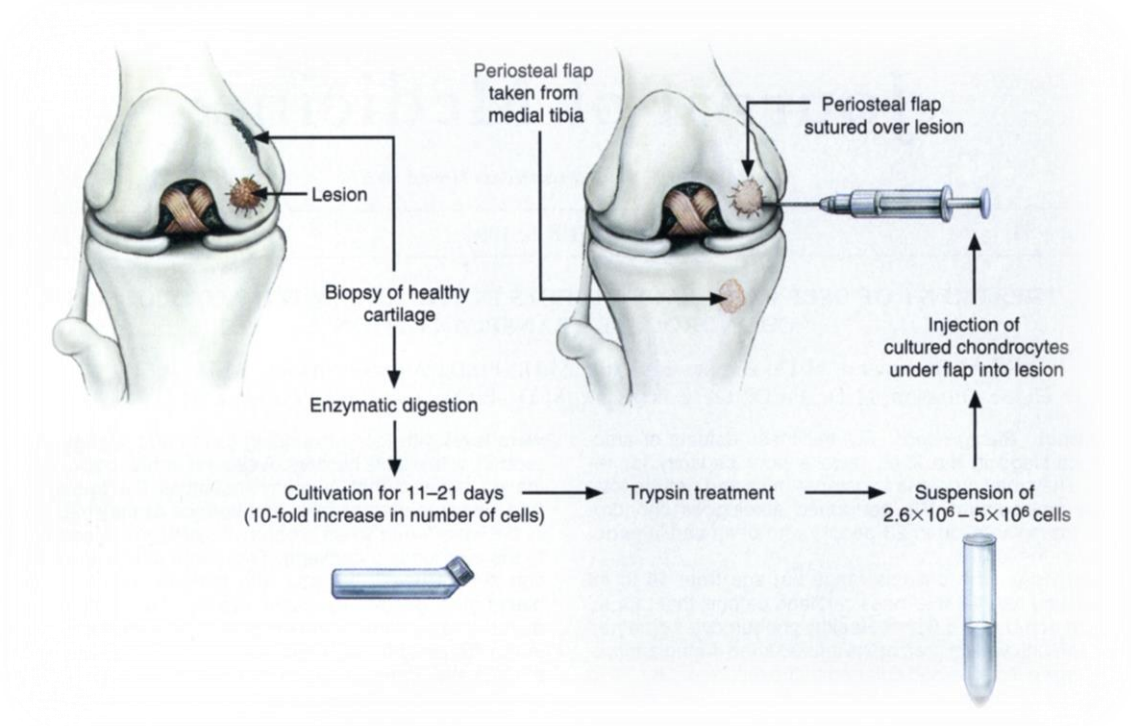

Figure 1-7. Schematic diagram for autologous chondrocyte implantation (ACI) technique. *Steps of chondrocyte harvesting, expanding in lab until final transplantation into defective area and periosteal flap cover. Arrows are indicative for stages of development. (Brittberg et al. 1994).*

1.7. Limitations of the current treatment

Current treatment modalities showed some good results regarding osteochondral repair and filling of defects (Steadman et al. 1997; Smith 2005; Hangody et al. 2008). According to a study by H. Chen et al (2009), the osteochondral repair was evaluated 24 hrs after microfracture and micro drilling techniques in a rabbit model. they pointed a less invasive aspects coming out from micro-drilling compared to micro-fracture techniques. They concluded that microfracture may causes bone compaction around the induced holes which prevent underlying bone marrow leakage and affect healing process. The clinical outcomes though have left some doubts concerning the type and functionality of the repaired tissue, especially when dealing with load bearing joints (Shahgaldi 1998). Shahgaldi et al, have demonstrated that new tissues formed were unable to withhold pressure loading of the joint. Further, these tissues do not present the same tissue properties or morphology. Although less invasive with low cost advantages, micro-drilling and micro-fracture techniques offer limited ability to functionally repair cartilage with the resultant formation of fibrous cartilage type that may have different morphological properties which affect cartilage structure integration (Clair et al. 2009; Chen et al. 2009b). Moreover, deterioration of the clinical condition occurs mostly within 18 months of the procedure and it is earlier in older patients (Steinwachs et al. 2008).

Donor site morbidity is also a common problem encountered with osteochondral autograft techniques, in addition to losing shape and curvature of articular surfaces, which probably have an impact on the joint contact pressure and load bearing strength (Swieszkowski et al. 2007; Clair et al. 2009). Moreover, osteochondral allografts are challenged by the availability of the appropriate donor, in addition to the possibility of transmitting infections and originating an immune response against the implanted tissue graft (Chu 2001).

1.8. Tissue engineering approaches

Tissue engineering represents an alternative solution to overcome the limited capabilities of current therapeutic options, utilizing biological, chemical, and engineering principles to create a modern technique for tissue restoration (Laurencin et al. 1999). It is considered as a better alternative for osteochondral tissue damage repair with the aim of establishing normal, mechanical and functional characteristics of articular cartilage and osteochondral regions (Panseri et al. 2012). The principle concept of tissue engineering depends upon the ability of cells to build-up new tissues when cultured in a 3-dimensional environment utilising a properly fabricated scaffold where other factors necessary for attachment and proliferation of cells are considered (Lavik & Langer 2004). In this regard, a balanced system of cells and suitable biomaterial is fabricated to engineer a scaffold that supports normal growth and integration of cells in a way that simulates the native tissue environment (Jagur-Grodzinski 2006). Numerous studies have been conducted in this field to gain a better understanding of the biomaterials and scaffold properties, their compatibilities with the cells and biological environment, in addition to extracellular matrix characteristics (Hutmacher 2001; Castro et al. 2012). Most of these studies were directed to examine the nature of biomaterials and their effects on steering cell behaviour and attachment (Lynch et al. 2005; Hirschfeld-Warneken et al. 2008). Some other aspects were investigated such as the chemistry (Thevenot et al. 2008), porosity (Bandyopadhyay et al. 2010; Hollister 2005), and stiffness (Xiao et al. 2013; J. Yang et al. 2017) of materials on affecting certain cell responses, viability and growth pattern. it has been concluded that specific materials features resulted in variable cell responses and tissue compatibilities. Eventually, these had affected the choice of material and tissue engineered fabrication technique for certain tissue regeneration (Lu et al. 2011; Chen et al. 2014). Chen et al. 2014 evaluated a gelatine-chitosan scaffold on variable cell responses including attachment and proliferation. They investigated their scaffold design and properties such as porosity and mechanical strength, fabricated using 3D printing to act as a tissue replacement. They concluded the suitability of the tissue engineered 3D scaffold as biocompatible tissue substitute to support the process of tissue regeneration.

1.9. Biomaterials

The term '*biomaterial*' is applied to any material that coordinates with a biological system in such a manner that it forms a construct for supporting cells and tissue development. It could be either natural, where it is normally produced by the biological systems of a living organism, or synthetic, where it constitutes a wide range of products synthesised in order to replace an impaired or damaged tissue construct (Hench 1998; Currie et al. 2007). The classical application of these biomaterials in the field of medicine to replace a specific organ or tissue in the body was governed by the nature and type of material, their physical and biological features and behaviour. Accordingly, biomaterials used were either metallic, as in hip replacement, textiles, as in vascular grafts, or polymers, as in intraocular lenses (Williams 2009).

The concept of biomaterial utilization in medicine has significantly changed since the introduction of nanotechnology and tissue engineering techniques (Binyamin et al. 2006; Williams 2009). Recently, biomaterials are produced to provoke a biological system response for the intended tissues, i.e. to be bioactive (Roach et al. 2007). In such a case a complex interactions between neighbouring cells and between cells and a biomaterial, will stimulate the release of certain chemicals and growth factors leading to further tissue regeneration (Ziats et al. 1988; El-Sherbiny & Yacoub 2013).

1.9.1. Types of biomaterials

The use of natural biomaterials provides a reasonable environment for supporting cells and tissue development, as it is closely related to the natural tissue construct (Gaharwar et al. 2011). Derivatives of ECM components are applicable as bio-composite implants such as proteins including collagen (type I or II), fibrin, and carbohydrate derivatives including agarose, GAGs, hyaloronan (Jagur-Grodzinski 2006; Currie et al. 2007). Metals such as magnesium, titanium, and platinum have been used as biomaterials in various fields of medicine depending on their purity and specific mechanical properties (Woo et al. 2005; Staiger et al. 2006). Other synthetic or semi-synthetic biomaterials which have been used for

tissue engineering include various forms of polymers and ceramics which are more controllable and can easily be processed to give a wide range of predictable properties (Liu et al. 2007). Synthetic polymers constitute a wide range of materials intended to be applied as tissue implants. Polymers are long chain organic materials formed by the combination of repeated monomeric units covalently bonded to produce their basic structure. They are of different types and categories, depending on their physical, chemical, mechanical and thermo-sensitive behaviours. Poly (lactic acid) (PLA) and poly(glycolic acid) (PGA) acid have largely been used as effective biopolymers (Binyamin et al. 2006). Ceramic biomaterials such as bioactive glass, hydroxyapatite (HA) and calcium phosphate derivatives have largely been used owing to their good biomimetic and bioactive behaviour within the biological system. They also possess specific osteoconductive properties allowing for osteogenesis and bone growth with applicability for musculoskeletal tissue engineering. Combinations of calcium phosphate with HA have also been demonstrated as effective osteoconductive bio-ceramics. Moreover, it has been shown that bioactive glass scaffolds for bone tissue engineering perform better than other applied bio-ceramics (Cao & Hench 1996; Van der Kraan et al. 2002; Jagur-Grodzinski 2006; Jones 2015).

1.9.2. Characteristic of suitable biomaterial

In order for a biomaterial to be applicable for use in tissue engineering repair techniques, it must fulfil certain characteristics (Table 1-2) to satisfy the requirement of biocompatibility with the host tissue environment (Cao & Hench 1996; Deb et al. 2018a).

Whenever a biomaterial is implanted in a living organism, tissue attachment becomes an important feature of the implant and is considered to be a function of tissue response to the implant at the tissue interface (Binyamin et al. 2006). Interfacial tissue fixation can be achieved through the use of porous biomaterials which enable the ingrowth of tissues either into the pores or throughout the surface of the implant, referred to as biological fixation (Hench 1991). Another feature of the implanted biomaterial, in terms of tissue attachment, is to be bioactive, where it can create a series of reactions between the tissues and the implant

surface with the resultant interfacial tissue attachment, described as bioactive fixation (Hench 1998; Cao & Hench 1996; Jones 2015). Bioactive glass materials have been presented in variable configurations and compositions to be incorporated with other biomaterials. These are basically act as an osteoconductive materials and are proven to be effective for bone tissue regeneration (Cao & Hench 1996; Hench 2006a; Jones et al. 2006).

Biodegradability is an important, but not obligatory, criteria of the implanted biomaterial, where the implant is able to degrade after a certain period of time and be substituted by natural host tissues (Cao & Hench 1996). For these materials two important points should be considered, one of which is that the resultant degraded products are able to be metabolically eliminated, the second point is that the degradation rate of implant must be as close as possible to the build-up rate of the host new tissues (Williams 2008; Williams 2009). As a rule, there should be a constant bond created between the implant and the host tissue at their interface, thereby offering good stability of the implant against physical stimuli. The biocompatibility could then be ascertained in all aspects concerning the biochemical and biomechanical properties (Wilson et al. 1981; Hench 1991).

Table 1-2. Biomaterials classifications and applications. *Nature and source of biomaterials with their further categorization and application.*

Nature of biomaterial	**Category**		**Applications**	**References**
Natural polymers	Proteins	Collagen Elastin Fibrin Elastin	Natural biodegradable polymers derived from human or animal sources, widely applied for most types of tissues including bone, cartilage, muscles, etc.	(Drury & Mooney 2003; Currie et al. 2007)
	Polyscacchar ide derivative	Agarose Chitosan Alginates GAGs Hyaloronan	Can form hydrogels, many derivatives synthesized, mainly applied for dermal wound healing, and tissue generation of certain types including cartilage	(Francis Suh & Matthew 2000; Currie et al. 2007)
Synthetic	Ceramics	Bioactive glass Bioactive ceramics HA and Ca salts	Osteoconductive and bioactive (bio-glasss and HA), applied for tissue engineering and regeneration of musculoskeletal system (bone, cartilage, teeth, and muscles)	(Hench 1991; Allo et al. 2012)
	Polymers and hydrogel	Poly ethylene glycol PEG, PLA, PGA, and their co-polymers	Biodegradable, biomimetic, hydrophilic polyesters, applied in tissue engineering as ECM substitutes	(Patterson et al. 2010)
	Metals	Mg Ti Pt	Proved application in load bearing tissues including bones, and for surface treatment of certain biomaterials	(Staiger et al. 2006)

.

1.10. 2D vs 3D scaffolds

The use of tissue engineering techniques to regenerate or reconstruct damaged or lost tissues, necessitates the presence of guidance for cells to proliferate or differentiate to yield the intended shape and composition of the natural tissues (Peter X. Ma 2004). This guidance can originate from a scaffold fabricated from certain biomaterial or a mixture of biomaterials chosen according to their chemical, mechanical, and biological behaviour that simulate the intended tissue environment (Peter X. Ma 2004; Grosskinsky 2006).

Scaffold materials should fulfil certain properties to be acceptable as a carrier for cells; such properties are closely related to the previously mentioned biomaterials characteristics with the most important criteria being biocompatibility enabling cells and tissue attachment, proliferation, and/or differentiation (Hutmacher 2001; Liu et al. 2007).

1.11. The impact of 2D surface characteristics

The biocompatibility of implanted scaffolds usually decided by the specific characteristics of implant surface, such as surface roughness (Elbert & Hubbell 1996a). Surface features play roles in cell adhesion, proliferation, and migration, characteristics of prime importance for successful tissue engineering (Roach et al. 2007). The existence of certain chemical functional groups on substrates surfaces and their effects on cell behaviours, suggests the feasibility of surface chemistry in directing cellular biological activity towards attachment (Boyan et al. 1996).

1.11.1. Surface micro-topography

In addition to environmental factors encountered at the site of implant, each implanted biomaterial is capable of provoking a specific cellular biological response. Such a biological response may be attributed to the morphological properties of the material, for instance the three dimensional structure, or to the specific surface topographical features and textures (e.g. the presence of grooves on the surface and the depth of these grooves) (Boyan et al. 1996; Deb et al. 2018a). Micro-topographical features of substrate surfaces are effective in

controlling cell behaviours and responses. For instance specific cells will display best attachment on grooved surfaces when compared to cells on flat surfaces within a specific time limit (Dalby et al. 2003).

1.11.2. Surface nano-topography

Other than micro topographical features it is also clear that nano-scale topography of substrates positively affects cell responses (Flemming et al. 1999). The natural ECM of tissues are composed from well-defined nano-fibers. Such nano-structures form an important aspect of living tissue which positively affects cell behaviour in terms of active adhesion and stimulating further release of growth and biological factors (Shi et al. 2010). Accordingly, nano-technology has been utilized for the fabrication of scaffolds with nano surface or topographical features (Shi et al. 2010). Certain procedures have produced a nano-scale topography on substrates, one of these methods was the spontaneous de-mixing of polymers producing nano-scale islands ranging in height from 13 to 95 nm (Dalby et al. 2002; Dalby et al. 2003). Observations proved better attachment and proliferation of cells on 13nm height islands compared to the 95 nm heights.

1.11.3. Surface chemistry

Surface chemical and functional groups exert their own impact on cell attachment and proliferation (Shin et al. 2003). Surface treatment and chemical modification, for example the incorporation of specific ions and surface coating of the biomaterials, has been proven to be effective in enhancing cellular adhesion and subsequent proliferation (Elbert & Hubbell 1996a; Roach et al. 2010).

Enhancing wettability of scaffolds surfaces through the inclusion of specific materials with active functional groups such as CH_3, OH, COOH, or NH_2 was shown to positively affect cell adhesion behaviour for certain cell types (Arima & Iwata 2007).

1.11.4. Surface biochemistry

Certain long chain ECM proteins such as fibronectin (FN), vitronectin (VN), and laminin (LN), have been applied as surface coatings of biomaterials to make them biomimetic (Underwood & Bennett 1989). However, after the discovery of the presence of signalling amino acid domains within the long chain ECM proteins, which are involved with cell membrane interactions, it is now more applicable to use these short peptide chains for surface treatment due to their increased stability and their relative ease of production at low cost (Shin et al. 2003). RDG peptide (Arg-Gly-Asp) is commonly used for surface management of certain implants along with certain other peptide sequences, for example a novel peptide sequence composed from Lys-Arg-Ser-Arg was proven to be efficient in improving osteoblast cell adhesion upon its use to modify specific biomaterials surfaces (Dee et al. 1998; Shin et al. 2003).

1.12. Fabrication of tissue engineering scaffolds

Engineering of scaffolds can be performed using specific fabrication techniques which may vary according to the type of materials included (either metal, polymer, ceramic, etc.) (Table 1-3), and to the final scaffold morphological characteristics (including micro or nano structure, pore size characteristics, etc. (Hutmacher 2001; Liu et al. 2007).

Several fabrication techniques have been used to create 3D scaffolds including some conventional methods such as solvent casting, particulate leaching, gas foaming, freeze drying, phase inversion and textile fibre technologies which involve fibre bonding and fibre knitting (Table 2) (Liu et al. 2007; Subia et al. 2010). Although these techniques are usually simple to conduct, they are time consuming and may require several processing stages in order to obtain the final desired scaffold (Figure 1-8) (Subia et al. 2010). In general, these techniques depend on the application of heat, or pressure, to a polymeric solution, or the use of salt particles to create a 3D scaffold with up to 95% pore density and pore sizes range of 50-1000 µm (Liu et al. 2007; Lu et al. 2013). However, the most important limitations of these techniques are related to lack of the uniform morphology and shape as there is variability in

moulds and containers used. Inconsistency and inflexibility of some techniques may have an impact on the final architecture and pore size of scaffolds. While toxic organic solvents used by most techniques for fabrication process may exert effects through the incomplete removal of the solvents which adversely affect the adherent cells and other bio-active materials (Leong et al. 2003).

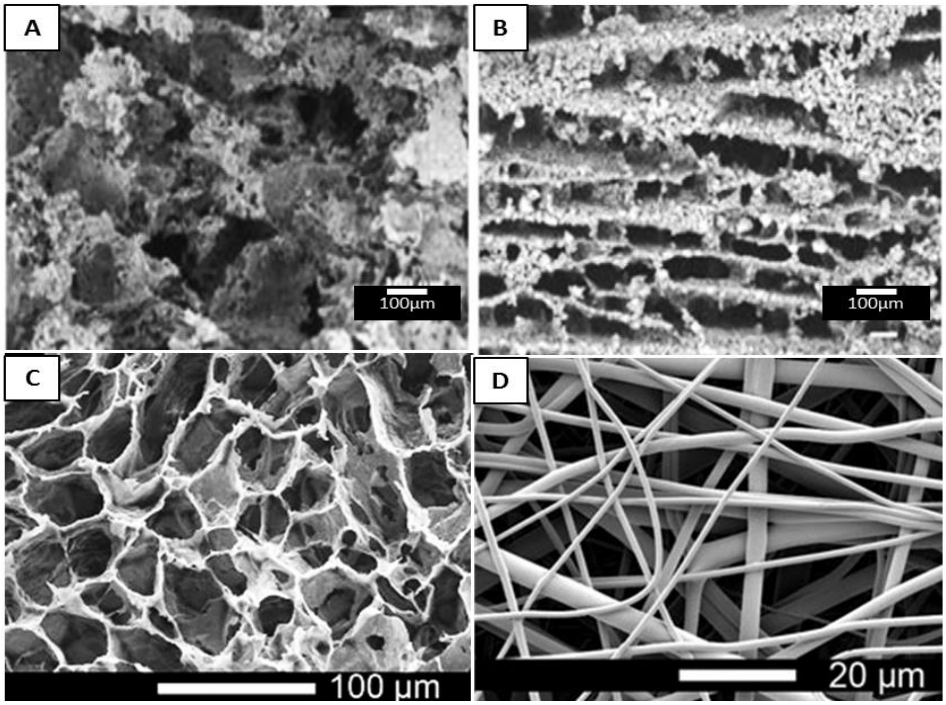

Figure 1-8. Examples of scaffold architecture fabricated using conventional techniques. *SEM imaging of scaffold's architecture shape produced according to (A) Particulate leaching, (B) freeze casting method, (C) phase separation (Solid-liquid), and (D) electrospinning. Scale bar measures 100 µm for (A, B, C) and 20 µm for (D) (Leferink et al. 2016; Darus et al. 2018)*

A further 3D scaffold fabrication technique is the solid freeform (SFF) or rapid prototyping (RP) technique (Figure 1-9), which utilises computer aided design (CAD) systems to control the process of scaffold fabrication through designing a computerized 3D scaffold shape (Yeong et al. 2004; Liu et al. 2007; Preethi Soundarya et al. 2018). The scaffold shape will then be synthesized via constructing layer by layer of the materials using a wide range of RP methods, the most applicable including 3D printing (3DP), fused deposition modelling (FDM), and selective laser sintering (SLS) (Leong et al. 2003; Sachlos & Czernuszka 2003). These CAD dependent techniques are advantageous in term of producing scaffolds with

reproducible architecture and control over pore size micro-structure and morphological characteristics (Hutmacher 2001; Hutmacher et al. 2004; Turnbull et al. 2018). It can also be applied to a wide range of materials including polymers (PLA, PGA, etc.), ceramics, and metals (Leong et al. 2003).

Apart from 3D scaffold production, the above mentioned fabrication techniques are also utilised for the fabrication of micro-structure surface characteristics (Leong et al. 2003). Other techniques have been used to yield a 2D scaffold with nano-surface characteristics, such as electron beam-induced deposition (EBID) which depends on the application of high energy electrons causing dissociation of the molecules on the substrate surface (Norman & Desai 2006). This technique is more applicable for use with metallic or metal-organic substrates, for instance copper, platinum, or titanium, to induce nanoscale surface features such as nanowires on the surface of these metallic constructs (Ueda & Yoshimura 2004). Electrospinning has been used as a popular technique utilised to produce 2D nano-fibrous scaffolds with promising results for tissue engineering (Vasita & Katti 2006). It utilises a high voltage electric power between two electrodes to yield a nanoscale fibres randomly arranged in a manor simulating the natural ECM construct.

Table 1-3. Conventional scaffolds fabrication techniques. *Type of technique, its description and pore size produced accordingly with their main limitations*

Technique	Description	Porosity	Limitations	Reference
Solvent casting /particulate leaching	Very simple, based on the evaporation of solvent from polymer solution in mould to create the scaffold, particulate leaching involve the addition of salt particles to the polymeric solution after evaporation the resulted scaffold immersed in water with the salt particles dissolved and leached out leaving a porous scaffold.	> 50 µm; porosity: 30 _ 90%	Problems with pore shape and internal pore openings with limited membrane thickness and low mechanical strength, in addition to residual solvent problems.	(Sachlos & Czernuszka 2003; Leong et al. 2003; Liu et al. 2007; Subia et al. 2010)
Gas foaming	The process rely on saturation of polymer with CO_2 gas at high pressure, and the dissolved gas will then be phase separated upon rapidly reducing pressure leading to a highly porous scaffold formation formed by the gas bubbles produced in the polymer, and there is no solvent involvement.	> 50 µm Porosity up to 95 %	Limited interconnected pore network	(Sachlos & Czernuszka 2003; Liu et al. 2007; Subia et al. 2010)
Freeze drying	The dissolved polymer mixture is freeze and then freeze dried to remove the ice particles produced in the polymer after freezing, producing a porous scaffold.	15-,200 µm; Porosity: > 90%	It is a time consuming process and usually results in small pore size scaffold	(Hutmacher 2001; Subia et al. 2010)
Phase separation (thermally controlled)	The principle is that a homogenous polymer solusion undergoes phase separation into polymer rich and polymer lean phases by lowering their temperature, then removing of solvent results in producing porous scaffold,	< 200 µm;Porosity: 70 _ 95%	Low control over pore size and microstructure, and problems with solvent residues	(Leong et al. 2003; Peter X Ma 2004; Liu et al. 2007)
Fibrebonding	May involve the use of heat to attack two fibre materials together, then using solvent to dissolve one of them producing fibre network with interconnected pores and high surface area.	Interconnected pore network 20-100 µm	Problems with residual solvent, and limited number of polymers.	(Hutmacher 2001; Leong et al. 2003; Liu et al. 2007; Subia et al. 2010)

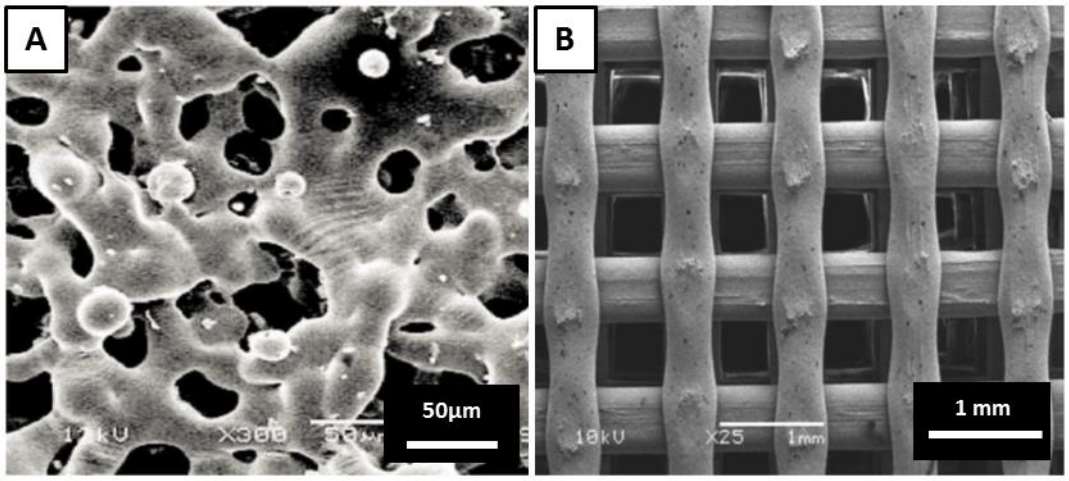

Figure 1-9. Examples of Scaffolds fabricated by solid free form (SFF) techniques. *(A) by SLS method, and (B) by FDM method. Scale bar measure 50 µm for (A) and 1mm for (B) (Leong et al. 2003; Yeong et al. 2004).*

1.13. From 2D to 3D cultures

Cells in natural tissues are normally existed in 3D environment which enables them to communicate in a multidirectional manner. Accordingly, this will impacted their further responses and signalling pathways and will decide their outcome behaviour and physiological function. In contrast, most of the tissues and cellular biological behaviour studies are dependent on monitoring growth of cells in two dimensional (2D) cell cultures which are deficient in tissue micro environmental conditions and requirements (Dutta & Dutta 2009; Huh et al. 2011). Consequently, 3D cell culture models were created to mimic these tissue requirements. These culture systems rely mostly on utilizing a specific biomaterial or a mixture of biomaterials to build-up a 3D scaffold fabricated to simulate the original tissue spacing and ECM needed for optimum ingrowth of cells (Pampaloni et al. 2007; Justice et al. 2009).

Attention must be offered towards providing a balanced combination between cells and the intended scaffold to create a suitable 3D culture environment that will promote native cellular

activities. Balanced systems may require the fabrication of scaffolds with certain bioactive molecules, growth factors, or enzymes that are necessary to stimulate natural cells responses including cell signalling and intercommunication that will result in further adhesion, proliferation, differentiation, and growth of tissues (Jagur-Grodzinski 2006; Huh et al. 2011). Additionally, scaffold characteristics, including surface features, spatial orientation, and bulk properties, are critically important considerations. For instance bone tissue engineering involves the fabrication of a scaffold with a suitable biomaterial combination that will provide optimum mechanical strength, and with reasonable interconnected pore size architecture (approximately > 200 μm) to enables vascular ingrowth and cellular migration (Hutmacher 2000). The success of building up tissues for any specific organ depends primarily on the scaffolds biomaterial type and properties besides their architectural design, as these factors determine the cells behaviour and final tissue morphology (Liu et al. 2007; El-Sherbiny & Yacoub 2013).

1.14. Fabrication of tissue engineered osteochondral scaffold

Tissue engineering aimed at regenerating osteochondral tissue is directed towards simulating the structural and histo-physiological criteria for the two types of tissues; bone and cartilage (Johnna S. Temenoff & Mikos 2000). Accordingly, a bi-phasic and tri-phasic scaffold has been developed and examined for these purposes (Figure 1-10), and specific biomaterials were chosen to best mimic each tissue type (Swieszkowski et al. 2007; Schaefer et al. 2002; Kon et al. 2014; Yousefi et al. 2015). The chosen biomaterials must be considered on the basis of their tissue biocompatibility and in this case to be able to support bone and cartilage cells performance (Di Luca et al. 2015a; Othman et al. 2018).

In general, the nature of the surrounding tissues and matrix will decide the choice of biomaterial to be used, for example, in certain trials HA and collagen type I were chosen for scaffold fabrication to regenerate bone tissues (Aydin 2011; Boyd et al. 2015; Sartori et al. 2017). Engineering of interfacial tissue grafts between bone and cartilage (osteochondral interface) constitute a challenge as the structural differences between tissues gradually change

from one tissue type towards the other one (Seidi et al. 2011; Camarero-Espinosa & Cooper-White 2017).

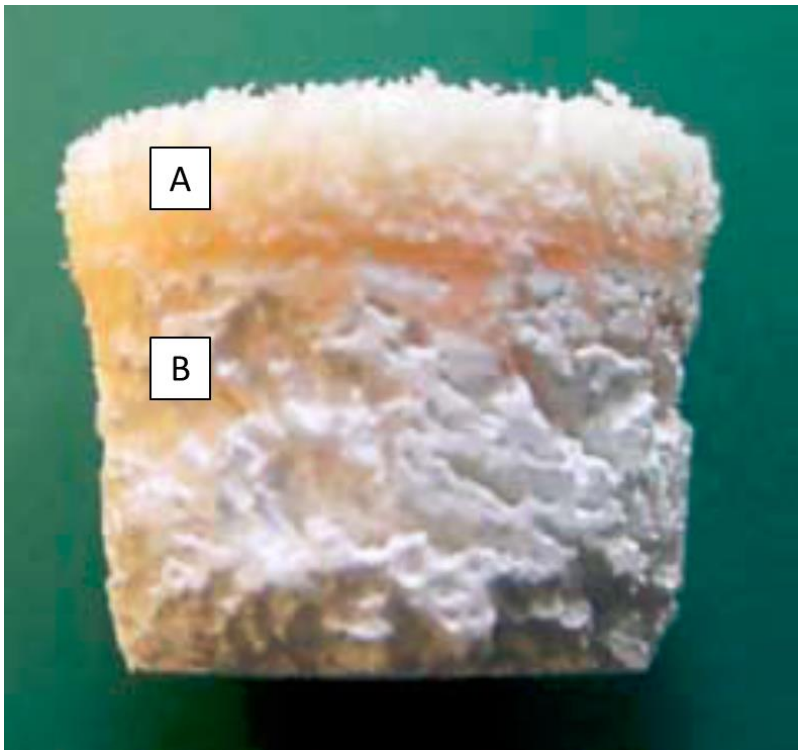

Figure 1-10. Example of a bi-phasic scaffold for osteochondral repair. *Image is showing two regions of biomaterials combinations (A) corresponding to the cartilage region and composed from copolymer poly(ethylene glycol)- terephthalate/poly(butylene)-terephthalate, (B) corresponding to the bone region and composed from HA and tri-calcium phosphate TCP (Martin et al. 2007).*

Accordingly, scaffolds should be fabricated to obtain a multiregional structure across the scaffold itself while simultaneously supporting tissue growth in a gradient manor mimicking the interfacial tissue growth environment (Seidi et al. 2011; Gadjanski 2017). Studies concerning multi-scaffold design have shown some promising results, for instance a multi-layer scaffold manufactured of agarose hydrogel and PLGA-bioactive glass showed good control of chondrocyte and osteoblast *in vitro* growth in each region of the scaffold, resulting in the formation of three distinct regions of cartilage, bone and calcified cartilage (Panseri et al. 2012). Another example displayed effective osteochondral repair in a knee joint of a porcine model using a bi-phasic scaffold made by fabricating HA with tri-calcium

phosphate (TCP) for the bone phase combined with a fabricated hyaluronic acid and atelocallagen (ultra-pure collagen) for the chondral phase (Panseri et al. 2012).

In reviewing osteochondral tissue structure (section 1.4), it seems applicable sometimes to use ECM components to fabricate an osteochondral scaffold. Lynn et al. (2010) fabricated a two-layer scaffold consisted from mineralized collagen I/GAG to regenerate sub-chondral bone and mineralized collagen II/GAG to regenerate cartilage. They studied the final scaffold nano-composition and concluded its suitability to mimic the natural osteochondral structure as per chemical composition and material distribution. It might also be useful to replicate the osteochondral architecture features when designing a multilayer scaffold such as the porosity and mechanical strength. Apart from chemistry, material's larger porous structure will facilitate osteoblastic cell growth and differentiation compared to a smaller porosity which proved more effectiveness for cartilage tissues (Di Luca et al. 2015b; Luca et al. 2016).

1.15. Summary

Articular cartilage is a unique avascular structure that surrounds bone ending at joints, aiding in lubrication and supporting low frictional joint mechanical functions (Kheir & Shaw 2009b; Gaharwar et al. 2011). It is a unicellular structure composed from chondrocytes which is responsible for ECM formation and lack vascularization. Unlike cartilage tissue, bone is a vascular multicellular structure composed from osteocytes, osteoblasts, and osteoclasts communicated together to preserve the internal bone microstructure and mineralization (Weiner & Wagner 1998). The base of cartilage is the sub-chondral bone layer from which cartilage is originated. The junction between bone and cartilage is an area that differs from bone and cartilage in terms of molecular density and mineralization potential, supporting the forward production of cartilage tissues and limiting further bone formation (Madry et al. 2010; Nukavarapu & Dorcemus 2013a). Cartilage layers constitute of three zones starting from the bottom with the calcified zone near the osteochondral bone region then the deep zone followed by the middle and then the superficial zones (Melero-Martin & Al-Rubeai 2007; Carballo et al. 2017a). Other than the calcified zone, the upper three zones of cartilage differ from each

other's by the way of arrangement and orientation of chondrocytes and ECM, where it is found to be perpendicular to the cartilage surface at the deep zone, irregular orientation at the middle zone, and are parallel to the surface of cartilage at the superficial zone (Sophia Fox et al. 2009). The calcified zone forms a transitional layer between bone and cartilage which is highly mineralized and is separated from the other zones by the tidemark which supresses further tissue ossification (Cohen et al. 1998; Sophia Fox et al. 2009; Hoemann et al. 2012b). Such an architecture and tissue orientations from bone to cartilage, provides an extreme resistance of joints against compressive and shear forces (Kheir & Shaw 2009b).

Damage or defective injury to cartilage may be difficult to heal due to lack of tissue vascularization and innervation, as this is the issue; treatment of cartilage injury had relied mainly on stimulating spontaneous tissue healing which must be performed by doing a small holes by drilling or micro-fracture on the sub-chondral bone surface after removing the damaged cartilage layers down to the sub-chondral bone (Hunziker 1999; Hunziker 2002; Douleh & Frank 2018), the result is bleeding with consequent leakage of accumulation of inflammatory mediators along with mesenchymal stem cells (MSCs) immigration from the bone marrow to the site of injury to start tissue repair and regeneration (Smith, Knutsen et al. 2005). Although simple and induce tissue healing, the outcome results of this treatment is the formation of fibrous cartilage with different mechanical properties that may not be able to withstand normal compressive forces as do the native cartilage, and this will lead to further deterioration upon certain period of time with the resultant osteoarthritis (Steinwachs et al. 2008; Clair et al. 2009; Erggelet & Vavken 2016).

Tissue engineering has emerged as a new tissue regeneration technique with a promising future towards correcting several forms of tissue damage including chondral and osteochondral injuries (Laurencin et al. 1999; Steward et al. 2011; Martin et al. 2007). The basic concept of tissue engineering is the utilization of cells to regenerate the damaged tissues by culturing them at the site of injury. Recently, tissue engineering have come out with several advances in this field, it utilizes biomaterials or mixture of biomaterials to fabricate 3D

scaffolds that mimic the ECM architecture and to be seeded by the cells to build up tissues in a manner that simulate natural tissue construct (Lavik & Langer 2004; Armiento et al. 2018). The biomaterials constitute a wide range of materials which could be natural (proteins and polysaccharides derivatives), or synthetic which may include certain types of polymers (PCL, PGA, PLLA, or their combinations), or bioactive ceramics (bio-glass, HA, and other Ca salts) (Hench 1998; Currie et al. 2007; Jones 2015; Deb et al. 2018b).

The choice of materials for scaffold fabrication is an important point to be considered as the bulk properties of these materials may be related directly or indirectly to the degree of biocompatibility along with the chemistry and surface characteristics of the fabricated scaffold (Cao & Hench 1996; Hench 1998; Binyamin et al. 2006; Steward et al. 2011). Accordingly, several fabrication techniques have been proposed to synthesize certain scaffolds with considerable biomimetic properties, these biomimetic features may involve controlling the pore size, changing the surface features by inclusion of functional groups or coating with bioactive materials that ensure best cellular responses and tissue regeneration (Hutmacher 2000; Shin et al. 2003; Ma 2008; Cao et al. 2017). Conventional fabrication techniques were first proposed which rely mostly on manual procedures with the application of heat, pressure, and solvents to synthesize the intended scaffold (Liu et al. 2007; Subia et al. 2010; Lu et al. 2013). However, these conventional procedures may carry certain limitations (Table 2) (Leong et al. 2003), which techniques such as SFF, which utilizes a CAD system to produce scaffolds with precisely controlled and reproducible architecture hope to eliminate (Hutmacher 2001; Yeong et al. 2004; Liu et al. 2007; Lu et al. 2013).

Osteochondral tissue engineering requires the fabrication of scaffold that should meet the criteria of two different types of tissues which are the bone and cartilage, consequently, a reasonable choice and combination of biomaterials should be made, for instance collagen type I with HA have been chosen for bone tissue and for cartilage tissues collagen type II and chitosan or other polysaccharides derivatives may be considered as a good choice (J.S. Temenoff & Mikos 2000; Martin et al. 2007; Levingstone et al. 2014; You et al. 2018).

Another point to be considered when designing multiphase scaffolds, is that the scaffold should involve a gradual change between the two phases by creating a gradient of materials between the two to ensure extreme simulation of the natural tissue environment (Schaefer et al. 2002; Seidi et al. 2011; Sola et al. 2016). Furthermore, surface topographical features of the substrate should be considered for impact on cell behaviours. In a study conducted on osteoblast-like cells (OCT-1), a better cellular adhesion was observed when cells were seeded on poly (L-lactide) (PLLA) polymer with micro topographical surface features (e.g., lines, grooves, pits, etc.) (Wan et al. 2005). A laser-induced micro and nano surface topography on titanium implant surface also showed an enhanced bone tissue attachment and growth (Brånemark et al. 2011).

1.16. Aims

The current project aims to fabricate a 3D hydrogel scaffold to regenerate the osteochondral interface (involving sub-chondral bone and calcified cartilage zone). This region presents a complex bone to cartilage transformation that hosts a minerals and tissue gradients. As such, the final scaffold should address for a multifunctional region with a hope to be achievable by joining two materials together to produce an integrated gradient scaffold. The chosen materials should be eligible to support osteogenic and chondrogenic cell activities with variable tendencies for mineralization. In this case, the scaffold should permit a higher rate of mineralization with higher osteogenic activity at one end that will gradually interchanged into more chondrogenic less mineralizable attitude towards the other. The current scaffold design should mimic the osteochondral interface replicating the sub-chondral bone and the calcified cartilage zone. In this prospective, and to optimize this design, bio-active glass fibres will be embedded longitudinally across the scaffold mass. These fibres are biodegradable and thus will leave empty channels to allow for cellular transplantation and vascularization. Moreover, the biodegradable elements from these fibres (calcium phosphate minerals) will provide a mineral environment by forming hydroxyapatite (HA) layer which in turn stimulate osteogenic and mineral cell behaviour (Cao & Hench 1996; Jones 2015).

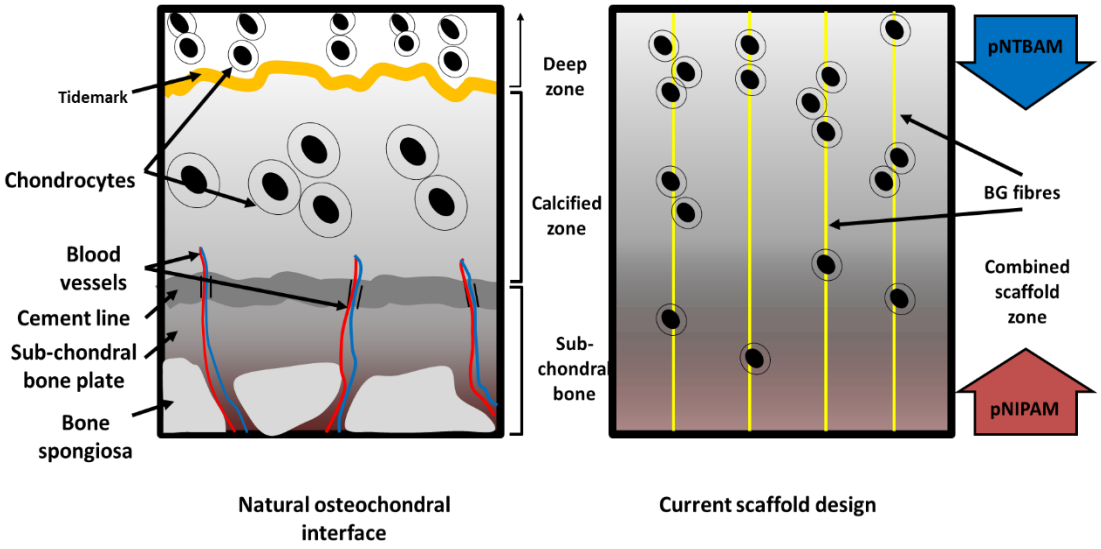

Figure 1-11. Current scaffold design compared to osteochondral interface region. *Suggested design for the current osteochondral scaffold illustrating scaffolds final shape and its principle components of polymers and BG fibres to match the osteochondral interface region. Black circles with dark cores represent cells.*

The choice of materials is mainly rely on the fact that both materials are belonging to the same category with slight difference in structure. As such, poly N-isopropylacrylamide (pNIPAM) and poly N-tert-butylacrylamide (pNTBAM) synthetic polymers were chosen. Both polymers are acrylamide based revealing the same chemical functional groups with only additional methyl group presented by pNTBAM. Accordingly, both polymers should present different features depending on the basic difference in their chemical structure and that these features will be reflected per cellular activities. The gaol is to inspect materials' characteristics such as surface chemistry, mechanical strength, porosity and architectural differences and then to investigate the relevant effects of these on cell survival, and proliferation. Variable monomeric concentrations of each polymer were inspected to investigate their effects on having larger pore size and eventually on cell migration. Based on the previous investigations, a specific monomeric concentration of each polymer will be chosen to proceed with testing osteogenic and chondrogenic cell functions. The final pNIPAM-pNTBAM composite will be inspected

to verify the development of multiregional scaffold architecture. The latter will then be tested to detect osteogenic and chondrogenic cell performances across scaffold regions. The individual hydrogels and the resultant composite scaffold will be compared between BG threaded and non-BG scaffolds to assess the impact of BG mass on cell functions and the rate of mineralization. The current project work can be summarized as follows:

- Characterization of pNIPAM and pNTBAM individual hydrogels to verify the main differences in terms of chemistry using FTIR spectroscopy and wettability by measuring water contact angle.
- Producing hydrogels in different monomeric concentrations (0.042 g/mL, 0.058 g/mL, and 0.079 g/mL) and compare them by measuring compressive force strength to assess materials stiffness, and SEM imaging to examine internal architecture and porosity. In addition, both hydrogels will be incubated with simulated body fluid (SBF) to test their ability to bind calcium minerals.
- Cell culturing of hydrogels with immortalized cell lines (MG63 osteoblast like cells and OK3H chondrocytes) to determine the impact of materials' various characteristics on cell attachment and survival in addition to cellular migration.
- Testing osteogenic and chondrogenic cell activities on hydrogels by seeding these hydrogels with primary human osteoblasts (hOBs) and primry human chondrocytes (hCHs).
- Joining the two polymers to produce a composite multiregional scaffold and examining the osteogenic and chondrogenic performances of cells upon the resultant architecture.
- Preparing hydrogels (individuals and composite) by vertically embedding BG fibres and assessing the degradation profile of these fibres within hydrogels at 37 °C incubated with PBS solution and followed using Raman microscopy and micro computed topography (micro CT).
- Testing the effects of embedding BG fibres within hydrogels on further mineralization activity and cell penetration across scaffold thickness.

Chapter 2

Materials and Methods

2.1. Materials

Table 2-1. list of the materials used in experimental work with their catalogue numbers and suppliers' names. *All chemicals were purchased as per table and used as received.*

Material	Catalogue number	Supplier
1,9-Dimethyl-methylene Blue zinc chloride double salt	341088	Sigma-Aldrich
2,2′-Azino-bis(3-ethylbenzothiazoline-6-sulfonic acid)	A3219	Sigma Aldrich
Acetic acid	A6283	Sigma-Aldrich
Alcian blue 8GX	A3157	Sigma Aldrich
Alizarin Red S	A5533	Sigma-Aldrich
Ammonium persulfate, reagent grade 98%	215589	Sigma-Aldrich
Anti-Collagen I antibody	ab34710	Abcam
Anti-Collagen II antibody	ab34712	Abcam
Anti-Collagen X antibody	ab58632	Abcam
Ascorbic acid	A4544	Sigma Aldrich
Bicinchoninic acid	B9643	Sigma Aldrich
Bovine Serum Albumin solution 7.5 %	A8412	Sigma Aldrich
Calcium chloride	C1015	Sigma Aldrich
Calcium Colorimetric Assay Kit	MAK022	Sigma-Aldrich
Cetyl pyridinium chloride	C0732	Sigma Aldrich
copper sulphate	C2284	Sigma Aldrich
CytoPainter Phalloidin-iFluor 555 Reagent	ab176756	Abcam
DAPI (4′,6-diamidino-2-phenylindole)	D9542	Sigma Aldrich
Dexamethasone	D2915	Sigma Aldrich
Dimethyl Sulfoxide	BP231-100	Fisher Scientific
DMEM (Dulbecco's Modified Eagle's Medium)-4.5g glucose	15-013-CVR	Corning
EDTA (ethaline diamine tetra-acetic acid)	E5134	Sigma-Aldrich

Eosin	SLBJ6425V	Sigma Aldrich
Ethanol 95%	E/0500DF/17	Fisher Scientific
Formaldehyde 37%	533998	Sigma Aldrich
Fetal bovine serum	FB-1001/500	Biosera
Goat Anti-Rabbit IgG H&L (FITC)	ab6717	Abcam
Goat Anti-Rabbit IgG H&L (TRITC)	ab6718	Abcam
Haematoxylin	GHS216	Sigma-Aldrich
Human chondrocytes (HCH) cryopreserved	C-12710	Promo Cell
Human osteoblasts (HOB) cryopreserved	C-12720	Promo Cell
Human Pro-Collagen I alpha 1 DuoSet ELISA	DY6220-05	R & D Systems
Human Pro-Collagen II DuoSet ELISA	DY7589-05	R & D Systems
Human TGF-beta 3 (E.coli)	100-36E	PeproTech
Human Total Annexin A2 DuoSet IC ELISA	DYC3928-5	R & D Systems
Hydrochloric acid	10125	VWR International
Insulin-Transferrin-Selenium-Ethanolamine (ITS -X) (100X)	51500056	Thermo Fisher scientific
L-Glutamine solution (200 mM)	G7513	Sigma-Aldrich
LIVE/DEAD® Viability/Cytotoxicity Kit, for mammalian cells	L3224	Thermo Fisher scientific
Magnesium chloride hexa-hydrate	M-2670	Sigma Aldrich
Methanol	320390	Sigma Aldrich
N,N,N′,N′-Tetramethylethylenediamine, reagent plus 99%	T22500	Sigma-Aldrich
N,N′-Methylenebisacrylamide	M7279	Sigma-Aldrich
N-Acetyl-L-cysteine	A7250	Sigma-Aldrich
N-Isopropylacrylamide	415324	Sigma-Aldrich
N-tert-Butylacrylamide 97%	411779	Sigma-Aldrich
Papain from papaya latex	P4762	Sigma-Aldrich

PBS (phosphate-buffered saline), 1X	21-040-CVR	Corning
Penicillin-Streptomycin	P4333	Sigma Aldrich
Phosphate buffered saline (Dulbecco A) tablets	BR0014G	Sigma Aldrich
Potassium chloride	p4333	Sigma Aldrich
Potassium phosphate tri-hydrate	p5504	Sigma Aldrich
Sodium bicarbonate	5-5761	Sigma Aldrich
Sodium chloride	S-7653	Sigma Aldrich
Sodium hydroxide	S8045	Sigma Aldrich
Sodium phosphate dibasic	S3264	Sigma Aldrich
Sodium phosphate monobasic	S5011	Sigma Aldrich
Sodium sulphate	238597	Sigma Aldrich
Tris (hydroxymethyl) amino-methane	252859	Sigma Aldrich
Trypan Blue 0.5% solution	L0990-100	Biosera
Trypsin EDTA solution 10X	59418C	Sigma Aldrich
Tween® 20	BP337	Fisher Scientific
β-Glycerophosphate disodium salt hydrate	G9422	Sigma Aldrich

2.2. Hydrogels synthesis procedure

The polymerization of NIPAM and NTBAM monomers to form hydrogel network was mediated by the process of atom transfer radical polymerization (ATRP). The process is dependent on the availability of enough monomers in solution in addition to a cross linker and an initiator to evoke the polymerization reaction. It is principally based on the formation of polymer using free radicals. The free radical is simply an unpaired electron which in this case will be supplied in the system by the inclusion of initiator (Lanzalaco & Armelin 2017). Ammonium persulfate (APS) will be used as the initiator to this reaction. It is an unstable compound and decomposes in solution to produce a very reactive free radicals that will elicit the polymerization process. The result is a chain of free radical monomers that reacts with the adjacent unreactive monomers thus the free radical will be passed through a series of monomers (Figure 2-1 A). This will lead to propagation of polymer chain until the monomers is finished in solution (Matyjaszewski 2012). A cross linker N,N′-methylenebisacrylamide (MBA) was used to link the polymer network. The accelerator N,N,N′,N′-tetramethylethylenediamine (TMED) will increase the reactivity of the APS initiator to elicit the polymerization process. As the APS is a highly reactive, it will react with oxygen present in solution and this will probably interrupt the polymerization process. Thus, purging the monomeric solution with nitrogen gas was performed before the addition of initiator to ensure optimum polymerization process.

NIPAM and NTBAM monomers were dissolved in their corresponding solvents at 0.079 g/mL, 0.058 g/mL, and 0.042 g/mL. MBA crosslinker was added to each solution at 0.0013 g/mL, then each mixture was bubbled with nitrogen gas for 10-15 minutes where the gas was pumped through an 18-gauge needle at a rate of approximately 10-15 bubbles/second. A 5 µL of TMED accelerator was added followed by 15 µL of the initiator solution (10% APS). Phase separation was induced causing the polymer phase to surround water phase vesicles to shape the final hydrogel porous construct (Figure 2-1 B)(Durmaz & Okay 2000; Kwok et al. 2003).

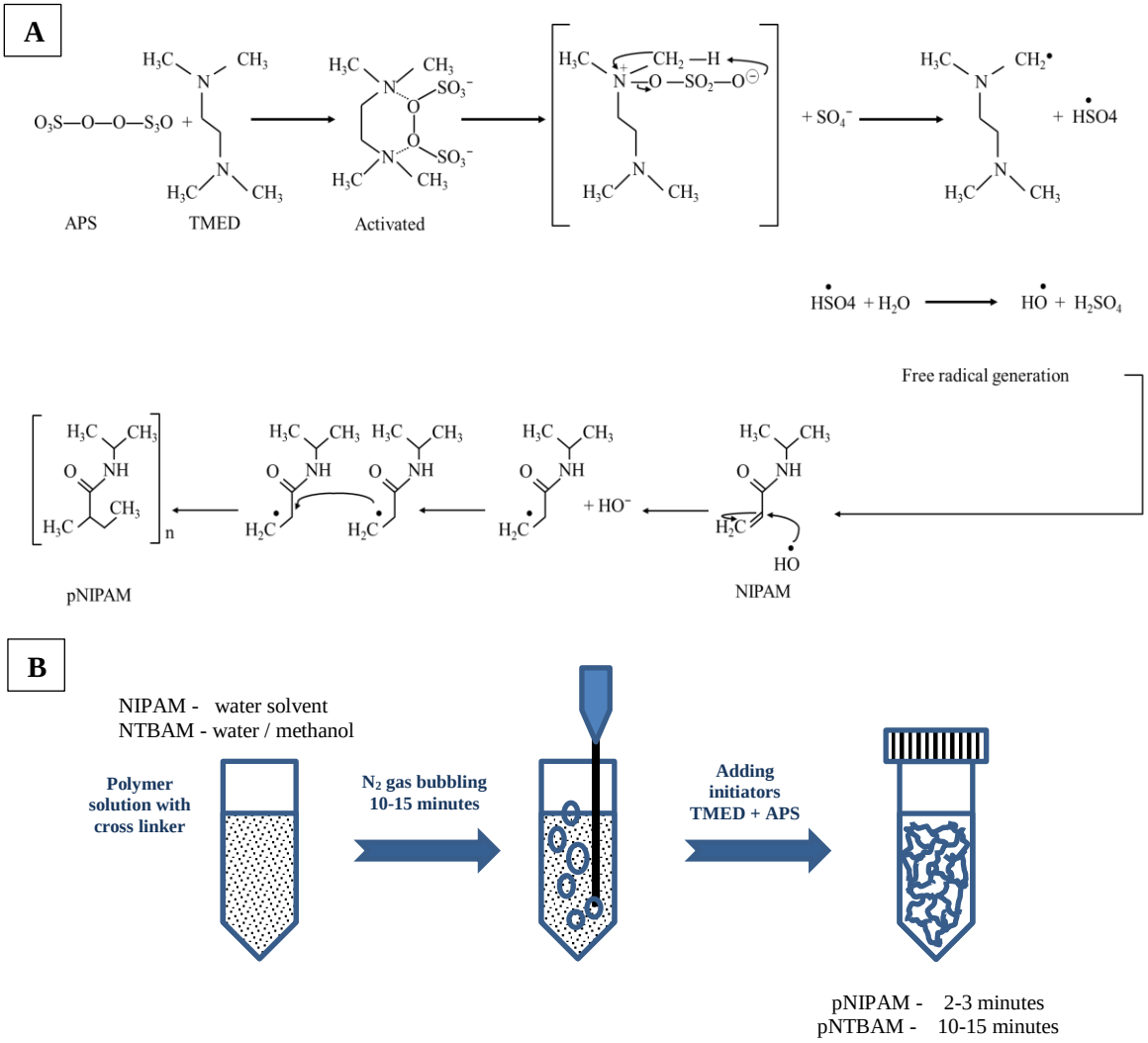

Figure 2-1. Schematic representation of the general procedure of polymer preparation by atom transfer radical polymerization inducing phase separation. *A) illustration of free radical generation and polymer formation. Adapted from (Mohan & Geckeler 2007) B) representation of lab procedure for polymer production.* **.**

2.2.1. Synthesis of pNIPAM hydrogel

NIPAM was dissolved in d H_2O and polymerised as per production method in 2.2. The hydrogel formed is a colourless soft gelatinous structure requiring 2-3 minutes to form after initiation.

2.2.2. Synthesis of pNTBAM hydrogel

NTBAM is insoluble in water at room temperature. Heating the mixture enhanced the solubility to some extent but the solution was more prone for recrystallization soon at room temperature. NTBAM, though, showed an excellent solubility in organic solvents (ethanol and methanol) at room temperature. However, the latter system failed to elicit polymerization after the addition of initiator. The combination of water and methanol in a ratio of 1:1 with heating to 37 °C had enabled solubility of NTBAM without recurrence or recrystallization after cooling. The resultant solution was stable and proved success in polymerization process. The formation of pNTBAM was at slower rate compared to pNIPAM and it takes about 10-15 minutes to completely produce.

2.2.3. Synthesis of pNIPAM/pNTBAM gradient hydrogel composite

The variable chemical and dissolution criteria for NIPAM and NTBAM polymers create a complex challenge in gradient hydrogel formation. In addition to the different solvents used for each polymer the timing required for hydrogel polymerisation must also be considered. pNIPAM hydrogels form within a few minutes (2-3 minutes) while the pNTBAM hydrogel can take up to 15 minutes to form and several hours to harden. We therefore proposed a dynamic method for gradient hydrogel preparation adjusted for the timing of polymerization required by each hydrogel. A stepwise pouring of previously prepared polymer solutions was performed starting with NIPAM (Figure 2-2). Each monomer solution was mixed with the APS initiator immediately before pouring into the intended container. The sequence of addition was determined by the speed of polymer formation where NIPAM was the first to be added. The second monomer solution was added only after the first layer had begun to polymerize, allowing polymer layers to infiltrate each other at their interfaces forming a stable bonding. The NIPAM-NTBAM monomeric mixture was added 40 seconds after the addition of NIPAM to create a combining region between the two variable layers. NTBAM within this layer extended the time for polymerization initiation to 1.5 minutes, thereafter the last

NTBAM layer was added. The gradient samples were covered and stored at room temperature overnight.

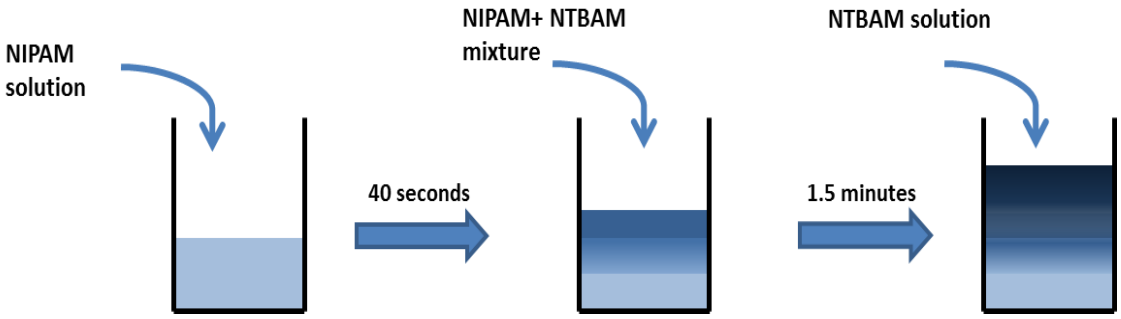

Figure 2-2. Gradient hydrogel composite preparation. *The steps of adding polymer solutions are revealed together with the specified timing for each one.*

2.3. Biodegradable glass fibres embedded hydrogel scaffold composite

Bio-glass (BG) fibres, $50P_2O_5$-24MgO-16CaO-$16Na_2O$-$4Fe_2O_3$ (Jones 2013), were incorporated within hydrogel constructs in an attempt to provide a mineralized environment and to create channels. These fibres are biodegradable and leave channels across the scaffold construct allowing cells to travel down the scaffold thickness. These were kindly donated by Dr. I. Ahmed, University of Nottingham.

2.3.1. Insertion of BG fibres across hydrogel

A 3D printed mould model comprised of a cylindrical polymeric base with channel holes was used to hold BG fibres vertically while casting the polymeric material (Figure 2-3). The mould was designed on Autocad 2012 software and printed on a Makerbot 3D printer. Base plate temperature was 120 °C, and nozzle temp 220 °C at the low (fastest) resolution. The material used was non-biodegradable acrylonitrile butadiene styrene (ABS). Mould dimensions were 15 mm diameter x 10 mm thickness. The holes were arranged in a 4x4 with diameter of 1 mm.

The fibres were aligned manually to the mould base with the aid of a dissection microscope. The whole set was enclosed by a plastic cylindrical cover, locked with a rubber ring, and the polymer solution (prepared as mentioned in section 2.2) was casted. The mould was then sealed and kept on the bench at room temperature to enable hydrogel formation. The time taken to remove the gel from the mould was polymer dependent (See Sections 2.2.1, 2.2.2, and 2.2.3). Hydrogels were removed and stored in dH_2O at 4 °C until ready for use.

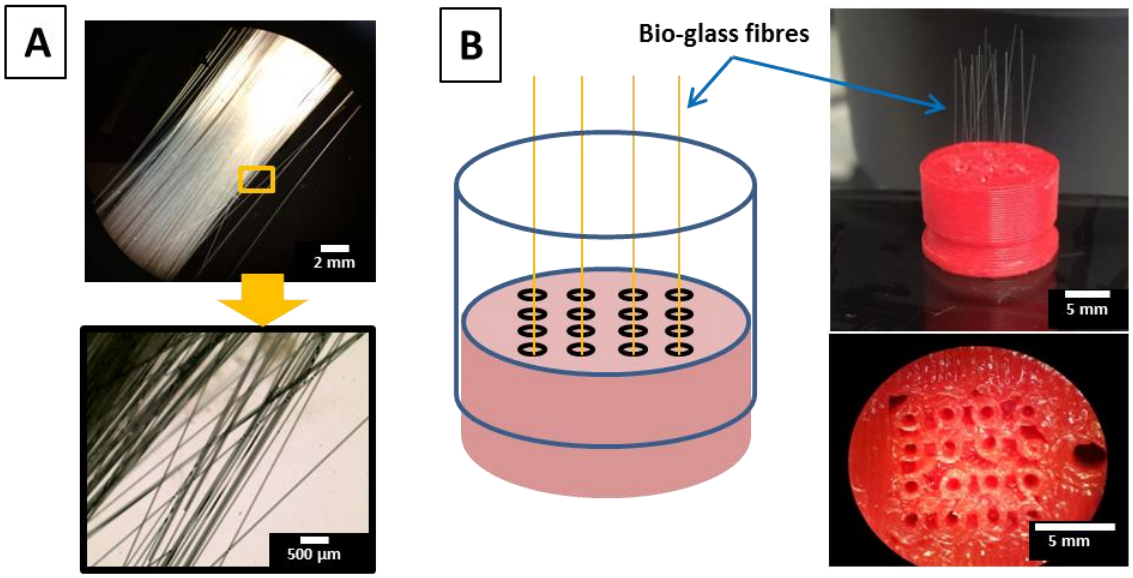

Figure 2-3. Processing of BG fibres in mould, *illustrating A) BG fibres and B) 3D mould shape and fibres loading onto the mould.*

2.3.2. Following degradation profile of BG fibres

2.3.2.1. Raman microscopy

Raman spectra were taken on a Thermo scientific DXR Raman microscope with a 532 nm laser, Olympus TH4 – 200 at magnification x10 lens. Hydrogel samples with embedded BG fibres were also observed under Raman microscope. Map spectra of the surface in proximity to fibre were taken as a day 0 measurement. Samples were then incubated with PBS at 37 °C and map spectra were taken on days 3, 7 and 15. Settings were optimized at 30 secs/ spectra,

2 spectra per point, no photo bleaching, 10x10 mapping and points spacing at 10x10 µm. Aperture was set at 25 µm slit. A map spectrum was also analysed using principle component analysis (PCA) function of Raman to differentiate and track specific peaks from BG and hydrogel. Analysing sample spectra using PCA is often used to distinguish between two or more components in sample by minimizing the sample spectra into specific easily recognized components. Accordingly, this will support pursuing a degradation profile of a material or monitoring the development of specific protein with time by eliminating other components spectra in sample while focusing on the targeted compound (Sato-Berrú et al. 2007; Hong Ong et al. 2012).

2.3.2.2. Micro-CT scanning for fibre density

Hydrogel perfused fibres were 3D scanned in an X ray Scano micro-CT40 with X ray settings at 55 kvp/ 71 µA. Hydrogel samples were placed in a cylindrical 2 cm diameter sample holder, wrapped with biofilm, and loaded over a machine robotic handle and scanned (Figure 2-4 A).

Scanned samples were analysed to verify the variable densities between hydrogel and bio-glass mass. The Scano micro-CT software enables two volume analysis of a sample by analysing the density for each component per material volume. The hydrogel and BG fibres had been considered as two components with different densities per sample. Sample scanning by µCT will recognize the variable densities between the hydrogel and BG mass.

The scanned samples were analysed to verify the fibre mass density per hydrogel by showing the dense object mass (BG fibres) in transparent low-density hydrogel mass. Each component was analysed according to specific density threshold revealing the BG mass at the higher threshold (134-1000) versus the hydrogel mass at the lower threshold (0-134) (Figure 2-4 B). 3D images were constructed revealing the BG fibres tracked for their degradation at 0, 7, 15, 21, and 28 days after incubation with PBS at 37 °C.

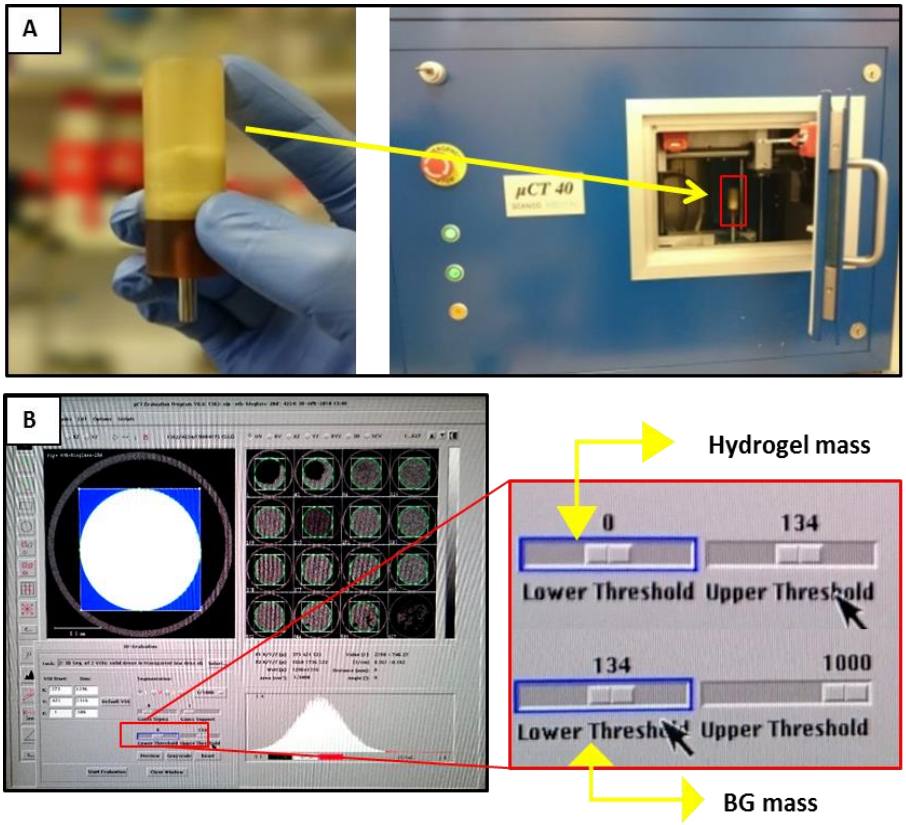

Figure 2-4. Micro-CT scanner processing of samples. *An illustration of A) sample holder and sample loading into machine robotic hand, B) a screen shot for 3D analysing setting of hydrogel sample using the micro-CT software to detect the dense BG fibres mass by analysing two volume threshold both of hydrogel and BG fibres.*

2.3.2.3. Revealing BG fibres channels after degradation

To observe the location of BG channels after BG degradation, samples were stained with alizarin red stain. After incubating samples with PBS at 37 °C for 28 days, hydrogel samples were washed 3 times with d H_2O at room temperature and then incubated with 1 mL 1% alizarin red stain for 30 minutes at room temperature. A washing step was followed with d H_2O 3 times (full protocol for alizarin red stain is mentioned in detail in section 2.4.5.1). Samples were then viewed using EVOS bright field microscope for the x10 and Leica dissection microscope for the x2 magnification (for the x10 magnification images captured by NIKON D5000 mounted to the dissection microscope).

2.4. Characterisation of hydrogels

Following synthesis of hydrogels, we next sought to determine chemical, physical, mechanical, and architectural characteristics.

2.4.1. Fourier transform infra-red (FTIR) spectral characterisation

2.4.1.1. individual hydrogels FTIR spectra

Chemical compsition for each hydrogel (Figure 2-5) was verified using FTIR spectroscopy. A ThermoScientific IS50 FTIR fitted with a single bounce germanium ATR was used. Freeze-dried samples (using Edwards freeze dryer machine) were used to minimise water noise in spectra. Data were recoreded in Omnic at 4 cm^{-1} resolution, with 32 scans being averaged between 4000-400 cm^{-1}.

Figure 2-5. Monomeric structure of NIPAM and NTBAM. *The main difference between the two materials in the basic chemical structure is illustrated by the red dotted circles.*

2.4.1.2. Composite gradient scaffold spectra

A pNIPAM-pNTBAM composite (prepared as mentioned in section 2.2.3) was freeze dried (as per section 2.4.1.1) and was sectioned using scalpl into several pieces both vertically and horizontally (Figure 2-6). FTIR analysis was performed to map across the gradient composite regions. Three samples were processed with seven regions from each scanned across the length of each gradient sample (the same instrument settings were used as per 2.4.1.1).

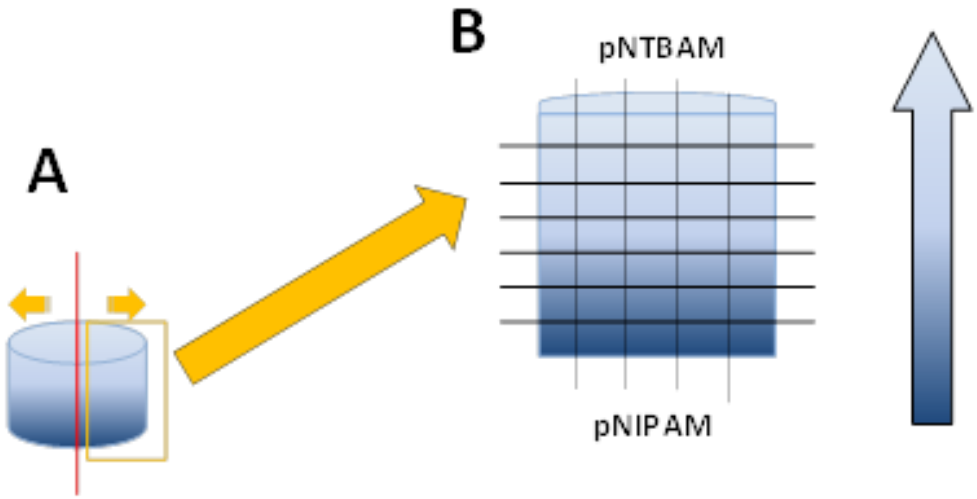

Figure 2-6. Schematic representation of how the gradient sample was prepared for FTIR measurement. *by A) spliting samples into two halfs and B) a grid figure of how the gradient wassliced into several regions where the spectra for each region collected out of multiple pieces.*

2.4.2. Water contact angle measurments

To verify wettability of the scaffold materials, both of the gels were assessed using water droplet contact angle measurements. A Thetalite version 2.4 operated by OneAttension software system was used. Hydrogels were placed over a glass petri dish, pressed using a glass coverslip to get a flat surface. The latter step was conducted to condense the polymer network by compressing the porous material. The materials dried at 70^{o} C in an oven for up to 2 hours. Contact angles were recorded automatically every 100 ms for the first 10 seconds following water placement on the surface via syringe. Each droplet was accurately measured at 1 µL, following sysetm-based calibration to measure droplet volume. A replicate of 4 samples were used and a 4 measurments were collected for each sample. All experiments were carried out on the bench at room temperature.

2.4.3. Compressive force mechanical testing

The compressive strength of hydrogels was measured using the BOSE Electroforce system equipped with a 20 N loading cell and cross head speed at 0.05 mm/s. The samples were

cylindrical in shape with dimensions of 4.5-5.0 mm hieght and 9.4- 11.5 mm diameter (Figure 2-7). The load was applied until strain reached 90%. The compressive strength was determined from the maximum load of the applied stress-strain curve. Four samples of each hydrogel were tested and an average obtained.

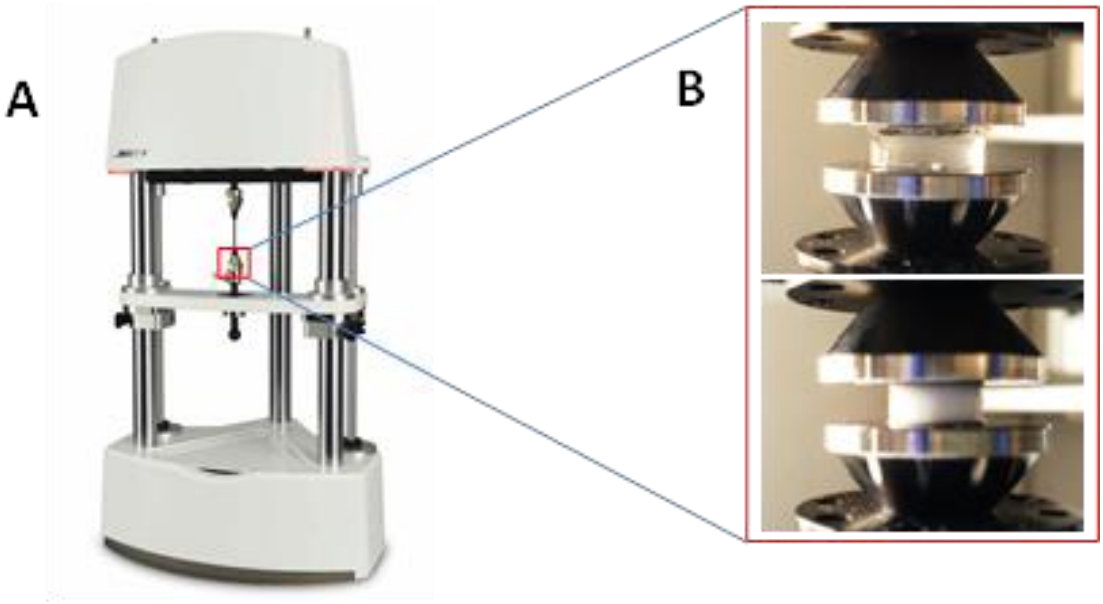

Figure 2-7. BOSE electroforce machine. *showing A) the device over all front appearance and B) sample loading to the machine holder.*

2.4.4. Scanning electron microscope (SEM) imaging

Hydrogels were observed using a bench top Hitachi S4500 scanning electron microscope (SEM) to examine the internal architecture, pore shape, and size. The basic principle of SEM technique is the application of high energy beam of electrons to the surface of sample. These electrons will excite the sample generating multiple signals from sample surface. These signals will be translated to reveal information about sample morphological characteristics and crystalline structure (Weinbrandt & Fatt 1969).

To preserve the internal architecture of hydrogels, samples were frozen at −20° C overnight (using traditional −20 lab freezer), and then freeze-dried using Edwards freeze dryer machine.

Freeze drying of samples is based upon removing water from hydrogel sample while frozen in a pressurized chamber, thus maintaining the pore shape and texture and preventing collapse of sample. Samples were sliced into small multiple sized pieces and mounted over a carbon plates covered metal holders. The small pieces of sample were glued at their edges to the carbon plate surface, making sure they are sufficiently fixed at position. Thereafter, gold coated samples were viewed by SEM at 5 kV. The gold coating step was conducted to cover samples with a thin electrically conductive layer. This process will prevent charging of samples (because of static electric field) and thus improve image quality. Multiple images collected for each sample at several magnifications.

Pore size measurements were performed with ImageJ programme to measure the diameter of pores depending on the magnification scale for the selected image (Figure 2-8). Information was collected into Excel sheet; the mean and standard deviation were measured along with the minimum and maximum pore diameter.

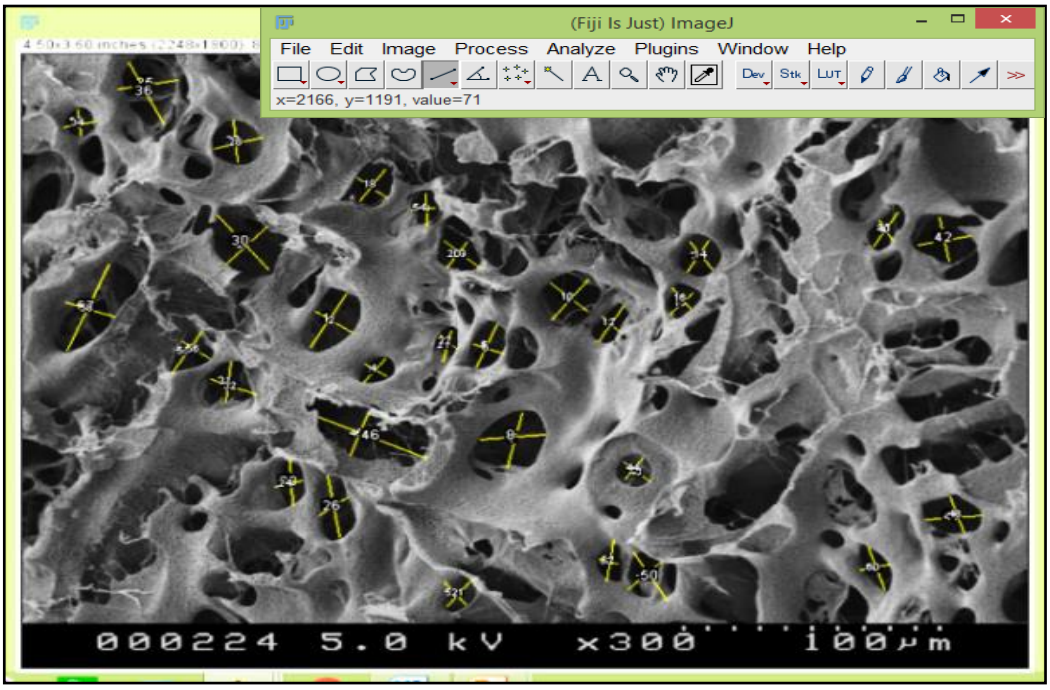

Figure 2-8. Pore characterisation with ImageJ software. *Yellow lines represents multiple measurements of pore diameter.*

2.4.5. Mineral association

To establish the degree of calcium mineralisation associated with hydrogels, a simulated boby fluid solution (SBF) was used as a source for calcium minerals. The solution represents a mixture of certain minerals in specific percentages similar to body fluid composition at pH 7 (Kokubo & Takadama 2006; Kepa et al. 2015).

All hydrogels were cast in 48 well plates and then immersed in SBF solution, incubated at 37 °C, and tested for calcium association at three time points (7, 15, and 21 days). Triplicate hydrogel samples were prepared for each time point. For control purposes a further triplicate set of hydrogels were incubated with phosphate buffered saline (PBS) and tested together with the other hydrogel samples at the specified times representing the control measurements for each sample set.

To further explore hydrogel mineral association, an osteogenic differentiation set supplmemented SBF was used as a further control measure.

2.4.5.1. Alizarin red staining test

Alizarin red solution (1%) was prepared and adjusted to pH 4.2, sealed, and stored at room temperature. Samples were taken out of solution at 7, 15, and 21 days, washed 3 times with d H_2O then incubated with 1 mL alizarin red solution (enough to cover the samples) for 30 minutes at room temperature. Alizarin stain were then removed and samples washed with d H_2O for 24 hours. Water was changed 6-7 times until no more dye was observed in washing solution. Microscopic images were taken using EVOS xl core brightfield microscope.

2.4.5.2. Alizarin red quantification

Alizarin stain was collected from each sample by incubation with 10% w/v cetylpyridenium chloride solution (CPC) in water. Each sample well was topped with 500 µL of CPC solution, sealed with biofilm, and incubated at room temperature overnight on a rotary shaker. The supernatant (200 µL) was collected from each sample and aliquoted into a 96 well culture plate at 200 µL each. A plate reader was used to measure absorption at 562 nm wavelength.

A serial dilution of the original dye stock concentration was prepared with the CPC solution. A standard curve was obtained, and the samples' dye concentrations calculated against the standard values.

2.4.5.3. Calcium assay

A colorimetric calcium assay kit (Sigma) was used to assess the concentration of calcium ions associated with hydrogels. The assay principle is based upon determining the chromogenic complex in solution. This complex is formed by the combination of O-cresolphthalein reagent with calcium ions (Morin 1974). The resultant colour change was detected by measuring the absorbance with microplate reader at 575 nm.

All hydrogel samples were removed from SBF solution (including controls), washed 3 times with d H_2O, and then freeze-dried making them ready for calcium extraction. A 0.5 M diluted HCl solution was used to break the calcium ion bonding to polymer surfaces, releasing calcium into solution. A 24 well plate was used as a base container for the hydrogel samples. Then, samples were incubated for 24 hours in 0.5 mL of HCl extraction solution, sealed with para-film, and placed upon rotary shaker set at medium speed. Next day, the seal was removed, and the solution collected from each sample well. Using a 96 well plate, 50 µL of each collected sample and control solutions were added. Into each of these, 90 µL of chromogen reagent was added to prompt the complex formation. To clearly illustrate the colour differentiation in solution, 60 µL of calcium buffer solution was added with gentle mixing. The whole reaction plates were incubated at room temperature protected from light for 5-10 minutes at room temperature. The absorbance then measured at 575 nm.

2.5. Cell culturing techniques

2.5.1. Choice of cells

A range of cell lines in addition to primary cells were utilized to test the variable aspects of the 3D culture environment.

A bone osteosarcoma cell line (MG63), and immortalised human primary chondrocytes (OK3H) were both utilised to investigate the attachment and viability profile for the cell scaffold system. Primary human osteoblasts (hOBs) and primary human chondrocytes (hCHs) were included to detect the specific osteochondral features of the selected cell scaffold systems.

2.5.2. Choice of media and nourishing culture environment

Dulbecco's Modified Eagle's Medium (DMEM) with 4.5 g/L glucose, and sodium pyruvate, was used in all cell culture experiments. The media was fortified with 10 % foetal bovine serum (FBS), 2% glutamine, and 1% penicillin-streptomycin antibiotic supplements.

Supplementations with osteogenic or chondrogenic promoting factors were considered as well. These were added in specific percentages to media enhancing further osteogenesis by osteoblasts or chondrogenesis markers by chondrocytes.

For osteogenic media preparation, factors to support osteogenic cell activity were added to the previously prepared DMEM media (Table 2-2). The percentage of addition had followed the below recipe. The media mixture was then kept in 50 mL universal tubes and frozen at −20 °C. Agents to promote chondrogenesis were added in the same way to DMEM media following the below recipe (table 2-3). Again, transferred in 50 mL universal tubes and frozen at −20 °C.

Table 2-2. Cell culture medium additives to enhance osteogenic cell behaviour.

Materials	Stock concentration	Final concentration	Volume /100 mL of media
Ascorbic acid	50 mM	0.05 mM	100 µL
Beta glycerophosphate	1000 mM	10 mM	1000 µL
Dexamethasone	0.5 mM	1×10^{-5} mM	20 µL

Table 2-3. Cell culture medium additives to enhance chondrogenic cell behaviour.

Chondrogenic factors	Stock concentration	Final concentration	Volume /100 mL of media
Insulin-Transferrin-Selenium-Ethanolamine (ITS)		1% v/v	1000 µL
Dexamethasone	0.5 mM	0.1 µM	20 µL
Ascorbic acid	50 mM	50 µM	100 µL
L-proline	40 mg/mL	40 µg/mL	100 µL
TGF-Beta 3	10 ng/µL	10 ng/mL	20 µL

2.5.3. MG63 and OK3H cell lines culture

The cell lines were selected to perform initial explorations of the suitability of the hydrogel 3D culture environment for cellular attachment and viability.

Frozen cryotubes of cells, each with 10^6 cells /mL were taken out of liquid nitrogen storage. The cells were brought to 37 °C by immersing in a water bath at 37 °C and once thawed quickly mixed with 10 mL DMEM media. The mixture was then centrifuged at 1400 rpm for 4-5 minutes. The supernatant was removed carefully, and a fresh 5 mL media added. The precipitated cell mass was then re-dispersed by gently pipetting up and down. Cell culture flask (T25) size were prepared and topped with 7 mL media. The cell suspension (500 µL) was added to each flask and then stored in 37 °C 5% CO_2 incubator. Media was changed after 24 hours and then every 3-4 days.

2.5.4. Primary human cells culture

Primary human osteoblasts and primary human chondrocytes were obtained commercially from Promo Cell®. The supplier protocol for culturing was followed for both types of cells (supplied by Promo Cell®).

A T25 flask was topped with 10 mL of media and warmed by incubating at 37 °C for 30 minutes. The cells were first removed from liquid nitrogen storage and defrosted in a 37 °C water bath for not more than 2 minutes. The tubes were immediately moved to the flow hood, sprayed extensively with 70% IMS, dried with tissues, before being added to the previously prepared T25 flask, then incubated at 37 °C, 5% CO_2 (Promo Cell 2016).

Media was changed after 24 hours and then every 3-4 days. Once get confluent the cells were passage into a T75 flask.

2.5.5. Cell passaging and trypsinization

At 80-90% confluence cells were dissociated from flasks by trypsinization. The media was first removed, and the cells washed with PBS solution for 10 seconds. The PBS wash solution was aspirated, and the cells incubated with 10 % trypsin solution in PBS for 5 minutes at 37 °C (primary cells were incubated at room temperature). The volume of trypsin solution was measured at 1 mL for T25 flasks and 3 mL for T75 flasks.

After incubation, cells were detached from the surface and the action of trypsin was terminated by adding 5-7 mL medium. The whole mixture was transferred into a 50 mL universal tube and centrifuged for 5 minutes at 1200 rpm. The supernatant was carefully aspirated, the cell pellet then topped with 5 mL medium and cells re-dispersed by gently pipetting up and down until cell suspension is produced. The cells are now ready for further passage or sample seeding.

2.5.6. Haemocytometer Cell counting technique

After trypsinization of cells and obtaining cell suspension, cell counting was performed using normal haemocytometer technique (Figure 2-9). Equal volumes of cell suspension and trypan blue reagent were mixed in an eppendroff tube, then 10 µL of this mixture was used to fill the haemocytometer chambers already covered with coverslip. The haemocytometer slide was then observed under light microscope and the shiny blue stained cells were counted at the four sides of the rectangular indentations grid.

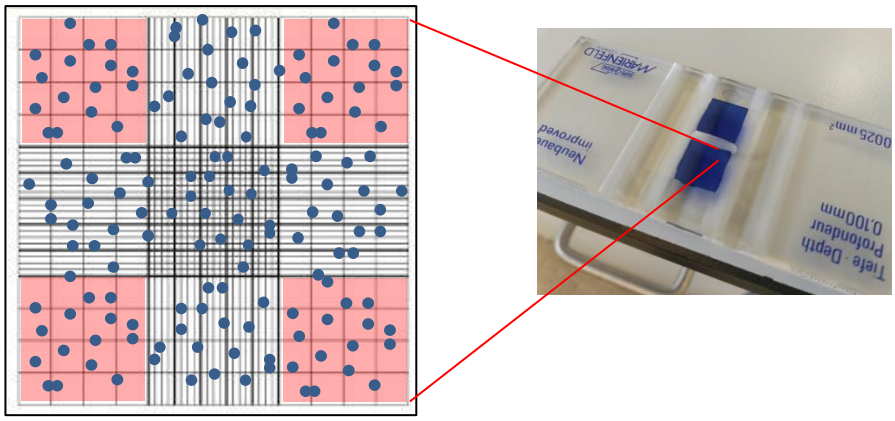

Figure 2-9. Haemocytometer cell counting. *A) Haemocytometer slide with cell suspension-trypan blue reagent mixture inserted underneath a coverslip, B) a magnified illustration of grid pattern where cells are counted in the red marked grid regions.*

2.5.7. Cell culture on 3D hydrogels

2.5.7.1. Preparation of samples for cell culture

Hydrogels samples were washed with PBS for 48 hours at 37 °C to remove any monomeric and chemical residues. The PBS solution was changed every 4-8 hours. A sterilisation process was followed by immersing the hydrogels in 99% ethanol solution for 20-30 minutes. Samples were then washed again with sterile PBS for 24 hours at 37 °C. A final washing step was performed by soaking the samples in media for 1-2 hours before seeding hydrogels with cells.

2.5.7.2. Hydrogels cell culturing

After trypsinizing cells from the flask into cell suspension and performing cell count, as mentioned in sections 2.5.5 and 2.5.6; cells were seeded on the top of the hydrogels at 10 µL volume of cell suspension counted at a concentration of 10^4 cells /sample (Figure 2-10). Samples were then incubated at 37 °C for 1-2 hours, to enable cell attachment and then topped with 500 µL medium per each well. Cell on tissue culture plastic surfaces were included as comparative samples. Cells were seeded at the same rate in a 24 well plate, incubated for 1 hour at 37 °C, and topped with 500 µL medium. Samples were prepared in triplicate for both the basic medium and the osteogenic/chondrogenic medium samples. Storage conditions were

set at 37 °C 5% CO_2, media was changed every 5 days. The same procedures were followed for both cell lines and the primary human cells.

2.5.7.3. Composite pNIPAM/pNTBAM gradient scaffold culture

The same procedure for trypsinization of cells and cell count was performed (sections 2.5.5 and 2.5.6). Scaffolds were washed and sterilized as mentioned in section 2.5.7.1., the only difference with composite scaffold is that the scaffolds were sliced vertically into 2 halves before performing the wash and sterilization step. In this case, the cell culture was conducted by applying 10 µL of cell suspension to the middle of the scaffold cross section with cell density counted at 10^4 cells/sample (Figure 2-10). Thereafter, the cell cultured scaffold's cross sections were incubated at 37 °C 5% CO_2 for 1-2 hours in a 24 well culture plate to enable adhesion and cell attachment at position. Then, each sample well was topped with 500 µL of media. Samples were prepared in triplicate for both the basic medium and the osteogenic/chondrogenic medium samples. Storage conditions were set at 37 °C 5% CO_2, media was changed every 5 days.

2.5.7.4. BG embedded samples culturing

Following BG samples preparation (section 2.3.1), samples were ejected from moulds then washed and sterilized as mentioned in section 2.5.7.1. cell seeding procedure was followed as per individual sample seeding i.e. to the top of hydrogels. Gradients scaffold composites with BG fibres were seeded according to the same protocol followed for the non-BG composites i.e. on the middle of cross sectioned samples. The volume of cell suspension and seeding density was set to be the same as per the previous samples (10^5 cells/sample). The same protocol was then followed to allow cell attachment and then topping plates with media as mentioned in the previous sections (2.5.7.2. and 2.5.7.3).

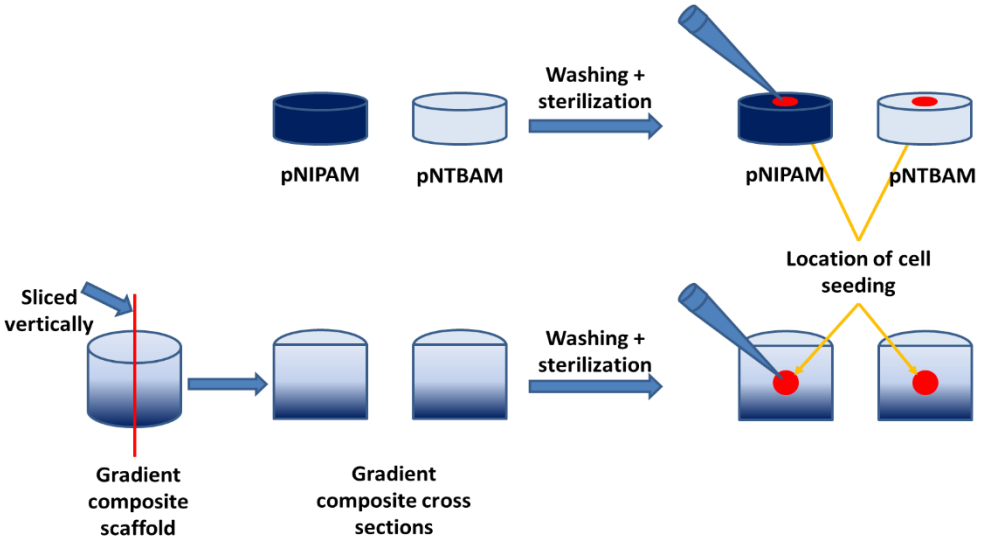

Figure 2-10 Schematic representation of 3D scaffolds cell culturing, *showing the location of cell seeding to the top of individual hydrogel samples and to the middle of gradients composites cross sections.*

2.6. Cell adhesion and attachment

2.6.1. Fixation of 3D hydrogel samples

In the current work, 10% paraformaldehyde in PBS was used to obtain fixed cells on hydrogel samples. Paraformaldehyde has widely been used for tissue samples fixation as it is easily handled and produce accurate results. It preserves cells and tissues architecture by terminating enzymatic reactions normally occurred in biological systems thus preventing its lysis. It principally acts by cross-linking proteins and biological molecules thus fixing them in position and preserving their original shape figure (Thavarajah et al. 2012). This will help in preparing samples and tissue sections for microscopic observations or immunohistochemical assessment.

Media was first removed from sample wells, then samples washed 3 times with PBS. Then, samples were incubated in 10% paraformaldehyde in PBS solution (enough amount to cover the hydrogel sample which is about 1 mL) for 30 minutes at room temperature. Thereafter, the fixing solution is removed, and samples washed again 3 times with PBS.

2.6.2. Histology staining by Haematoxylin and Eosin

Evidence for cells adhesion was investigated after 7 days. Media was removed from well and hydrogel samples washed 2-3 times with PBS. Samples were then fixed with 10% paraformaldehyde solution in PBS (mentioned in section 3.6.1.). For hydrogel samples each washing step was performed over 2-3 minutes to ensure adequate washing was performed.

Hydrogel samples were first washed with haematoxylin stain for 2-3 minutes, the stain was then removed, and the hydrogels washed 3 times with PBS. Thereafter, samples were washed with eosin stain 2-3 minutes, followed by removal of dye and 3 times washing steps with PBS. Hydrogels were then observed under bright light microscope.

2.6.3. Confocal microscopy

2.6.3.1. Actin filaments and nuclear staining

To review the attachment pattern of cells on hydrogels cytoskeletal actin filament and nuclear staining were performed using CytoPainter phalloidin-iFlour 555 and DAPI staining reagents.

Samples were fixed as mentioned in section 2.6.1; samples were then incubated with 1:500 phalloidin solution in PBS for 20 minutes at room temperature while protected from light. The stain was then removed, and samples washed 3 times with PBS. Incubation with 1:1000 DAPI stain in PBS was followed for 30 minutes at room temperature while protected from light. Washing with PBS was then performed 3 times before samples were viewed by Olympus U-TBI90 laser fluorescent confocal microscope.

2.6.3.2. Cells migration within scaffold construct and BG fibres channels

The impact of the hydrogel porous architecture on cell behaviours was investigated by locating the DAPI stained nuclei through scaffold thickness. Cell migration tracking was then performed after 21 days culture. Sample fixation and DAPI staining was followed as in steps 2.6.1 and 2.6.2.1. Samples were then scanned by confocal microscope through their thickness by Z stack function. The 3D image scanning was acquired with a 2 µm step size reaching a

maximum of 150 slices of sample down from the top layer. The scanned distance for each sample was set to a maximum of 300 μm starting from the surface.

Scanned files were processed via Image J software to detect DAPI. The location was determined by generating a graph curve illustrating intensity versus distance.

BG imbedded hydrogel samples were investigated as well to detect any cell infiltration within the channels left by degraded BG fibres. The same protocol for sample fixation and DAPI staining was followed as for previous samples. This was followed by confocal microscope sectioning (options chosen as before) through hydrogel thickness with only focusing this time on the BG fibres location. A 3D images were created and observed for cells location and behaviour per BG fibre opening.

2.7. Viability and cell survival

Testing the ability of cells to survive on hydrogels and the impact of cell-scaffold system on the viability of cells was carried with the live/dead® cytotoxicity/viability kit (Thermo Fisher scientific). The major components of the assay kit are calcein AM and ethidium homodimer-1 reagents. Calcein AM identifies the presence of live cells by detecting intracellular esterase activity and cell membrane integrity. This is carried out by enzymatic conversion of the calcein AM into the green fluorescent calcein. Ethidium homodimer-1 is a red fluorescent dye which binds to nucleic acids of the membrane damaged cells and produces an intense red fluorescence indicating the presence of dead cells. A live/dead staining solution was prepared by mixing both reagents with PBS at the following rates; 1:200 of calcein AM and 1:50 of ethidium homodimer-1 in PBS.

The assay procedure involved staining for a non-fixed hydrogel sample. Medium was removed from sample wells, samples washed with PBS 2-3 times, and then incubated with the live/dead staining solution for 30 minutes at room temperature while protected from light. The stain solution was then aspirated, and samples washed 2-3 times with PBS. Hydrogels were

observed for green versus red fluorescence as indicators for live/dead cells by confocal microscopy.

The percentage of viable cells was identified by calculating the number of live and dead cells per specific region of each sample (Figure 2-11). The number of live cells (green) and dead cells (red) were counted over a 1 mm^2 area for a maximum of 5 regions of a captured x4 microscopic images obtained for individual samples and the average was taken. The whole process was carried out using the cell counting tool of Image J software.

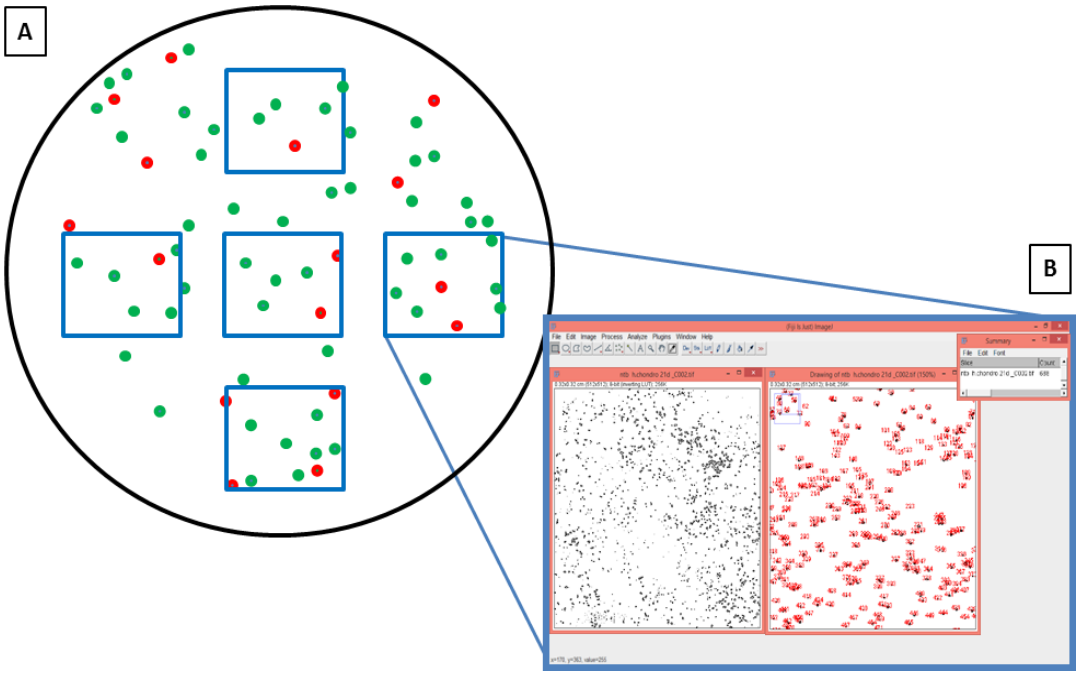

Figure 2-11. Schematic representation of live/dead stained hydrogel sample seeded wih cells. *A) cell counting live/dead methodology per captured x4 images (around 3 mm^2) of confocal microscope, with an illustration of the chosen regions per sample, B) counting the number of cells on each captured image using Image J software.*

2.8. Detecting osteogenic and chondrogenic activities of cells on hydrogels

2.8.1. Osteogenic cell behaviour

Cells had been tracked for 7, 15, and 21 days to record their further osteogenic activities. An osteogenic and control media were utilised, and samples collected in triplicate from each condition.

2.8.1.1. Alizarin red staining

Alizarin red pigment is used to identify calcium minerals in tissue or cell culture sample. A chelation process produces an alizarin red s-calcium complex indicating evidence of calcium minerals association via red colouration (Virtanen & Isotupa 1980).

A 1% alizarin red solution was prepared in the lab at room temperature. This was performed by dissolving 1g of alizarin red S powder in 100 mL of dH_2O and adjusting the pH to 4.2. The solution was then filtered through a 0.2 µm filter, sealed and stored at room temperature.

Samples were removed from medium and fixed with 10% formaldehyde (mentioned in section 2.6.1). In a 24 well culture plate, enough volume of alizarin red dye solution was poured per sample well, ensuring that each sample was adequately covered (1 mL per each). Samples were left on a rotary shaker for 30 minutes at room temperature. The dye was then removed and samples washed with dH_2O for 24 hours with water being changed 5-6 times. Washing was repeated until no significant dye was apparent in water. A final PBS wash step was carried out for 15 minutes at room temperature to remove any nonsignificant staining. Samples were observed under bright-field microscope and images collected.

2.8.1.2. Quantification of Calcium ions

Calcium mineral quantification was performed through a colorimetric calcium assay kit procedure. It provides a quantitative measure for calcium locally associated with each hydrogel sample (details of the assay were mentioned in sections 2.4.5.3).

Samples were taken out of media in a 24 well culture plate and fixed with 10% formaldehyde for 30 minutes at room temperature. This was followed by washing 3 times with d H_2O, and the same procedure was applied as in section 2.4.5.3 for calcium assay.

2.8.1.3. Alkaline phosphatase (ALP) activity

To determine the cells potential for mineral deposition in their surrounding matrix, ALP activity was measured in each sample medium. This is a potential indicator that the cell,

weather osteoblast or chondrocyte, is being engaged or promoted for such an action by producing higher levels of this enzyme (Gillette & Nielsen-Preiss 2004; Kirsch et al. 2000).

The test was performed using ALP colorimetric assay kit (Abcam). The assay principle depends on the reaction between the substrate materials, p-nitrophenyl phosphate (*p*NPP), with ALP enzyme in the sample. The reaction results in the production of the yellow coloured p-nitrophenyl (*p*NP) as the ALP hydrolyse the phosphate ester and releases an organic phosphate.

The assay was performed according to the protocol instructions supplied with the product. Medium was collected from hydrogel samples (in triplicate) at days 1, 7, 14, and 21 in eppendorff tubes and frozen at −80 °C. The assay was performed at room temperature, although the reagents were all kept on ice during the test. A 96 well culture plate was used to host the assay reactions. An 80 µL volume of each sample was supplemented with 50 µL substrate reagent of *p*NPP. Another triplicate of samples was prepared by mixing with 20 µL stop solution before being supplemented with *p*NPP substrate reagent, these will represent the sample control set. A standard solution was prepared by diluting *p*NPP substrate solution into aliquots of serial dilutions which were added to the same 96 well culture plate in triplicate at 120 µL /well. An ALP enzyme, supplied with the kit, was reconstituted with 1 mL assay buffer and 10 µL added to each standard well and mixed by pipetting up and down. The plate was then gently shaken and incubated at room temperature for 60 minutes in the dark. A 20 µL stop solution was added to the samples and standard wells after which the absorbance was immediately measured at 405 nm.

2.8.2. Chondrogenic cell behaviour

The primary hCHs were used to reflect the extent of chondrogenic cell activity upon hydrogel culture. The same tracking time points were followed as for osteoblasts which are 7, 15, and 21 days. Basic medium as well as a chondrogenic medium were used for cell culturing, making two equal sets of samples.

2.8.2.1. Alcian blue staining

This test was conducted to detect mucopolysaccharides and glycoproteins (sulphated and non-sulphated). The presence of these is a possible indication of active chondrogenic matrix formation.

A 1% stain solution was prepared by dissolving 0.5 g of alcian blue 8GX (sigma) powder in 50 mL of 3% acetic acid solution at room temperature. The pH was adjusted at 1.5. In a 24 well culture plate, samples were covered with 1 mL alcian blue stain. Samples were sealed, and incubated for 24 hours at room temperature upon a rotary shaker. Thereafter, the stain solution was aspirated from sample wells and samples washed with dH_2O for 24 hours. The washing solution was changed 5-6 times to ensure adequate elimination of non-significant dye out of hydrogel mass. Microscopic observation and imaging of samples was carried out via dissection and bright field microscopes at different magnifications.

2.8.2.2. Dimethylmethylene blue (DMMB) assay

Dimethylmethylene blue is an active colorimetric reagent that reacts with sulphated glycosaminoglycans (GAGs) forming a major component of cartilage matrix. The reaction is sensitive and leads to a change in spectral absorption of the reagent at 525 nm wavelength (Farndale et al. 1986).

Working solution was prepared by mixing 0.008 g DMMB reagent, 1.52 g glycine, and 1.185 g sodium chloride with 500 mL d H_2O. DMMB powder is not easily dissolved in water; as a result, it was solubilized first with 2 mL absolute ethanol before mixing. The whole mixture was covered with aluminium foil and stirred for 3-4 hours at room temperature. The pH of solution was adjusted to 3 with 1M HCl, and then stored in a glass bottle at room temperature protected from light. Chondroitin sulphate was used as a standard solution to identify sulphated GAGs associated with samples. It was prepared by dissolving 2.5 mg chondroitin sulphate in 50 mL d H_2O at room temperature. A serial dilution was then prepared from the stock solution to reflect the standard readings.

The assay procedure involves the use of non-fixed samples by first removing them from culture media and washing 3 times with PBS. Samples were freeze dried and then, in a 24 well culture plate, smashed into small pieces with scalpels. Each sample was then digested with 500 µL papain digestion buffer, sealed with biofilm and incubated at 60 °C overnight. The volume of the lysate buffer was decided depending on sample size. As the hydrogel samples composed from a 5 mm thickness and 1 cm width, even after being crushed, the minimum amount required to cover the sample was 500 µL. In a 96 well culture plate, sample lysates and standards (both in triplicate) were added at 50 µL each. Using a multichannel pipette, a 250 µL of DMMB working solution was then added and the absorption immediately taken using Synergy II BioTek plate reader plate reader at 525 nm.

2.8.3. Matrix proteins identification

To identify specific proteins associated with bone and cartilage matrices, collagen types (I, II, and X), and annexin A2 had been chosen as reflective measure to indicate cells functionality. Hydrogel samples were checked for possible protein expressions after 21 days of culturing.

2.8.3.1. Immunostaining

Primary antibodies for collagens type I, II, and X were used to detect sample proteins association. These were visualised with secondary antibodies labelled with red (TRITC) or green (FITC) fluorescent dye. The whole kit was purchased from Abcam.

Hydrogel samples were fixed with 10% formaldehyde at room temperature (mentioned in section 2.6.1). Samples were blocked with 5% bovine serum albumin (BSA) in PBS for 2-3 hours at 4°C. This was followed by sample incubation with primary antibody solution overnight at 4 °C. The primary solution was prepared by mixing primary antibody (directed to type I, II, or X collagens) with 5% BSA in PBS at a 1:200 ratio.

The primary solution was then aspirated and samples washed four times with a 1% BSA in PBS solution. Each wash was 5-10 minutes to ensure adequate removal of the primary solution residues. Next, samples were incubated with secondary antibody (FITC or TRITC) in 5% BSA

in PBS solution at 1:200 ratio. Samples were incubated at 4 °C for 4 hours in the dark. Then, samples were thoroughly washed with 1% BSA in PBS 5-6 times (5-10 minutes each), followed by 2 times washing with PBS.

Nuclear staining was performed by incubating samples with DAPI stain for 30 minutes at room temperature, then washing 3 times with PBS. Hydrogels were observed under a confocal microscope to locate any fluorescent indication of protein expression.

2.8.3.2. Sandwich enzyme-linked immunosorbent assay (ELISA) quantification

Sandwich ELISA efficiently detects specific antigens between two layers of antibodies, capture antibodies and detection antibodies (Osmekhina et al. 2010). Experimental samples were tested for the collagens I and II, as well as for annexin A2. The assayed markers should indicate the way the cells are reacting to their 3D environment and weather they are in line with their function. Annexin A2, however, should reflect the cells response in laying out minerals to the surrounding matrix.

Samples were washed 3 times with PBS before freeze drying and digesting with papain digestion buffer overnight. Samples lysates were then collected in eppendorf tubes and frozen at −80 °C for later detection.

All samples lysates were assessed for total protein content using Bicinchoninic acid protein assay (sigma). The assay principle depends on the reduction process of cupric ions to cuprous which will be parallel to the amount of protein present in sample. A 7.5% bovine serum albumin solution was used as a standard to verify the total protein amounts of samples. According to results, samples were normalised to the lowest protein content by diluting with the original digestion buffer previously used for samples.

The assay procedure was carried out at room temperature. Nunc® immunoassay 96 microplates were used to hold ELISA assay reactions. All the assay kits were supplied by R&D systems. Assay procedure was followed according to the protocol provided with each kit.

Assay reagents were all brought to room temperature before starting the test, these included anti-human (capture and detective) antibodies for human collagen (I and II), or human total annexin A2. Other reagents included streptavidin conjugated to horseradish peroxidase and standard solution. All reagents were diluted to the working concentration using the intended diluent recommended by the assay protocol. A 1% BSA in PBS was used as a blocking buffer, whereas 0.05% Tween® 20 in PBS was used as a washing buffer to carry out washing after each assay step. A substrate material of 2,2′-azino-bis(3-ethylbenzothiazoline-6-sulfonic acid) (supplied by Sigma) was used to complete the reaction series for the final identification step.

The general assay procedure involved coating microplate wells with 100 µL /well of capture antibody solution. The plates were sealed with biofilm and incubated at room temperature overnight. Then the capture antibody solution was removed, and the plates were washed 3 times with 400 µL/well of wash buffer. This was followed by blocking plates with 300 µL/well of blocking buffer for 2 hours at room temperature. The same washing steps were followed using the washing buffer, and then samples and standards were applied at 100 µL/well in diluent buffer. The plates were sealed with biofilm and incubated at room temperature for 2 hours. Plates were then washed again as before, and detection antibodies added after being diluted to the intended concentration at 100 µL /well and again sealed and incubated at room temperature for 2 hours. Following on from washing samples were incubated with streptavidin reagent added at 100 µL /well for 20 minutes at room temperature.

The plates were then washed as mentioned previously, and a final incubation was performed with the substrate reagent at 100 µL /well for 20 minutes at room temperature. Then, a stop solution was added at 50 µL /well and the absorbance was measured immediately with microplate reader to 450 nm wavelength.

The above assay procedure was followed for each marker to be measured including reagents' and samples' dilution buffers in addition to washing buffers. The only difference was annexin

A2 reagents dilution buffers. Annexin A2 assay kit uses a particular dilution buffer for each reagent including samples and standard.

2.9. Data collection and statistics

Characterization of samples were conducted using a triplicate of 4. Other biological assessments including cell attachment, a triplicate of 3 samples were analysed in 3 time points (7, 15, and 21 days). All data were collected and analysed with Microsoft XL 2010 to calculate the mean, standard deviation and resulting graphs. Results obtained were compared using one and two-way ANOVA with Tukey's multiple comparisons test. Statistics were analysed using Origin Pro 8, the level of significance was set at $P \leq 0.05$.

Chapter 3

Osteochondral tissue regeneration materials preparation and characterisation

3.1. Introduction

Osteochondral defects are a serious problem leading to painful and disabling syndromes. They affect a wide range of populations around the world and occur across variable age groups from 20 years and above (Nukavarapu & Dorcemus 2013b; Pape et al. 2010). A number of therapeutic options have been applied drawn from multidisciplinary field, but these mostly result in unsatisfactory outcomes (Swieszkowski et al. 2007; Steadman et al. 1997).

Advances in regenerative medicine and tissue engineering have resulted in substantial progress in finding new approaches for the regeneration of the osteochondral region (Nukavarapu & Dorcemus 2013b). Several biomaterials have been the subject of investigations into cellular responses in regeneration of bone and cartilage (Bichara et al. 2014; Solchaga et al. 2005; Emans et al. 2013). The impact of chemical and physical biomaterial characteristics defines the exact cellular responses helping to identify suitable cell-biomaterial combinations.

The design of osteochondral scaffolds has largely seen combinations of two or three biomaterials and fabrication techniques to create multi-layered scaffolds with variable characteristics including surface chemistry (Chang & Wang 2011), topographical features (Lord et al. 2010) , specific pore size and interconnectivity (Griffon et al. 2006), etc., to promote successful osteochondral regeneration. These results show variable cellular response in terms of attachment, proliferation, and migration for the relevant scaffolds intended for osteochondral tissue regeneration (Tampieri et al. 2008).

In designing an osteochondral scaffold, the choice of biomaterials is an important point for consideration. Biomimetic is an essential aspects depending primarily on the chemical, physical, and mechanical properties of the selected biomaterial and its ability to simulate the natural environment of the intended tissues. (Karageorgiou & Kaplan 2005; Ma 2008). The resultant biomimetic behaviour of these biomaterials ultimately supports the final morphological and physiological outcomes of the intended tissue regeneration including

osteochondral tissues (Williams 2008; Williams 2009). Natural products like collagen could be a perfect choice as it is already present in natural tissues, however there still some issues concerning contamination and evoking of immune response (Patterson et al. 2010). Synthetic products constitute a huge number of materials with encouraging properties and behaviour supportive of cellular proliferation and tissue replacement. Certain polymers, hydrogels, and bio-ceramics have proved effective as ECM substitutes for bone and cartilage tissues repair in which hydroxyapatite, poly(lactic acid) (PLA), and poly lactic-co-glycolic acid (PLGA) polymers have been widely used with good biocompatible and osteo-conductive behaviour (Nukavarapu & Dorcemus 2013b; Fan et al. 2013). The internal architecture and porosity of a specific biomaterial directly affects cellular behaviour in terms of migration and tissue development (Hollister 2005; Miao & Sun 2010). Surface chemistry and topography are widely used as surface characteristics with a major role in determining cellular attachment and further proliferation (Elbert & Hubbell 1996b; Hollister 2005). Together all these factors work in synergy to give a biomaterial its distinctive properties. The above understanding of materials' properties can be utilized to design scaffolds with optimum characteristics for our intended purpose. The production of scaffolds is a complex process which involves certain steps for processing and fabrication of biomaterials to yield the intended scaffold construct (Liu et al. 2007).

N-isopropylacrylamide (NIPAM) and N-tert-butylacrylamide (NTBAM) were selected for the current work in light of the previous reports that indicated their tuneable properties and biomimetic behaviour towards cellular system (Lynch et al. 2005; Barnes et al. 2016; Haq et al. 2017). This is possibly related to their surface charge density and their ability to simulate extracellular matrix environment of tissues (Lynch et al. 2005). Further to that, both polymers are of the acrylamide derivatives with only a slight difference in structure. These criteria might have an impact on certain characteristics of the resultant polymer's construct such as the wettability.

The current chapter investigates materials' differences in terms of chemistry, mechanical strength, and architecture and the outcome criteria relevant to their biological application in cell survival and proliferation.

3.2. Chapter aims

This chapter aims to prepare and characterise synthetic polymeric hydrogels that are close in terms of basic structure. Synthetic polymers including N-isopropylacrylamide (NIPAM) and N-tert-butylacrylamide (NTBAM) were prepared and investigated to address the following objectives.

- Determine the variable chemistry and wettability profile between selected polymers.
- Identify the internal architecture, porosity and the impact of different monomeric concentrations on the overall architecture.
- Calculate compressive strength and hydrogel stiffness.
- Quantify the potential for calcium mineral association.

3.3. Methods

Hydrogels preparation and characterisation procedures were described in detail in sections 2.2 and 2.4 of Chapter 2.

3.3.1. Hydrogel preparation

Hydrogels were prepared via atom transfer radical polymerization utilizing chemical initiator to elicit the process of polymer formation. Hydrogels were cast in a 48 well culture plate giving a uniform cylindrical shape of hydrogels with dimensions of about 10 mm diameter and 5 mm thickness; the process was carried out on the bench at room temperature. Once set, hydrogels were immersed in dH2O, sealed and stored at 4°C (details in section 2.2, Chapter 2).

3.3.2. FTIR spectra

A ThermoScientific IS50 FTIR fitted with a single bounce germanium ATR unit was used to collect hydrogel spectral pattern. A freeze dried-samples were tested to reduce the impact of water noise (details are mentioned in section 2.4.1, Chapter 2).

3.3.3. Wettability and water contact angle

Measurement of water contact angle was performed using a Thetalite OneAttension version 2.4 system. Samples were placed on a glass petri dish and compressed with a coverslip to get a flat surface while being dried at 70 °C in an oven. Water droplets, measured at 1 µL, were slowly placed onto test surfaces. Four measures were collected from each sample out of four samples and the average was taken (details are mentioned in section 2.4.2, Chapter 2).

3.3.4. Investigating internal architecture and porosity

Hydrogel samples were frozen at −20 °C and freeze dried in readiness for SEM imaging. Multiple pieces of sample were mounted over a carbon plate holder and imaged with Hitachi S4500 electron microscope. Three monomeric concentrations for each hydrogel were prepared (0.042 g/mL, 0.058 g/mL, and 0.079 g/mL) to investigate the impact of using lower concentrations on pore size and shape. Captured images were analysed using ImageJ software to calculate the average pore diameter for each polymer structure (section 2.4.4, Chapter 2).

3.3.5. Compressive mechanical strength

To observe hydrogel behaviour under applied compression, samples were tested using BOSE electroforce system. Cylindrical shape hydrogel samples were used with thickness of 4.5-5.0 mm and 9.5-11.5 mm diameter. Data were collected and analysed to obtain the stress/strain curve and Young's modulus (section 2.4.3, Chapter 2).

3.3.6. Mineral association

The ability of polymers to support calcium mineral association to their surfaces was tested by incubating polymers with SBF solution at 37 °C (a solution with mineral composition similar to that of body fluids). The amount of calcium mineral associated with each hydrogel sample

was detected using calcium assay kit (abcam) and alizarin staining test (section 2.4.5, Chapter 2).

3.4. Statistics

All data were collected and analysed with Microsoft XL 2010 to calculate the mean, standard deviation and resulting graphs. Results obtained were compared using one and two-way ANOVA with Tukey's multiple comparisons test. Statistics were analysed using Origin Pro 8, the level of significance was set at $P \leq 0.05$.

3.5. Results

3.5.1. General hydrogels appearance:

Though produced according to the same procedure, pNIPAM and pNTBAM revealed distinct external figures. These were distinguished readily by the different colour and overall texture between them (Figure 3-1 A and B). In general, the pNIPAM hydrogel formed a colourless viscous material which was flexible and soft when handled (Figure 3-1 C). On contrast, pNTBAM fomed a white, rigid, and easy to handle mass, this could be fragmented into pieces using lab tools (Figure 3-1 D).

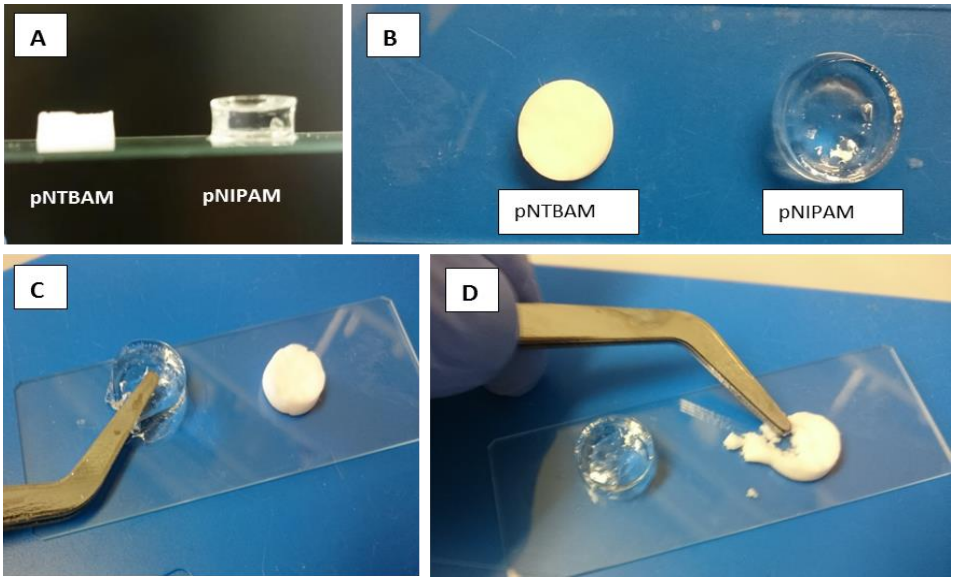

Figure 3-1. pNIPAM and pNTBAM have distinct visual and physical characteristics. *Illustration of general hydrogels outcome figures and their main apparent differences, showing top and side view (A, and B). pNIPAM was more elastic in nature compared to pNTBAM which is stiffer in nature (C and D).*

3.5.2. FTIR spectral assessment

The major chemical variances between the two polymers were identified at the lower energy level of spectral chart. The fingerprint band region at 1200 cm^{-1} displayed distinctive spectral peaks for isopropyl and t-butyl compounds. The rest of the spectra demonstrated the main functional groups at the higher energy level for both polymers' structures (Figure 3-2). A basic identification was for the CH3, NH, and C=O stretch spectral bands, the same groups showed deformation spectral band below 1600 cm^{-1} for both compounds.

Table 3-1. Identifying pNIPAM and pNTBAM FTIR spectral bands components. *An illustrative description of pNIPAM and pNTBAM specific functional groups and their corresponding bands reflected at certain infra-red energy levels showing the relative resemblance between the two polymers.*

Polymers / **Peak maximum**		**pNIPAM /cm^{-1}**	**pNTBAM /cm^{-1}**
CH stretch	Asymmetric	CH_3 2971 CH_2 2929	CH_3 2966 CH_2 2930
	Symmetric	CH_3 2881 CH_2 2854	CH_3 2872 CH_2 2849
CH deformation	Asymmetric	1458	1454
	Symmetric	Split band at 1367 and 1387	Split band at 1364 cm^{-1} and 1362
NH stretch		3286	3317
NH deformation		1594	1539
C=O stretch		1646	1651
Specific band region		Two bands 1131 and 1171, for isopropyl compounds.	One big band 1224, for t-butyl compounds

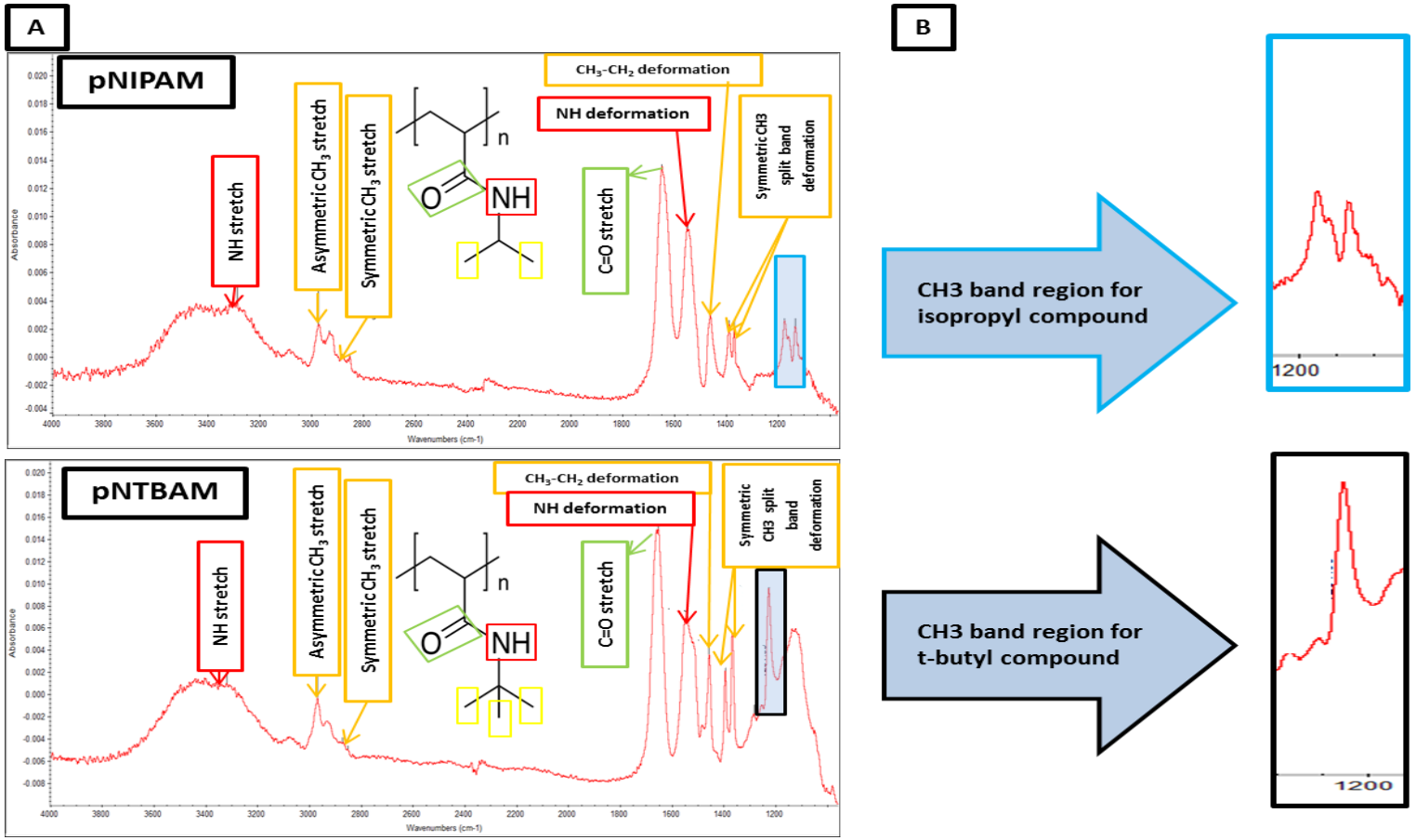

Figure 3-2. FTIR spectra for pNIPAM and pNTBAM polymers. *A) Spectral peaks for pNIPAM and pNTBAM indicating the main functional groups as referred by each polymer chemical structure, B) the major spectral difference band region between the two compounds owing to the aliphatic chain difference (measured using ThermoScientific IS50 FTIR)*

3.5.3. Water contact angle measurements

Data for contact angle were collected reflecting the time and the angle measured since water drop been positioned to surface. The results for both polymers were compared with that obtained from a plastic surface which was considered as baseline. A higher contact angle was recorded for pNTBAM compared to pNIPAM whereas the highest measure was for plastic surface. Results indicated a more hydrophilic behaviour presented by pNIPAM polymer where a significantly higher ($p \leq 0.05$) mean contact angle was measured for pNTBAM compared to pNIPAM contact (Figure 3-3).

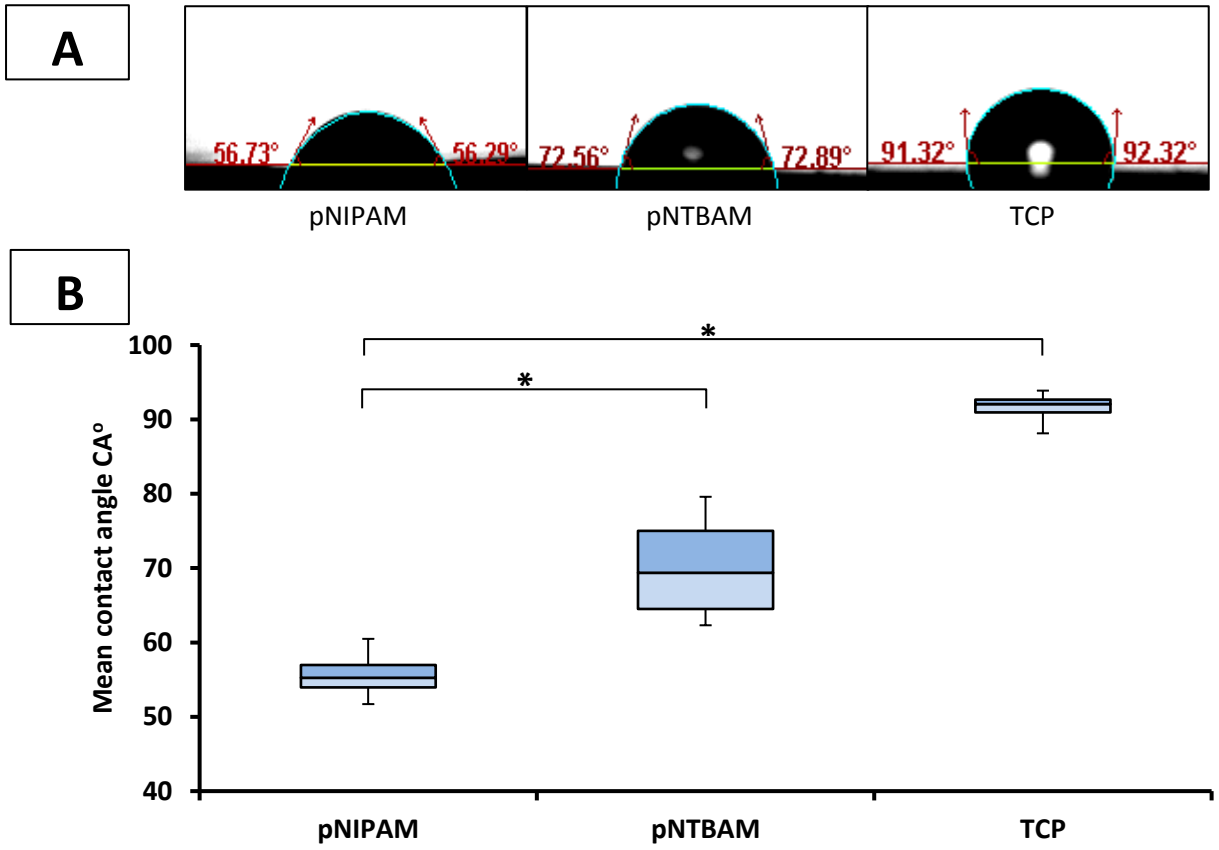

Figure 3-3. Differences between pNIPAM and pNTBAM hydrophilic behaviour compared to plastic surface. *The water contact angle records for pNIPAM and pNTBAM polymers compared to TCP surface demonstrating A) shape of water drop upon contact with tested surfaces with contact angle marked for each (image captured 3 seconds of setting water drop), B) comparison between the mean contact angles for the tested materials illustrated by box plot and means plot showing significant values between pNIPAM and pNTBAM. Asterisks indicate significance at P≤0.05 results correspond to mean± SD, n=4.*

3.5.4. SEM imaging and pore characterisation

According to SEM images, pore diameter measurements revealed pNIPAM as having significantly larger pore size when compared to pNTBAM. Larger pores were identified when using lower monomeric concentration of polymer with the 0.042 g/mL polymer concentration having the largest pore diameter (Figure 3-4). Results indicated significantly increased pore diameter with the lower monomeric polymer concentration for both hydrogels. Captured SEM images revealed internal hydrogel architectural differences. Both hydrogels showed a porous matrix with different pore size and shape according to hydrogel nature (Figure 3-5).

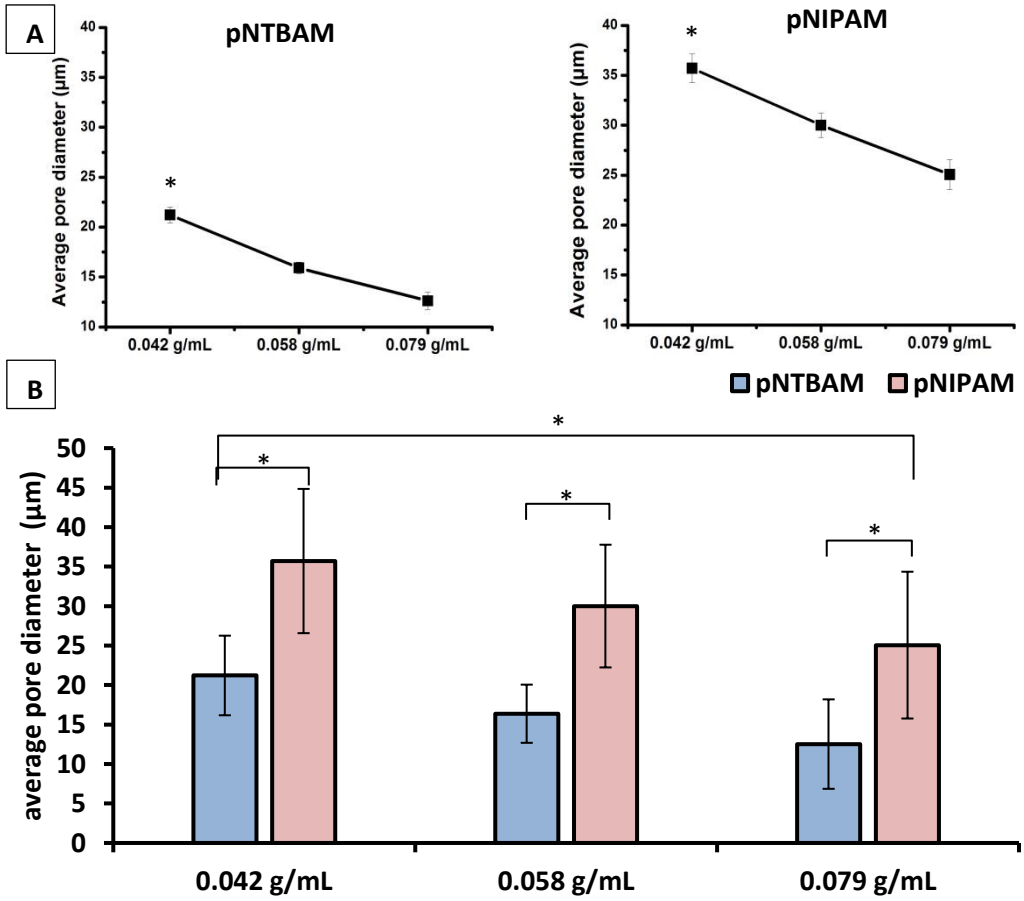

Figure 3-4. Pore size differences between pNIPAM and pNTBAM hydrogels' subgroups. *The figure is illustrating pore diameter in µm showing (A) the impact of reducing monomeric concentration on pore diameter for each hydrogel, (B) comparing pore diameter measurements between the two hydrogels and their subgroups. Measurements were made using ImageJ software. Asterisks indicate significance at P ≤0.05 results corresponds to mean± SD, n=4.*

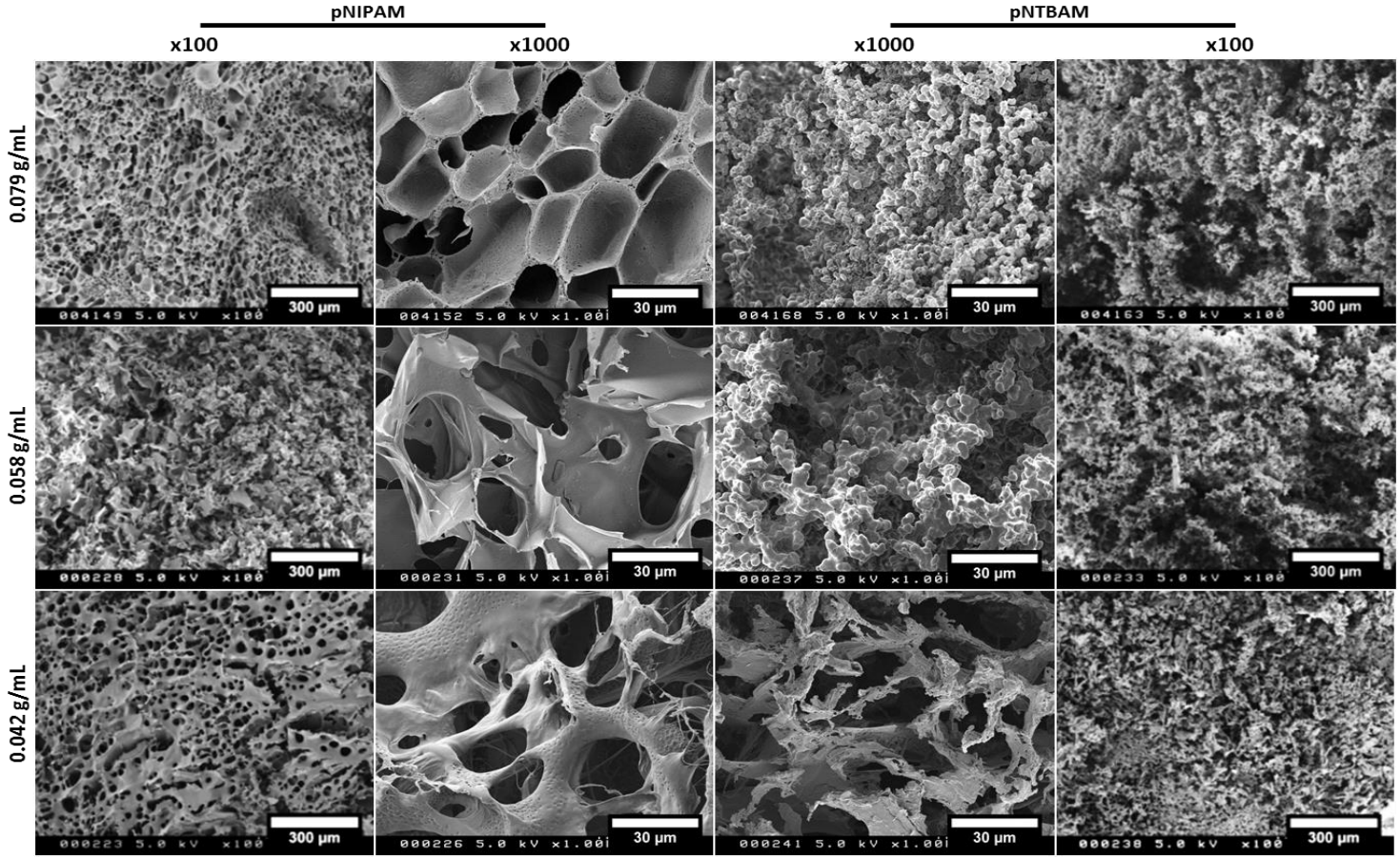

Figure 3-5. SEM imaging of pNIPAM and pNTBAM revealing internal architectural differences between their subgroups. *Images were captured at two magnifications (x100, and x 1000) arranged in columns. Images rows correspond to each hydrogel's different monomeric concentration. Scale bar 300 µm for x100 and 30 µm for the x1000 images.*

3.5.5. Compressive force mechanical strength

Data from compression test, representing the applied force and the compressed distance of sample, was collected. The stress was calculated by dividing the applied force by the sample surface area (which was circular); the strain for a sample was calculated by dividing the compressed distance over the sample thickness. These were then used to obtain the stress/strain curve and Young's modulus which indicated the rate of stiffness of samples.

A more flexible behaviour was noticed for pNIPAM when the sample recovers its normal shape after releasing applied stress unlike pNTBAM which deformed into a flattened mass after compression (Figure 3-6). Results showed each hydrogels' different monomeric subgroups were in the same region when responding to the applied force as shown in the stress vs strain curve with no significant differences observed. However, pNTBAM's higher monomeric group (0.079 g/mL) was significantly stiffer than the others (Figure 3-7 A). Comparing both hydrogel's stiffness indicated significantly higher stiffness for pNTBAM compared with pNIPAM (Figure 3-7 B). pNTBAM resisted force up to 25 N (which was the upper limit for the equipment) whereas a maximum of 12 N for pNIPAM was resisted at the same strain level (90%).

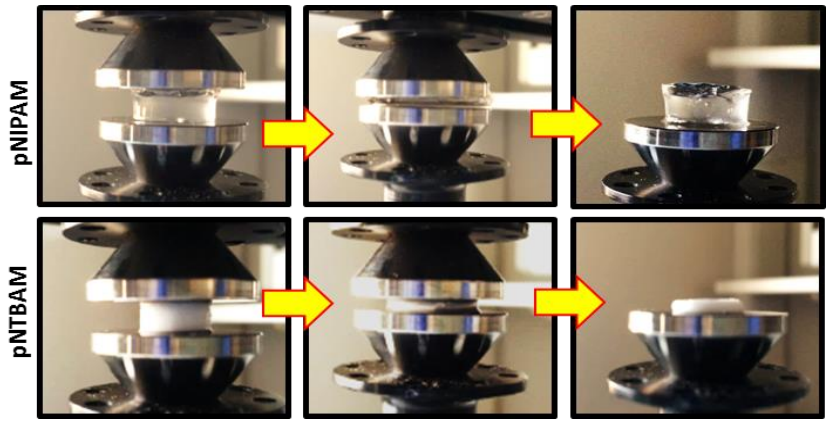

Figure 3-6. Response of pNIPAM and pNTBAM to compressive force was quite different. *Images of samples while doing compression test showing the way each hydrogel respond to compression and how pNIPAM is recovering after applying pressure compared to pNTBAM which turned into a flattened shape. Arrows indicating steps of applying compression (before, during maximum stress, after stress release).*

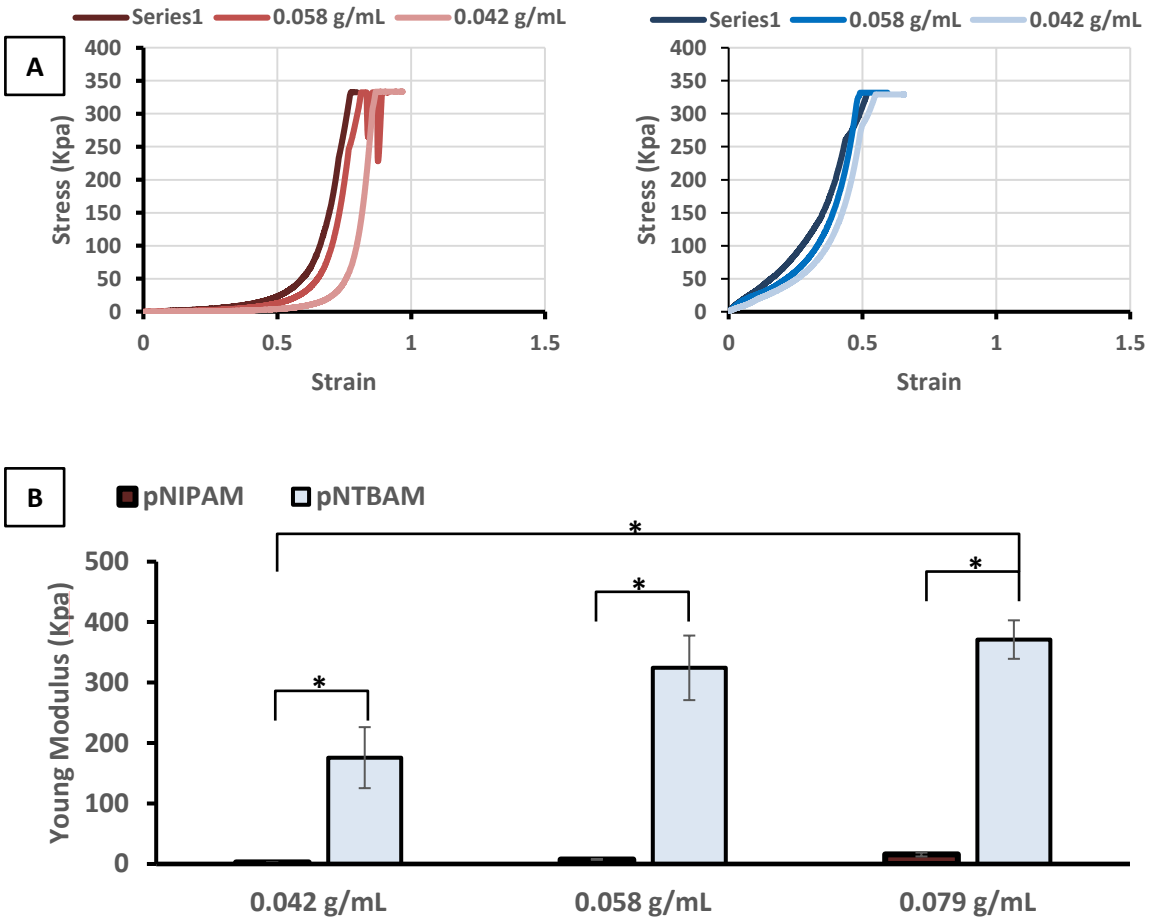

Figure 3-7. Mechanical testing of pNIPAM and pNTBAM hydrogels, *clarifying A) the stress/strain curve for pNIPAM and pNTBAM and their corresponding monomeric concentrations, where the stress is expressed in Pascal (Pa.). (B) Comparing Young's modulus measured in Pa between the two hydrogels, bars are representing each monomeric subgroup. Asterisks indicate significance at P≤0.05 results correspond to mean± SD, n=4 .*

3.5.6. Calcium mineral association

Results from alizarin staining and calcium assays for hydrogels immersed in SBF solution showed a positive association of calcium minerals with tested polymers. Images from alizarin stained samples revealed these results as observed from red stained minerals on hydrogel samples at day 21. These were compared with images from stained controls incubated with PBS solution at 37 °C for 21 days (Figure 3-8). Control hydrogel samples incubated with PBS had shown some background staining which include remnants of redness that still can be observed after complete sample washing. The amount of stain was quantified to differentiate between the positive and negative (control) staining of hydrogels by incubation with 10 %

cetylpyridenium chloride (Chapter 2 section 2.4.5.2). The alizarin stain assessed from each sample had significantly increased after 21 days of incubation with SBF solution at 37 °C including all tested monomeric concentrations. Monitoring levels of alizarin and calcium ions indicated significant increases with time for all monomeric subgroups. Alizarin amounts showed no significant ($P > 0.05$) variations between each hydrogel's sub-groups and all were in-line together. Calcium assay results had shown the same apart from some segregation between levels observed after day 15. These levels indicated no significant ($P > 0.05$) differences between pNTBAM sub-groups. No significant ($P > 0.05$) differences were observed between osteogenic and non-osteogenic stimuli containing set of samples and both were on the same line of development (Figure 3-9).

Significantly, increased alizarin levels were detected when compared with control hydrogel samples incubated with PBS solution at day 21. Both hydrogel control samples showed no significant alizarin staining when incubated with PBS solution between hydrogels and even after 21 days. These results were parallel to those obtained from the calcium assay (Figure 3-10, A and B). Significantly higher levels of alizarin red staining and calcium mineralisation were noted for pNTBAM when compared to pNIPAM, this was applicable to all monomeric sub-groups of pNTBAM. Values compared between monomeric sub-groups for each hydrogel showed no significant variations with alizarin and calcium ions assessment. Significant differences, however, were observed in the amount of calcium minerals between pNIPAM sub-groups, with the higher value obtained for pNIPAM 0.079 g/mL.

The comparison of osteogenic and non-osteogenic stimuli containing samples indicated no significant difference between them or between the two hydrogels, their corresponding concentrations, or between controls. This was noted for both alizarin and calcium ions assessments (Figure 3-10 A and B).

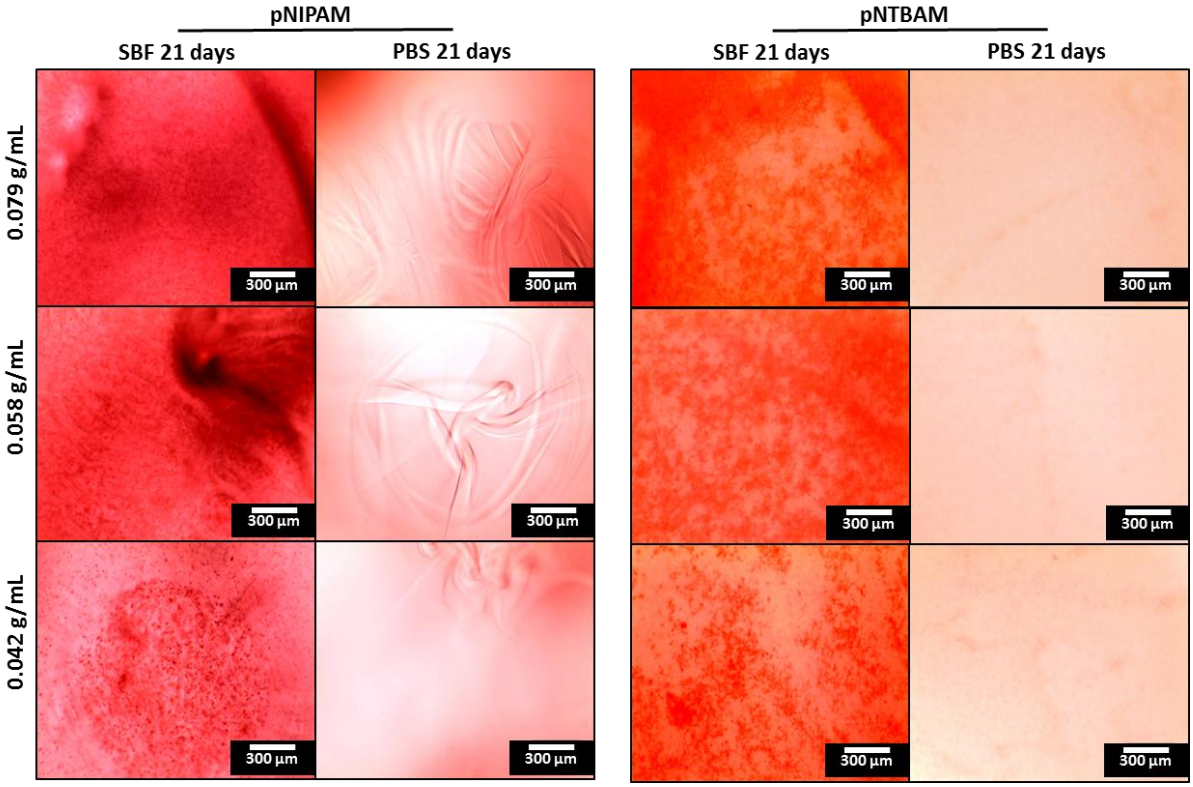

Figure 3-8. Alizarin staining of pNIPAM and pNTBAM hydrogels incubated with SBF at day21. *Images are revealing in columns both hydrogels stained with alizarin red and each compared with its control. Images rows are correspond to each hydrogel monomeric sub-group. Scale bar measure 300 µm.*

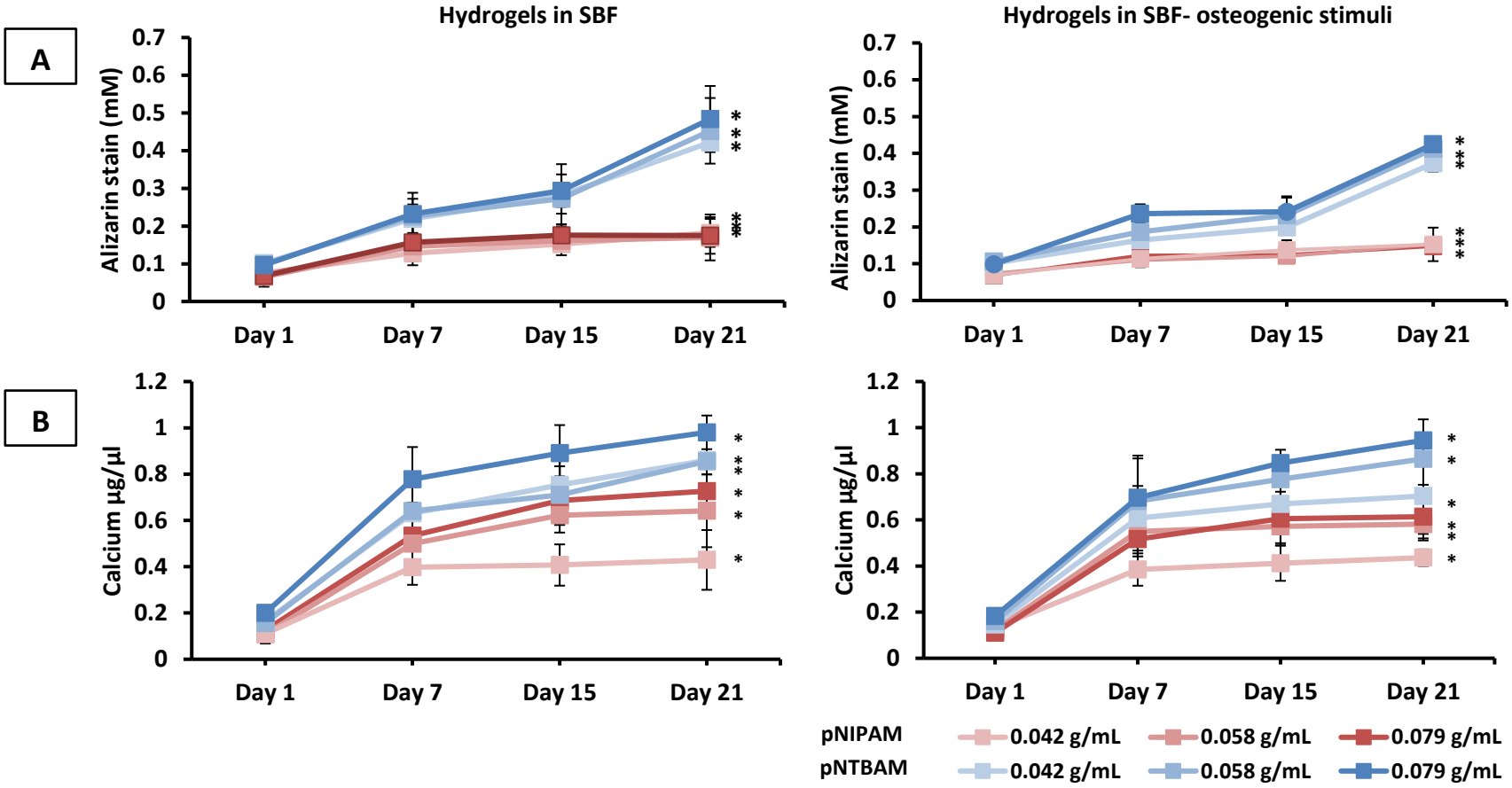

Figure 3-9. Monitoring calcium minerals associated with hydrogels and their monomeric sub-groups. *Figures are illustrating (A) the amount of alizarin stain quantified from each sample in mM, (B) calcium ions assessed upon each sample in µg/µL of sample lysate. Figures columns represent hydrogel samples incubated with SBF solution at 37 °C in two sets with and without osteogenic stimuli. Each figure compares the development of minerals with time up to day 21 for each hydrogel's monomeric sub-groups where the blue markers are for pNTBAM while the red markers for pNIPAM. Asterisks indicate significant level with time at P ≤0.05. Results corresponds to mean± SD, n=3.*

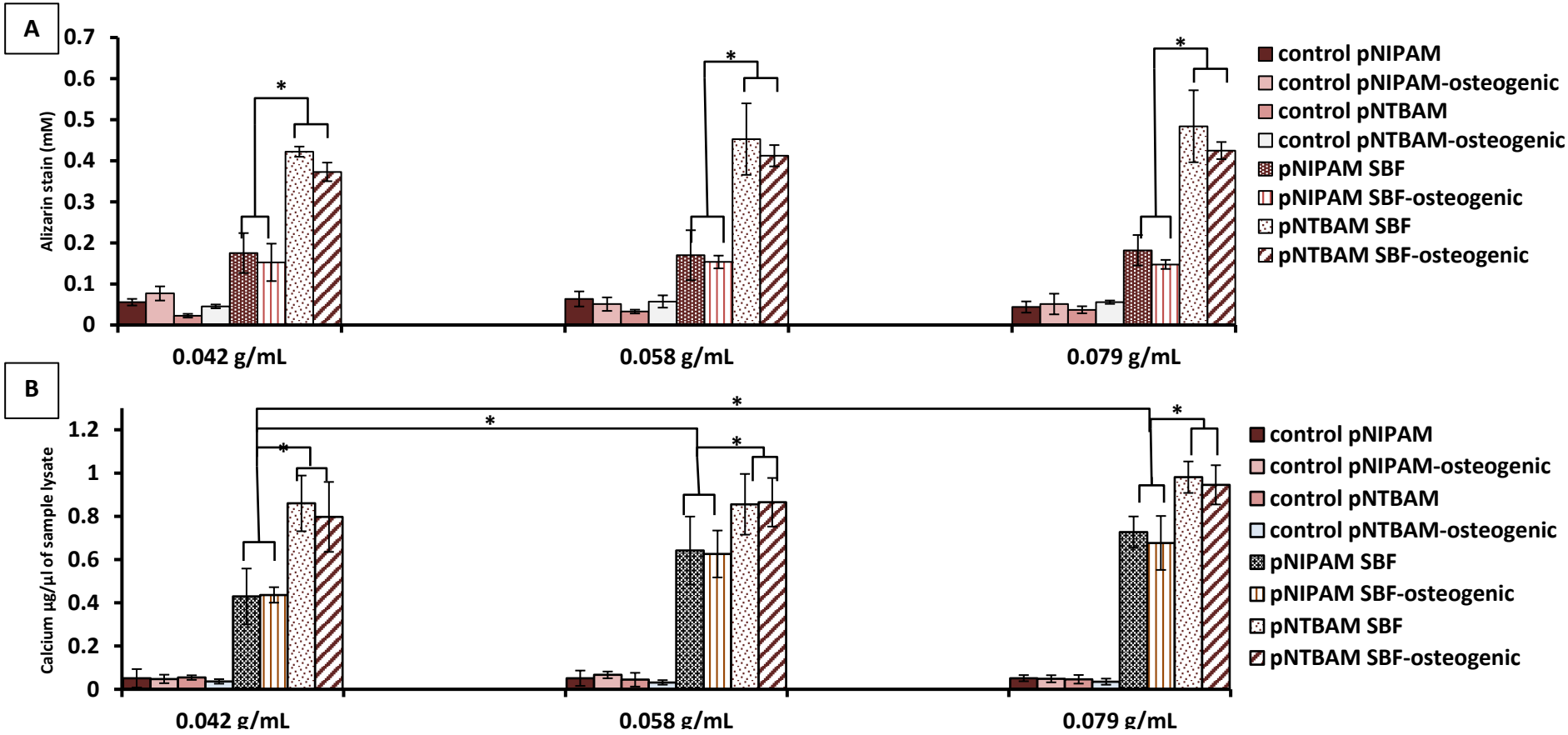

Figure 3-10. Calcium ions and alizarin assessment of hydrogels at day 21., *indicating (A) amount of alizarin stain quantified in mM concentration, (B)calcium ions levels in µg/µL of sample lysate. Each marker levels were compared between hydrogels monomeric sub-groups. Solid fill bars correspond to hydrogels' controls, while patterned fill bars are for pNIPAM and pNTBAM samples incubated with SBF with and without osteogenic stimuli.. Asterisks indicate significant level with time at P ≤0.05. Results corresponds to mean ±SD, n=3.*

3.6. Discussion

Biomaterials science offers a profound range of materials with specific characteristics to serve the target of regenerating old or damaged tissues (Mano 2015; Hutmacher 2001; Jones 2013; Kurtz & Devine 2007). Quite a lot of features may decide the choice of materials which include, in addition to the intended tissue type, plenty of physicochemical and biological factors that directly impact cell-materials interaction (H G Craighead et al. 2001; Patterson et al. 2010; Grover et al. 2006; Jones 2015). For the current work, the choice of materials relied on previous studies that indicated pNIPAM and pNTBAM as non-toxic biocompatible materials (Akiyama & Okano 2015; Muramatsu K Wada T, Hirai H, Miyawaki F 2012; Lynch et al. 2005). Proceeding forward, current results from FTIR and water contact angle confirms the main difference between these materials in chemistry and wettability. And as revealed by FTIR both polymers expressing the same functional groups mainly –NH, =O, and CH.

The active functional groups presented by pNIPAM and pNTBAM hydrogels, as indicated by the FTIR spectral measurements, may reflect some of the materials behaviours when they come in contact with cells (Figure 3-2). The presence of C=O and NH- functional groups allow for a more hydrophilic behaviour of the polymer surface which may promote active osteoblast differentiation and activity (Chang & Wang 2011; Keselowsky et al. 2003). It has been shown that more hydrophilic behaviour is connected to increased cellular adhesion and proliferation (Thevenot et al. 2008). Some hydrophobic behaviour may be related to the presence of CH_3- groups (Chang & Wang 2011), and as more CH_3- groups are being presented by pNTBAM this may explain the slight hydrophobic behaviour of this polymer compared to pNIPAM. The water contact angle measurements may indicate such behaviour for both hydrogels where a larger water angle has been measured with pNTBAM (about 70^o) compared to pNIPAM (about 50^o), i.e. as expected from the chemical structure pNTBAM presents a more hydrophobic surface (Figure 3-3). These results were in accordance with other studies that stated the hydrophobic behaviour of pNTBAM versus hydrophilic for pNIPAM

Wettability of surfaces can be judged according to specific variables such as surface roughness and porosity in addition to the chemical nature of the material (Shirtcliffe et al. 2005; Lee 2013). For the current study, the lower water contact angle obtained may be due to the porosity of the selected polymers. Such features will enable water entrapments from the surface into the pores, and because the pore diameter for pNIPAM was measured to be higher than that of pNTBAM (Figures 3-4), water will imbibe within these pores more rapidly in pNIPAM resulting in a lower contact angle measurement. This figure may explain the impact of porosity and surface roughness on determining the water contact angle and the wettability of such surfaces (Roach et al. 2010; Lu et al. 2011). Therefore, the wettability of the hydrogels in the current study was a function of their porous structure in addition to their hydrophilic-hydrophobic active functional groups.

Both hydrogels were produced according to thermally induced phase-separation technique which is widely used for the production of porous polymer scaffolds (Hutmacher 2001). The hydrgels are formed when the polymer solution thermodynamically separates into polymer-rich and polymer-poor phases. The water droplets are entrapped within the crosslinked polymer network and are responsible for the micro-or macrostructure of the resultant hydrogels, specific variables may control the pore size limit according to this technique including the monomer concentration of the polymer and the solvent mixture used (Nam & Park 1999). According to the current results, reducing the monomeric concentration of polymers did indicate a significantly increased pore diameter for both hydrogels. It was manifested as well, from SEM images, that variable internal figures were generated by changing the intended polymer concentration. This technique has shown its eligibility for controlling internal hydrogel microstructure and interconnected porous architecture. Pore size modification may also be performed while keeping the same surface chemistry, the graded porosity of scaffolds have an enormous impact on supporting variable tissue generation and will be useful for osteochondral region encouraging bone and cartilage gradient growth (Lien et al. 2009; Miao & Sun 2010)

In view of the porosity and pore size effects of biomaterials, Vassilis Karageorgiou and David Kaplan (2005) showed the impact of high concentration of polymer solution on yielding a smaller pore size compared to a lower concentration, they reviewed the positive correlation as well between porosity and osteogenesis which have been mainly observed at 50-100 µm pore size ranges. Although being highly porous, pNIPAM and pNTBAM hydrogels have average smaller pores as regard to the larger pores of cancellous bone (average of 300 µm) (Lee et al. 2012; Cooper et al. 2016). However, current hydrogel porosity is comparable to that of the sub-chondral bone plate, which is a more compact layer with a smaller pore openings range from 20-30 µm in diameter (Bian et al. 2016).

Material stiffness is an essential property of tissue regeneration. Such properties may decide the potential for cells to proliferate, their final configuration, and growth pattern (Wells 2008). According to several studies, biomaterials showed a variable degree of mechanical strength and stiffness relative to their nature and method of production (Hollister et al. 2002; Vijayavenkataraman et al. 2017). For the current work, pNIPAM and pNTBAM revealed the variable degree of rigidity with a significantly higher value of 371 KPa for pNTBAM compared to 16 KPa pNIPAM (Figure 3-7). Perhaps the hydrophobic nature of pNTBAM and the small porous structure are the reasons behind having a more compact and stiffer composition compared to the highly porous hydrophilic pNIPAM (Cha et al. 2011). Several studies have reported cartilage compressive modulus range between 200-500 KPa depending on the region and cartilage layer (Swann & Seedhom 1993; Franz et al. 2001; Little et al. 2011) . Current results were promising concerning pNTBAM as it is closely related to native cartilage records. On the other hand, both hydrogels were way less than the measured compressive modulus for bone tissues which could reach up to hundreds of megapascals (Pal 2014; Keaveny et al. 2004). It has been suggested, according to some studies, that the material's stiffness is not necessarily to be identical to the native's tissue one, because it serves as a temporary matrix template that supports biological function of cells and native tissue so that retaining the regular strength (J. Yang et al. 2017). Moreover, tuning of these materials

could be an onward step in the direction of enhancing their mechanical properties, thereby improving the chance for obtaining more suitable material composite (Little et al. 2011; Cha et al. 2011; Vijayavenkataraman et al. 2017).

As the basic plan was to target the osteochondral tissue regeneration, it is essential to test the materials' ability for the calcium minerals association and to adapt the mineral environment of the osteochondral region. It is known that an active process of mineralisation is involved in generating the osteochondral region starting from the sub-chondral bone up to the calcified cartilage zone. This process will be opposed biochemically at the tidemark of the calcified cartilage layer (Bullough & Jagannath 1983; Hoemann et al. 2012a). Such an arrangement provides a gradient of minerals from the sub-chondral bone plate up to the first cartilage layers (Bian et al. 2016). It was indicated according to Kokubo & Takadama 2006 that the materials ability to combine to calcium and form apatite layer in vivo can be examined by incubation in SBF solution at 37 °C *in vitro*. Materials intended for bone and ostechondral tissue regeneration, are required to adequatly form a strong combination with these tissues which eventualy requires these materials to be able to meniralize when examinedin an *in vitro* assessment (Kepa et al. 2015). In a study cnducted by Vo et al. 2016, the mineralization capacity was evaluated for acellular pNIPAM based thermogellling macromer and another cocolymeized with dimethyl-γ-butyrolactone acrylate that advice for more hydrophobicity, both being injected in rat cranial defect. They concluded a positive ability of these polymers to mineralized based in an *in vivo* and *in vitro* experiments (SBF incubation) with increased levels obsrved for the more hydrophobic polymer (Vo et al. 2015). The present results revealed both materials are capable to bond with calcium ions and form mineralized layer upon their surface using *in vitro* SBF incubation. This was in accordance with certain studies that explain the usefullness of SBF solution composition to test materials mineralization tendencies and hydroxyapatite coating when targeting osteochondral tisuues regeneration (Kokubo & Takadama 2006; Jones et al. 2007; Wu & Xiao 2009; Kepa et al. 2015; Jones 2015; Camarero-Espinosa & Cooper-White 2017). The current materials showed different tendencies to be

associated with calcium minerals evident by the significant ($P \leq 0.05$) amount of calcium ions and alizarin red stain measured for pNTBAM compared to pNIPAM, which may be important when combined with cellular activity. Both tests were parallel in indicating the amount of calcium mineralization except that alizarin red staining may involve more of the HA components i.e. semi quantitative while calcium assay is more specific for calcium ions (Moriguchi et al. 2003). The significant mieral associatino with thes polymers may also be related to their surface charges and the resultant hydrophilic versus hydrophobic surface behaviour which could possibly enhanced their ability for mineralization (Castillo Diaz et al. 2014; Mai et al. 2018). However, no significant variations were observed between hydrogel's sub-groups of different monomeric concentrations as per alizarin staining and quantification and calcium assay of pNTBAM sub-groups. Calcium assay though indicated significant calcium ions associated with the pNIPAM 0.079 g/mL compared the other pNIPAM sub-groups. This could serve the target of generating a mineral gradient when combining these two hydrogels in one scaffold making use of the variable calcium association tendencies observeed between these polymers and the relavent sub-groups.

The present results had shown that pNIPAM and pNTBAM polymers produced as a 3D hydrogels with relatively different criterias. A more wettable surface with larger pores diameter were recorded for pNIPAM. Whereas, a stiffer mass together with more potential for mineral association were the main distinguishing factors for pNTBAM. The slight chemical difference between the two polymers had possibly acounted for the relavant variations monitored in the current results. All these distinguishing features between the tested hydrogels may suggest that these two materials could support various types of tissue regeneration with the possible impact on cells proliferation. It also holds promising trends towards joining these hydrogels to produce a gradient scaffold owing to their distinctively variable behaviours.

Chapter 4

Determining the biological suitability of the scaffold system

4.1. Introduction

Cell-biomaterial interactions are a function of material characteristics that will ultimately guide cells and determine the outcomes of their behaviour. The physico-chemical properties and architectural construct specific to each material will determine the potential for cell attachment, proliferation (Wan et al. 2005; H. G. Craighead et al. 2001; Murphy et al. 2010). Furthermore, these materials characteristics will decide whether the chosen cells are performing their natural biological function (Currie et al. 2007; Chen et al. 2018). As such, matching the cells natural environment, with a biomaterial, is critical in bringing these cells activity as close as possible to their normal behaviour. For instance, surface charge and chemistry in addition to material stiffness impacts on cell number, adhesion profile, and morphology (Deligianni et al. 2000; Yang et al. 2009; Wang et al. 2016). The presence of additional surface cues such as peptides, growth factors, or bioactive materials has also proven to be effective in the promotion of appropriate cellular behaviour (Cao & Hench 1996; Arima & Iwata 2007; Chang & Wang 2011; Emans et al. 2013; Wang et al. 2016; Jones 2015).

Several materials were investigated to address bone and cartilage tissue regeneration (Hutmacher 2000; Nukavarapu & Dorcemus 2013a; Correa & Lietman 2017; Camarero-Espinosa & Cooper-White 2017). Many of these materials were capable of supporting osteogenic cell behaviour and mineralization owing to their porous architecture and surface features (Karageorgiou & Kaplan 2005; Durante 2012). Promoting chondrogenic behaviour has been reported using materials with nano surface features or nano-fibres scaffolds (Puppi et al. 2010a; Izadifar et al. 2012). A hydrophilic versus hydrophobic surface functional groups is another factor that impacted chondrogenic or osteogenic cell differentiation (Glennon-Alty et al. 2013; Li et al. 2018). Tailoring of these materials by altering surface chemistry or incorporating certain cues had impacted cellular functions for instance bio-active glass and carbon nono-tubes enhanced mineralization and osteogenic cell behaviour (Fu et al. 2011; Gajendiran et al. 2017)

Distilling the above introduction further we aim to fabricate materials for use in 3D culture systems enabling a sophistication of architecture greater than that achievable with standard 2D culture alone. In doing so, we seek to enable cells to sense their surrounding 3D environment and to communicate more efficiently. The selected method of biomaterial production will also impact the manner in which cells interact with the final material shape. It has been hypothesized that manufacturing of materials into hydrogels would support appropriate biological function owing to their water content and having a porous structure that is closely related to that seen in a number of tissues (Hoffman 2012).

In this chapter the basic characteristics of pNIPAM and pNTBAM on cell survival and behaviour are explored. We hypothesize that the differences between these hydrogels (as described in Chapter 3) will result in variable cellular responses. This will rely on the type of cells to be seeded upon tested hydrogels, which in this case will be bone and cartilage cells as we are aiming at regenerating osteochondral region. The outcome results should enable us to identify the biological responses of cells and to make judgment upon the best cartilage- and bone-matched environment based on the previously identified materials properties.

4.2. Chapter aims

The current chapter aims to examine the following

- Cell attachment and distribution on each hydrogel surface.
- Cell survival and proliferation rate for immortal and primary cell lines seeded at the same density and tracked for 21 days.
- The capability of cells to migrate towards the core of hydrogel connecting this to the porous structure of each hydrogel.
- Osteogenic and chondrogenic behaviour of primary human osteoblasts (hOBs) and primary human chondrocytes (hCHs) upon each hydrogel tracked for 21 days.

4.3. Materials and methods

All Materials and Methodology utilised in this Chapter are fully detailed in Chapter 2.

Hydrogels were prepared for cell culture by 3 X PBS washes at 37° C for 48 hours each followed by sterilization with 99% ethanol for 30 minutes at room temperature before being washed again with PBS for 24 hrs at 37° C with PBS changed every 6-8 hrs (mentioned in detail in section 2.5 of Chapter 2).

Primary human chondrocytes (hCHs) and human osteoblasts (hOBs) were seeded on the top of hydrogels at 10^4 cells /15 µL of cell suspension and topped with either basic or specialized (osteogenic and chondrogenic) media. Samples were examined after 7, 15, and 21 days for specific cells responses (mentioned in detail in section 2.5 of Chapter 2).

Confocal assessment of the cell-scaffold system was conducted to verify cell attachment, viability, and specific protein expression by primary cells. Histological H&E staining of 3D samples was an aid to confirm that cells had adhered to the hydrogel surface. Settings for confocal imaging, including laser intensity, brightness and contrast, were adjusted at the same levels for all hydrogel samples to minimize noise and auto-fluorescence obtained normally gained due to hydrogel mass (details of confocal imaging are given in Chapter 2 sections 2.6 and 2.7).

Biochemical assessment of calcium minerals and GAGs was carried out via alizarin red and alcian Blue staining. Images were captured on a EVOS light microscope. Quantitative measures applied to samples were Calcium and DMMB assays (detailed in chapter 2 section 2.8.1)

Detection of protein and specific markers was quantified with ELISA immune assays (procedures are mentioned in detail in chapter 2 section 2.8.2).

4.4. Statistics

All data were collected and analysed with Microsoft XL 2010 to calculate the mean, standard deviation and resulting graphs. Results obtained were compared using one and two-way ANOVA with Tukey's multiple comparisons test. Statistics were analysed using Origin Pro 8, the level of significance was set at $p \leq 0.05$.

4.5. Results

4.5.1. Attachment and cell shape

4.5.1.1. Haematoxylin and Eosin (H&E) staining

The depth of the hydrogel samples created difficulties in viewing cells directly on their surfaces. However, H&E staining revealed apparent cells, which were not present in control samples, as dark spots on the hydrogel surface (Figure 4-1).

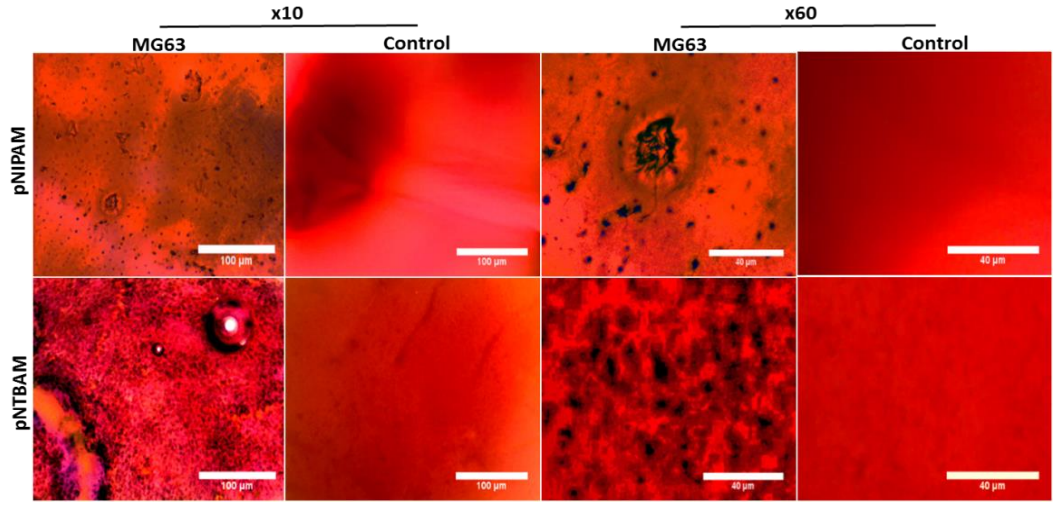

Figure 4-1. Haematoxylin and eosin staining of pNIPAM and pNTBAM hydrogel samples indicates cell attachment. *Images are showing pNIPAM (the top row) and pNTBAM (the dawn row) both compared between MG63 seeded and control (without cells). Images were captured at two magnifications (x10 and x60), scale bar measure 100 µm for the x10 images and 40 µm for the x60.*

4.5.1.2. Cytoskeletal actin filaments and nuclear stain

Confocal imaging of hydrogels indicated cell attachment to hydrogel surfaces with variable morphologies as indicated from actin fibre staining. Images also revealed the difference between the cells are attachment upon each hydrogel.

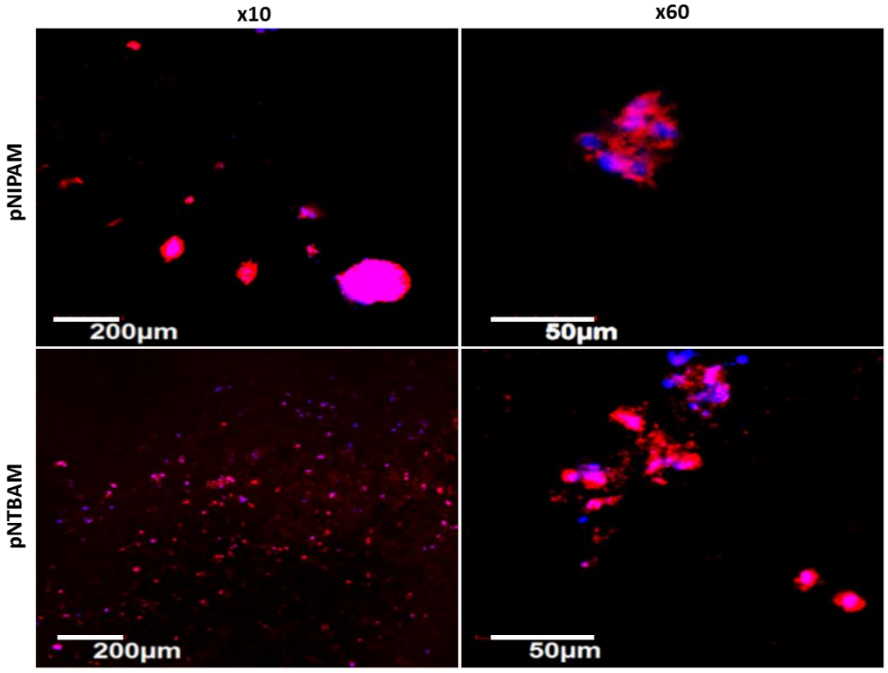

Figure 4-2. Cytoskeletal fibrin and nuclei staining of MG63 cells seeded on hydrogels at day 21. *Confocal images illustrating pNIPAM (top row) and pNTBAM (down row) hydrogels in two magnifications (x10 and x60). Both hydrogels were stained with phalloidon ifluor (red) indicating actin filaments and DAPI (blue) indicating cell nuclei. Scale bar measure 200 µm for x10 and 50 µm for x60.*

Image interpretation suggested that seeding upon pNIPAM tended to result in cell aggregates or clusters. This was readily evident when images were captured at higher magnifications indicating groupings of two to ten nuclei per aggregate. In contrast, cells seeded onto pNTBAM displayed a tendency to distribute evenly across the hydrogel surface (Figure 4-2).

4.5.2. Viability and cell proliferation

Cell seeded hydrogel samples were live/dead stained to determine the prevalence of viable versus dead cells after 21 days of culture. Cells were seeded at 10^5 cells/sample, this number was replicated to all samples and was considered as the starting cell density to judge the rate of cell proliferation upon each hydrogel. Confirming our previous observations cells on pNIPAM samples formed aggregates or clusters unlike pNTBAM where cells spread out

across the hydrogel surface (Figure 4-3). This scenario was replicated across all monomeric subgroups indicating hydrogel-specific behaviour. However, there were a significantly high number of cells counted on pNTBAM vs. pNIPAM hydrogel which was consistent for both MG63 and OK3H seeded samples (Figure 4-4).

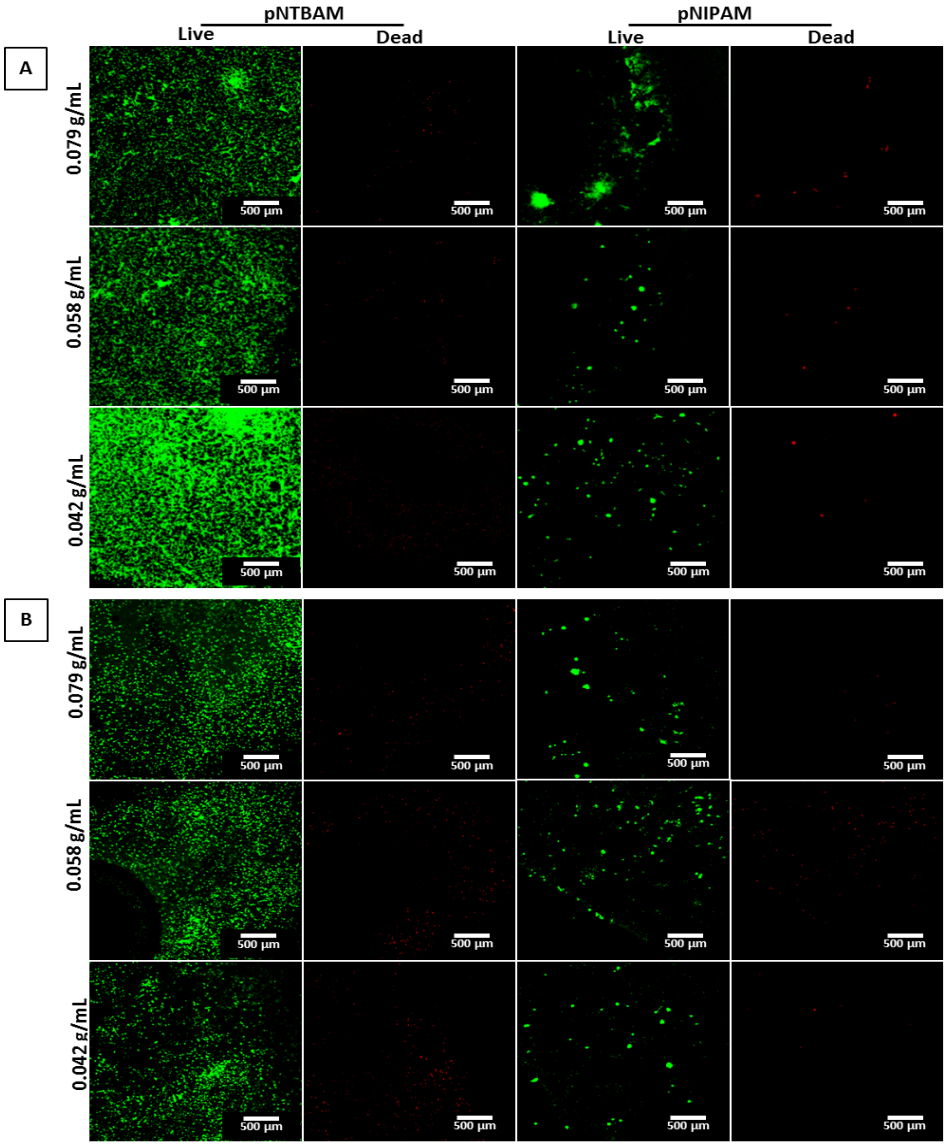

Figure 4-3. Confocal imaging of live /dead stained hydrogels at day 21 seeded with MG63 and OK3H cells. *Images are showing green fluorescent colour indicating live cells and red fluorescent colour indicating dead cells (images columns) for pNIPAM and pNTBAM hydrogels. Subgroups of multiple monomeric concentrations are represented by images rows with the top 3 rows set (A) correspond to MG63 cells and the bottom 3 rows (B) are for OK3H cells. Scale bar measures 500 µm.*

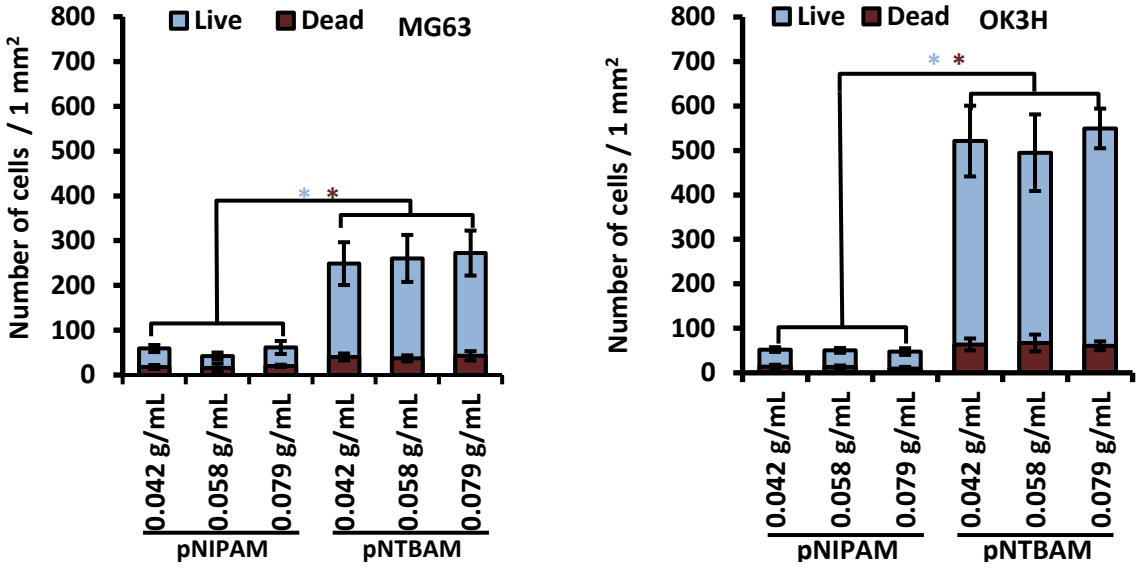

Figure 4-4. Cell count of live/dead MG63 and OK3H cells seeded on hydrogels at day 21. *Figures are revealing the average number of cells counted per 3 mm^2 of hydrogel's surface. The light blue colour bars represent the live cells number while the dark red colour bars are the dead cells number. Each set of bars (live and dead) corresponds to the relevant monomeric concentration of hydrogel. Both asterisks indicate significance at P ≤0.05, the light asterisk (*) is for the live cell count and the dark one (*) is for dead cell count comparisons (results represent the mean ±SD, n=3).*

Tracking DAPI stained cells' nuclei enabled us to determine whether the cells are traveling towards the core of hydrogel. 3D image sections from confocal microscope were analysed via ImageJ software to define DAPI fluorescent intensity across hydrogel thickness. A plot was created to measure the pixel colour intensity of DAPI (blue) through an identified distance (the depth) in micrometres (μm). The deepest distance at which a higher intensity obtained was averaged and compared between hydrogel's sub-groups (Figure 4-5).

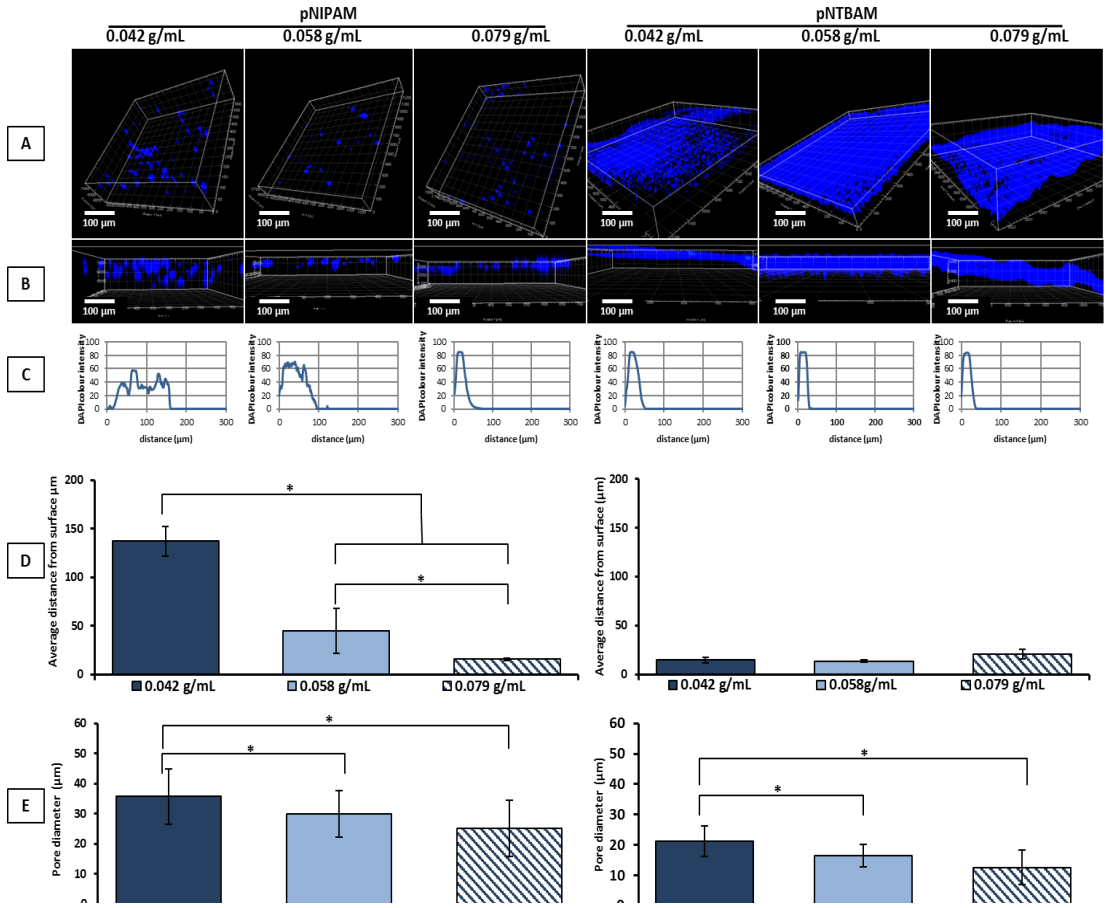

Figure 4-5. The assessment of MG63 cells migration within the hydrogel's construct at day 21.*Figure is showing hydrogels' monomeric sub-groups arranged in columns and compared between each other's according to A, B, C, and D. (A, B) are confocal 3D image sections of DAPI stained hydrogels illustrating cells (blue) position from hydrogels' surface, scale bar is 100 µm, where (A) represent side view of sections, (B) 3D configuration of the scanned sections. (C) Graph presentation of DAPI colour intensity obtained across the depth (distance in µm) of each hydrogel's monomeric group. (D) Is a bar figure representing the average distance travelled by cells from hydrogel surface compared between each hydrogel's monomeric sub-groups. Graphs in (B) are created by ImageJ software. Asterisk (*) indicate significance at P ≤0.05, results representing mean± SD, n=3.*

Reviewing the whole set of samples, confocal images of 3D representation of sectioned sample (Figure 4-5 A) and side view of sample (Figure 4-5 B) have shown how cells are acting on hydrogels. The cells were obviously slicked to the surface of pNTBAM hydrogels with all monomeric concentrations. In contrast, penetration was increased towards the lowest monomeric sub-group of pNIPAM as the cells start infiltrating through surface. The colour intensity was captured at the highest level only a few micrometres from the surface (averaged

15-20 µm) of pNTBAM hydrogel samples. The same result was obtained for pNIPAM 0.079 g/mL sample, however, evidence of higher colour intensity was witnessed at deeper distance for the 0.058 and 0.042 g/mL monomeric concentrations (Figure 4-5 C). The far distance measured was for pNIPAM 0.042 g/mL (averaged at 137±15 µm) which was significant ($P \leq 0.05$) compared to the other hydrogels. The pNIPAM 0.058 g/mL has gained as well some penetration of cells which was significant to the other measurements but less than the 0.042 g/mL sub-type. The pNIPAM 0.079 g/mL and pNTBAM subgroups were all parallel to each other's with no significant alteration (Figure 4-5 D). These results were compared with the pore size measurements for each hydrogel to reflect the impact of porosity on enabling cell penetration (Figure 4-5 E).

Our previously described compression testing and porosity (Chapter 3) coupled with the viability and migration data provided crucial information to inform the final working hydrogel monomeric subtypes suitable for further experimentation. As pNTBAM did not show signs of cell migration using the lower monomeric concentrations we elected to utilise the higher concentration subtype (0.079 g/mL). In contrast pNIPAM displayed strong of cell penetration through the porous structure when using the lower monomeric subtype (0.042 g/mL) without displaying any loss of mechanical strength vs. other subtypes which supported its selection.

We next confirmed the viability profile of hOBs and hCHs seeded on the chosen hydrogel subtypes. Confocal images indicated the same growth profile difference between hydrogels as observed with MG63 and OK3H (Figure 4-6). Similarly, live/dead cell counts were parallel to previous results noting that significantly greater levels of proliferation were noted for hCHs when compared to hOBs on pNTBAM. We again noted that pNIPAM displayed reduced cell numbers when compared to pNTBAM while maintaining cell viability (Figure 4-7).

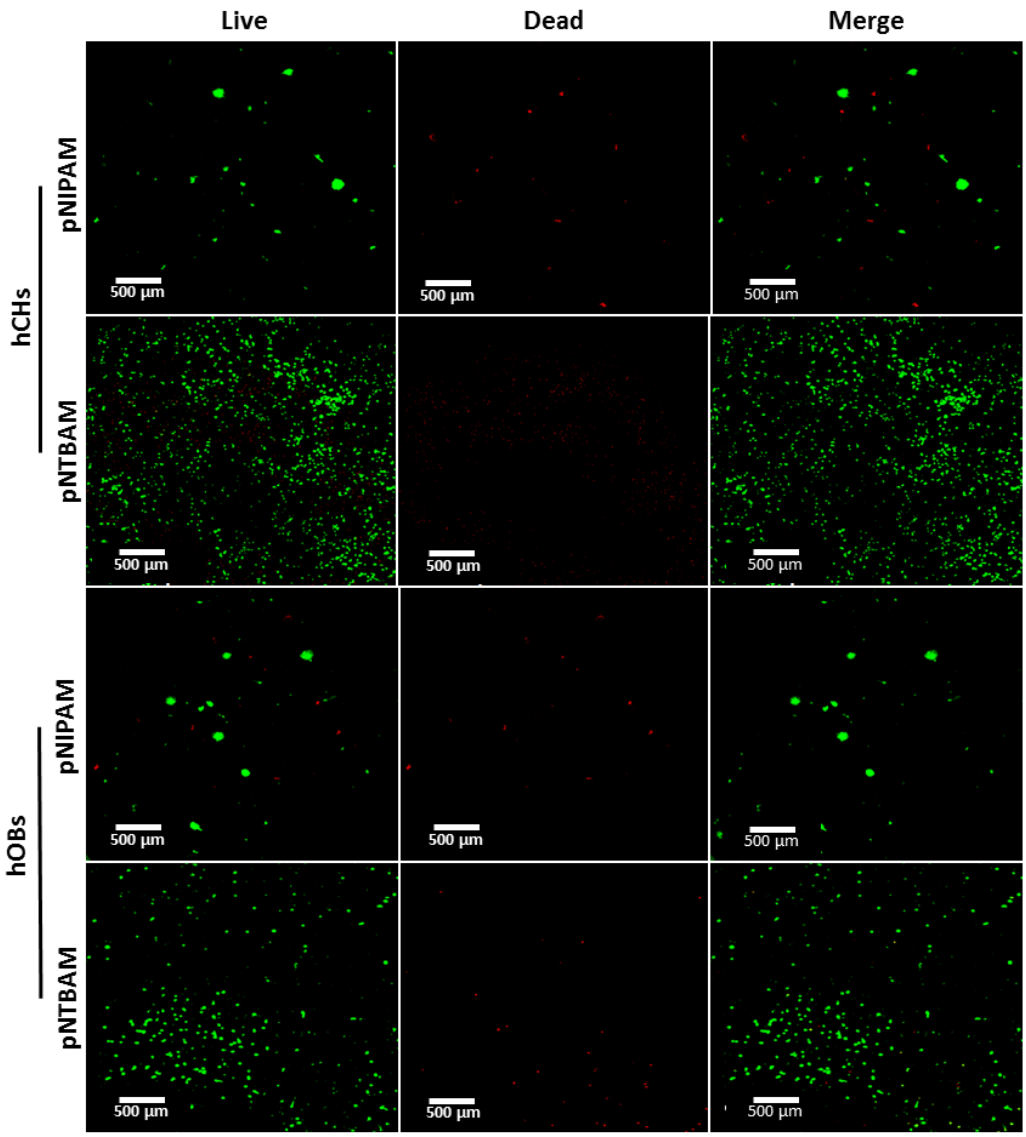

Figure 4-6. Live/dead staining of hydrogels at day 21 indicates viability profile of hOBs and hCHs. *Images showing live cells (green) and dead cells (red) in addition to a combination of both (merged) represented in columns along figure. Each hydrogel staining profile (live, dead, and merged) was indicated in rows with top two rows are for hCHs and the down two rows for hOBs. Scale bar measure 500 µm.*

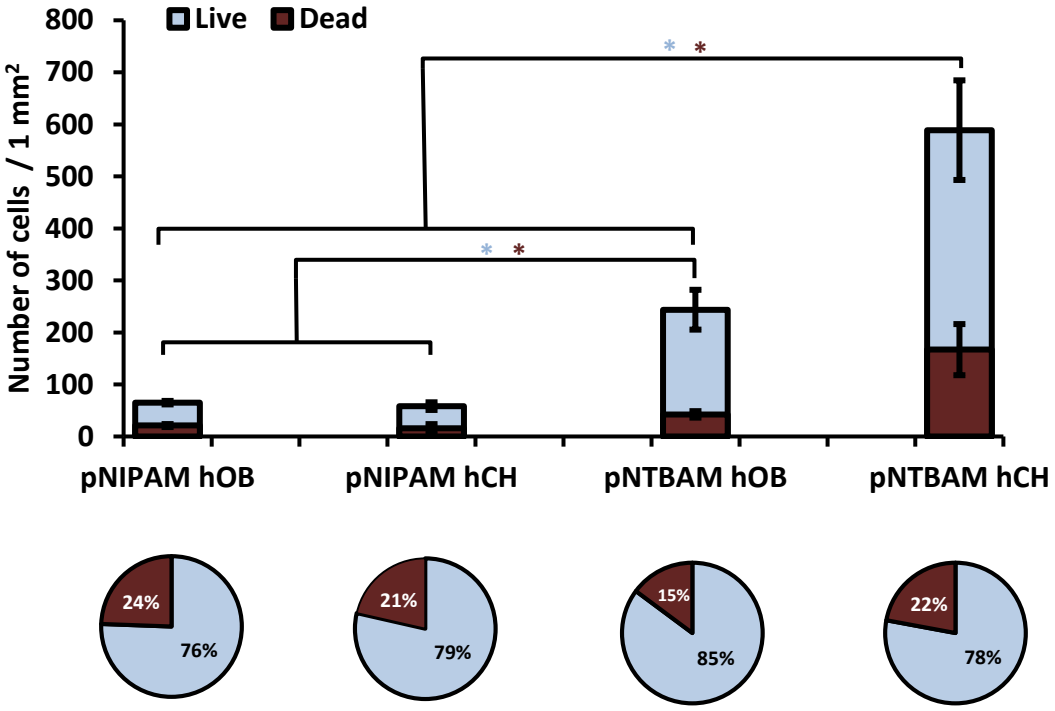

Figure 4-7. Live/dead cells counting for primary hOBs and hCHs upon hydrogel constructs. *Figure is illustrating the number of cells counted per 3 mm² of each hydrogel's surface. Bars are corresponding to each hydrogel seeded with specific cell type. Pie charts represent the percentage of live/dead cells. The light colour corresponds to the number and percentage of live cells while the dark colour is for the number and percentage of dead cells (reflected in bars and pie chart figures). Both asterisks indicate significance at P ≤0.05, the light asterisk (*) is for the live cell count and the dark one (*) is for dead cell count comparisons (results represent the mean ±SD, n=3).*

We wanted to check the chosen polymer concentrations on enabling the primay hOBs and hCHs to penetrate through the hydrogel's thickness. Tracking the blue fluorescent from DAPI staining of these cells has come out with almost the same results as for the tested cell lines (Figure 4-8). Confocal images are showing hOBs and hCHs cells infiltrating within pNIPAM hydrogel while accumulating at the surface of pNTBAM hydrogel (Figure 4.8 A and B). The blue colour intensity was higher at a deeper distance as measured with ImageJ for pNIPAM hydrogel and indicating that cells and cells clusters are traveling within hydrogel structure. In contrast, pNTBAM is still showing high colour intensity at the surface (Figure 4-8 C). Cells

upon pNIPAM indicated evidence of migration within hydrogel construct at an average distance of around 133 µm for both hOBs and hCHs which was significant to that obtained for pNTBAM (Figure 4-8 D).

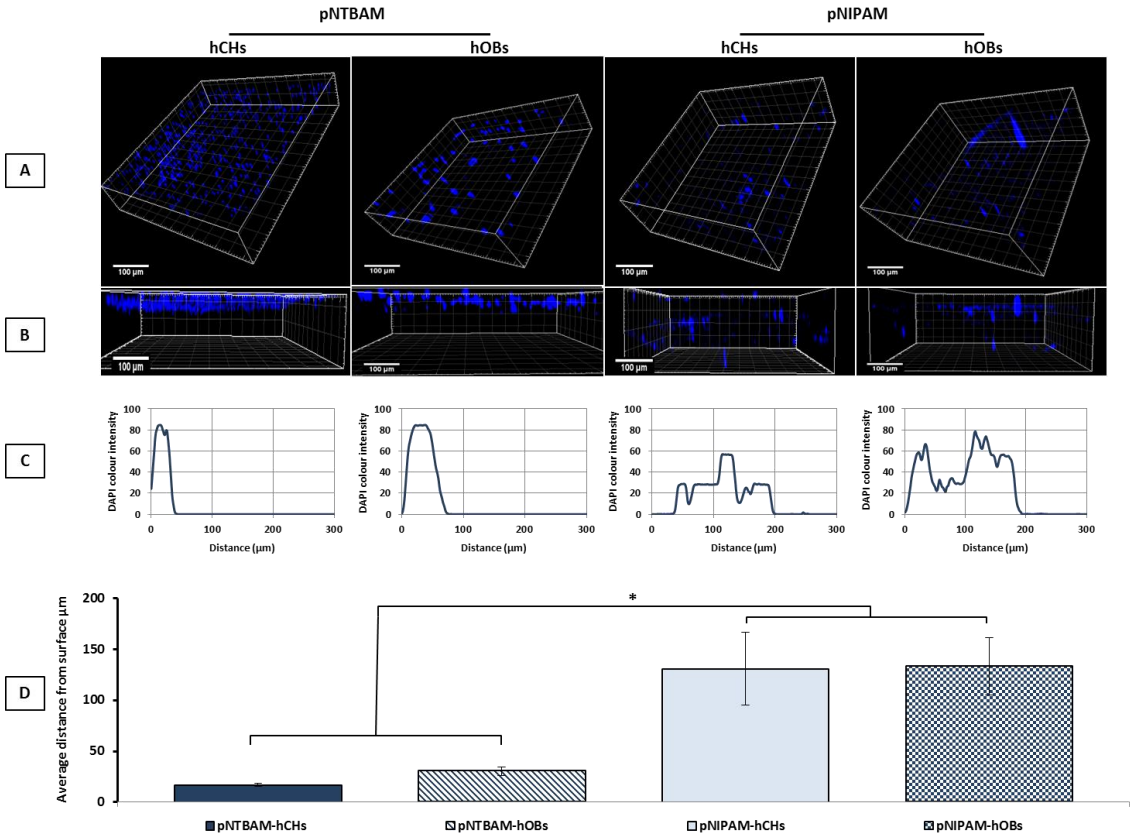

Figure 4-8. The impact of hydrogel's internal porous structure on enabling primary hCHs and hOBs penetration within pNIPAM and pNTBAM. *showing pNTBAM and pNIPAM hydrogels seeded with hCHs and hOBs arranged in columns while rows are (A, B) confocal 3D image sections of DAPI stained hydrogels illustrating cells (blue) position from hydrogels' surface, scale bar is 100 µm, where (A represent side view of sections, (B) 3D configuration of the scanned sections. (C) Graph presentation of DAPI colour intensity obtained across the depth (distance in µm) of each hydrogel for hCHs and hOBs, and (D) a bar figure comparison of the average distance travelled by cells measured in µm and showing results obtained for each hydrogel with the corresponding cell type seeded upon surface. Graphs in (B) are created by ImageJ software. Asterisk (*) indicate significance at P ≤0.05, results representing mean± SD, n=3.*

As per the above results, the number of cells count upon pNIPAM 0.042 g/ml sub-group may be a little higher as some of the cell were infiltrated beneath the hydrogel surface. The viability though still showing higher viable versus dead cell number.

4.5.3. Biochemical testing of specific cells behaviour

4.5.3.1. Alkaline phosphatase (ALP) activity

ALP activity assessment revealed wide variations between cell type and hydrogel (Figure 4-9). Increased ALP activity was noted for hOBs, irrespective of hydrogel, relative to control levels, which became detectable after 15 days of culture. Levels for hOBs indicated significant increase with time and was significantly altered compared to control ($P \leq 0.05$). The chondrogenic media did not promote ALP activity in the hCHs with a gradual reduction observed over time. The higher levels seen with basic media indicated that the chondrogenic media was having a refractory role on ALP activity levels. For hCHs on pNTBAM samples, the picture indicated a regression of ALP activity measured in media samples with significant decline with time seen for samples with chondrogenic media and was significantly lower at day 21 compared to control samples (Figure 4-9).

Comparing the activity levels of ALP at day 21, including all samples and cell types, have shown a progress for pNTBAM with hOBs. Samples with hOBs were significantly higher compared to their control peers of basic media and to that seeded with hCHs. In contrast, samples with hCHs were significantly lower in ALP activity compared to their control peers (Figure 4-10).

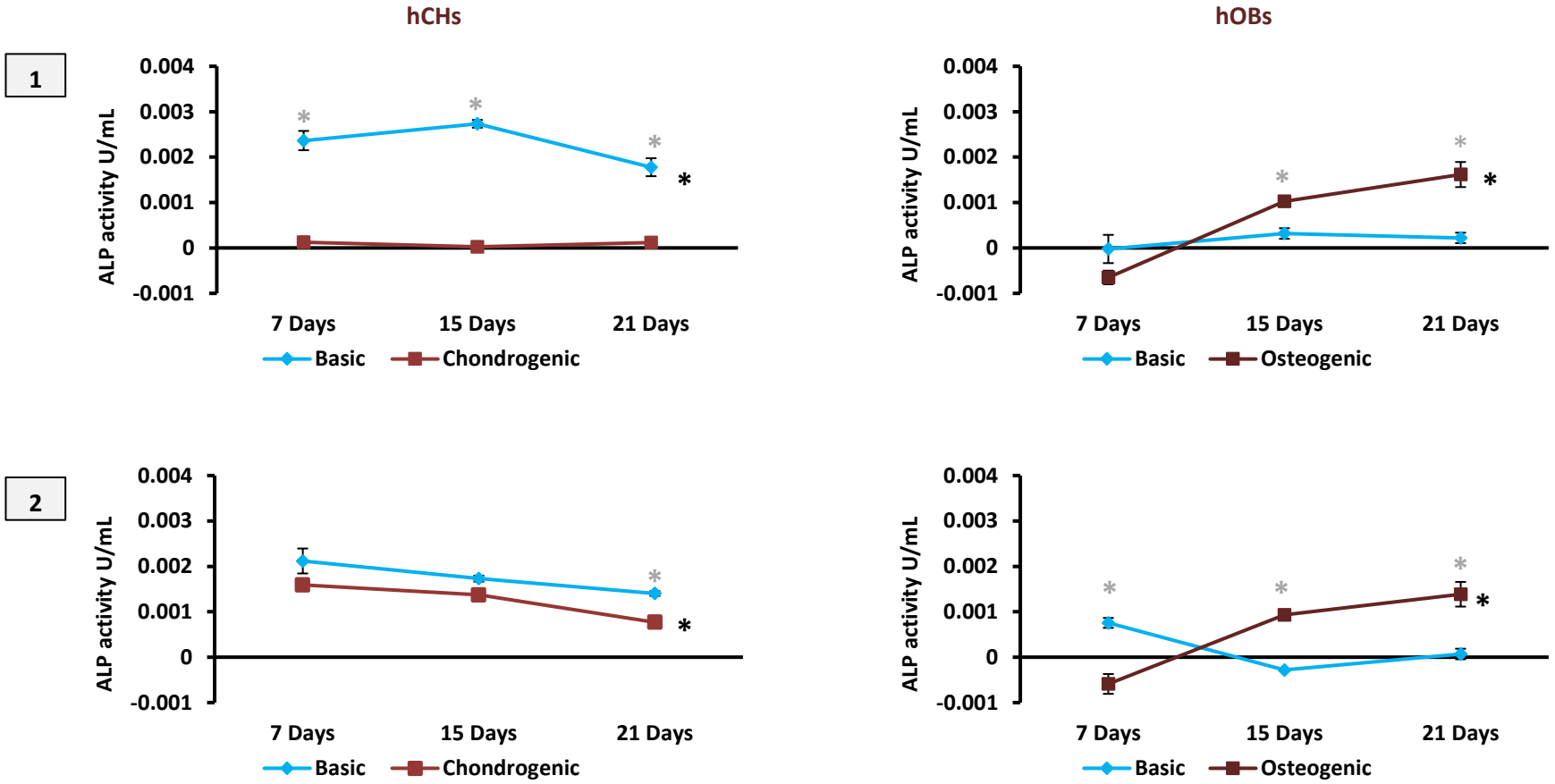

Figure 4-9. Monitoring ALP activity of hOBs and hCHs seeded upon hydrogels. *pNIPAM (1), and pNTBAM (2), each with the corresponding measurements of ALP activity for hCHs and hOBs. ALP activity was expressed in U/mL of media sample tracked for 7, 15, and 21 days. In each measurement was comparing between samples in osteogenic or chondrogenic media (dark square mark lines) and control sample cultured with basic media (light diamond mark lines). Asterisks indicate significance at P ≤0.05, the light asterisk (*) is the significance between sample and control at each time point and the dark one (*) is indicative for significance with time (results represent the mean ±SD, n=3).*

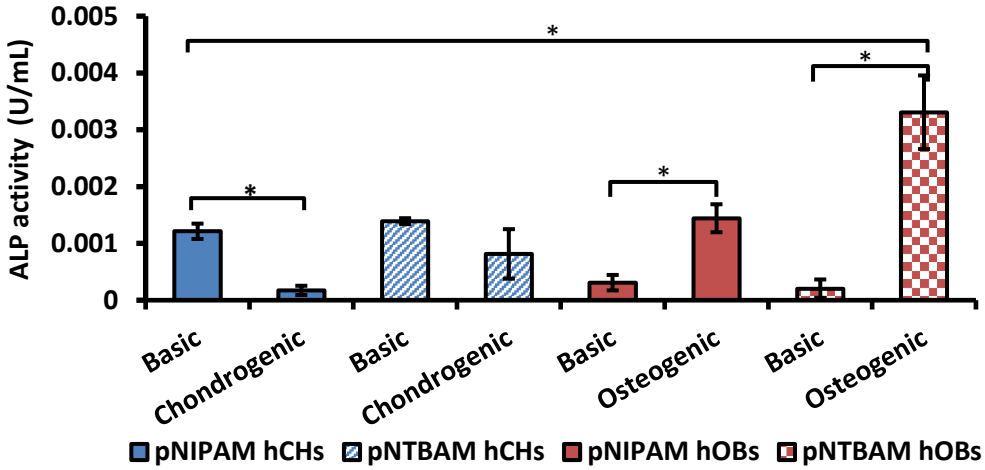

Figure 4-10. Levels of ALP activity for hCHs and hOBs seeded on pNIPAM and pNTBAM hydrogels compared at day 21. *The levels of ALP activity in U/mL of samples media. Bars are representing each sample with specific cell type presented with its control (basic media) and compared to other hydrogel samples. Asterisks indicate significance at P ≤0.05. (Results represent the mean ±SD, n=3).*

4.5.3.2. Alizarin Red and Calcium Ion evaluation

Histological staining of Alizarin Red-stained cell-seeded hydrogels via microscopic image revealed positive staining on both pNIPAM and pNTBAM samples indicating active mineral production. This was strongest with hOBs seeded on either hydrogel after 21 days. Samples seeded with hCHs showed low levels of staining with pNIPAM but no clear staining observed with pNTBAM (Figure 4-11). Calcium assay results similarly showed higher levels of calcium ion association with pNTBAM compared to pNIPAM samples seeded with hOB ($P \leq 0.05$). We also observed significant increases of calcium ion association after 21 days of culture. Hydrogel samples seeded with hCHs showed some elevation of calcium mineral levels over time for pNIPAM samples, but these were not significantly increased with pNTBAM (Figure 4-12).

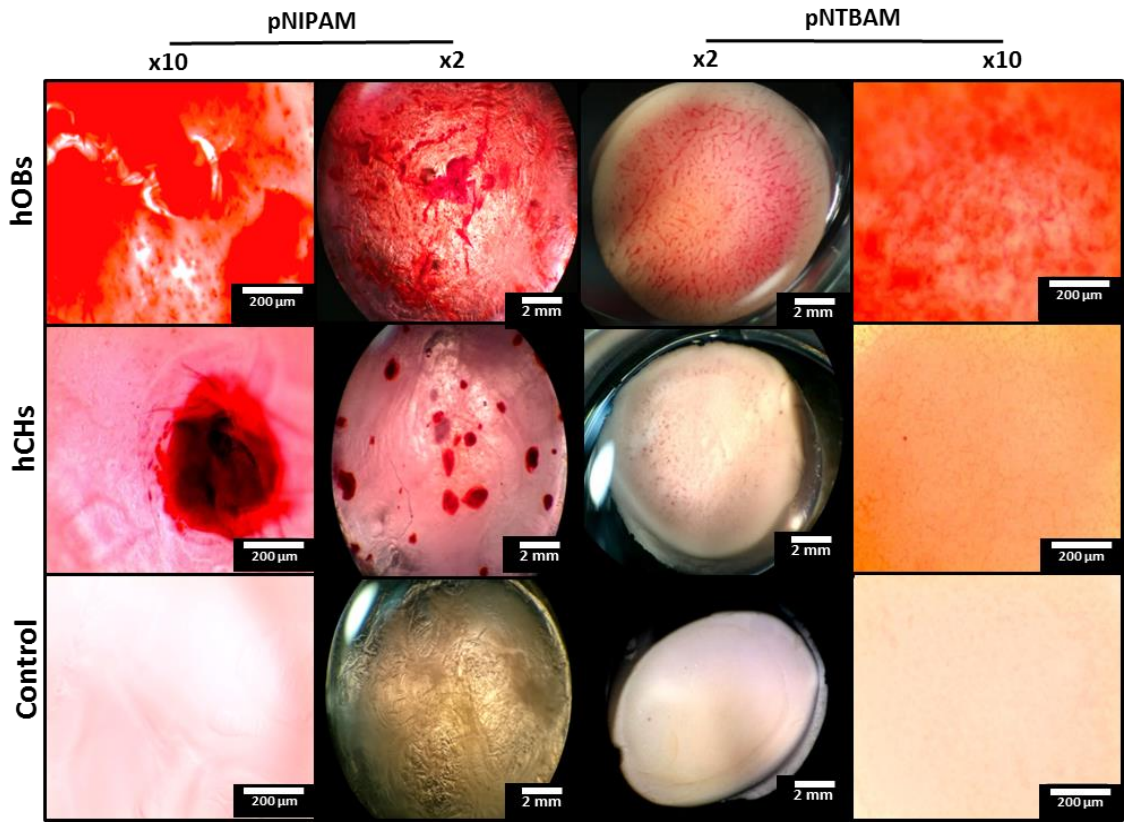

Figure 4-11. Mineral association illustrated by alizarin staining of hydrogels. *Images were captured at x2 and x10 magnifications and were arranged in columns for each hydrogel. Images rows correspond to the cell types (hOBs and hCHs) in addition to control hydrogel (no cells). Images scale bar measure 2 mm for x2 and 200 µm for x10.*

Results from calcium assay showed significant calcium ions association with hOBs samples, more often with pNTBAM samples and significantly higher level ($P \leq 0.05$) with osteogenic media samples. In contrast, hCHs were at the minimum level of calcium minerals with pNTBAM hydrogels. However, more tendencies for calcium mineralization were observed for hCHs in pNIPAM samples with no significant differences between basic or chondrogenic media samples (Figure 4-12 A).

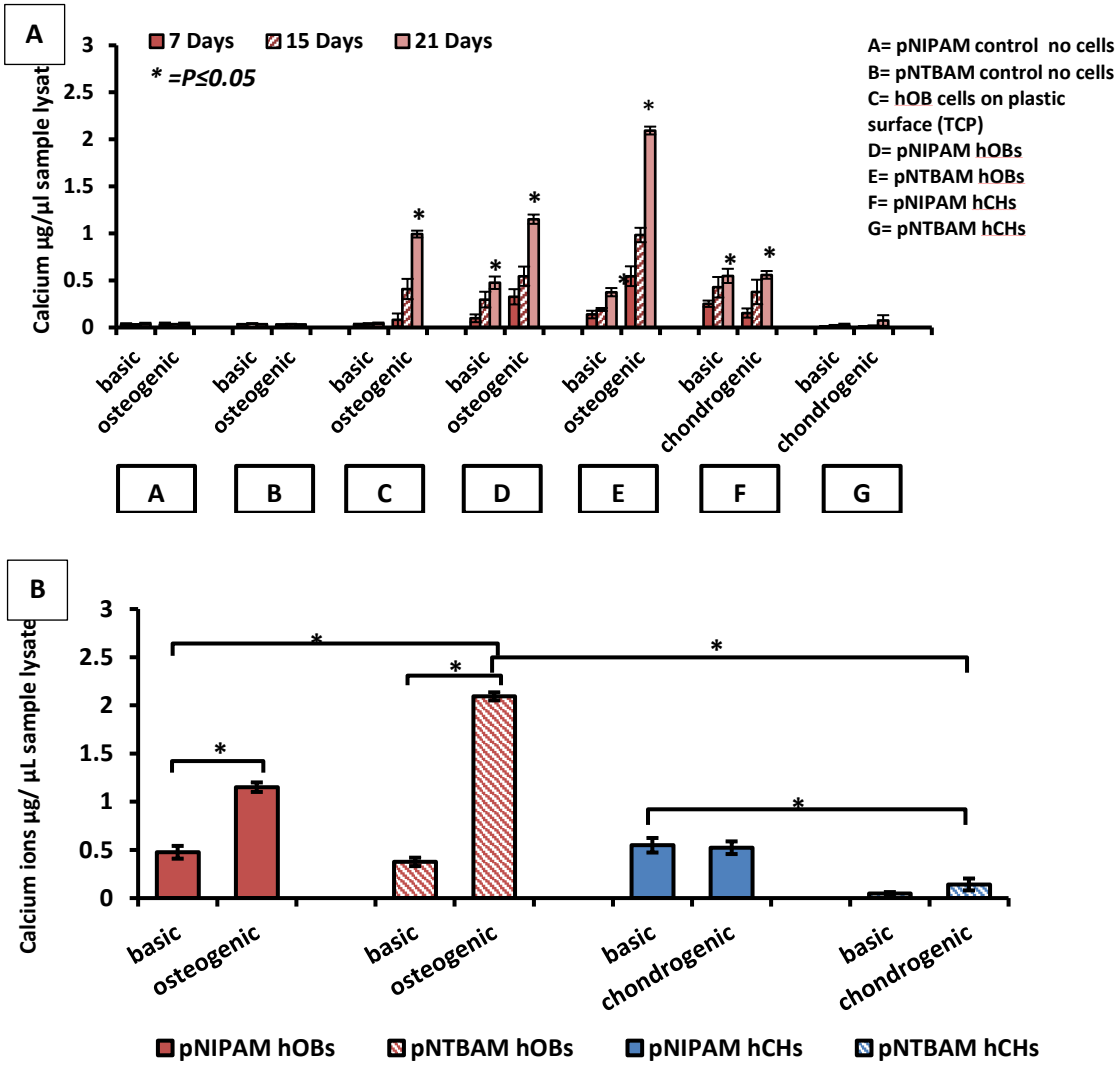

Figure 4-12. Assessment of calcium ions associated with hydrogel samples seeded with hOBs and hCHs. *Figure is illustrating the amount of calcium ions in µg/µL of sample lysate. (A) is the comparison of levels at different time points (7, 15, 21 days), bars are indicating each sample set with specific media (osteogenic or chondrogenic) and basic media (control) and indicated by letters (A-G) defined in the top right list. (B) Is the comparison between calcium ions associated with hydrogels at day 21. The bars are representing each sample compared to its control (basic) samples compared at day 21. Asterisks indicate significant levels at P ≤0.05 (Results are representing mean ±SD, n=3).*

Results of calcium ions were then compared between hydrogels at day 21 to observe the main differences between cells behaviour upon each hydrogel type. A significant increase was noted for pNTBAM samples with hOBs vs their controls and compared to pNIPAM samples as well. Levels with pNIPAM were significant to their control and when compared to the hCHs

samples. Evidence of calcium minerals was noted for pNIPAM with hCHs which was significant when compared to pNTBAM-hCHs (Figure 4-12 B).

4.5.3.3. Assessment of GAGs

Histological staining with alcian blue and subsequent evaluation via microscopic images was utilised to evaluate cell response to hydrogel and chondrogenic differentiation. Positive staining was readily observed with pNTBAM samples seeded with hCHs while hOB-seeded and control samples showed little evidence (Figure 4-13).

To evaluate GAG levels, we next performed the DMMB assay. This revealed high levels of GAGs in pNTBAM gels seeded with hCHs. As per the methodology, hydrogel samples where incubated with 500 µL papain lysate buffer, thus the amount of GAGs was assessed per 500 µL of each sample. GAG levels gradually increased across the 21 days of culture. Reduced amounts of GAGs were noted for pNIPAM hCHs seeded gels (vs. pNTBAM) which gradually increased over the culture period (Figure 4-14 A). Notably, GAG levels in pNIPAM samples were unaltered using either basic or chondrogenic cell culture media. In contract, pNTBAM samples showed highly increased levels of GAGs when using chondrogenic medium. The hCHs on TCP samples revealed some increased levels especially with chondrogenic medium but still significantly lower than cells on hydrogel samples. Samples with hOBs, included for control purposes, had significantly lower levels of GAGs. This was to the greatest extent with pNIPAM samples while some increases were seen with pNTBAM. When comparing the GAGs content between hydrogels with hCHs and hOBs, at day 21, the results came out with significantly higher levels for hCHs upon pNTBAM hydrogels mostly when using chondrogenic media (figure 4-14 B).

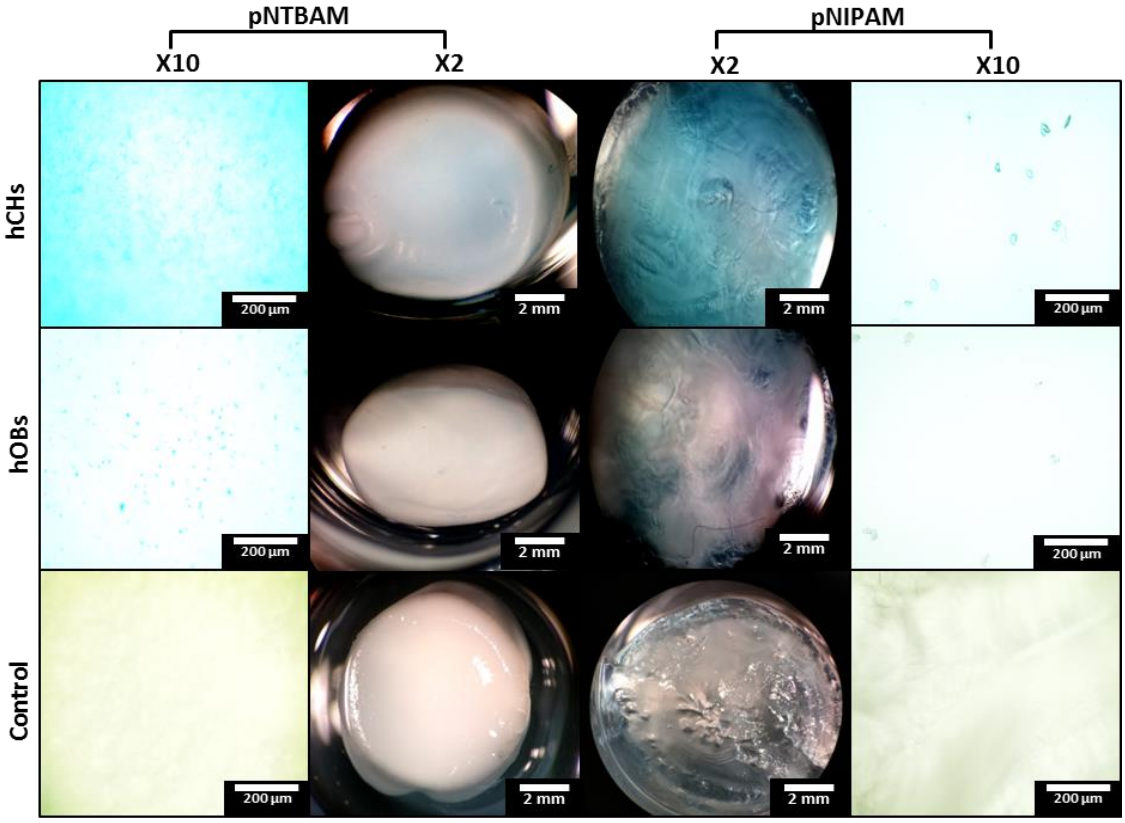

Figure 4-13. Alcian blue staining of hydrogel samples seeded with hCHs and hOBs. *Images were captured at x2 and x10 magnifications for each hydrogel and were arranged in columns for each hydrogel. Images rows correspond to the cell types (hOBs and hCHs) in addition to control hydrogel (no cells). Images scale bar measure 2 mm for x2 and 200 µm for x10.*

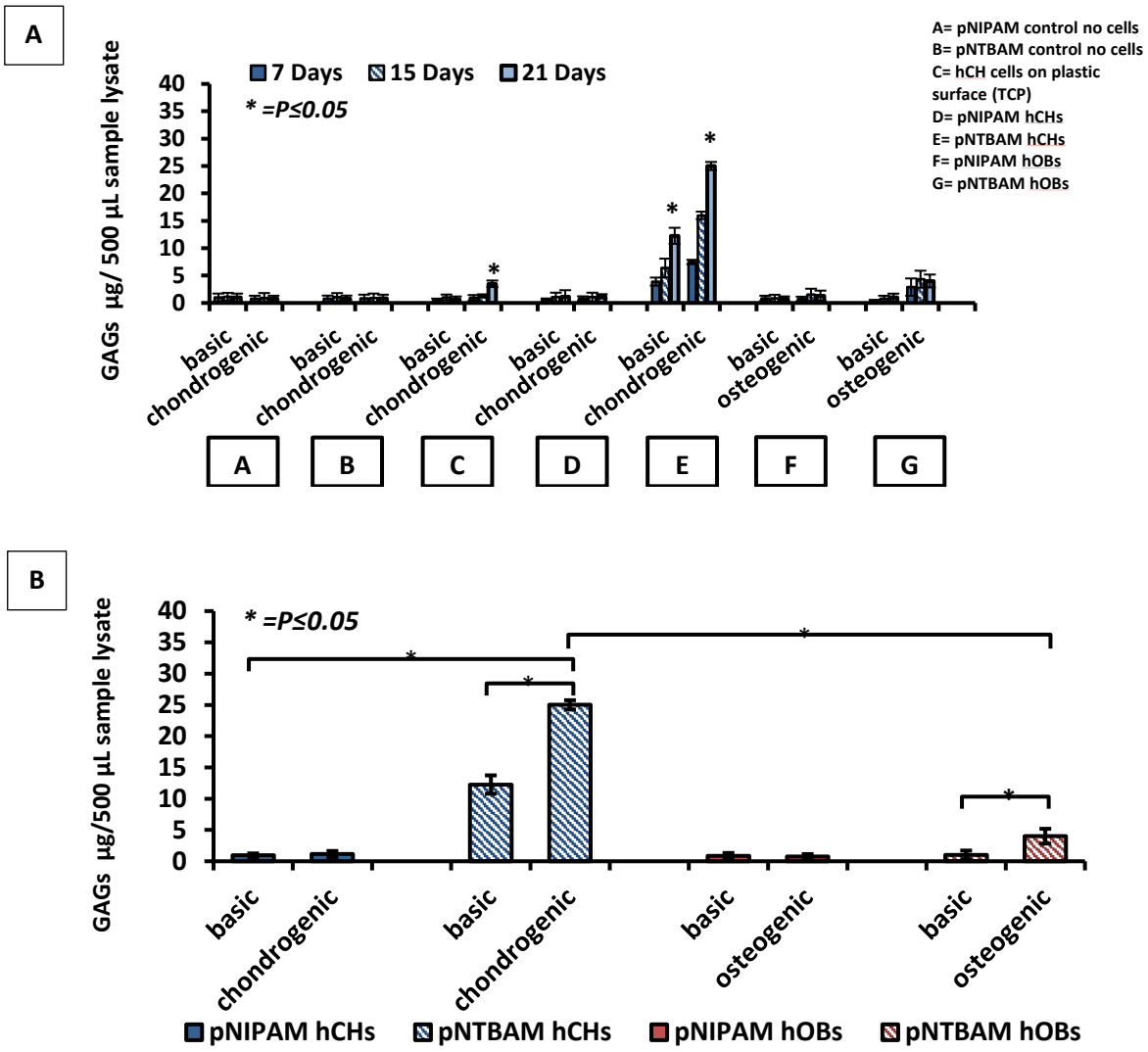

Figure 4-14. Assessment of GAGs content in hydrogels seeded with hCHs and hOBs. *Figures are revealing the amount GAGs measured in µg/500 µL where (A) is the comparison of levels at different time points (7, 15, 21 days), bars are indicating each sample set with specific media (osteogenic or chondrogenic) and basic media (control) and indicated by letters (A-G) defined in the top right list. (B) is a comparison between the levels of GAGs in hydrogels where the bars are representing the hydrogel samples with hCHs and hOBs compared at day 21. Asterisks indicate significant levels at P ≤0.05 (Results are representing mean ±SD, n=3)*

4.5.4. Determining collagen expression in cell-seeded hydrogels

4.5.4.1. Immunostaining for collagens I, II, and X

Positive collagen immunostaining was evident across all samples to a variable extent depending on cell type, hydrogel combination, and differentiation cocktail applied.

Collagen I expression was noted across both hOB and hCH-seeded hydrogel samples with a qualitatively noted more intense colour expression was noticed with pNIPAM-hOBs samples (Figure 4-15). Collagen II staining was more specifically-linked to hCH-seeded hydrogels with strong staining noted with pNTBAM and to a lesser extent pNIPAM. hOB-seeded hydrogels displayed low levels of collagen II expression in comparison (Figure 4-16). Collagen X expression was seen with both hOB and hCH seeded on both types of hydrogels. However, different rate of expression was observed between hydrogels rather than cell type, with higher extent involving pNIPAM including both cell types. Expression on pNTBAM has also been obvious with hCHs and hOBs with variable extents. Generally, this had involved wide range of cells but sometimes looks more intense with pNTBAM (Figure 4-17).

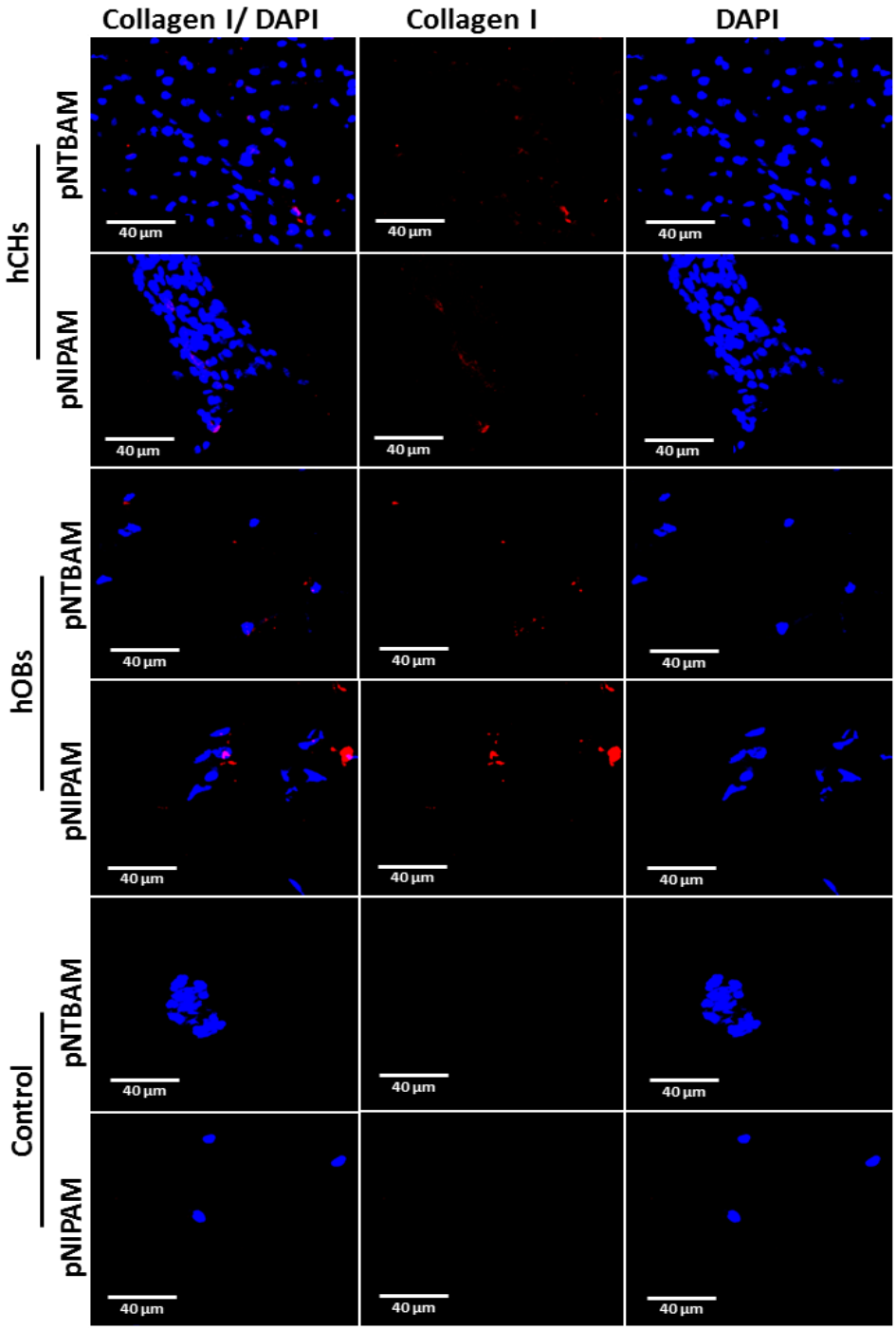

Figure 4-15. Immune stained hydrogel samples for collagen I expression. *Confocal images of hydrogel samples with hOBs and hCHs captured using x40 magnifications and revealed in columns separating channels for DAPI and collagen stain plus a merged channels image. Samples were stained with DAPI (blue) for cell nuclei and TRITC (red) fluorescent for collagen. Control samples involve hydrogels seeded with hOBs and incubated with secondary antibodies coupled with TRITC red fluorescent stain without primary antibodies and DAPI stained. scale bar measure 40 µm.*

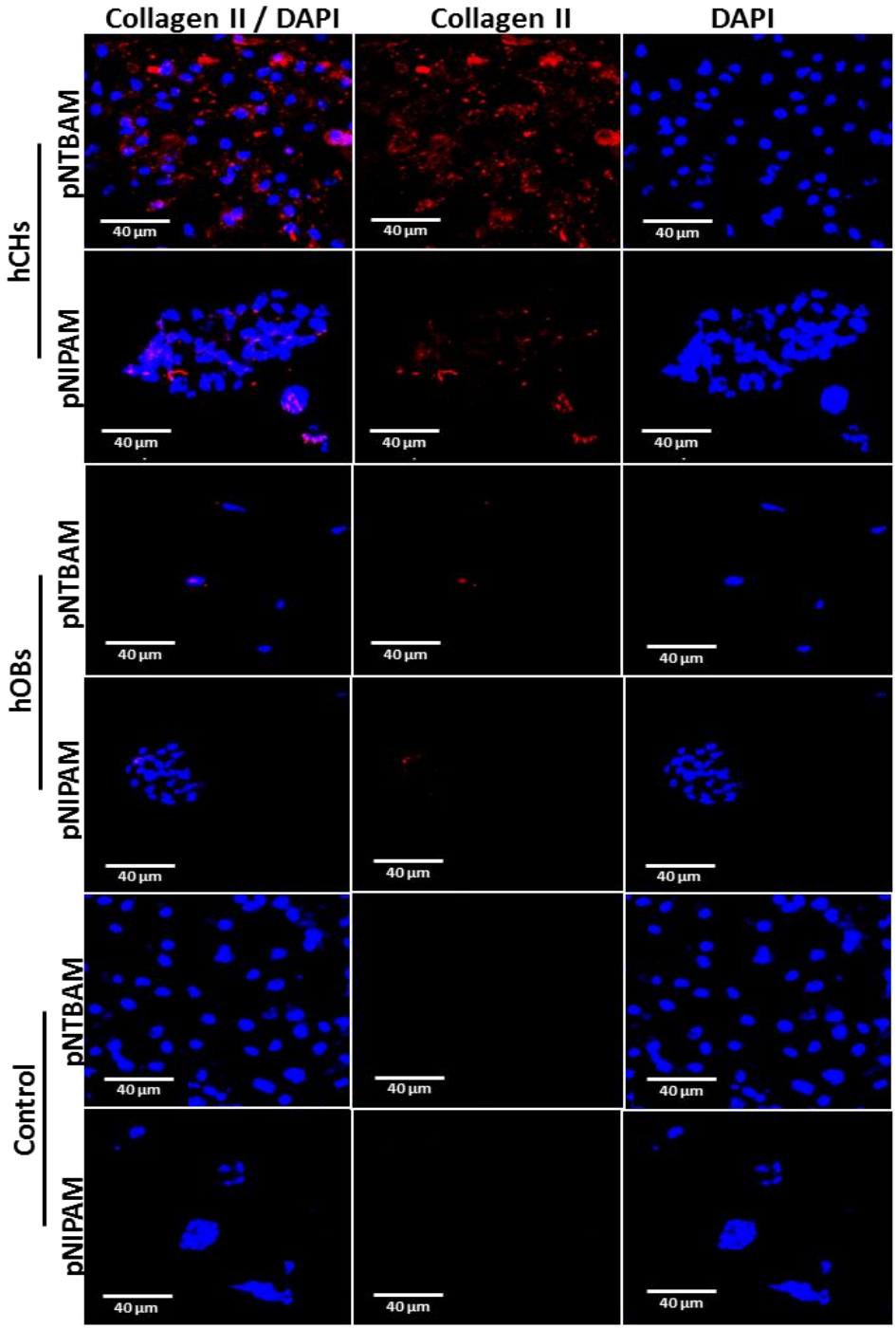

Figure 4-16. Immune stained hydrogel samples for collagen II expression. *Confocal images of hydrogel samples with hOBs and hCHs captured using x40 magnifications and revealed in columns separating channels for DAPI and collagen stain plus a merged channels image. Samples were stained with DAPI (blue) for cell nuclei and TRITC (red) fluorescent for collagen. Control samples involve hydrogels seeded with hCHs and incubated with secondary antibodies coupled with TRITC red fluorescent stain without primary antibodies and DAPI stained. Scale bar measure 40 µm.*

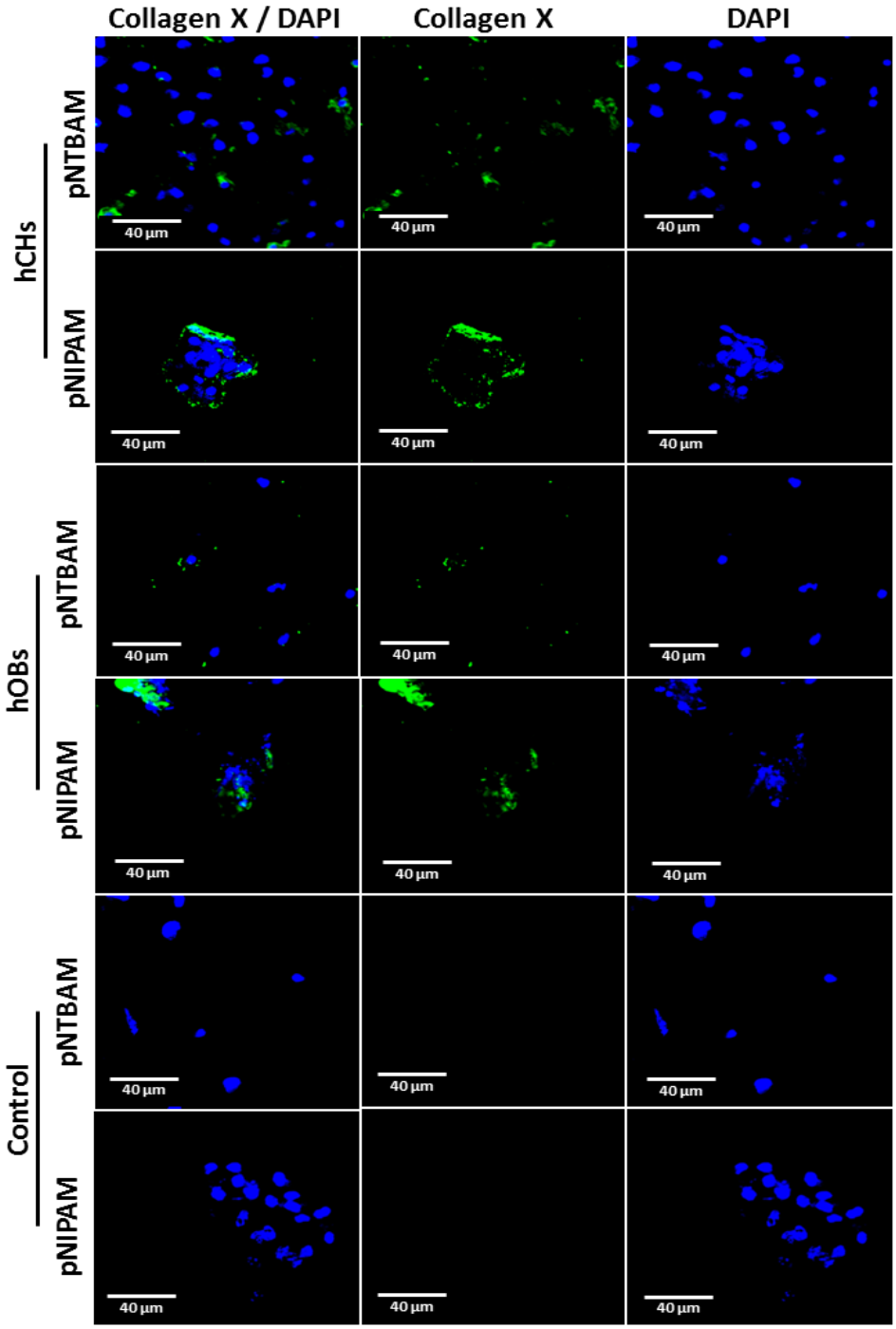

Figure 4-17. Immune stained hydrogel samples for collagen X expression. *Confocal images for hydrogel samples with hOBs and hCHs captured x40 magnifications and revealed in columns separating channels for DAPI and collagen stain plus a merged channels image. Samples were stained with DAPI (blue) for cell nuclei and FITC (green) fluorescent for collagen. Control samples involve hydrogels seeded with hOBs and incubated with secondary antibodies coupled with FITC green fluorescent stain without primary antibodies and DAPI stained. Scale bar measure 40 µm.*

4.5.4.2. ELISA-based collagen detection

ELISA testing was applied to determine and confirm collagen presence on cell-seeded hydrogels. Collagen I production was elevated over time with osteogenic media compared to control. This was observed to the greatest extent with pNTBAM and less so with pNIPAM. Hydrogels seeded with hCHs displayed less robust collagen I production although some increases were detected, particularly for pNTBAM (Figure 4-18).

Collagen II levels displayed significant increases over with time with hCHs upon pNTBAM in the presence of chondrogenic factors compared to basic media samples. However, little evidence of collagen II production by hCHs on pNIPAM was noted, irrespective of media system. Similarly, hOB-seeded hydrogels displayed little evidence of meaningful change irrespective of media/hydrogel pairing (Figure 4-19).

In tracing the levels for Annexin A2, as a marker for cell engagement in mineral activity, hOBs indicated significant increase with time which was mostly evident with osteogenic samples and for both hydrogels, although higher for pNTBAM. Lower levels were noticed for hCHs samples especially with pNTBAM samples which showed less increase with time; however, a significant increase was seen for pNIPAM samples even with chondrogenic media samples (Figure 4-20). The measured quantities for all proteins were then compared at day 21 to examine the difference possibly concluded between tested hydrogels. Eventually collagen I was significantly higher for hOBs seeded upon pNTBAM hydrogel. Levels were significantly ($P \leq 0.05$) higher using osteogenic media compared to the basic media control set. (Figure 4-21 A). Collagen II levels were significantly higher for hCHs upon pNTBAM samples using chondrogenic media and in comparison to other hydrogel samples. (Figure 4-21 B). Annexin A2 was evidently significant with hOB but with higher level for pNTBAM samples compared to other samples (Figure 4-21 C).

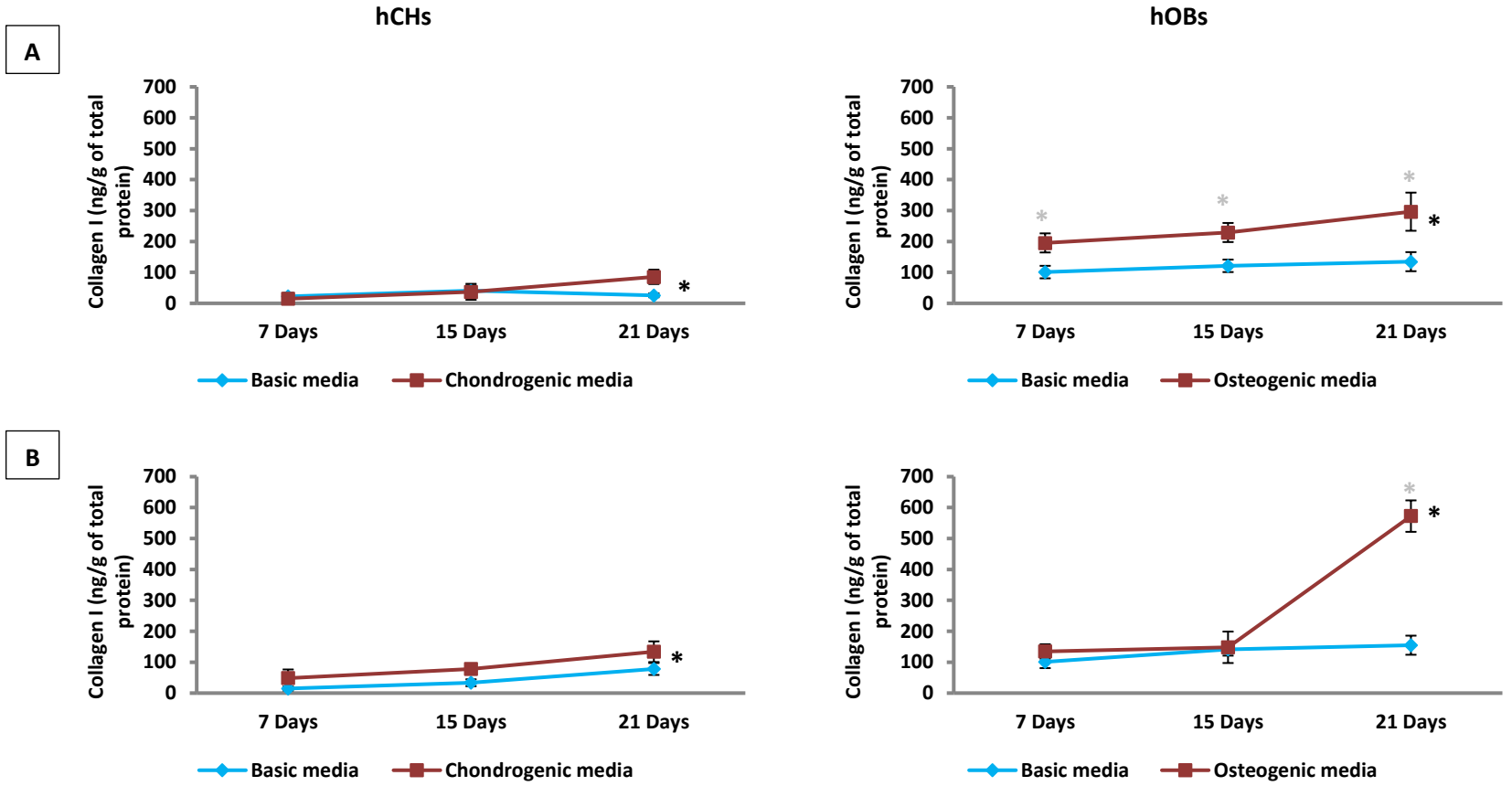

Figure 4-18. Assessment of collagen I on hydrogels seeded with hCHs and hOBs. *The amount of collagen I in ng/g of total protein measured in sample lysate, samples expressed in columns to indicate each cell type and in rows corresponding to each hydrogel where (A) is pNIPAM hydrogel and (B) is pNTBAM both with hCH and hOB. The amounts were followed in three time points (7, 15, and 21) where the dark square marks line represents specific media set (osteogenic or chondrogenic) while the light colour diamond marks line is the basic media set (control). Asterisks indicate significance at P ≤0.05, the light asterisk (*) is the significance between sample and control at each time point and the dark one (*) is indicative for significance with time (results represent the mean ±SD, n=3).*

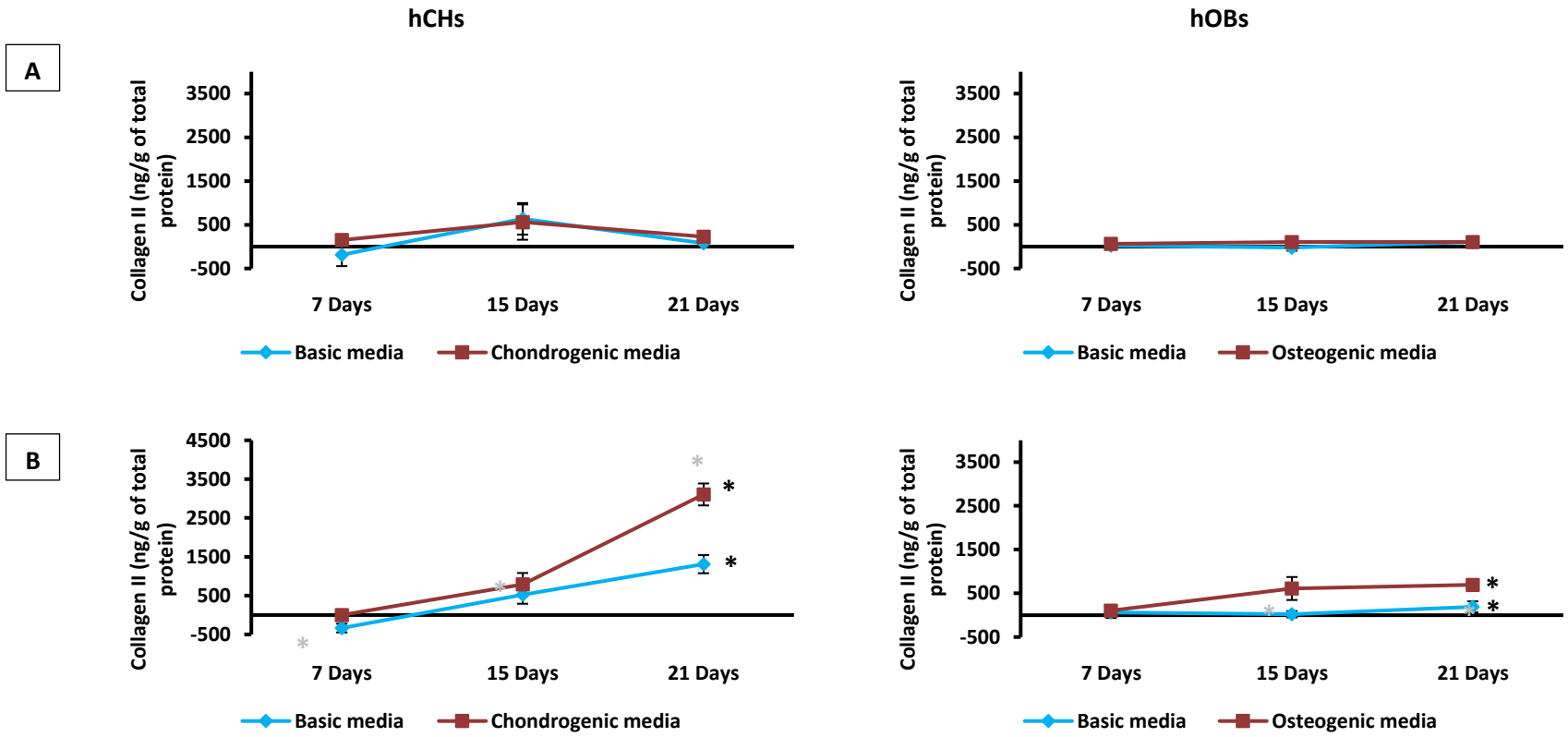

Figure 4-19. Assessment of collagen II on hydrogels seeded with hCHs and hOBs. *The amount of collagen I in ng/g of total protein measured in sample lysate, samples expressed in columns to indicate each cell type and in rows corresponding to each hydrogel where (A) is pNIPAM hydrogel and (B) is pNTBAM both with hCH and hOB. The amounts were followed in three time points (7, 15, and 21) where the dark square marks line represents specific media set (osteogenic or chondrogenic) while the light colour diamond marks line is the basic media set (control). Asterisks indicate significance at P ≤0.05, the light asterisk (*) is the significance between sample and control at each time point and the dark one (*) is indicative for significance with time (results represent the mean ±SD, n=3).*

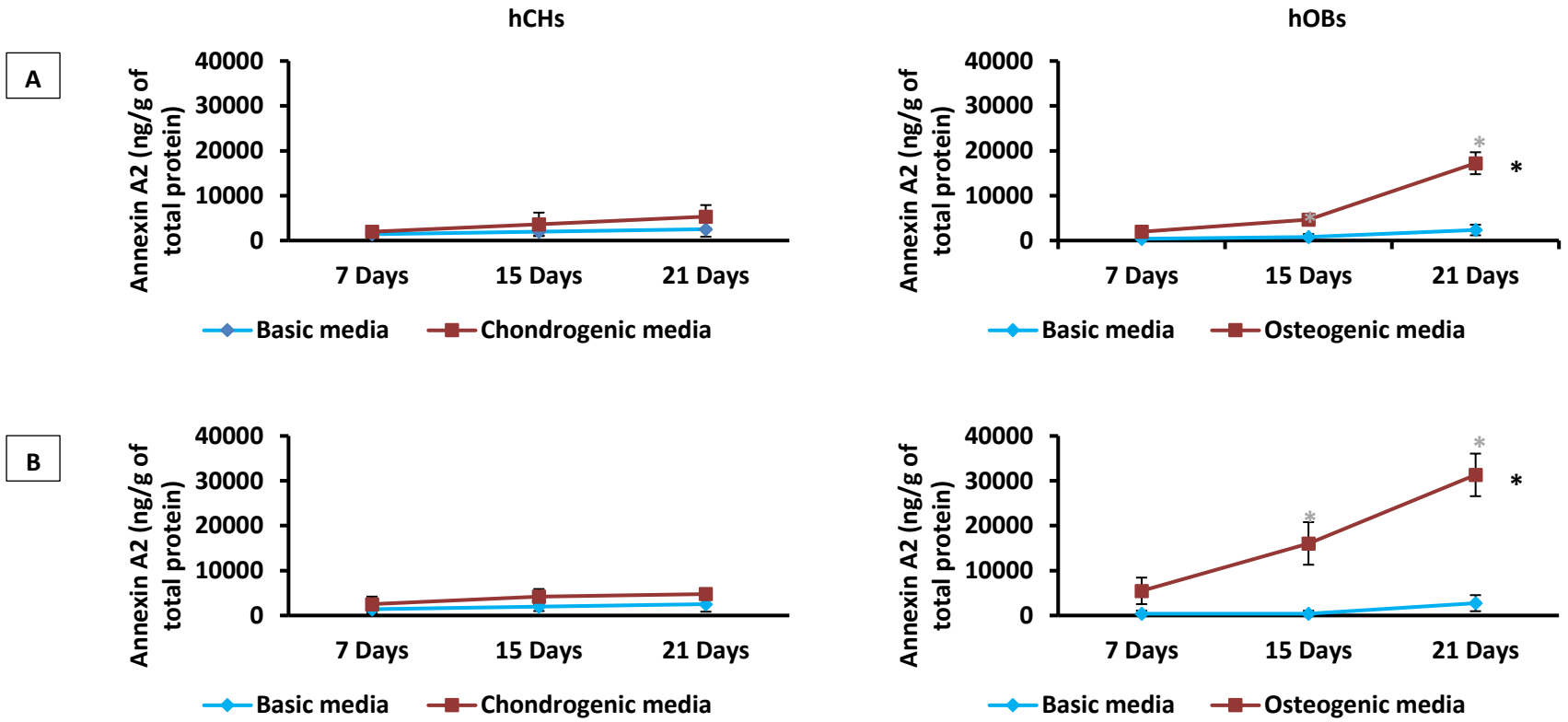

Figure 4-20. Assessment of annexin A2 on hydrogels seeded with hCHs and hOBs. *The amount of Annx A2 in ng/g of total protein measured in sample lysate, samples expressed in columns to indicate each cell type and in rows corresponding to each hydrogel where (A) is pNIPAM hydrogel and (B) is pNTBAM both with hCH and hOB. The amounts were followed in three time points (7, 15, and 21) where the dark square marks line represents specific media set (osteogenic or chondrogenic) while the light colour diamond marks line is the basic media set (control). Asterisks indicate significance at P ≤0.05, the light asterisk (*) is the significance between sample and control at each time point and the dark one (*) is indicative for significance with time (results represent the mean ±SD, n=3).*

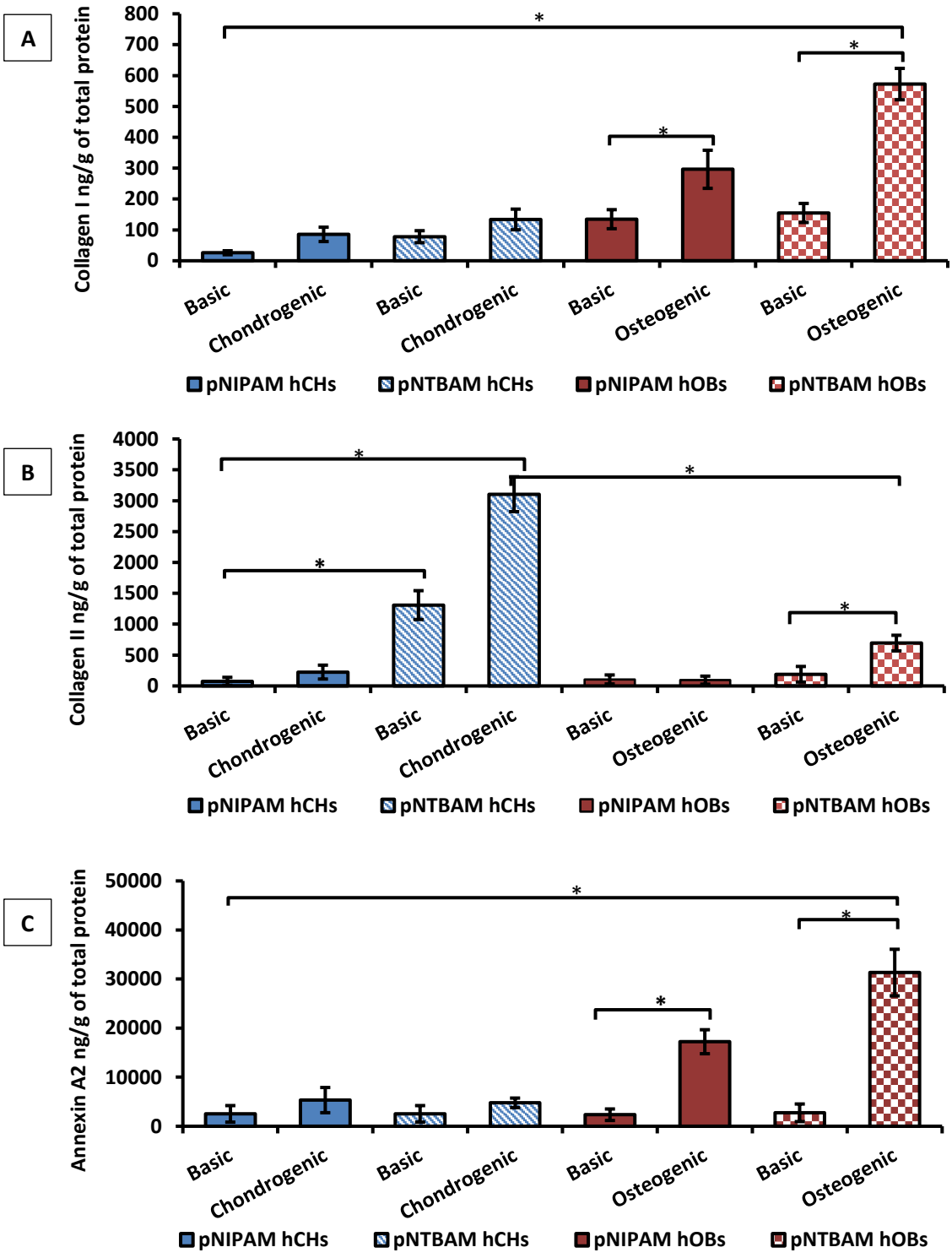

Figure 4-21. Comparing levels of collagens, I, II and annexin A2 between hydrogels at day 21. *Levels are expressed in ng/g of total protein measured in sample lysate for (A) collagen I, (B) collagen II, and annexin A2. Bars with different colours and patterns are indicating both hydrogels with either hCH or hOB. Asterisks indicate significant levels at P ≤0.05 (Results are representing mean ±SD, n=3).*

4.6. Discussion

An important aspect of material intended for the promotion of tissue regeneration is the ability to communicate with the biological system including the cells (Williams 2009). In our current study we have displayed a positive association between cells and materials. H&E and confocal imaging revealed cell attachment upon hydrogel surfaces which was distinct between pNIPAM and pNTBAM (Figures 4-1, 4-2). Chemical and architectural differences between the two materials, as outlined in Chapter 3, clearly impacted cell behaviour and potentially their capacity for tissue regeneration. For instance, the promotion of aggregate formation on pNIPAM vs. the cell spreading seen with pNTBAM could provide focus for when targeting each material towards intended tissue regeneration. Reviews of material properties and their effects on overall cellular behaviour indicate that materials with intermediate hydrophilic or hydrophobic characteristics are generally supportive of cell adhesion and attachment (Bačáková et al. 2004; Lynch et al. 2005). It is also proposed that materials with soft surfaces promote a round shape, reduced attachment, and reduced proliferation compared to hard surface materials (Bačáková et al. 2000; Bačáková et al. 2001; Bačáková et al. 2004).

Viability of cells on prospective materials is an important tool in determining material eligibility and biomimetic, non-toxic characteristics for cells (Tsou et al. 2016; R. Yang et al. 2017). The current study established a higher rate of viable vs. dead cells for all cells involved on both polymers (Figure 4-3). Cell number counts however indicated a dramatic difference between pNTBAM and pNIPAM with higher cell numbers evident on pNTBAM (Figure 4-4). Cells seeded on pNIPAM, although remaining viable at day 21, stayed at or around the original seeding density. The soft surface features of pNIPAM may not be suitable for the support of cell proliferation. These results have confirmed the impact of hydrogel chemistry on different cell shape, growth pattern, and cell number. pNIPAM hydrophilic behaviour has likely increased the percentage of water content forming a more flexible, soft surface, promoting growth in clusters without an increase in cell number (Keselowsky et al. 2003; Bačáková et al. 2004; Tan et al. 2005). The current finding were in agreement with certain

studies that indicated the effects of material stiffness on impacting cell shape and proliferation in addition to cell attachment (Rehfeldt et al. 2007; V Thomas et al. 2017; Basu et al. 2018). Engler et. al. studied the performance of cells in response to their mechanical microenvironment. They revealed the importance of stiffness on having a flattened and higher proliferation rate and viability versus a spherical cell shape and more aggregates using softer surfaces. This is probably related to alter cell signalling when the cells are sensing their ground matrix (Engler et al. 2004; Engler et al. 2006)

The ability of cells to migrate within the hydrogel construct is determined by the porosity and internal architecture of the tested material. Several previous studies have indicated the importance of interconnected porous structures on guiding cell behaviour. This enables penetration of cells towards the core of the scaffold optimising signalling communication throughout (Karageorgiou and Kaplan 2005; Murphy et al. 2010; Sobral et al. 2011; Turnbull et al. 2018). The current data indicated that pNIPAM (0.042 g/mL) supported cell migration below the surface region. This was observed with both primary human cells and immortal cell lines (Figures 4-5, 4-8). In contrast pNTBAM did not support cell penetration, even with the lower monomeric concentration, which may be due to the smaller average pore size obtained for pNTBAM versus pNIPAM (Chapter 3). There may also be a correlation to the more hydrophobic behaviour of pNTBAM. As the production of these hydrogels involves phase separation, less monomeric concentration is associated with more water being incorporated between polymer phase when using a hydrophilic polymer like pNIPAM with water solvent. However, the more water repelling properties presented by pNTBAM in addition to the use of methanol solvent ultimately promoted more dense mass with less water being enclosed within polymer part and less interconnected porosity (Mane 2016; Remanan et al. 2018; Khoryani et al. 2018).

Illustrating the above facts, it can be assumed that pNIPAM 0.042 g/mL may advice for a higher number of cells compared to the other subgroups. this is possibly attributed to the cells are being migrated within the hydrogel. The cell number may still lower than pNTBAM

relevant to the significantly increased cell population upon pNTBAM sub-groups. However, this could be an added bonus to the pNIPAM 0.042 g/mL sub-group indicating more eligibility for hosting vital number of cells in addition to allowing cells migration owing to its porous structure.

In line with the main goal of creating an osteochondral scaffold, the current work proceeded to examine primary cells responses to culture upon pNIPAM and pNTBAM hydrogels. The findings from ALP and mineral association determined that the highest mineral association was observed from hOBs seeded on pNTBAM, although a progressive increase was obvious for pNIPAM. This is also noticeable from alizarin staining showing a clearly positive staining with pNIPAM samples which was more evident with hOBs. Signs of active mineralization were significantly lower with hCHs upon pNTBAM which again was evident from alizarin staining (Figures 4-11, 4-12). In contrast, GAG content was highest for hCHs on pNTBAM which progressively increased with time according to DMMB assay. These preliminary findings might be an indication of each hydrogel's possible trend towards supporting specific cell behaviour (Figure 4-14). It is evident that both hydrogels were able to host mineralization production with higher tendency for hOBs upon pNTBAM, whereas pNTBAM has supported hCHs GAGs production to significantly higher degree compared to pNIPAM.

In an attempt to create an osteochondral scaffold, the above results are of importance as we need to mimic the natural tissue. The region spanning the sub-chondral bone up to the articular cartilage layers normally hosts a mineral gradient that gradually shifts from bone cells to hypertrophic chondrocytes at the calcified cartilage layer. This gradient is restricted by the tidemark junction before the middle cartilage zone where no further mineralization is formed by cells (Burr 2004; Hoemann et al. 2012b; Pal 2014). The current results might suggest the validity of these hydrogels to create a scaffold that will host variable mineralization tendencies from variable cell types (bone and cartilage).

Immunostaining coupled with ELISA established that the level of collagen I showed significant elevation with both hydrogels more specifically with pNTBAM. This was shown as intense colour expression with immunostaining images (Figure 4-15). Collagen II indicated higher expression with hCHs on pNTBAM and less with pNIPAM; confirmed by ELISA which revealed significant levels of collagen II from hCHs on pNTBAM at day 21 (Figures 4-16, 4-21). The normal physiology of bone and cartilage highlights that these tissues are associated with collagens I and II but to different extents. This is identified normally by higher collagen I levels in bone which contrasts with cartilage tissues where collagen II is the major matrix protein. Between these regions the level of matrix proteins will increase or decrease along the tissue gradient depending on the cell type and the level of mineralization. This is basically recognized at the calcified cartilage region where hypertrophic chondrocytes started some increase in collagen II in addition to elevation of collagen X as an indicator of mineral association activity by cells (Hoemann et al. 2012b; Pal 2014). In locating mineralization parameters, the expression of collagen X was notably higher with hOBs and hCHs on pNIPAM compared to pNTBAM (Figure 4-17). This was in line with annexin A2 that showed significant increases with hOBs and hCHs upon pNIPAM compared to pNTBAM (Figures 4-20, 4-21). Annexins family are group of proteins of which annexin A2 is highly expressed by hypertrophic chondrocytes and bone cells and is one among 6 proteins of the same family whom are involved in promoting active matrix mineralization (Kirsch et al. 2000; Gillette & Nielsen-Preiss 2004; Genetos et al. 2014). In view of the current results, we could have a possible involvement of hCHs in a calcium mineralization process when seeded upon pNIPAM which was opposite to their behaviour on pNTBAM that went for a more chondrogenic activity.

Hydrogel surface chemistry and stiffness therefore have the potential to impact the final cell behaviour. Studies have shown that increased hydrogel's stiffness to beyond 33Kpa will enhance GAGs production by chondrocytes while materials presenting more NH- and OH- with less CH_3- chemical groups are involved in promoting osteogenic cell activity (Wells

2008; Wang et al. 2016; Cao et al. 2017b). The present findings might predict our materials properties as a factor in deciding cell behaviour owing to their different stiffness and variable percentage of CH_3- groups. All these facts might suggest the usefulness of the current hydrogels in creating a gradient scaffold mass that will support osteogenic and chondrogenic tissue regeneration at bone-cartilage interface.

4.7. Conclusion

The current results proven the ability of pNIPAM and pNTBAM polymers hydrogel construct to support cells adhesion to their surfaces. It also indicates good percentage of viable cells, including primary cell lines, upon their surfaces for up to 21 days. Calcium mineralization was hosted to a certain degree by both hydrogels, but a high tendency was noted with pNTBAM. Moreover, pNTBAM revealed higher tendency to promote chondrogenic behaviour unlike pNIPAM. This might refer to the variable tendencies for pNIPAM and pNTBAM to promote bone and cartilage cells respectively, and how the distinctive polymers properties impacted their relevant biological performances. Moreover, this could give a clue for a possible engagement of both hydrogel to create unique scaffold construct utilizing the variable behaviours obtained to reconstruct osteochondral region.

Chapter 5

Generating 3D (pNIPAM-pNTBAM) bio-glass enforced gradient scaffold to regenerate osteochondral region

5.1. Introduction

Osteochondral region has a unique structural variation that includes cells and tissues. It ranges from hard highly mineralised sub-chondral bone to a more flexible cartilage region. Within this region, a gradual transformation is developed allowing for a mineral and structural gradient that support the functional integrity of these tissues (Izadifar et al. 2012). Damage to the osteochondral region eliminates the consistency of this structure causing serious functional disabilities that demand medical intervention. Variable treatment strategies basically depend on the inflammatory response and cellular ability to regenerate damaged tissues, showed some positive results, however with certain limitations.

Tissue engineering approaches principally use an ECM substitute that will act as a template to support cells' growth and differentiation. A surplus range of materials with tissue-specific features may support this goal by promoting cells' specific functions to regenerate damaged tissues. The complex multi-structure of the osteochondral region may require a combination of two or more biomaterials in order to mimic the natural tissue construct. Studies have shown some progress by joining materials together to create a multi (bi- or tri-phasic) scaffold to guide the regeneration of certain tissues including the osteochondral region. However, the main challenge is the combining of these materials together into one unit; many have used protein glue to attach scaffold's layers producing an integral multi-layered construct. Problems from de-mixing or delamination were still existed and challenging such scaffold production.

This Chapter focuses on testing the possibility of joining pNIPAM and pNTBAM hydrogels, to produce a 3D gradient scaffold with multi-architectural features. As both hydrogels are produced using the same technique, we will make use of this feature to generate the gradient scaffold in a single manufacturing operation. The process of polymer elongation and cross-linking will be the bonding step to join these materials and at the same time generating gradient region while moving From one polymer to the other. The resultant scaffold construct will be tested furtherly regarding cells behaviour by focusing on the gradient interface region.

In an attempt to promote optimum cell performance across the proposed scaffold construct, bioactive glass (BG) fibres were introduced by vertically embedding them through the scaffolds mass. The BG material is a known osteoconductive mass that will support further mineralization and encourage osteogenic behaviour of cells (Hench 1996; Jones 2015). Several types of BG materials were existed and applied for biomedical researches. The current BG fibres are the phosphate based glass which their main constituents (calcium and phosphate) are extremely important for bone mineralization once they degrade to release these minerals (Hench 2006b; Hossain et al. 2018). The use of these fibres will aid the design of the current scaffold in two dimensions; they will leave empty channels after degradation allowing for cells migration; they will promote mineralization of this region enhancing bone cells function and promoting calcification of chondrocytes with the hope for matching the calcified cartilage region. These will be tested accordingly to assess the impact of BG fibres on cells behaviour.

5.2. Chapter aims

The current Chapter aims for the followings

- Testing the possibility of joining pNIPAM and pNTBAM to generate a gradient scaffold construct with further characterization.
- Embedding biodegradable glass fibres (BG) within scaffolds construct with evaluation of their degradation profile.
- Biological assessment of osteogenic and chondrogenic cell behaviour across gradient scaffold surface.
- Determining the impact of BG fibres on the resultant osteogenic and chondrogenic performances of cells compared to the non-BG samples.

5.3. Materials and methods

A detailed methodology for the current Chapter experiments is mentioned in Chapter 2.

5.3.1. Generating gradient scaffold

The same synthesis procedure used for single hydrogel production was applied to obtain the gradient hydrogel scaffold. The two main characteristics that differentiate between these polymers in terms of synthesis are the type of solvent and the timing required for hydrogel formation. These differences were used as a base to prepare gradient scaffold. Both polymers solutions were prepared individually; pNIPAM polymer solution was added to the container at the beginning and initiated for polymerization using TMED. After 40 seconds (enough time for the polymerization to start) pNIPAM-pNTBAM mixture was added followed by adding pNTBAM solution exactly after 1 minute. The timing was critical for obtaining the final scaffold construct. Samples were sealed with a cover and left overnight at room temperature for complete hardening (**C**hapter 2 section 2.2.3).

5.3.2. Characterisation of gradient scaffold regions

To identify regional differences across the resultant scaffold mass, an FTIR spectrum was taken. Gradient scaffold was sliced into pieces and scanned for spectral gradual change from the top to the bottom of the entire mass (Chapter 2 section 2.4.1.2). SEM imaging was performed as well to architectural differences across gradient regions (Chapter 2 section 2.4.4)

5.3.3. The inclusion of bioactive glass (BG) fibres

A 3D printed model was proposed as a mould to hold the BG fibres in a vertical direction. The mould was designed to host 16 fibres per sample evenly spaced throughout the base. Mould dimensions were 15 mm diameter x 10 mm thickness and fitted with a cylindrical plastic container. The polymer solution was prepared normally and cast over the mould; the whole unit was then sealed with a cap and stored at room temperature. The degradation pattern for BG fibres mass was tracked using a Raman microscope and micro CT scan (Chapter 2 section 2.3)

5.3.4. Biological assessment of gradient and BG enforced scaffolds

All complex scaffold structures (including combined polymers and BG enforced) were inspected to monitor cells behaviour upon their surfaces. Samples generally were washed several times with PBS at 37 °C before cell culturing upon their surfaces. Gradients samples were sliced vertically into 2 halves and cells were seeded upon the surface of section basically to the middle zone where polymer gradient is located. Alizarin red and alcian blue staining were applied to observe mineral and GAGs distribution over gradient hydrogel surface. Samples were tested furtherly for evidence of cell functional protein association including immunostaining and ELISA testing. Samples with BG fibres followed the same washing steps before cell culture, cells were seeded to the top of hydrogels. These samples were compared with the previously tested BG free hydrogels including gradients to verify the impact of BG fibres on cell overall behaviour (Chapter 2 sections 2.5.7, 2.7).

5.4. Statistics

All data were collected and analysed with Microsoft XL 2010 to calculate the mean, standard deviation and resulting graphs. Results obtained were compared using one and two-way ANOVA with Tukey's multiple comparisons test. Statistics were analysed using Origin Pro 8, the level of significance was set at $P \leq 0.05$.

5.5. Results

5.5.1. Gradient hydrogel architectural properties

The resultant scaffold appearance revealed the gradual change from one end to another, basically showing predominant white colour mass from pNTBAM layer with gradual transformation into transparent shape towards pNIPAM end layer (Figure 5-1 A).

The SEM imaging of three scaffold's compartments showed relatively parallel architectural features to the original hydrogels (Figure 5-1 B). This was mostly notable at both ends of the scaffold that corresponds to pNIPAM and pNTBAM. The interface region though showed variable pore shape and size, but mostly more dense, flake-like polymer aggregates.

The FTIR scan though revealed progressive change from one side of scaffold to the other one detected by tracking the specific bands regions of spectra for each polymer at around 1200 cm^{-1} of FTIR spectra (two bands at 1131 cm^{-1} and 1171 cm^{-1} for pNIPAM and one big band 1224 cm^{-1} for pNTBAM). The interface region spectra reveal the interference between the two polymers with gradual spectral peak reduction as moving from pNTBAM to pNIPAM area (Figure 5-1 C).

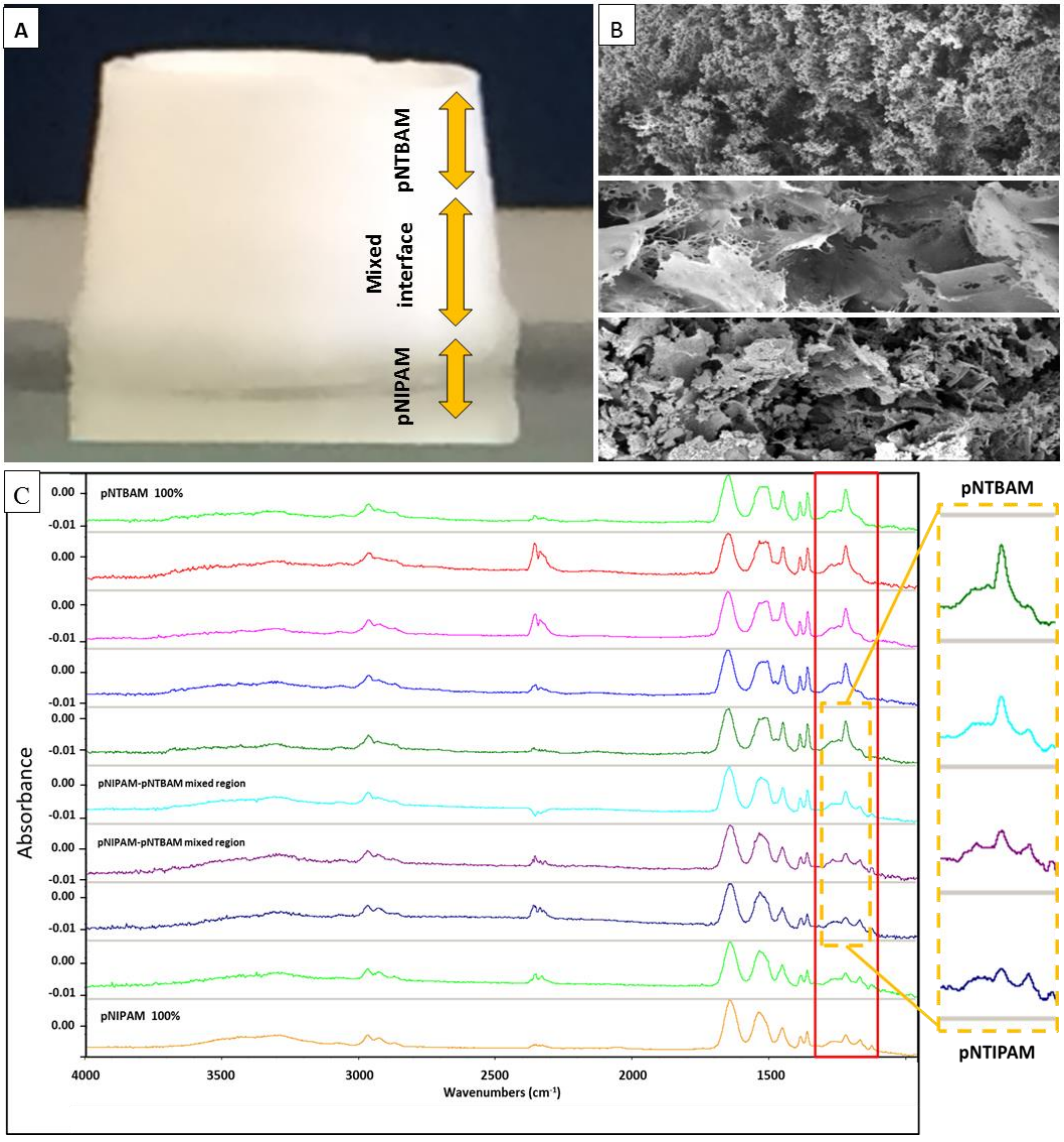

Figure 5-1. Characterisation and physical appearance of gradient hydrogel scaffold. *(A) Showing scaffold general appearance, arrows indicating the range of each polymer regions. (B) SEM imaging showing architectural variations between scaffold compartments where pNTBAM at the top and pNIPAM at the bottom layer and in between a mixed layer of the two polymers. (C) The FTIR spectra of several regions across the length of gradient scaffold starting from pNTBAM layer towards pNIPAM layer, the region marked with red rectangle corresponds to the finger print region specific for each polymer where the elevated peak from*

pNTBAM gradually transformed into two small peaks at the pNIPAM region. yellow dotted marked region represents the mixed polymer regions and peaks transformation.

5.5.2. Bio-glass (BG) mass evaluation

5.5.2.1. Raman microscopy

Raman mapping of hydrogel surface, where BG fibres included, enables us to identify the relevant regions of these components as a heat map. Raman spectra of pNIPAM-BG scaffold show the BG and hydrogel's spectral region indicating high peak elevation for the BG mass at 700 cm^{-1} and 1150 cm^{-1} (Figure 5-2 A). The pNIPAM spectrum corresponds to the CH- and NH- stretching bands at the higher Raman shift area (2800-3000 cm^{-1}). The BG spectral regions equivalent to to the P=O stretching bands at 1100-1170 cm^{-1} and P=O bending at 500-700 cm^{-1}. Mapping of sample surface, focusing on the BG region at 1150 cm^{-1}, generates a heat map that illustrates the Raman intensity of the BG band at this region (P=O stretch bands). The heat map comprises coloured areas indicative to the components peaks where the red reflects the higher Raman intensity (in this case the BG) down to the lowest intensity represented by blue. Tracking the BG fibre with time showed expanding of the green zone region across days 7 to 15 while shrinking of the red zone which reflects blending of these elements with hydrogel. The principal component analysis (PCA) of Raman enables the direct comparison of peaks within a number of ranges, in this case between 2800 and 3000 cm^{-1} (corresponding to the hydrogel) and 1100-1200 cm^{-1} (to illustrate the BG fibre band).

The starting point clearly shows that where there is BG present there is not hydrogel and vice versa. From day 7 the distinction between BG and hydrogel becomes less apparent. Further noticeably at day 15, where the correlation between the two peaks is unclear, indicating the diffusion and thus interaction of the ions with pNIPAM as a function of time. The heat maps illustrate the shrinking of the area where there is fibre as it degrades (Figure 5-2 B).

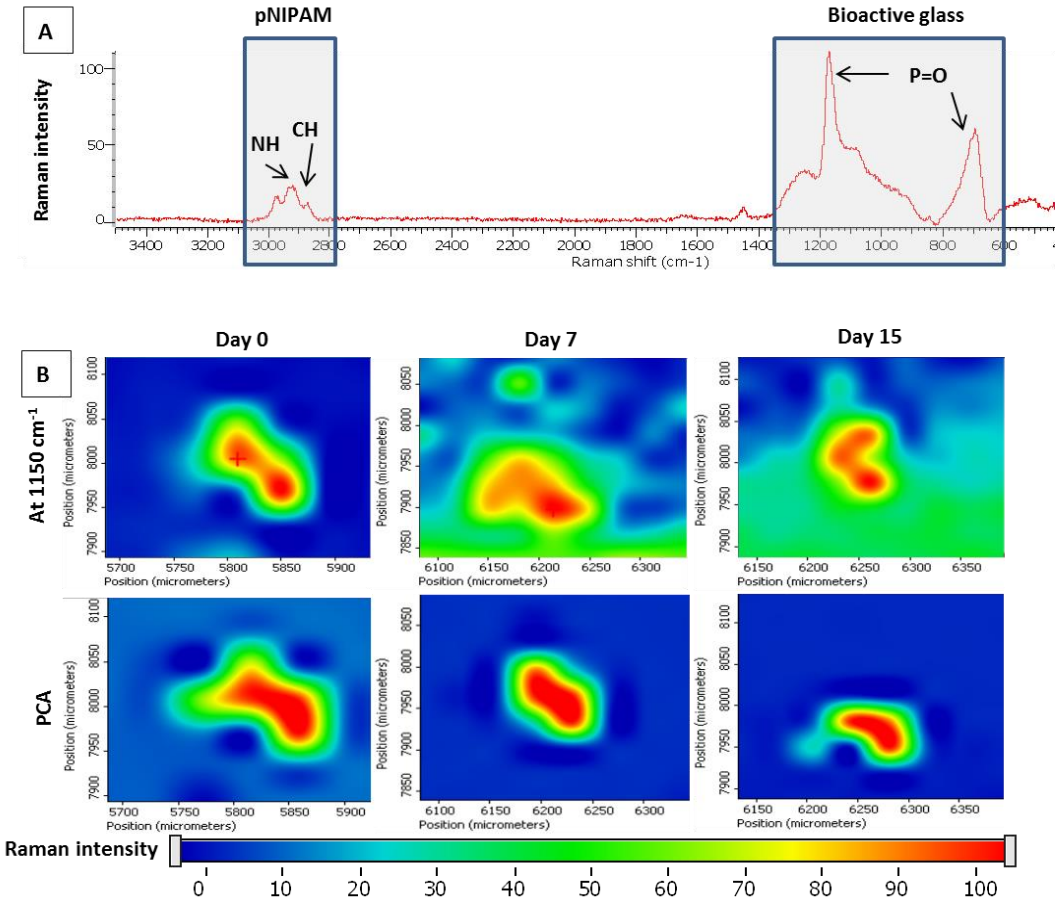

Figure 5-2. Raman mapping of BG mass embedded in hydrogel. *The figure is showing (A) spectral regions of pNIPAM and BG located in different regions, (B) heat map of sample surface focusing on single BG fibre at 1200 cm $^{-1}$ revealing the BG mass (red core), the green zone spreading at days 7, and 15 is indicating BG mass disintegration with time, analysis using PCA indicated mass shrinking from day 7 to 15.*

5.5.2.2. Micro computed tomography (µCT)

The use of µCT enables us to recognize the degradation of BG fibres within hydrogels by detecting the different densities between the hydrogel and BG fibres. As per the µCT, the hydrogel-BG composite was analysed to show the dense BG mass (brown colour) in transparent mass of hydrogel. The dense fibre mass was clearly fading with time reaching up to 28 days of incubation in PBS at 37 °C (Figure 5-3 A). The condition was almost the same for both hydrogels as both showed quite similar mass density. Density values assessed by the µCT, was plotted against time to reveal the BG mass reduction. the BG mass ratio was

evaluated in percentage of BG per the total volume of sample. results showed the reduction of BG fibres mass volume with time reaching the lowest level at day 28 (Figure 5-3 B).

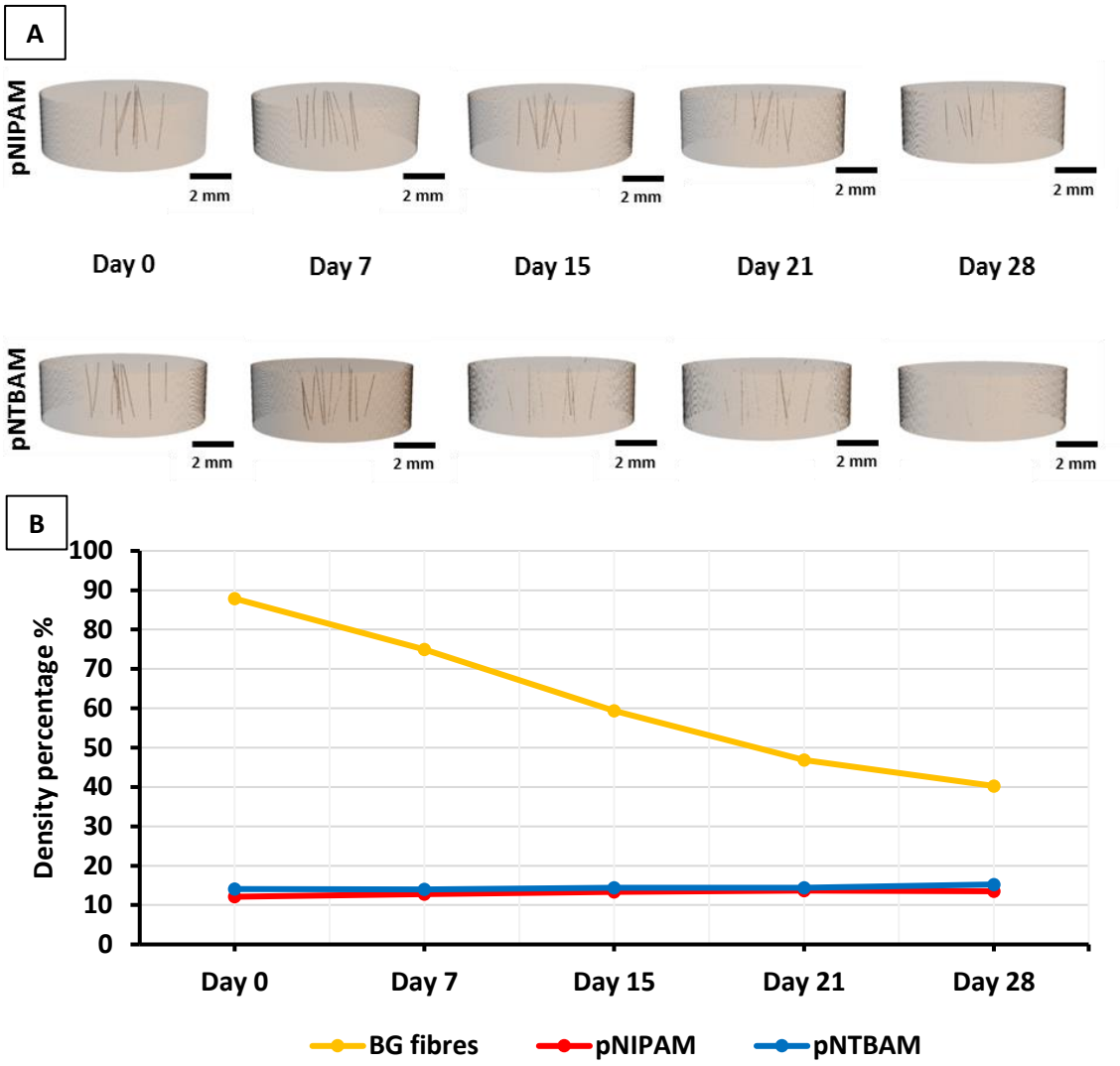

Figure 5-3. µCT scanning of hydrogel embedded BG mass for pNIPAM and pNTBAM. *A) Images are showing BG mass (brown colour) threaded within hydrogels (transparent) using µCT scanned with time (7, 15, 21, and 28 days). Images scale bar at 2 mm. B) BG fibres percentage of density reduction tracked with time up to day 28 compared to hydrogel density.*

5.5.2.3. Alizarin red stain as an evidence of BG degradation

hydrogel samples with BG fibres were assessed to locate BG fibres openings and evidence of mineral traces by staining with alizarin red. samples were stained after being incubated with PBS at 37 °C for 28 days. images from alizarin red stained sample revealed signs of BG

channels appeared as a red stained mark on the top of hydrogels. pNIPAM-BG samples though were easier to illustrate the BG channels when viewed microscopically, as it is transparent. alizarin staining showed the linings of the BG channels and most of the core stained red reflecting a diffused zone of redness surrounding the BG channel (Figure 5-4).

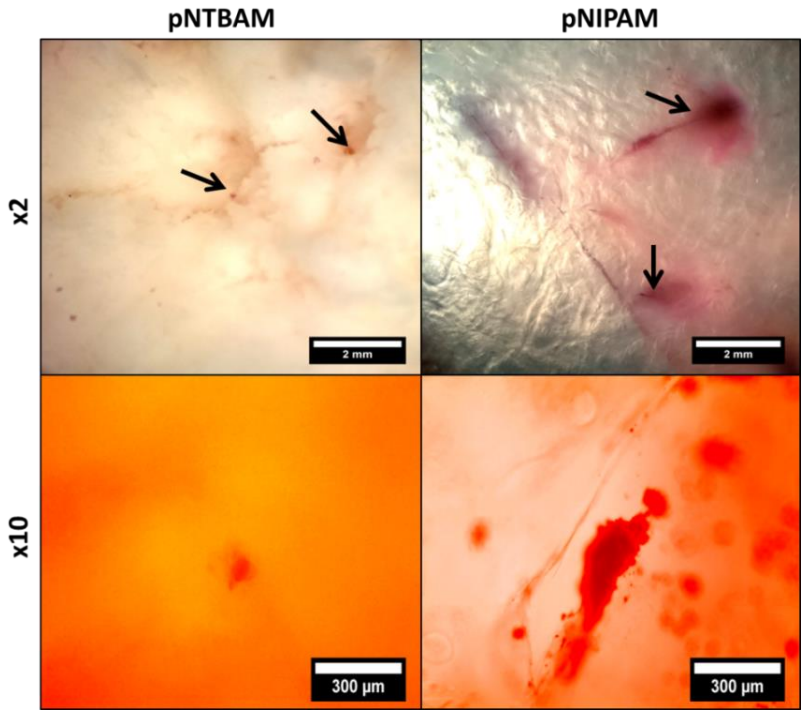

Figure 5-4. BG embedded hydrogels incubated with PBS at 37 °C and stained with alizarin red at day 21. *pNIPAM and pNTBAM hydrogels imaged at two magnifications (x2, and x10) showing the magnitude of staining for BG fibres and their degradation elements for both hydrogels. Scale bar measure 2 mm for x2 and 300 µm for x10 images.*

5.5.3. Biological assessment of gradient scaffold

5.5.3.1. Quantification of minerals and GAGs

Staining of gradient scaffold sections showed the arrangements of minerals and GAGs across the gradient area corresponding to each cell type. Alizarin stained hOBs samples obviously pointed out the prevalence of red stained calcium minerals throughout the surface (Figure 5-5). An increased minerals level towards pNIPAM region was noticeable by the slightly enhanced redness. Gradient samples with hCHs obviously showed less alizarin red

staining for the whole sample surface, however, with evidence of calcium minerals association observed at the interface region.

GAG contents, according to alcian blue stain, revealed fewer amounts associated with hOBs samples mostly close to control samples. An enormous staining was clear with hCHs samples towards pNTBAM region which seems to be opposed at the junction before pNIPAM side.

Quantifying calcium ions over 21 days of cell culture has shown significantly increased levels with time when tracking hOBs samples mostly with osteogenic media which also was significant compared to basic media samples (Figure 5-6 A). These results were obviously significantly higher than samples with hCHs seeded at the same cells density. Gradient samples with hCHs were not significantly different between basic and chondrogenic media sample sets.

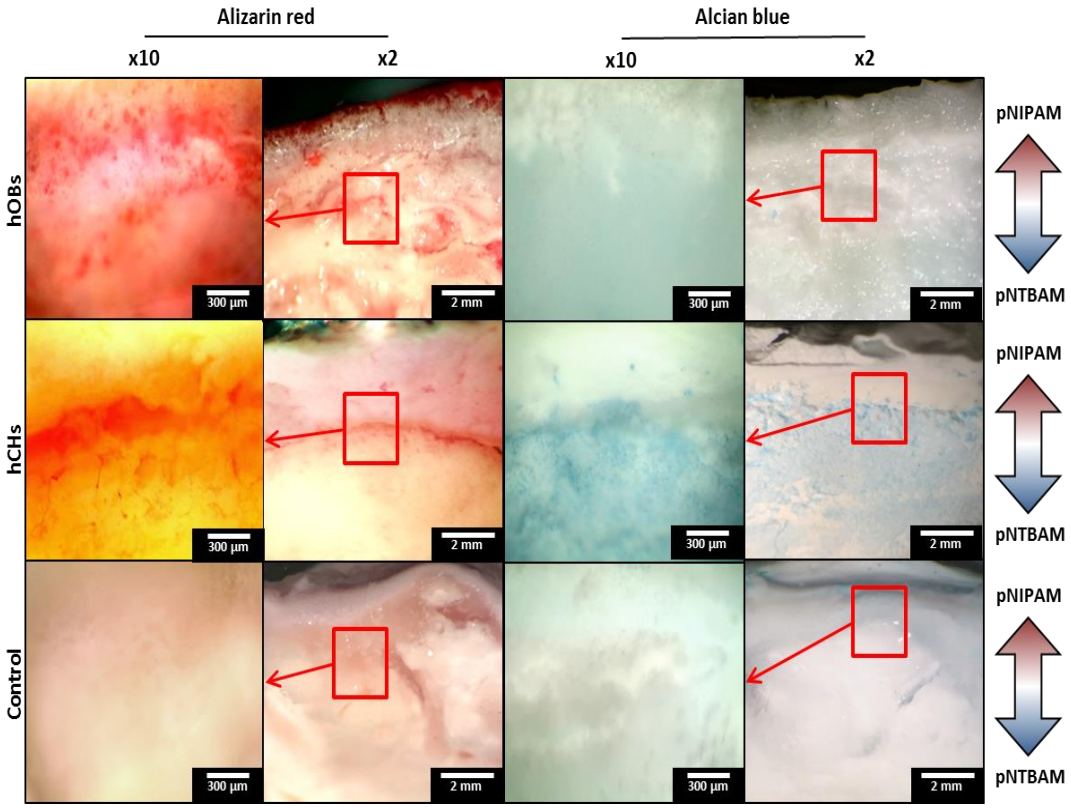

Figure 5-5. Alizarin and alcian blue stained gradient hydrogel sections seeded with hOBs and hCHs. *Images are illustrating gradients samples captured at two magnifications (x2) for the whole sample and (x10) for the interface region (marked red square). Images rows are referring to each cell type in addition to control samples at the bottom. The far right up-down arrow key-figures are indicative for the scaffold's regions between pNIPAM and pNTBAM for images row. Scale bar measure 2 mm for the x2 and 300 µm for the x10 images.*

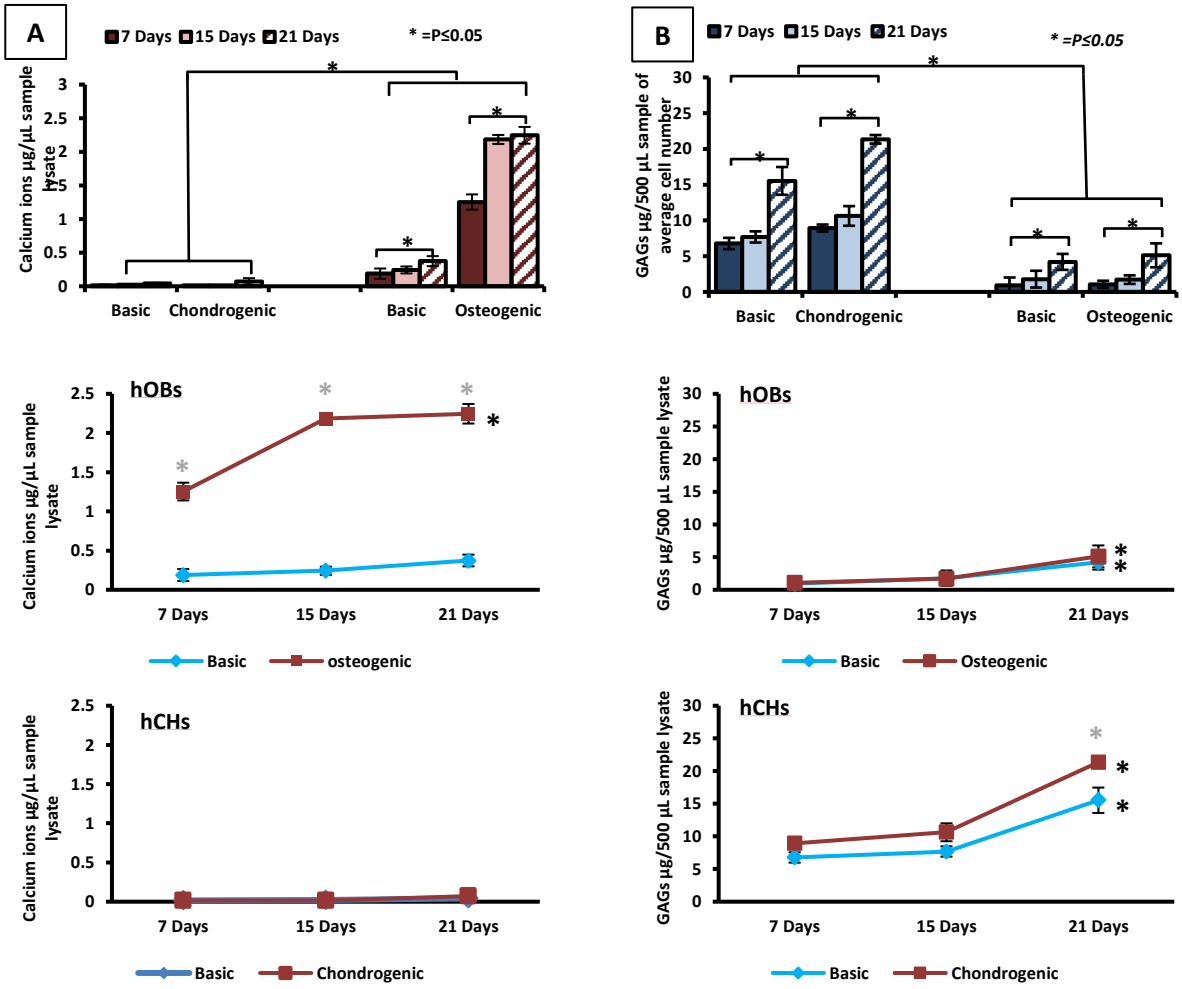

Figure 5-6. Quantifying calcium ions and GAGs contents upon gradient hydrogels. *(A) Calcium ions in µg/µL of sample lysate, (B) the amount of GAGs in µg/500µL of sample lysate. The top bar figures are comparing all samples with hOBs and hCHs for the levels of calcium ions and GAGs, the bottom figures are the relevant monitoring of these levels per each cell type compared to their control. Asterisks indicate significance at P ≤0.05, for the bottom figures the light asterisk (*) is the significance between sample and control at each time point and the dark one (*) is indicative for significance with time (results represent the mean ±SD, n=3).*

DMMB assay clearly revealed higher GAGs associated with gradient sample seeded with hCHs (Figure 5-6 B). The levels were significantly higher with chondrogenic media compared to basic media control samples and compared to other samples seeded with hOBs. Monitoring GAGs amounts with time showed a progressive increase with time up to day 21 for all tested samples including hOBs samples.

5.5.3.2. Immune staining for collagens I, II, and X

Images from immune-stained samples showed the expression of collagen I and II relevant to each cell type in addition to collagen X (Figure 5-7). Red fluorescent level indicated intense colour for collagen I in hOBs samples. Some staining was seen for hCHs which might be higher when compared to the same cells upon original hydrogels (Chapter 4, Figure 4-15). Expression for collagen II revealed less strength for hOBs and medium to low stages for hCHs which is lower when compared to the previous imaging for individual hydrogels (Chapter 4, Figure 4-16). The green fluorescent (FITC), indicative for collagen X, revealed higher expression for both cell types observed at the middle zone of gradient samples. The fluorescent level seems to be evenly expressed for hOBs and hCHs with a bit more intensity for hOBs.

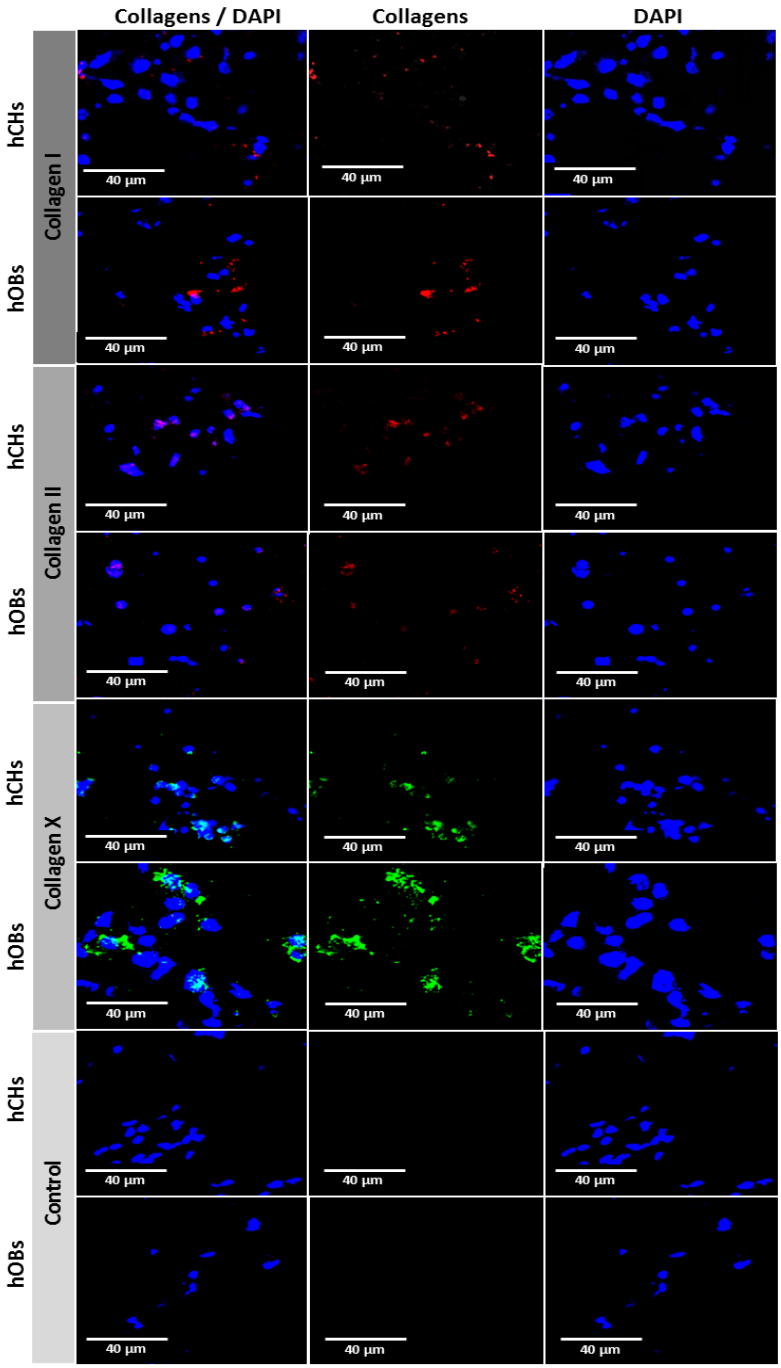

Figure 5-7. Immune-stained gradients samples seeded with hOBs and hCHs for collagens I, II, and X. *Confocal images are explained in columns for the magnifications x40 showing collagens expressions and cells nuclei plus a merged x40. Images rows are corresponding to collagen types each with particular cell type. Controls are samples with hOBs and hCHs incubated with secondary antibodies marked with TRITC (red) and FITC (green) without primary antibodies. Images scale bar measure 40µm for the x40 and 200µm for the x10 images (Images were captured using Olympus U-TBI90 laser fluorescent confocal microscope).*

5.5.3.3. ELISA immune assay

Monitoring of collagen I level exposed a progressive significant increase with hOBs samples using osteogenic media. Levels were apparently shifted to a greater value after day 15. Results, however, were not significant using basic media with variable measures reaching day 21 (Figure 5-8 A). Some elevations in collagen I was recorded for hCHs gradient samples which was not significantly altered, neither by day 21 nor between basic or chondrogenic media sets. When compared at day 21, hOBs using osteogenic media clearly indicated significantly higher levels compared to hCHs samples or other basic media samples.

Collagen II levels were very low at day 7 that barely can be recognized with both cell types. However, gradient samples with hCHs evoked a significant increase from day 15 which was parallel in terms of basic or chondrogenic media at this point. Levels with chondrogenic media though were recorded to be significantly higher than basic control samples reaching day 21 of culturing (Figure 5-8 B). Gradient hydrogels with hOBs had also shown significant ($P \leq 0.05$) elevation using osteogenic media which were plateaued after day 15 towards day 21, this was significant compared to basic media sample set. When reviewing the whole results set at day 21, hCHs samples with chondrogenic media showed a significant amount comparing to the other basic or hOBs samples.

Gradient samples with hOBs and hCHs revealed significantly increased annexin A2 levels with time which might refer to increased mineral layout activity. Amounts were significantly shifted to higher level with hOBs osteogenic media set compared to basic media (Figure 5-8 C). The situation with hCHs indicated parallel increase with time for both chondrogenic and basic media sample set with no significant difference. The final comparison revealed significant amounts for hOBs samples compared to hCHs and controls at day 21.

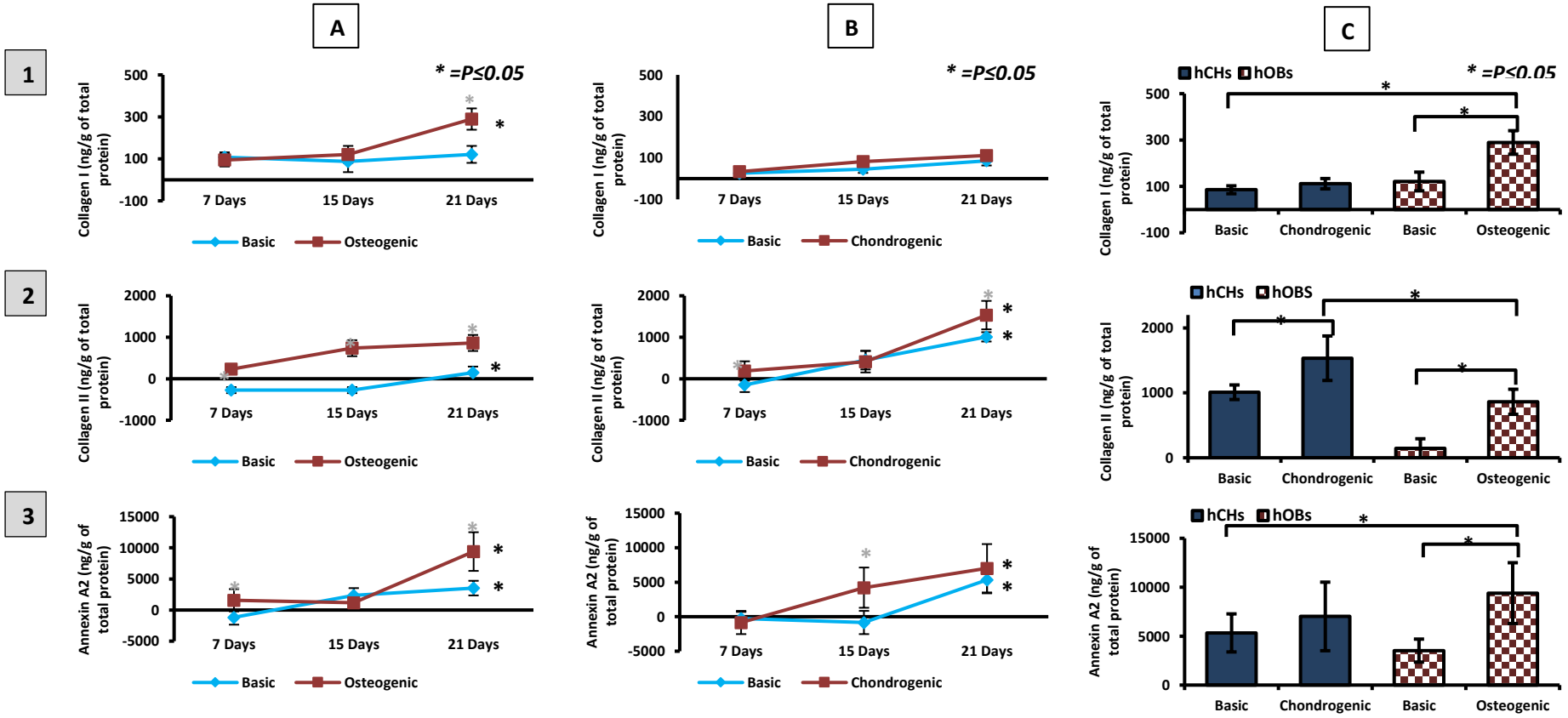

Figure 5-8. Quantifying collagens I, II and annexin A2 on gradient hydrogels seeded with hOBs and hCHs. *Figures rows represent each marker level (1) collagen I, (2) collagen II, and (3) annexin A2. Figure columns are revealing marker level monitored with time for (A) hCHs and (B) hOBs respectively with the final comparison of levels at day 21(C) illustrated in the right side column bar figure. Each marker quantified in ng/g of total protein measured in sample lysate. Asterisks indicate significance at P≤0.05, for the time monitoring figures the light asterisk (*) is the significance between sample and control at each time point and the dark one (*) is indicative for significance with time (results represent the mean ±SD, n=3).*

5.5.4. BG embedded scaffold assessment

5.5.4.1. Assessment of cells travelling through BG fibres channels

3D images from confocal microscope showed cells (DAPI stained MG63 cells) gathering into BG fibre location with little evidence of infiltration through these channels for both pNIPAM and pNTBAM hydrogels. Cells may appear forming clusters or accumulates at the openings of these channels. pNIPAM samples also shows cells migration within porous structure (mentioned in Chapter 4) surrounding BG fibres region. This was in contrast to pNTBAM where cells set on the surface while some are clustering trying to migrate through BG openings (Figure 5-9).

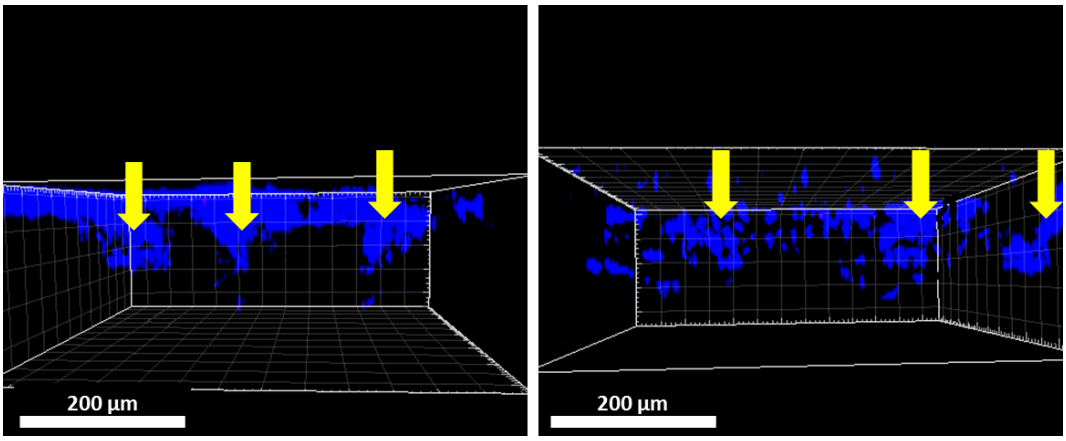

pNTBAM **pNIPAM**

Figure 5-9. Assessment of MG63 travelling through degraded BG fibres channels of pNTBAM and pNIPAM hydrogels. *Confocal 3D image sections for pNIPAM and pNTBAM showing DAPI stained MG63 cells (blue) to the surface of hydrogels and accumulating around BG fibre channels. Yellow arrows indicate BG fibres locations.*

5.5.4.2. Calcium minerals and GAGs

The comparison between hydrogel samples based on the existence or absence of BG fibres were all held using cell-specific functional media set (osteogenic or chondrogenic media).

The assessment of calcium ions upon hydrogel samples with BG fibres has shown elevation when compared to hydrogels with no BG mostly with hOBs samples. Samples of hOBs with BG encountered significantly increased values with time with a shifted increase at day 21, these were noticeable for both pNTBAM (Figure 5-10 A) and pNIPAM samples (Figure 5-10 B). The situation with hCHs has also witnessed significant elevation of calcium ions with time. However, these were mostly observed with pNIPAM samples and reported no significant difference as to the presence or absence of BG fibres. The pNTBAM samples with hCHs reveal no apparent increase in calcium ions with time. BG samples though indicated an increase whitch was obvious at day 21 only.

The evaluation of GAGs for BG hydrogel samples indicated progressively increased amounts with time recognized only for pNTBAM (Figure 5-11 A) with hCHs and was significantly higher than hOBs samples. Surprisingly, the levels of GAGs were significantly higher with pNTBAM-BG samples. However, the impact of BG fibres on hOBs for pNTBAM samples showed no apparent difference. Additionally, the whole set didn't expose relevant increase with time. The GAGs content for pNIPAM (Figure 5-11 B) samples was quite parallel compared to all samples weather according to cell types or BG enforced ones and has shown non-significant alteration with time.

Comparing results of calcium ions and GAGs at day 21 clearly revealed significant elevation of calcium ions for hOBs-BG samples indicated for both pNIPAM and pNTBAM samples with higher levels seen for hOBs on pNTBAM-BG samples. The least amount was measured for hCHs on pNTBAM with no obvious difference between original and BG containing samples (Figure 5-10 C). The GAGs content notably was higher with pNTBAM-BG seeded

with hCHs, while no significant (P >0.05) variation has been recorded for hOBs between BG and non-BG samples (Figure 5-11 C).

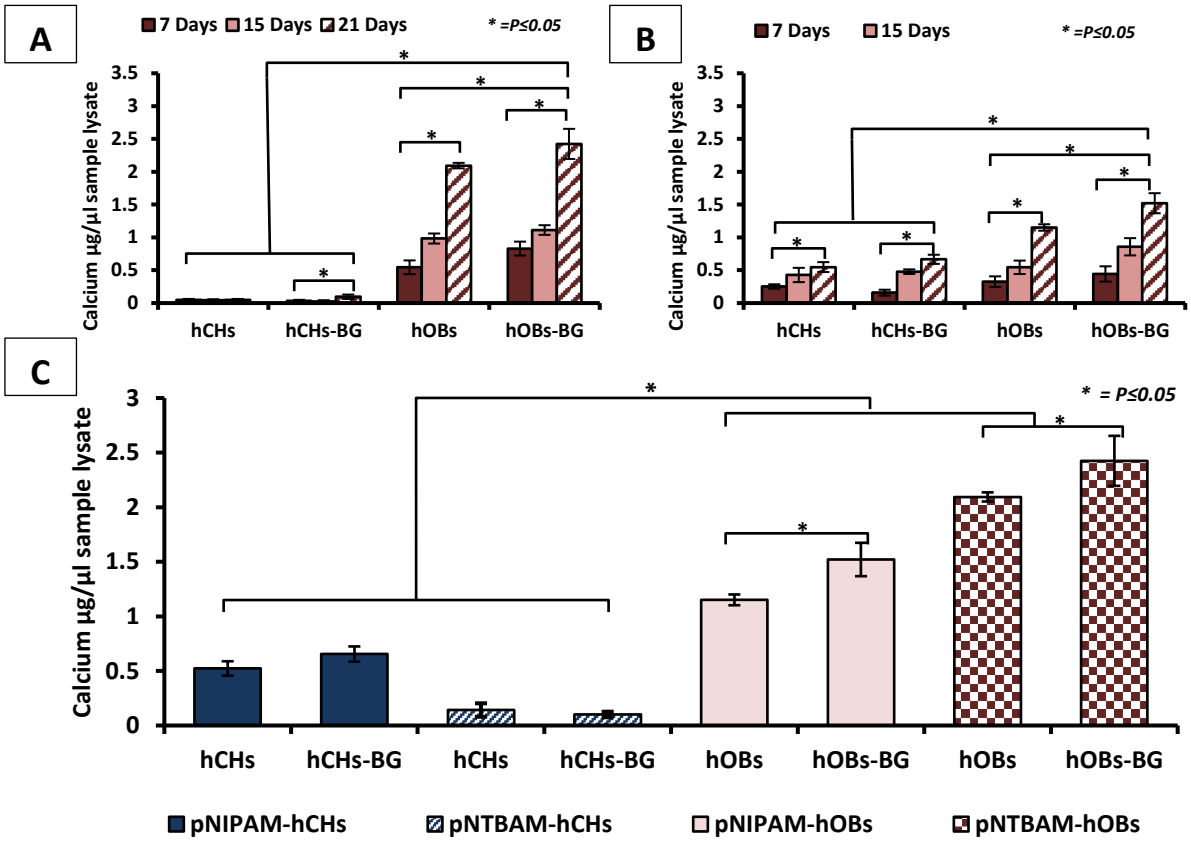

Figure 5-10. Comparing calcium mineral association between plain and BG enforced hydrogels seeded with hOBs and hCHs. *Figures are revealing the calcium ions measured in µg/µL of sample lysate for (A) pNTBAM and (B) pNIPAM compared between BG and non-BG samples while (C) represents the comparison between BG and non-BG of all samples at day 21. Asterisks indicate significant levels at P≤0.05 (Results are representing mean ±SD, n=3)*

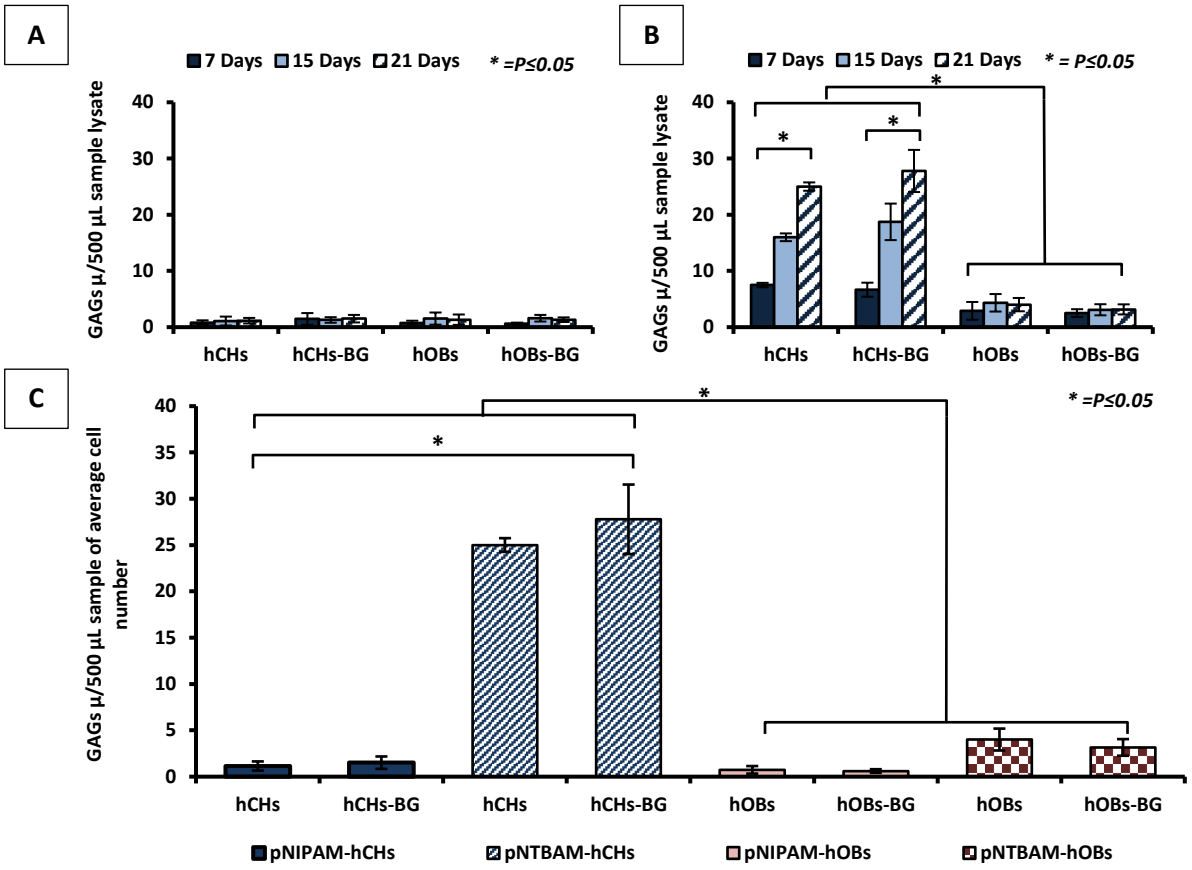

Figure 5-11. The amounts of GAGs measured in BG versus non-BG hydrogel samples seeded with hOBs and hCHs. *The amounts of GAGs measured in µg/500 µL of sample lysate for (A) pNTBAM and (B) pNIPAM compared between BG and non-BG samples while (C) represents the comparison between BG and non-BG of all samples at day 21. Asterisks indicate significant levels at P ≤0.05 (Results are representing mean ±SD, n=3).*

Evaluation of calcium minerals upon gradient scaffold showed manifested impact of BG fibres on cells overall mineral association. This was mostly observed with hOBs when calcium ions started gradual increase up to day 15 then obviously boosted to a maximum level at day 21 (Figure 5-12 A). The hCHs samples revealed some increased levels of calcium minerals with the BG samples evident by day 15, further increase was then plateaued reaching day 21. Overall comparison at day 21 defines a significant alteration in BG samples versus the original gradient scaffold measured for hOBs samples (Figure 5-12 B).

In determining the effects of BG fibres upon GAGs level, results indicated no significant difference observed for BG samples. The amount of GAGs was significantly higher for hCHs

and in line with that measured for non-BG samples when monitored with time (Figure 5-13 A). The final comparison at day 21 showed no significantly altered results relevant to introducing BG fibres (Figure 5-13 B).

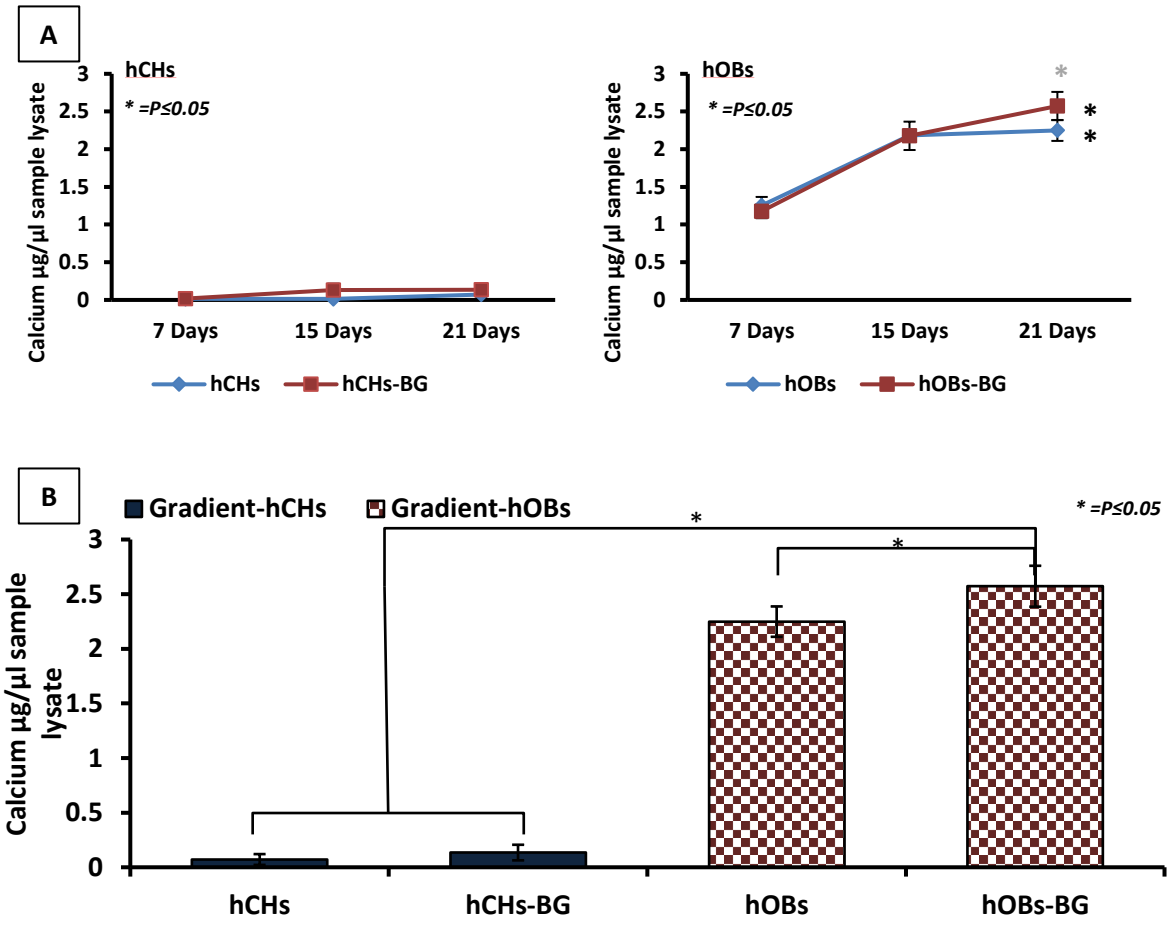

Figure 5-12. Assessment of calcium ions in BG and non-BG gradient scaffolds seeded with hOBs and hCHs. *(A) Calcium ions level monitored with time for each cell type compared between BG and non-BG samples, (B) comparing all samples for the level of calcium ions at day 21. Asterisks indicate significant levels at P ≤0.05 (Results are representing mean ±SD, n=3).*

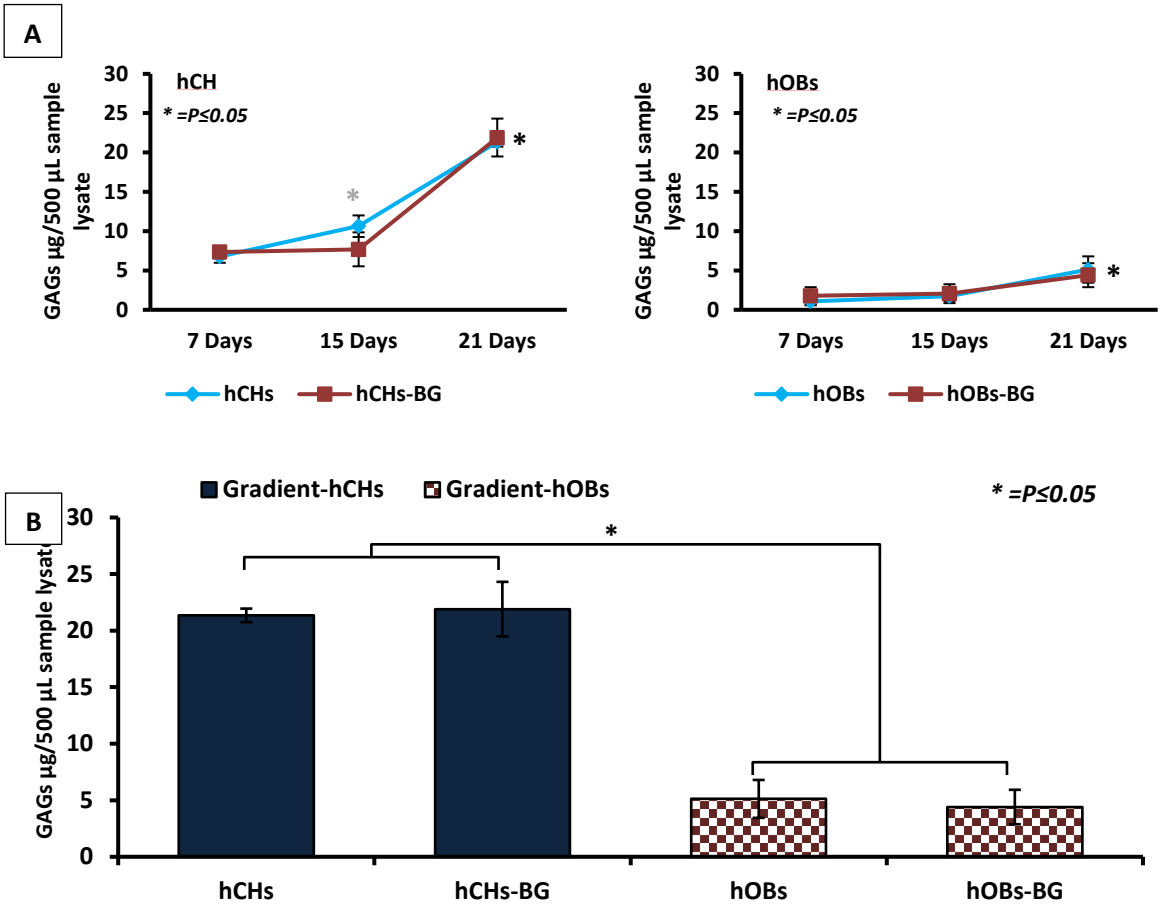

Figure 5-13. The amount of GAGs in BG vs non-BG gradient scaffolds. *(A) GAG contents monitored with time for each cell type compared between BG and non-BG samples, (B) the levels of GAG compared between all samples at day 21. Asterisks indicate significant levels at P ≤0.05 (Results are representing mean ±SD, n=3)*

5.5.4.3. ELISA detection of proteins for BG scaffolds

Results according to ELISA revealed the effects of embedding BG fibres within hydrogels construct on the relevant cells' activity. Collagen I showed an advanced level in pNIPAM-BG samples seeded with hOBs compared to the non-BG samples. Results reported significant amounts with time up to day 21, but a further increase was obvious in BG samples (Figure 5-14 A). The pNTBAM-BG samples seeded with hOBs had also indicated a significant increase of collagen I with time. The BG samples measured significantly higher

levels at day 7 reaching to day 15, but thereafter continue to rise to be in line with the non-BG samples reporting around the same level at day 21 (Figure 5-14 B). The pNIPAM-BG samples with hCHs have a little increase with time as previously monitored for non-BG samples, though some elevation was observed at day 7 and 15 which then returned to be in line with the non-BG samples at day 21. The pNTBAM-hCHs samples seem to present around equal levels of collagen I for both the BG and non-BG samples, even though, fewer amounts were noticed in general for BG samples.

In monitoring collagen II levels, non-significantly altered measures between BG and non-BG samples were observed for pNIPAM samples seeded with hCHs (Figure 5-15 A). The situation with pNTBAM-hCHs carried significant variation between BG and non-BG samples manifested by extremely lowered collagen II levels compared to the non-BG. The levels actually have significant elevation with time, but the amounts of collagen II retreated to be less since day 7 and reaching day 21 (Figure 5-15 B). Hydrogel samples with hOBs had only little elevation of collagen II manifested for pNIPAM and pNTBAM. Levels for BG samples were in line with the non-BG samples with only some increase over the non-BG samples observed with pNIPAM. Such increase was significant at some points notably from day 15-21. The pNTBAM-BG samples were not significantly altered from the non-BG ones and were fluctuated around the same levels.

Results of measuring annexin A2 clearly showed significant elevation with BG samples relevant to non-BG. Altered levels were mostly obvious with hCHs weather pNIPAM (Figure 5-16 A) or pNTBAM (Figure 5-16 B), these were notably started progressive elevation away from non-BG samples since day 7. Samples with hOBs have shown overall significantly higher levels for pNTBAM-BG compared to non-BG at all time points. The pNIPAM-BG samples though had a significant increase at the early time points, it went to be close to the level of non-BG samples.

Comparing results between BG and non-BG hydrogel samples at day 21, revealed the variation between cells' activities upon each specific hydrogel type and the impact of embedding BG fibres to their construct. BG fibres obviously impacted a significant increase in collagen I level for hOBs with pNIPAM-BG compared to non-BG but no significant difference between pNTBAM-BG and non-BG. Other hydrogel samples indicated non-significant variation of collagen I for BG introduction with hOBs or hCHs, lower level was recorded to pNTBAM-hCHs (Figure 5-17 A). Collagen II has significantly lower value with pNTBAM-BG samples of hCHs. Significantly increased level, however, were reported with pNIPAM-BG samples weather hOBs or hCHs (Figure 5-17 B). Annexin A2 values had significantly ($P \leq 0.05$) elevated with pNIPAM-BG and pNTBAM-BG samples seeded with hCHs. These value also witnessed significant elevation with hOBs upon pNTBAM-BG, but still with no significant ($P > 0.05$) variation revealed with hOBs on pNIPAM-BG samples (Figure 5-17 C).

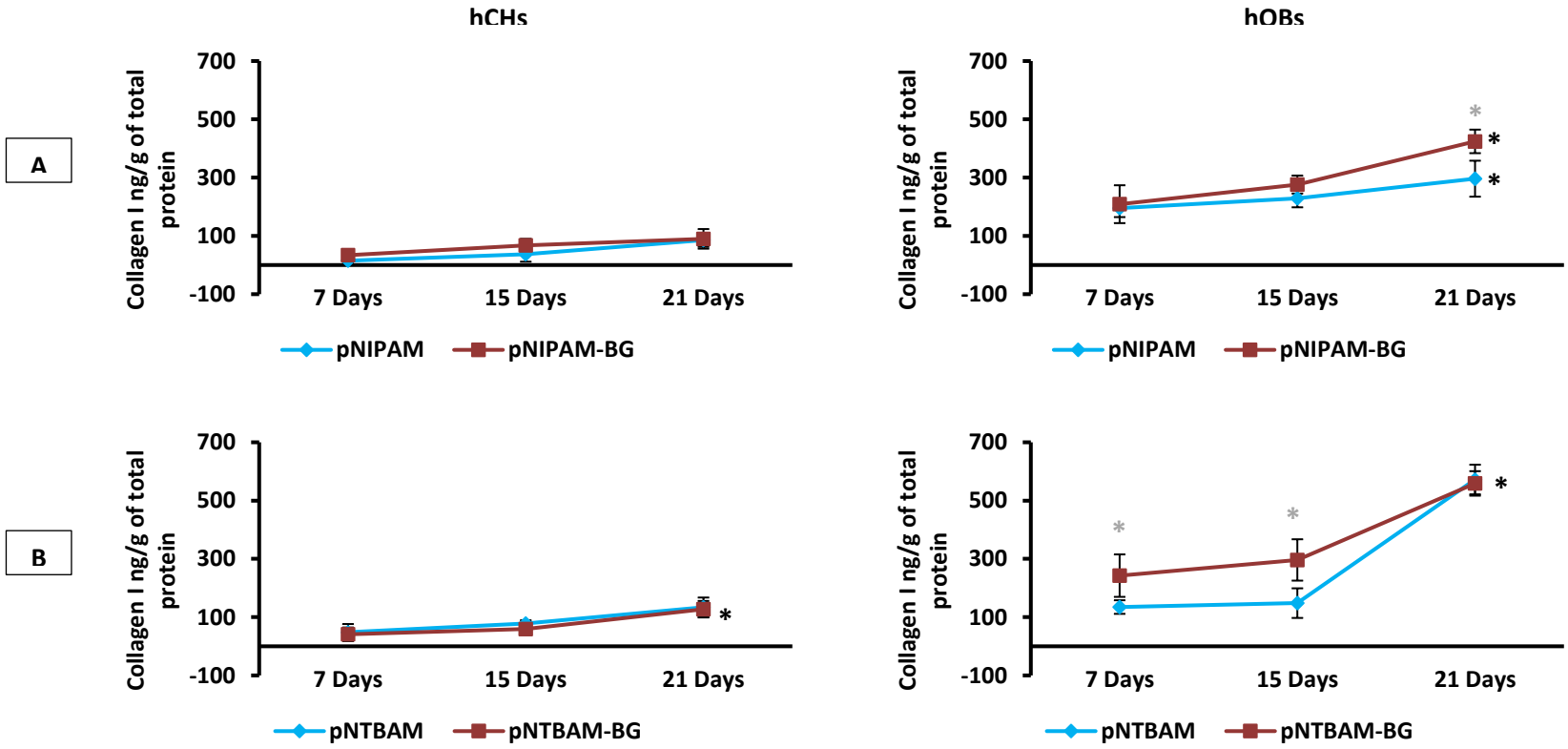

Figure 5-14. Comparing collagen I level measured in BG versus non-BG hydrogels seeded with hOBs and hCHs. *The level of collagen I in ng/g of total protein measured in sample lysate. The figures are arranged in columns indicating each cell type (hCHs and hOBs) and in rows representing each hydrogel type where (A) is pNIPAM and (B) is pNTBAM. Each comparison was held between BG (red square marks line) and non-BG (blue diamond marks line) samples monitored with time. Asterisks indicate significance at P ≤0.05, the light asterisk (*) is the significance between sample and control at each time point and the dark one (*) is indicative for significance with time (results represent the mean ±SD, n=3).*

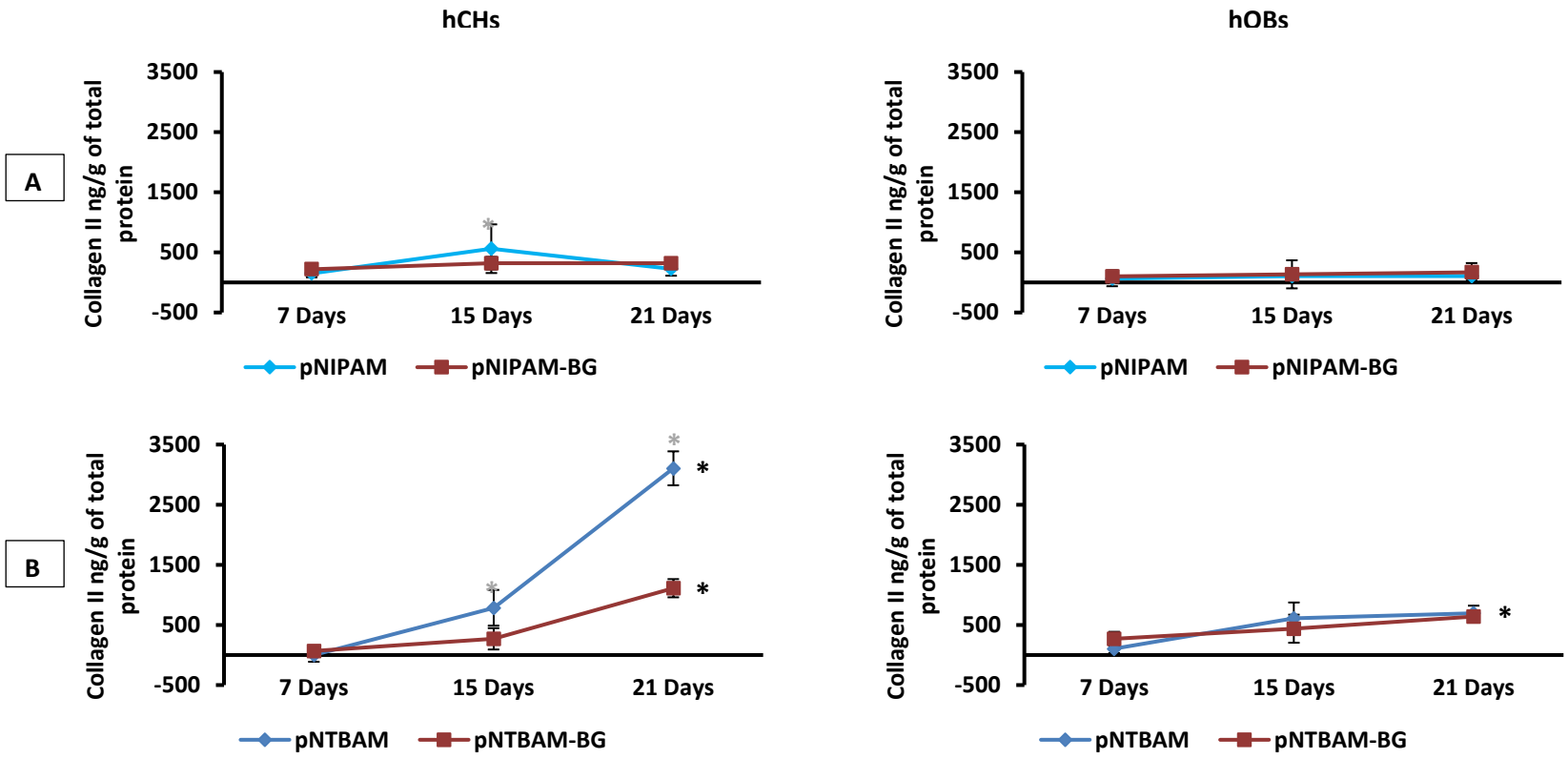

Figure 5-15. Comparing collagen II levels measured in BG versus non-BG hydrogels seeded with hOBs and hCHs. *The level of collagen II in ng/g of total protein measured in sample lysate. The figures are arranged in columns indicating each cell type (hCHs and hOBs) and in rows representing each hydrogel type where (A) is pNIPAM and (B) is pNTBAM. Each comparison was held between BG (red square marks line) and non-BG (blue diamond marks line) samples monitored with time. Asterisks indicate significance at P ≤0.05, the light asterisk (*) is the significance between sample and control at each time point and the dark one (*) is indicative for significance with time (results represent the mean ±SD, n=3).*

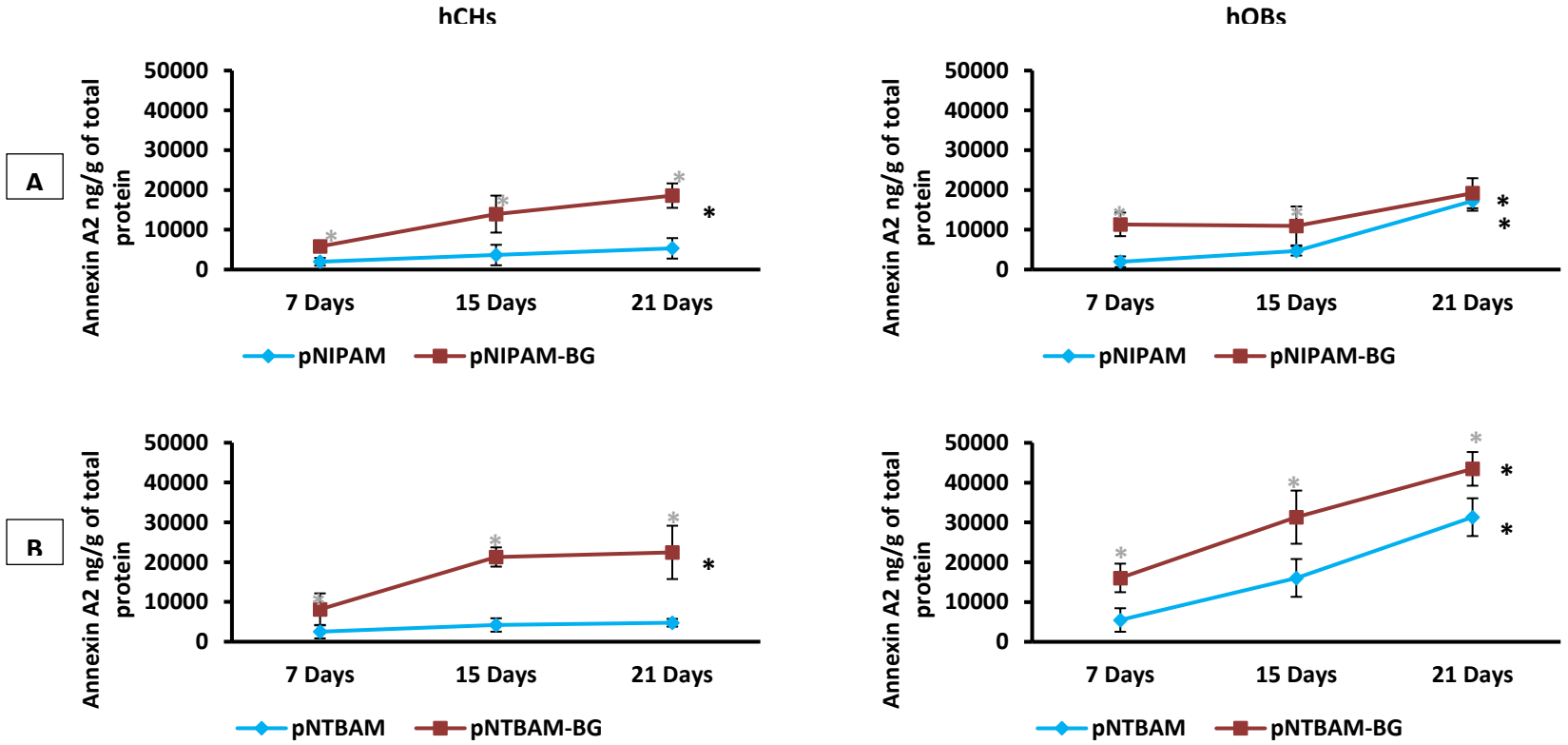

Figure 5-16. Comparing annexin A2 levels measured in BG versus non-BG hydrogels seeded with hOBs and hCHs. *The level of annexin A2 in ng/g of total protein measured in sample lysate. The figures are arranged in columns indicating each cell type (hCHs and hOBs) and in rows representing each hydrogel type where (A) is pNIPAM and (B) is pNTBAM. Each comparison was held between BG (red square marks line) and non-BG (blue diamond marks line) samples monitored with time. Asterisks indicate significance at P ≤0.05, the light asterisk (*) is the significance between sample and control at each time point and the dark one (*) is indicative for significance with time (results represent the mean ±SD, n=3).*

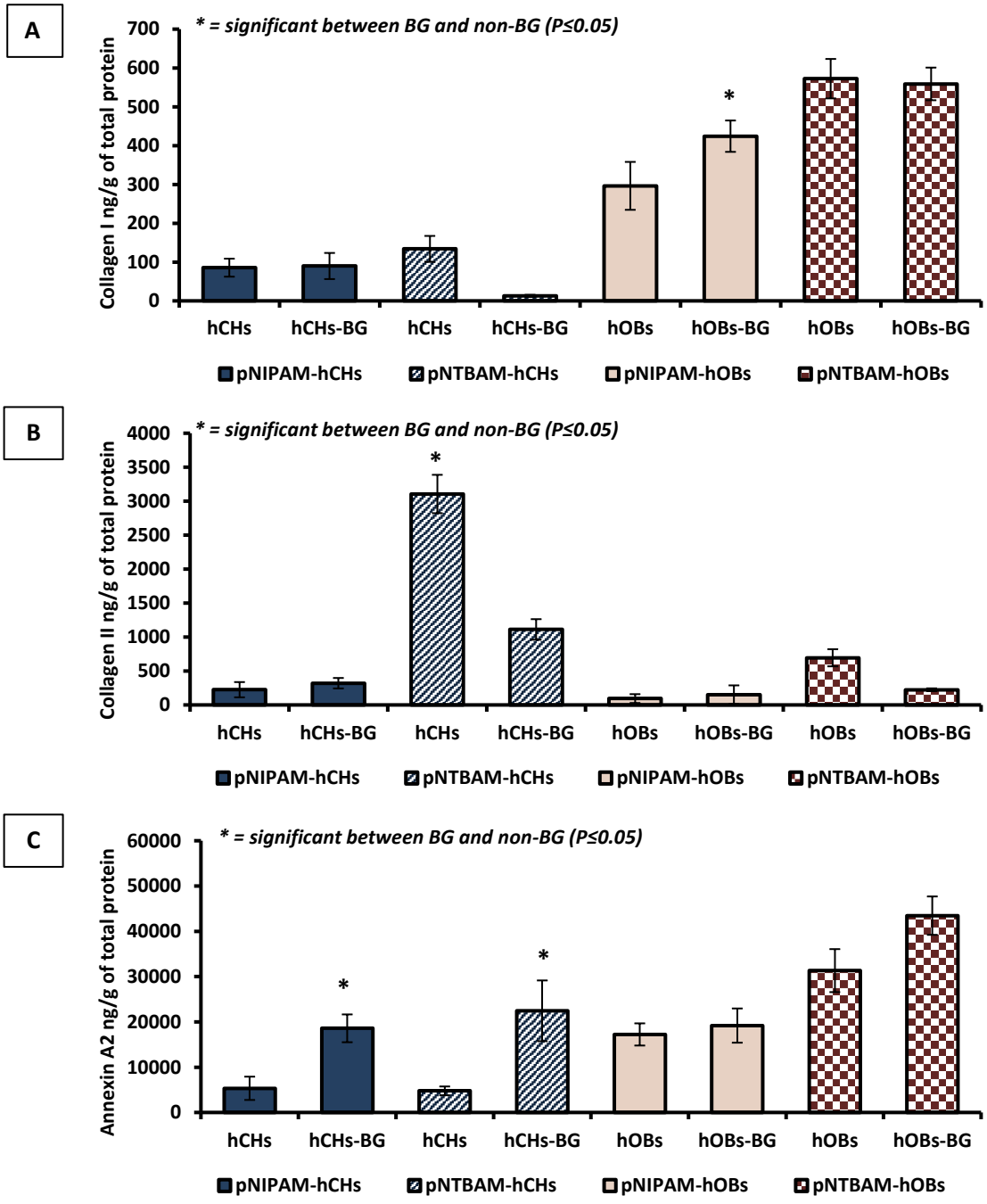

Figure 5-17. The assessment of collagens I, II and annexin A2 in BG vs non-BG at day 21. *Comparison between (A) collagen I levels (B) collagen II levels and (C) annexin A2 levels measured in ng/g of total protein of sample lysate. The bars in each figure are corresponding to each hydrogel sample with a specific cell type with BG or without BG. Asterisks indicate significant levels at P ≤0.05 (Results are representing mean ±SD, n=3).*

In determining the final impact of embedding BG fibres within gradient scaffold, results indicated significant alterations in almost all samples with BG fibres. Collagen I have shown a significant increase with time for gradient-BG samples with hOBs and encountered for a huge variation at all time points compared to non-BG samples. Gradient samples with hCHs were not significantly altered ($P > 0.05$) from the non-BG samples and both have only little increase with time (Figure 5-18 A).

The levels of collagen II revealed a significant lower level for gradient-BG samples seeded with hCHs compared to a higher level observed for the non-BG samples. The values were in line together at the early time points, but the further elevation after day 15 witnessed some retreat up to day 21 for the BG samples. For hOBs samples, collagen II had some variations between BG and non-BG with higher levels for non-BG samples until day 15, however, levels were back to be in line together at day 21 (Figure 5-18 B).

A significant elevation of annexin A2 was noticed for gradient-BG samples, this was inclusive to all time points and with both cell types which might indicate the engagement of cells with further mineral activities (Figure 5-18 C).

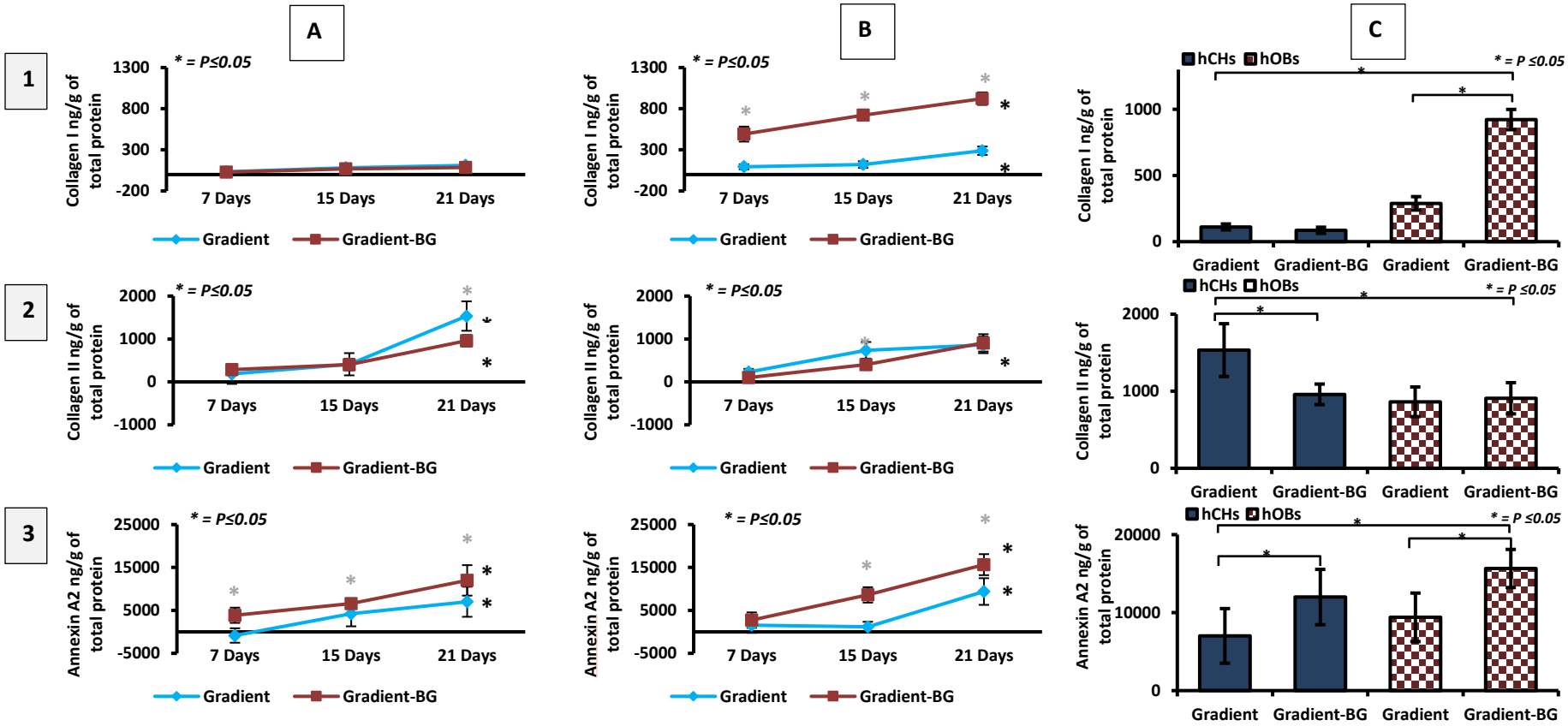

Figure 5-18. Quantifying collagens I, II and annexin A2 in BG vs non-BG gradient scaffolds seeded with hOBs and hCHs. *Figures rows represent each marker level (1) collagen I, (2) collagen II, and (3) annexin A2. Figure columns are revealing marker level monitored with time for (A) hCHs and (B) hOBs respectively with the final comparison of levels at day 21(C) illustrated in the right side column bar figure. Each marker quantified in ng/g of total protein measured in sample lysate. Asterisks indicate significance at P ≤0.05, for the time monitoring figures the light asterisk (*) is the significance between sample and control at each time point and the dark one (*) is indicative for significance with time (results represent the mean ±SD, n=3).*

5.6. Discussion

In the physiological perspective, the cartilage-bone interface is a well-integrated region offering a gradual transition between bone and cartilage tissues (Chan et al. 2012). In the present work, the previously tested pNIPAM and pNTBAM hydrogels were assembled together to produce a 3D multi-regional scaffold with the hope that this will advice for a gradient tissue development.

Studies have been directed to explore the role of biomaterial scaffolds as a template to guide the process of tissue regeneration. Several studies had established the usefulness of a multi-layer scaffold to regenerate complex tissue constructs such as the osteochondral region (Martin et al. 2007; Levingstone et al. 2014; Sartori et al. 2017). Materials of variable characteristics have proven success to guide multiple tissue regeneration (Liu et al. 2013). Recent trends are focusing on creating integrated materials scaffold making use of a functional gradient between layers to perform as a natural tissue match (Leong et al. 2008; Sola et al. 2016; Kang et al. 2018).

The current scaffold design looks intact with no apparent margins to differentiate the two polymers, apart from a thin transparent layer of pNIPAM at one ends of the scaffold (Figure 5-1 A). Several techniques have been used to fabricate materials into gradient constructs with variations as per materials different characteristics and the targeted tissue regeneration (Chatterjee et al. 2011; Seidi et al. 2011; Sola et al. 2016; Di Luca, Ostrowska, et al. 2016; Bracaglia et al. 2017). It was stated according to Matyjaszewski et al. 2000 that atom transfer radical polymerization (ATRP) has been approved for gradient polymers production making use of the polymerization process to blend variable materials properties. The proposed method of joining the current materials had allowed for the development of integrated regions between the two polymers. The timing of addition of each polymer layer was set to be just after the polymerisation process had started in the previous layer i.e. while polymer formation is in the midway. This had ensured that the process of polymerisation initiated in the first layer will continue to build up polymer chains up to the next layer. Now,

the process of polymerisation will include chains from the second layer and continue onward until forming the whole composite. Accordingly, the interface region between the layers was integrated properly by infiltrating polymer chains together forming intact bonding region. This has aided to create a single construct advised for three architectural regions avoiding the problem of delamination that would occur when combining different materials in traditional multilayer scaffolds (Izadifar et al. 2012). Current results illustrated the development of multiregional scaffold as per SEM imaging and FTIR characterisation. SEM images revealed similar architectural build to pNIPAM and pNTBAM at both ends. The interface part though exposed some change in configuration presented by larger pores with flake-like shape polymer boundaries (Figure 5-1 B). Variations between the two polymers in terms of wettability had impacted the process of their production; this was clear as different solvent system is required for each. Such a different property was reflected when both monomers solutions come in contact with each other in preparing gradient scaffold. It was obvious according to Biswas et al. that the presence of alcoholic component such as ethanol in pNIPAM solvent mixture will affect the swelling properties of the polymer leading to formation of macro-porous hydrogel. This could be interpreted by the different configuration observed in the interface region of the combined polymers scaffold according to SEM image. The FTIR identifications showed the gradual transition from pNTBAM to pNIPAM with a proposed interface section as indicated from the spectral fingerprint region (Figure 5-1 C). Notably, prevalence from pNTBAM phase was observed which might be related to the slower polymer formation speed. This is possibly led to a wide area formed from pNTBAM region which has had gradually narrowed towards pNIPAM. Accordingly, the current scaffold design indicated architectural integration between the two polymers to form an intact scaffold unit. Although the FTIR measurements reflect gradual transformation from one polymer region towards the other, the resultant scaffold construct apparently may not show a gradient architectural development from pNIPAM to pNTBAM region as indicated by the variable porosity at the interface. However, the scaffold internal architecture refers to a multiregional porous characteristic. According to the natural osteochondral interface architecture, the sub-chondroal bone region represents a

larger porous structure that is followed by the sub-chondral bone plate which is a more dense bony region before moving to the calcified cartilaginous region (Burr 2004; Hoemann et al. 2012a; Madry et al. 2010). The current design could be useful as the interface region give rise to a larger porous structure which can host higher rate of mineralization when tested with cellular behaviour (Karageorgiou & Kaplan 2005).

Preliminary findings from histological staining of gradient samples, showed the gradual alteration of cells response across the area between the two polymers (Figure 5-5). As a general outcome, calcium minerals association was enhanced across a wide area of scaffold regions including the interface, mostly with hOBs. The production of GAGs was distinctive for hCHs at the pNTBAM side which has been interrupted at the interface towards pNIPAM side. This might indicate the role of the background architecture of the current scaffold in guiding cells behaviour i.e. cells are changing their behaviour accordingly while moving across matrix layers. According to a study conducted by Di Luca et al. 2016 chondrogenic differentiation was guided by a smaller pore architecture. They tested the differentiation of human mesenchymal stem cells (hMSCs) on a scaffold with gradient porous structure; the cells were showing an increased chondrogenic behaviour and GAGs production towards the smaller pore gradient region. Both polymers were able to support mineral association either with SBF solution or when seeded by cells (Chapters 3 and 4). The mineral activity though was more pronounced with cells using osteogenic supported media. As such, the current scaffold architecture has shown the propagation of mineralization across scaffold regions. Di Luca et al. 2015 also stated that osteogenic differentiation coupled with increased mineralization was enhanced by larger porous architecture of a gradient scaffold. An evidence of mineral association with hCHs might be seen at the interface region, this was less observed towards pNTBAM region. This is a possible finding that the mixed polymer interface region provides a supportive background for a more mineral layout by hCHs. The latter may be explained by the effect of macro-porous architecture of the region in allowing more mineralisation activity by cells. It has been indicated that the larger porous architecture is an

excellent promoter for enhanced osteogenic and mineralization behaviour of cells (Karageorgiou & Kaplan 2005). These results revealed the impact of the current structure and porosity on influencing osteochondral cell behaviour. In this case, the mixed polymer region of the current scaffold may advice for a dense mineral region owing to the larger porous structure. The findings from immune staining and ELISA may support such a claim; this was obvious in monitoring confocal images for collagen X expression that revealed intense green fluorescent for both cells at the interface region. ELISA identification of annexin A2 in hCHs has had an enhanced value as well when monitored with gradient scaffold for both cells, which could be another evidence for these cells as being involved in the mineralization process. Markers like annexin A2 and collagen X have been proven as indicators for calcium mineralization of the extracellular matrix observed for hypertrophic chondrocytes and osteoblasts. Annexin A2 normally expressed in matrix vesicles produced by these cells (Bottini et al. 2018). Reviewing other markers, collagen I, II are both showing reasonable amounts corresponding to hOBs and hCHs respectively on gradient scaffold (Figure 5-8). This probably referring that the cells are still functioning normally relevant to their type.

In review of the above results, the produced multiregional scaffold presented a gradual mixture of both polymers towards scaffold ends. The mixed region develops some changes to the architectural structure. Accordingly, this had impacted cell's behaviour differently when compared to the individual hydrogels. Relevant to functional proteins levels, cells seeded on the current combined polymers scaffold revealed intermediate levels of proteins as per the same cells upon single hydrogels. The level of annexin A2, as an indicative of mineralization, presented variable levels which was significantly lower with hOBs while no significant difference with hCHs when compared to individual hydrogels (Figure 5-19).

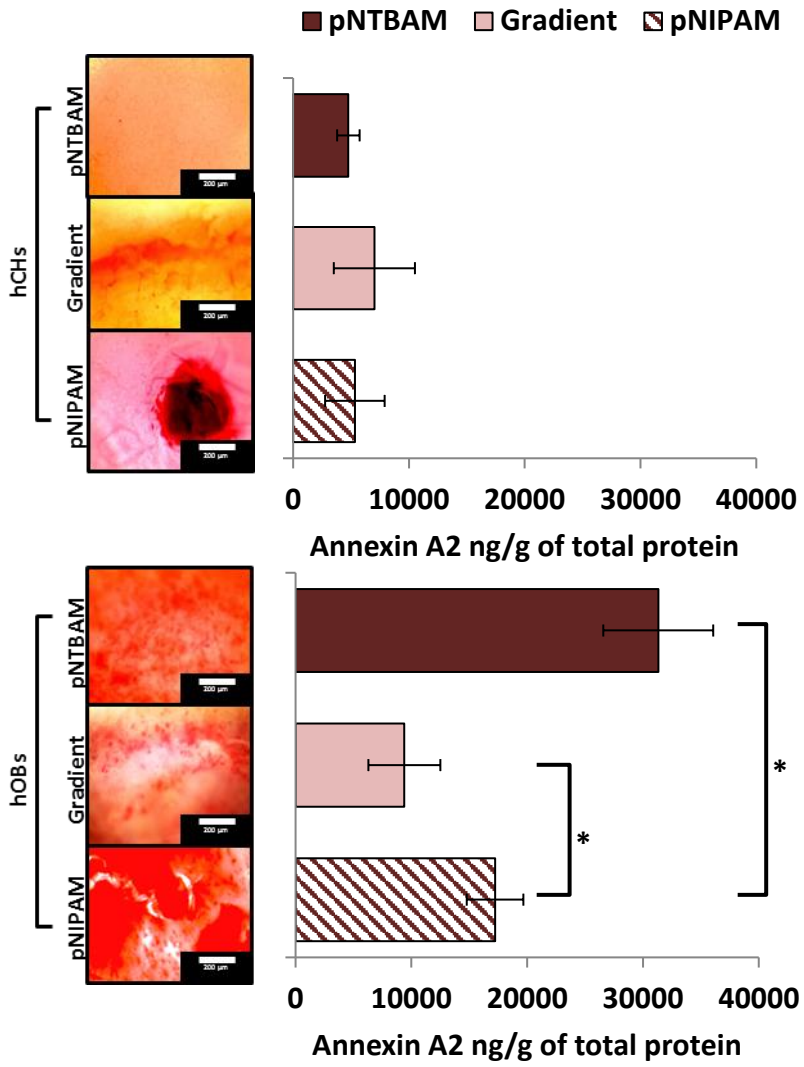

Figure 5-19. Comparing mineralization activity presented by cells on hydrogels at day 21. *Mineral association as per alizarin red staining and annexin A2 protein level for hCHs and hOBs. Bars are corresponding to each hydrogel type revealing annexin A2 level for each. Scale bar 200 µm, asterisks represent significance at P ≤0.05, results indicate mean ±SD, n=3.*

This is probably referring to a more controllable aspect presented by the mixed polymer interface which apparently hold mineralization process by cells within a specific limit. These might explain the variable trends of cells as per the scaffold's different characteristics which will eventually help in designing scaffold to regenerate complex tissue interface.

Designing of osteochondral scaffold might necessitate a consideration regarding tissue vascularization and further cellular nourishment, which might be a function of the porous

architecture or may be improved by the inclusion of certain cues (Seo et al. 2014; J. Yang et al. 2017; Camarero-Espinosa & Cooper-White 2017). Accordingly, the embedding of BG fibres was proposed for the current scaffold design in the hope of enabling cells traveling and further vascular infiltration from the sub-chondral layer. Furthermore, elements from these fibres degradation were considered as potent stimulators for osteogenic activity and bone matrix formation (Jones 2015; Turnbull et al. 2018). Diffusion of BG elements was described by Raman mapping. The heat maps illustrate the diffusion of the BG mass by day 15 of incubation at 37 °C (Figure 5-2 B). This was indicated by the expanded green zone band of the BG mass and shrinkage of the red zone referring to the reduced Raman intensity while the mass is disintegrating with time. This might indicate the formation of a hydroxyapatite layer by dissolution of these fibres and diffusion of the main elements (calcium and phosphate) to infiltrate the hydrogel phase (Turnbull et al. 2018). The potential of bioactivity of the BG material is determined by the rate of comprising HA layer which is basically depend on BG type and composition (Notingher et al. 2002; Kwiatkowska et al. 2012; Hossain et al. 2018). Relevant to μCT density scanning, reduction of fibre mass reached the maximum at day 28; however, remnants still can be sought within hydrogel's construct revealed from last time point images (Figure 5-3 A). This might reflect the existence of degradation elements from BG fibres after complete dissolution which possibly confirms the findings from Raman spectroscopy. Additional prove was the BG fibres mass volume reduction with time reaching the lower level which was then appeared to be a little plateaued at day 28. This was furtherly enforced by the alizarin stained BG channels after 28 days of PBS incubation at 37 °C (Figure 5-3 B).

Testing cells traveling through BG fibres empty channels reveals no true evidence of cells being migrated through these openings. Although BG fibres should leave about 60-70 μm channels across hydrogel thickness, the cells were only accumulating around the beginning of these channels at the top of hydrogels. It is possible that cells may lack enough oxygenation or nutrition while traveling through toward the core of hydrogel whether through pores or

empty channels (Ahearne 2014). In this respect, it could be more reasonable to use fibres with larger diameter thus enabling nutrients to infiltrate more across hydrogel. Additionally, testing oxidative stress of cells on these hydrogels may be required in future prospective to assess this condition.

The presence of BG fibres impacted for significant calcium minerals in samples with hOBs seeded on pNTBAM while no significant levels observed with pNIPAM samples seeded with the same cells (Figure 5-10). This has been reflected also in the level of annexin A2 which revealed a significant increase with hOBs but only with pNTBAM seeded with hOBs (Figure 5-17). Gradient scaffold seeded with hOBs though showed significantly higher annexin A2 level compared to non-BG. This might be proving that these BG mass has encouraged more cellular mineral activity thus expressing higher marker level.

In assessing samples with hCHs, little has been observed relevant to calcium ions evaluation with no significant difference seen with BG samples for single or gradient hydrogels (Figures 5-10, 5-12). However, ELISA measurements identify a significant increase in annexin A2 level for BG samples with hCHs. It also showed that BG samples with hCHs had witnessed some reduction, which was significant with pNTBAM, in collagen II levels for both single hydrogels and gradients (Figures 5-16, 5-17). This is another clue which could possibly indicate that these hCHs were engaged within active mineralization behaviour in the presence of BG fibres. These findings agreed with the previous claims that BG material increase the potential for mineral activity by cells (Jones et al. 2007; Jones 2015). This is important especially when chondrocytes revealed the intention to associate with minerals (as per increased annexin A2 levels) which is one of the characteristics of the hypertrophic chondrocytes that forms the calcified cartilage matrix (Hoemann et al. 2012a). It is not recognized whether these cells had been transformed into hypertrophic chondrocytes; however the current data might indicate some of these aspects as referred to the mineralization markers measured. Although the levels of calcium ions did not significantly increase with BG

samples seeded with hCHs, the expression of annexin A2 might reflect a future trend of these cells to produce matrix vesicles and mineralize the surrounding matrix.

5.7. Conclusion

Joining pNIPAM and pNTBAM presented a multiregional scaffold between the two polymers that showed different architectural regions including the polymers interface. Inspecting the mixed scaffold region illustrate the ability to host osteoblastic and chondrocytes activities in a way that reveal different cells attitude compared to individual hydrogels. The variations in cell responses across this region refer to a gradual transformation in cell functions while moving from one side to the other end of the scaffold. Introducing BG fibres into scaffolds' construct encountered for an enhanced mineral activity mostly with hCHs. This might increase the chance for establishing a mineralized interface by engaging chondrocytes to produce a calcified matrix. This is a vital aspect when the main goal is to regenerate the osteochondral interface as the current scaffold advised for a different potential of cells across its multi-architectural regions.

Chapter 6

Summative discussion, conclusion, and future work

6.1. Summative discussion

The prevalence of osteochondral defects, especially through the last decades, has brought it to be one of the serious worldwide problems that adversely impacted individuals lifestyle (Nukavarapu & Dorcemus 2013b; Pape et al. 2010). Treatment went through several options, one of which is to stimulate further tissue growth by drilling and micro-fracture techniques. These techniques are less invasive and have shown acceptable success rate, however some concerns have been reported about the nature of tissues produced. These were manifested mainly by the formation of fibrous cartilage that cannot withstand the normally applied pressure on the joints resulting in further deterioration after specific period of treatment (Swieszkowski et al. 2007; Steadman et al. 1997). Another treatment option, which is tissue transplantation of osteochondral allo-grafts or auto-grafts, has shown a greater success rate as being observed from a wide range of studies performed on animals and humans (Detterline et al. 2005). However, the availability of the intended grafts in addition to donor site morbidity have been regarded as a major limitations of these techniques (Detterline et al. 2005; J.S. Temenoff & Mikos 2000). Autologous chondrocyte implantation (ACI) has been accepted to be a superior solution for correcting osteochondral damage through utilizing a fresh chondrocytes, which have been harvested from nearby cartilage, expanded in the laboratory. The site of damage will be covered with a periosteal flap or membrane, then the cells injected through this membrane (Brittberg 2008; Hangody et al. 2008). ACI proved effectiveness in producing hyaline like articular cartilage, however, clinical studies have shown positive results only to specific cartilage sites like the femoral condyle (J.S. Temenoff & Mikos 2000).

The limitations observed for the above mentioned treatment options, necessitate the existence of a new therapeutic clues. Tissue engineering, as part of regenerative medicine, represents a wide field of therapeutic strategies that utilizes a specific biomaterials to construct an artificial extracellular matrix (ECM) or scaffolds, these scaffolds are designed and manufactured in a way that preferably support cellular proliferation and further tissue growth so that mimicking the natural tissue structure and property (Martin et al. 2007; Steinwachs et al. 2008; Chen et

al. 2009b; Vahdati & Wagner 2013). Engineering of the osteochondral interface should consider the complex tissue transformation from the sub-chondral bone to the cartilage region (Cancedda et al. 2003; Martin et al. 2007; Chiang & Jiang 2009). As such, studies was performed utilizing multilayer scaffolds to simulate the variable bone-cartilage tissue environment and the different stages of mineralization across this region (Dado & Levenberg 2009; Chen et al. 2014; Liu et al. 2013; Kon et al. 2014). The variable materials' features were explored such as the porosity, mechanical and surface chemistry to determine their impact on relevant cell performances (Puppi et al. 2010a; Shapiro & Oyen 2013; Patterson et al. 2010; Deb et al. 2018b). Indeed, challenge still existing as to establish an optimum scaffold design that address for a gradient tissue regeneration and avoid the problem of delamination of a multilayer construct (Sherwood et al. 2002; Liu et al. 2007; Steward et al. 2011; Chatterjee et al. 2011; Castro et al. 2012; Chen et al. 2014).

The current thesis work aimed to search the suitability of certain biomaterials to fabricate a multi-architectural scaffold unit to guide the regeneration of the osteochondral interface. Investigating certain materials and materials combination revealed the effects of different characteristics on guiding cell functions towards a specific tissue regeneration (Ito 1999; Flemming et al. 1999; Arima & Iwata 2007; Patterson et al. 2010; O'Shea & Miao 2008; Chang & Wang 2011). Material's preferences were based on the intended tissue to be regenerated with the synthetic materials gaining most interest because of their easily controlled features (Williams 2009; Puppi et al. 2010b; Jones 2015; Hossain et al. 2018). Accordingly, pNIPAM and pNTBAM were chosen for the current study relevant to their background reports for being biomimetic, non-toxic, and tuneable materials (You et al. 2008; Lynch et al. 2005; de Vries-van Melle et al. 2014; Haq et al. 2017; Ayat et al. 2016). Both are synthetic polymers bearing the acrylamide group in their structure with slight variations in chemical composition represented by additional methyl group in pNTBAM. These polymers were investigated to advise the basic chemical, mechanical and architectural characteristics that would possibly impacted the outcome biological results (Chapter 3). Findings elucidate

the main difference indicating more hydrophobic stiffer mass for pNTBAM compared to pNIPAM. A wettable versus less wettable surface of materials is a function of surface charge and chemical functional groups. Thus, pNTBAM revealed more hydrophobic surface compared to pNIPAM. This was recognized from the drop shape and larger water contact angle measured for pNTBAM (Figure 3-3). These findings were in agreement with certain studies stated the wettability profile difference for pNIPAM and pNTBAM and its correlation with their surface chemistry (Lynch et al. 2005; Muramatsu K Wada T, Hirai H, Miyawaki F 2012; Pelton 2010; Ayat et al. 2016). The C=O and NH- chemical functional groups presented by materials promote more hydrophilic behaviour of polymer, such an aspect may be linked to promoting osteoblastic cells activity and mineralization (Chang & Wang 2011; Keselowsky et al. 2003). A more hydrophobic behaviour presented by pNTBAM is possibly connected to the presence of higher percentage of CH_3- groups (Chang & Wang 2011).

Results from compressive strength revealed stiffer mass presented by pNTBAM compared to a more flexible soft pNIPAM. Mechanical strength is another criteria that impacted cells proliferation and attachment which could be the result of material's natural properties and their method of production (Hollister et al. 2002; Wells 2008; Vijayavenkataraman et al. 2017). Studying architectural difference and porosity showed pNIPAM as having significantly larger pore diameter compared to pNTBAM. The pore size variations measured for the current materials might contributed to the difference in stiffness obtained as agreed with certain studies stated the impact of increased porosity on decreasing material stiffness (Karageorgiou & Kaplan 2005; Bandyopadhyay et al. 2010; O'Brien 2011; Turnbull et al. 2018).The inspection of several monomeric sub-groups for each polymer declared the influence of reducing monomeric concentration on having a larger pore diameter as reflected according to SEM imaging. These were in accordance with studies that showed the influence of high monomeric concentration of polymer solution on yielding a smaller pore size compared to a lower concentration (Baugher et al. 1995; Karageorgiou & Kaplan 2005). Studies also concluded the correlation between larger pore size and osteogenic cell behaviour and the

impact of this on promoting mineralization (Lee et al. 2012; Cooper et al. 2016; Karageorgiou & Kaplan 2005). Both polymers showed a positive tendency to promote calcium minerals association *in vitro* (relevant to SBF incubation) with variations that indicated a higher tendency for pNTBAM (Figure 3-10). These relative differences in mineralization may be of value when planning for an osteochondral scaffold, as this region physiologically originate a mineral gradient between sub-chondral bone and cartilage (Bullough & Jagannath 1983; Hoemann et al. 2012a; Bian et al. 2016). The above variable characteristics captured for both hydrogels predisposed for the next observations in terms of cells attitude and biological assessment that we carried out in chapter four.

The study proceeded forward to investigate the influence of hydrogels' variable features (outlined in Chapter 3) on relevant cell survival and their biological function. The chemical and architectural differences between tested hydrogels revealed their impact on cells attachment and viability. An obvious observation was the growth pattern of cells on each hydrogel. It seems that cells grow in aggregates or clusters on pNIPAM while spread on pNTBAM. Studying the viability of cells indicates higher rate of viable vs. dead cells for both hydrogels. However, proliferation rate was quite different as the number of cells counted on pNIPAM was around seeding density at day 21 unlike pNTBAM which showed significantly increased number of cells. These results may be the outcomes from different materials' characteristics including soft versus stiff surfaces and hydrophilic versus hydrophobic properties obtained for pNIPAM and pNTBAM respectively. Certain studies proved the impact of these variable features on cells behaviour, viability and growth pattern (Keselowsky et al. 2003; Bačáková et al. 2004; Tan et al. 2005). Cells attachment can be improved using materials with intermediate hydrophilic to hydrophobic surface characteristics. Results were in agreement with other findings that indicated the impact of soft surfaces on affecting cell attachment and proliferation rate compared to a stiffer surfaces (Bačáková et al. 2000; Bačáková et al. 2001; Bačáková et al. 2004). The examined monomeric sub-groups of hydrogels did not reflect any major differences in terms of viability and proliferation rate.

Though, an evidence of cells migration within hydrogel's matrix of pNIPAM 0.042 g/mL sub-type was spotted. This feature might reflect the development of interconnected porous structure as per the lower monomeric concentration used which eventually could serve a better 3D environment and cells transportation. As such, the decision was made to move forward in the present study with this concentration of pNIPAM. In case of pNTBAM, the highest monomeric sub-type was chosen as no apparent variations in viability or migration had recognized among pNTBAM sub-groups. This monomeric sub-type was stiffer in terms of hardness compared to the others.

The outcome results from tracking osteogenic and chondrogenic cells behaviour revealed some differences between these hydrogels. hOBs showed active mineralization when seeded on both hydrogels, though, pNTBAM showed higher results. Findings regarding hCHs, indicated little or no evidence of mineralization especially with pNTBAM. In evaluating chondrogenic activity and GAGs production, pNTBAM was superior in revealing highest GAGs content. These results were then confirmed with the findings from immunostaining of hydrogels and ELISA assay for collagens. The levels of collagen I showed significant elevation with hOBs sample of both hydrogels but mostly with pNTBAM. In contrast, collagen II showed significant elevation with hCHs on pNTBAM samples whereas only little evidence was noted with pNIPAM. Collagens I and II are normally associated with bone and cartilage tissues but with different extents. This is identified normally by higher collagen I levels in bone which is in contrast to cartilage tissues where collagen II is the major matrix protein. Between these regions the level of matrix proteins will increase or decrease along the tissue gradient depending on the cell type and the level of mineralization. This is basically recognized at the calcified cartilage region where hypertrophic chondrocytes started some increase in collagen II in addition to elevation of collagen X as an indicator of mineral association activity by cells (Hoemann et al. 2012b; Pal 2014). The current results explain how cells were reacted to the different configuration previously characterised for both hydrogels. Hydrogels' chemistry, stiffness, and porosity apparently revealed their impact on

overall cell proliferation, viability, and relevant functions. These were in accordance with studies that described the increased stiffness of hydrogel to beyond 33 Kpa (evidenced with pNTBAM) will enhance GAGs production by chondrocytes while materials presenting more NH- and OH- with less CH_3- chemical groups are involved in promoting osteogenic cell activity (Wells 2008; Wang et al. 2016; Cao et al. 2017b). Another study by Di Luca et al. 2016 indicated the effect of smaller pore size of a material on guiding MSCs for more chondrogenic differentiation.

The above results from Chapters 3 and 4 clearly revealed the variations between pNTBAM and pNIPAM hydrogels in terms of basic characteristics reaching to biological observations. Indeed, both hydrogels proved their tendency to host calcium mineralization in variable degrees showing greater values with pNTBAM. The chondrogenic cell activity was supported mainly by pNTBAM with little or no extent with pNIPAM.

In an attempt to regenerate the osteochondral region, making use of various properties collected from the current materials as per mineralization and chondrogenic behaviour, these two hydrogels were combined together in an attempt to produce a gradient scaffold unit. Joining these polymers has had to follow the same synthesis procedures originally used for each polymer. However, a stepwise addition of each polymer solution in one container was regulated by a critical timing between the steps. The proposed method and timing of addition was dependent on the speed of polymerization and the nature of each polymer's solvent. Accordingly, pNIPAM was added in the beginning followed by mixture of the two polymers and finally pNTBAM layer. Initial characterization of the resultant scaffold showed the development of a multiregional scaffold construct between the polymers. Each polymer constitutes one end of the scaffold with mixed interface region that showed variable architecture. the interface different architecture was related to the polymers variable solubility properties and different solvent system. this had impacted polymer formation when the two polymers met at the interface resulting in a macro-porous structure. Consequently, combining the two polymers did not actually created a gradient architecture between them. This was

verified by SEM imaging, although the FTIR measurements across the scaffold's regions showed gradual polymer to polymer transformation (Figure 5-1).

Assessment of cells behaviour and biological activities on gradient scaffold showed increased calcium mineralization for hOBs in gradient interface region with evidence also being noted for hCHs. Chondrogenic cells activity was obviously increased towards pNTBAM side of the scaffold, which was evident from GAGs assessment. These were confirmed as well via ELISA measurements of collagens and annexin A2 as a mineralization marker. The activity of cells at the gradient scaffold interface showed variable trends presented by expressing intermediate levels of cell functional proteins when compared with the individual hydrogels. The level of mineralization as well was measured at a lower level compared to individual hydrogels with both cell types. This fact probably confirms that the gradient interface architecture resulted in moderate activities of cells while moving from each side of the scaffold towards the other side. Therefore, presenting three functional regions that will guide a gradual transformation of cells activities.

BG fibres were included within hydrogels' structure to aid the production of the final scaffold. The proposed role of these fibres was to facilitate cellular transportation across scaffold compartments or enabling vascularization and cells nourishment (Seo et al. 2014; J. Yang et al. 2017; Camarero-Espinosa & Cooper-White 2017). Although the current observations indicated evidence of cell migration for pNIPAM, limitations still existed with pNTBAM. That's why the use of these fibres might add additional significance. The other purpose of using these fibres originates principally from their ability to degrade with time leaving traces of minerals within the produced channels. These residues will support a mineral environment that will encourage osteogenesis and mineralization activity of the cells (Jones 2015; Turnbull et al. 2018). Degradation profile of BG fibres was described in Chapter 5 according to Raman and μCT analysis. Indeed, results indicated diminished BG mass up to day 28 with evidence of traces of these fibres still being measured after 28 days. Cells seeded on BG embedded scaffolds revealed an elevation of calcium minerals and annexin A2 levels compared to the

non-BG samples. Results also indicated the positive engagement of hCHs in mineralization activity with the presence of these fibres. This is probably evident by the increased annexin A2 and calcium ions with reduction of collagen II levels observed in BG samples. Annexin A2 has been proven as indicator for the involvement of cells in mineralization of the extracellular matrix. This marker is mainly expressed in matrix vesicles (MV) observed in hypertrophic chondrocytes and osteoblasts (Bottini et al. 2018). This could be a possible indication of the development of a multifunctional scaffold's regions that refer to a variable mineral cell behaviour which involves both cell types. However, tracking penetration of cells across the empty fibres' channels showed no obvious signs of cell migration. Accordingly, the current scaffold might serve the purpose of regenerating complex tissue construct, such as the osteochondral interface, making use of the BG mass to potentiate osteogenic cell activity and supporting the calcified matrix by chondrocytes.

6.2. Conclusions

Assessment of the current materials showed the development of hydrogels with different criteria's as relevant to their background chemistry. Results concluded that pNTBAM labelled as more hydrophobic, stiffer hydrogel with smaller pore diameter. On the other hand, pNIPAM was more hydrophilic, soft hydrogel with larger pores. These variations impacted cells attachment and viability assessment. The two hydrogels supported higher percentage of viable versus dead cells. However, cells were forming aggregates on pNIPAM with low proliferation rate whereas on pNTBAM they spread on the surface showing significantly increased number. The lowest monomeric concentration of pNIPAM indicated more interconnected pore architecture. This was proven by the evidence of cell migration observed with this sub-type compared to the other concentrations including pNTBAM monomeric sub-groups. Both hydrogels' architecture supported mineral association to variable tendencies. The levels were high when tracked with hOBs while only little with hCHs mostly evident with pNIPAM. Chondrogenic activity was promoted by pNTBAM compared to little or no evidence with pNIPAM hydrogel. The final scaffold generated by joining the two hydrogels

showed the integration between the two polymers to form a joint interface region. The resultant scaffold though may not actually refer to a gradient architectural development between the two polymers regions. This was evident by the pore shape and architectural difference at the interface. However, the resultant joined scaffold features a variable mineralization and chondrogenic activity across the multi-architectural regions. The inclusion of BG fibres within scaffold's construct indicated enhanced mineralization activity of cells whether with single or gradient hydrogels. Such a property would probably promote the establishment of mineral gradient across the osteochondral interface. However, we couldn't establish evidence of cell transport through fibres openings. The current study proved that materials with slight variation in chemistry advised for different materials' features which in turn impacted cell activities in the favour of multiple tissue regeneration. It also concluded the possibility of joining these materials to produce gradient scaffold promoted for multi-functional architectural regions. On the other hand, tuning of these materials by changing the monomeric concentration or by introducing bio active materials (BG fibres) had positively impacted some of their features including cell migration and enhanced mineral activity. These outcome measures might be of interest when trying to regenerate complex regions such as the osteochondral interface. The current scaffold design reveals variable cells activities per the different scaffold zones. Although the gradient architectural feature of the scaffold wasn't completely achieved as required, the cells performances refer to an interchangeable mineral and chondrogenic tendencies across scaffold multiple regions. This was influenced further by the embedding of BG fibres which ultimately enhanced mineralization tendency involving chondrocytes. Thus, it could be assumed that this had led to an imitation to the calcified cartilage together with the sub-chondral bone.

6.3. Future work

Considering the current results, future trends would recommend the application of this model study on other materials featuring the variable wettability, architectural and mechanical properties. This could be helpful to present wide range of models that would serve the

regeneration of complex tissues such as the bone-cartilage interface. Further recommendations suggest investigating gradient scaffolds' regional characteristics on guiding cell differentiation of mesenchymal stem cells (MSCs). This will clarify the osteogenic versus chondrogenic alignment of cell behaviour across scaffold regions and would benefit from addressing certain gene expression specific to cell functions.

It is also recommended to investigate BG fibres with larger diameter (100-150 μm). The current work summarizes an enhanced mineral potential of cells with BG embedded samples. However, fibre thickness may be not enough in enabling adequate cell migration across these fibres' openings. The proposed recommendation may probably provide an option that supports a better cellular transportation by enabling cells to infiltrate through larger openings.

The application of bioreactor system while testing *in vitro* cell culturing of the current materials. These probably involve hydrostatic pressure or shear stress which intended to simulate the *in vivo* mechanical stimuli especially when targeting osteochondral tissues.

A future recommendation may also involve the application of this scaffold model in an animal studies by subcutaneous implantation of the final gradient scaffold. This is a useful trend towards investigating *in vivo* versus *in vitro* environment and the quality of tissues produced under physiological conditions.

Chapter 7

References

Ahearne, M., 2014. Introduction to cell − hydrogel mechanosensing. *Interface Focus*, *4*(2), 20130038..

Akiyama, Y. & Okano, T., 2015. Temperature-responsive polymers for cell culture and tissue engineering applications. *Switchable and Responsive Surfaces and Materials for Biomedical Applications*, pp.203–233.

Allo, B.A. et al., 2012. Bioactive and Biodegradable Nanocomposites and Hybrid Biomaterials for Bone Regeneration. *Journal of Functional Biomaterials*, 3(4), pp.432–463.

Ando, W. et al., 2007. Cartilage repair using an in vitro generated scaffold-free tissue-engineered construct derived from porcine synovial mesenchymal stem cells. *Biomaterials*, 28(36), pp.5462–5470.

Arima, Y. & Iwata, H., 2007. Effect of wettability and surface functional groups on protein adsorption and cell adhesion using well-defined mixed self-assembled monolayers. *Biomaterials*, 28(20), pp.3074–3082.

Armiento, A.R. et al., 2018. Biomaterials for articular cartilage tissue engineering: Learning from biology. *Acta Biomaterialia*, 65, pp.1–20.

Ayat, ", Al-Massaedh, A." & Pyell, U., 2016. Mixed-mode acrylamide-based continuous beds bearing tert-butyl groups for capillary electrochromatography synthesized via complexation of N-tert-butylacrylamide with a water-soluble cyclodextrin. Part I: Retention properties. *Journal of Chromatography A*, 1477, pp.114–126.

Aydin, H.M., 2011. A three-layered osteochondral plug: Structural, mechanical, and in vitro biocompatibility analysis. *Advanced Engineering Materials*, 13(12), pp.511–517.

Bačáková, L. et al., 2001. Adhesion and proliferation of rat vascular smooth muscle cells (VSMC) on polyethylene implanted with O+ and C+ ions. *Journal of Biomaterials Science, Polymer Edition*, 12(7), pp.817–834.

Bačáková, L. et al., 2004. Cell Adhesion on Artificial Materials for Tissue Engineering. *Physiological Research*, 53(Suppl. 1), pp. S35-45.

Bačáková, L. et al., 2000. Molecular mechanisms of improved adhesion and growth of an endothelial cell line cultured on polystyrene implanted with fluorine ions. *Biomaterials*, 21(11), pp.1173–1179.

Bandyopadhyay, A. et al., 2010. Influence of porosity on mechanical properties and in vivo response of Ti6Al4V implants. *Acta Biomaterialia*, 6(4), pp.1640–1648.

Barnes, A.L. et al., 2016. Collagen-Poly(N-isopropylacrylamide) Hydrogels with Tunable Properties. *Biomacromolecules*, 17(3), pp.723–734.

Basu, S., Sutradhar, S. & Paul, R., 2018. Substrate stiffness and mechanical stress due to intercellular cooperativity guides tissue structure. *Journal of Theoretical Biology*, 457, pp.124–136.

Baugher, B. et al., 1995. Porosity in hexylene-bridged polysilsesquioxanes: Effects of monomer concentration. *Materials Research Society Symposium Proceedings*, 371, pp.253–259.

Benjamin, M. & Ralphs, J.R., 2004. Biology of Fibrocartilage Cells. *International Review of Cytology*, 233, pp.1–45.

Bhosale, A.M. et al., 2007. Combined autologous chondrocyte implantation and allogenic meniscus transplantation: A biological knee replacement. *Knee*, 14(5), pp.361–368.

Bian, W. et al., 2016. Morphological characteristics of cartilage-bone transitional structures in the human knee joint and CAD design of an osteochondral scaffold. *BioMedical Engineering Online*, 15(1), pp.1–14.

Bichara, D. a et al., 2014. Osteochondral defect repair using a polyvinyl alcohol-polyacrylic acid (PVA-PAAc) hydrogel. *Biomedical materials (Bristol, England)*, 9(4), p.045012.

Binyamin, G., Shafi, B.M. & Mery, C.M., 2006. Biomaterials: A primer for surgeons. *Seminars in Pediatric Surgery*, 15(4), pp.276–283.

Biswas, C.S. et al., 2011. Synthesis and characterization of porous poly(N-isopropylacrylamide) hydrogels prepared in ethanol-water mixtures. *Journal of Applied Polymer Science*, 121(4), pp.2422–2429.

Bottini, M. et al., 2018. Matrix vesicles from chondrocytes and osteoblasts: Their biogenesis, properties, functions and biomimetic models. *Biochimica et Biophysica Acta - General Subjects*, 1862(3), pp.532–546.

Boyan, B.D. et al., 1996. Role of material surfaces in regulating bone and cartilage cell response. *Biomaterials*, 17(2), pp.137–146.

Boyd, A.R. et al., 2015. The deposition of strontium-substituted hydroxyapatite coatings. *Journal of Materials Science: Materials in Medicine*, 26(2), pp.1–14.

Bracaglia, L.G. et al., 2017. 3D printing for the design and fabrication of polymer-based gradient scaffolds. *Acta Biomaterialia*, 56, pp.3–13.

Brånemark, R. et al., 2011. Bone response to laser-induced micro- and nano-size titanium surface features. *Nanomedicine: Nanotechnology, Biology, and Medicine*, 7(2), pp.220–227.

Brittberg, M., 2008. Autologous chondrocyte implantation-Technique and long-term follow-up. *Injury*, 39(1 SUPPL.), pp.40–49.

Brittberg, M. et al., 1994. Treatment of Deep Cartilage Defects in the Knee with Autologous Chondrocyte Transplantation. *New England Journal of Medicine*, 331(14), pp.889–895.

Buchmann, S. et al., 2012. Early clinical and structural results after autologous chondrocyte transplantation at the glenohumeral joint. *Journal of Shoulder and Elbow Surgery*, 21(9), pp.1213–1221.

Bullough, P.G. & Jagannath, A., 1983. The morphology of the calcification front in articular cartilage. Its significance in joint function. *The Journal of Bone and Joint Surgery British Volume*, 65(1), pp.72–78.

Burr, D.B., 2004. Anatomy and physiology of the mineralized tissues: Role in the pathogenesis of osteoarthrosis. *Osteoarthritis and Cartilage*, 12(SUPLL.), pp.20–30.

Camarero-Espinosa, S. & Cooper-White, J., 2017. Tailoring biomaterial scaffolds for osteochondral repair. *International Journal of Pharmaceutics*, 523(2), pp.476–489.

Cancedda, R. et al., 2003. Tissue engineering and cell therapy of cartilage and bone. *Matrix Biology*, 22(1), pp.81–91.

Cao, B. et al., 2017. Effects of Functional Groups of Materials on Nonspecific Adhesion and Chondrogenic Induction of Mesenchymal Stem Cells on Free and Micropatterned Surfaces. *ACS Applied Materials and Interfaces*, 9(28), pp.23574–23585.

Cao, W. & Hench, L.L., 1996. Bioactive materials. *Ceramics International*, 22(6), pp.493–507.

Carballo, C.B. et al., 2017. Basic Science of Articular Cartilage. *Clinics in Sports Medicine*, 36(3), pp.413–425.

Castillo Diaz, L.A. et al., 2014. Human osteoblasts within soft peptide hydrogels promote mineralisation in vitro. *Journal of Tissue Engineering*, 5, p.204173141453934.

Castro, N.J., Hacking, S.A. & Zhang, L.G., 2012. Recent progress in interfacial tissue engineering approaches for osteochondral defects. *Annals of Biomedical Engineering*, 40(8), pp.1628–1640.

Cha, C. et al., 2011. Tuning the dependency between stiffness and permeability of a cell encapsulating hydrogel with hydrophilic pendant chains. *Acta Biomaterialia*, 7(10), pp.3719–3728.

Chan, E.F. et al., 2012. Association of 3-Dimensional Cartilage and Bone Structure with Articular Cartilage Properties in and Adjacent to Autologous Osteochondral Grafts after 6 and 12 Months in a Goat Model. *Cartilage*, 3(3), pp.255–266.

Chang, H.-I. & Wang, Y., 2011. Cell Responses to Surface and Architecture of Tissue Engineering Scaffolds. *Regenerative Medicine and Tissue Engineering - Cells and Biomaterials*, pp.569–588.

Chatterjee, K., Young, M.F. & Simon, C.G., 2011. Fabricating Gradient Hydrogel Scaffolds for 3D Cell Culture, *Combinatorial chemistry & high throughput screening*, 14(4), 227-36.

Chen, H. et al., 2014. Cell-scaffold interaction within engineered tissue. *Experimental Cell Research*, 323(2), pp.346–351.

Chen, H. et al., 2009a. Drilling and microfracture lead to different bone structure and necrosis during bone-marrow stimulation for cartilage repair. *Journal of Orthopaedic Research*, 27(11), pp.1432–1438.

Chen, H. et al., 2009b. Drilling and microfracture lead to different bone structure and necrosis during bone-marrow stimulation for cartilage repair. *Journal of Orthopaedic Research*, 27(11), pp.1432–1438.

Chen, S. et al., 2018. Tuning surface properties of bone biomaterials to manipulate osteoblastic cell adhesion and the signaling pathways for the enhancement of early osseointegration. *Colloids and Surfaces B: Biointerfaces*, 164, pp.58–69.

Chiang, H. & Jiang, C.-C., 2009. Repair of Articular Cartilage Defects: Review and Perspectives. *Journal of the Formosan Medical Association*, 108(2), pp.87–101.

Chu, C.R., 2001. Chondral and osteochondral injuries: Mechanisms of injury and repair responses. *Operative Techniques in Orthopaedics*, 11(2), pp.70–75.

Clair, B.L., Johnson, A.R. & Howard, T., 2009. Cartilage Repair: Current and Emerging Options in Treatment. *Foot & Ankle Specialist*, 2(4), pp.179–188.

Cohen, N.P., Foster, R.J. & Mow, V.C., 1998. Composition and Dynamics of Articular Cartilage: Structure, Function, and Maintaining Healthy State. *Journal of Orthopaedic & Sports Physical Therapy*, 28(4), pp.203–215.

Cooper, D.M.L. et al., 2016. Cortical Bone Porosity: What Is It, Why Is It Important, and How Can We Detect It? *Current Osteoporosis Reports*, 14(5), pp.187–198.

Correa, D. & Lietman, S.A., 2017. Articular cartilage repair: Current needs, methods and research directions. *Seminars in Cell and Developmental Biology*, 62, pp.67–77.

Craighead, H.G., James, C.D. & Turner, A.M.P., 2001. Chemical and topographical patterning for directed cell attachment. *Current Opinion in Solid State and Materials Science*, 5(2–3), pp.177–184.

Crist, B.D. et al., 2016. Optimising femoral-head osteochondral allograft transplantation in a preclinical model. *Journal of Orthopaedic Translation*, 5, pp.48–56.

Da Cunha Cavalcanti Filho, M.M. et al., 2012. Updating on diagnosis and treatment of chondrallesion of the knee [Atualização no diagnóstico e tratamento das lesões condrais do joelho]. *Revista Brasileira de Ortopedia*, 47(1), pp.12–20.

Currie, H.A. et al., 2007. Natural and Artificial Hybrid Biomaterials. In *Hybrid Materials: Synthesis, Characterization, and Applications*. pp. 255–299.

Dado, D. & Levenberg, S., 2009. Cell–scaffold mechanical interplay within engineered tissue. *Seminars in Cell & Developmental Biology*, 20(6), pp.656–664.

Dalby, M.J. et al., 2002. Increasing fibroblast response to materials using nanotopography: Morphological and genetic measurements of cell response to 13-nm-high polymer demixed islands. *Experimental Cell Research*, 276(1), pp.1–9.

Dalby, M.J. et al., 2003. Nucleus alignment and cell signaling in fibroblasts: Response to a micro-grooved topography. *Experimental Cell Research*, 284(2), pp.274–282.

Darus, F. et al., 2018. Techniques for fabrication and construction of three-dimensional bioceramic scaffolds: Effect on pores size, porosity and compressive strength. *Ceramics International*, 44(15), pp.18400–18407.

Deb, P. et al., 2018. Scaffold Development Using Biomaterials: A Review. *Materials Today: Proceedings*, 5(5), pp.12909–12919.

Dee, K.C., Andersen, T.T. & Bizios, R., 1998. Design and function of novel osteoblast-adhesive peptides for chemical modification of biomaterials. *Journal of Biomedical Materials Research*, 40(3), pp.371–377.

Deligianni, D.D. et al., 2000. Effect of surface roughness of hydroxyapatite on human bone marrow cell adhesion, proliferation, differentiation and detachment strength. *Biomaterials*, 22(1), pp.87–96.

Detterline, A.J. et al., 2005. Treatment options for articular cartilage defects of the knee. *Orthopaedic nursing / National Association of Orthopaedic Nurses*, 24(5), pp.361-6; quiz 367-8. Available at: http://www.ncbi.nlm.nih.gov/pubmed/16272915.

Douleh, D. & Frank, R.M., 2018. Marrow Stimulation: Microfracture, Drilling, and Abrasion. *Operative Techniques in Sports Medicine*, 26(3), pp.170–174.

Drury, J.L. & Mooney, D.J., 2003. Hydrogels for tissue engineering: Scaffold design variables and applications. *Biomaterials*, 24(24), pp.4337–4351.

Durante, S., 2012. Osteogenic differentiation of MG63 cells in biodegradable scaffolds based on gelatin and genipin., *Italian Journal of Anatomy and Embryology*, 117(2), pp.67.

Durmaz, S. & Okay, O., 2000. Phase separation during the formation of poly (acrylamide) hydrogels. *Polymer*, 41, pp.5729–5735.

Dutta, R.C. & Dutta, A.K., 2009. Cell-interactive 3D-scaffold; advances and applications. *Biotechnology Advances*, 27(4), pp.334–339.

Edmondson, R. et al., 2014. Three-Dimensional Cell Culture Systems and Their Applications in Drug Discovery and Cell-Based Biosensors. *ASSAY and Drug Development Technologies*, 12(4), pp.207–218.

El-Sherbiny, I. & Yacoub, M., 2013. Hydrogel scaffolds for tissue engineering: Progress and challenges. *Global cardiology science & practice*, 2013(3), pp.316–42.

Elbert, D.L. & Hubbell, J.A., 1996. Surface Treatments of Polymers for Biocompatibility. *Annual Review of Materials Science*, 26(1), pp.365–394.

Emans, P.J. et al., 2013. Tissue-engineered constructs: the effect of scaffold architecture in osteochondral repair. *Journal of tissue engineering and regenerative medicine*, 7(9), pp.751–756.

Engler, A.J. et al., 2006. Matrix Elasticity Directs Stem Cell Lineage Specification. *Cell*, 126(4), pp.677–689.

Engler, A.J. et al., 2004. Myotubes differentiate optimally on substrates with tissue-like stiffness: pathological implications for soft or stiff microenvironments. *The Journal of Cell Biology*, 166(6), pp.877–887.

Erggelet, C. & Vavken, P., 2016. Microfracture for the treatment of cartilage defects in the knee joint – A golden standard? *Journal of Clinical Orthopaedics and Trauma*, 7(3), pp.145–152.

Erickson, B.J., Strickland, S.M. & Gomoll, A.H., 2018. Indications, Techniques, Outcomes for Matrix-Induced Autologous Chondrocyte Implantation (MACI). *Operative Techniques in Sports Medicine*, 26(3), pp.175–182.

Falah, M. et al., 2010. Treatment of articular cartilage lesions of the knee. *International Orthopaedics*, 34(5), pp.621–630.

Fan, W. et al., 2013. Biomaterial scaffolds in cartilage-subchondral bone defects influencing the repair of autologous articular cartilage transplants. *Journal of Biomaterials Applications*, 27(8), pp.979–989.

Farndale, R.W., Buttle, D.J. & Barrett, A.J., 1986. Improved quantitation and discrimination of sulphated glycosaminoglycans by use of dimethylmethylene blue. *BBA - General Subjects*, 883(2), pp.173–177.

Filardo, G. et al., 2013. Treatment of Knee Osteochondritis Dissecans With a Cell-Free Biomimetic Osteochondral Scaffold. *The American Journal of Sports Medicine*, 41(8), pp.1786–1793.

Flemming, R. et al., 1999. Effects of synthetic micro-and nano-structured surfaces on cell behavior. *Biomaterials*, 20(1999), pp.573–588.

Fox, A.J.S., Wanivenhaus, F. & Rodeo, S.A., 2012. The basic science of the patella: structure, composition, and function. *The journal of knee surgery*, 25(2), pp.127–141.

Francis Suh, J.K. & Matthew, H.W.T., 2000. Application of chitosan-based polysaccharide biomaterials in cartilage tissue engineering: A review. *Biomaterials*, 21(24), pp.2589–2598.

Franz, T. et al., 2001. In situ compressive stiffness, biochemical composition, and structural integrity of articular cartilage of the human knee joint. *Osteoarthritis and Cartilage*, 9(6), pp.582–592.

Freemont, A.J., 1996. the Pathophysiology of Cartilage and Synovium. *British Journal of Rheumatology*, 35(soppL 3), pp.10–13.

Fu, Q. et al., 2011. Bioactive glass scaffolds for bone tissue engineering: State of the art and future perspectives. *Materials Science and Engineering C*, 31(7), pp.1245–1256. Available at: http://dx.doi.org/10.1016/j.msec.2011.04.022.

Gadjanski, I., 2017. Recent advances on gradient hydrogels in biomimetic cartilage tissue engineering. *F1000Research*, 6(0), p.2158.

Gaharwar, A., Schexnailder, P. & Schmidt, G., 2011. Introduction to Polymer Nanocomposite Biomaterials for Tissue Repair. *Nanobiomaterials Handbook*.

Gajendiran, M. et al., 2017. Conductive biomaterials for tissue engineering applications. *Journal of Industrial and Engineering Chemistry*, 51, pp.12–26.

Gelber, P.E. et al., 2018. Fresh Osteochondral and Meniscus Allografting for Post-traumatic Tibial Plateau Defects. *Arthroscopy Techniques*.

Genetos, D.C. et al., 2014. Impaired osteoblast differentiation in annexin A2- And -A5-deficient cells. *PLoS ONE*, 9(9), pp.3–10.

Getgood, A., Bhullar, T.P.S. & Rushton, N., 2009. Current concepts in articular cartilage repair. *Orthopaedics and Trauma*, 23(3), pp.189–200.

Gillette, J.M. & Nielsen-Preiss, S.M., 2004. The role of annexin 2 in osteoblastic mineralization. *Journal of cell science*, 117(Pt 3), pp.441–9.

Glennon-Alty, L. et al., 2013. Induction of mesenchymal stem cell chondrogenesis by polyacrylate substrates. *Acta Biomaterialia*, 9, pp.6041–6051.

Griffon, D.J. et al., 2006. Chitosan scaffolds: Interconnective pore size and cartilage engineering. *Acta Biomaterialia*, 2(3), pp.313–320.

Grosskinsky, U., 2006. Biomaterial regulations for tissue engineering. *Desalination*, 199(1–3), pp.265–267.

Grover, L.M. et al., 2006. Biologically mediated resorption of brushite cement in vitro. *Biomaterials*, 27(10), pp.2178–2185.

Hangody, L. et al., 2008. Autologous osteochondral grafting-Technique and long-term results. *Injury*, 39(1 SUPPL.), pp.32–39.

Haq, M.A., Su, Y. & Wang, D., 2017. Mechanical properties of PNIPAM based hydrogels: A review. *Materials Science and Engineering C*, 70, pp.842–855.

Hench, L.L., 1991. Bioceramics: From Concept to Clinic. *Journal of the American Ceramic Society*, 74(7), pp.1487–1510.

Hench, L.L., 1998. Biomaterials: a forecast for the future. *Biomaterials*, 19(16), pp.1419–1423.

Hench, L.L., 2006. The story of Bioglass®. *Journal of Materials Science: Materials in Medicine*, 17(11), pp.967–978.

Hirschfeld-Warneken, V.C. et al., 2008. Cell adhesion and polarisation on molecularly defined spacing gradient surfaces of cyclic RGDfK peptide patches. *European Journal of Cell Biology*, 87(8–9), pp.743–750.

Hoemann, C.D. et al., 2012. The cartilage-bone interface. *The Journal of Knee Surgery*, 25(2), pp.85–97.

Hoffman, A.S., 2012. Hydrogels for biomedical applications. *Advanced Drug Delivery Reviews*, 64(SUPPL.), pp.18–23.

Hollister, S.J., 2005. Porous scaffold design for tissue engineering. *Nature materials*, 4(7), pp.518–24.

Hollister, S.J., Maddox, R.D. & Taboas, J.M., 2002. Optimal design and fabrication of scaffolds to mimic tissue properties and satisfy biological constraints. *Biomaterials*, 23(20), pp.4095–4103.

Homminga, G.N. et al., 1990. Perichondral grafting for cartilage lesions of the knee. *The Journal of bone and joint surgery. British volume*, 72(6), pp.1003–7.

Hong Ong, Y., Lim, M. & Liu, Q., 2012. Comparison of principal component analysis and biochemical component analysis in Raman spectroscopy for the discrimination of apoptosis and necrosis in K562 leukemia cells, Optics Express, 20(22), pp.25041-25043

Hossain, K.M.Z. et al., 2018. Porous calcium phosphate glass microspheres for orthobiologic applications. *Acta Biomaterialia*, 72, pp.396–406.

Huber, M., Trattnig, S. & Lintner, F., 2000. Anatomy, biochemistry, and physiology of articular cartilage. *Investigative Radiology*, 35(10), pp.573–580.

Huh, D., Hamilton, G.A. & Ingber, D.E., 2011. From 3D cell culture to organs-on-chips. *Trends in Cell Biology*, 21(12), pp.745–754.

Hunziker, E.B., 1999. Articular cartilage repair: Are the intrinsic biological constraints undermining this process insuperable? *Osteoarthritis and Cartilage*, 7(1), pp.15–28.

Hunziker, E.B., 2002. Articular cartilage repair: Basic science and clinical progress. A review of the current status and prospects. *Osteoarthritis and Cartilage*, 10(6), pp.432–463.

Hutmacher, D.W., 2001. Scaffold design and fabrication technologies for engineering tissues — state of the art and future perspectives. *Journal of Biomaterials Science, Polymer Edition*, 12(1), pp.107–124.

Hutmacher, D.W., 2000. Scaffolds in tissue engineering bone and cartilage. *Biomaterials*, 21(24), pp.2529–43.

Hutmacher, D.W., Sittinger, M. & Risbud, M. V, 2004. Scaffold-based tissue engineering: rationale for computer-aided design and solid free-form fabrication systems. *Trends in Biotechnology*, 22(7), pp.354–362.

Ito, Y., 1999. Surface micropatterning to regulate cell functions. *Biomaterials*, 20(23–24), pp.2333–2342.

Izadifar, Z., Chen, X. & Kulyk, W., 2012. Strategic Design and Fabrication of Engineered Scaffolds for Articular Cartilage Repair. *Journal of Functional Biomaterials*, 3(4), pp.799–838.

Jagur-Grodzinski, J., 2006. Polymers for tissue engineering, medical devices, and regenerative medicine. Concise general review of recent studies. *Polymers for Advanced Technologies*, 17(6), pp.395–418.

Jobanputra, P. et al., 2001. Effectiveness of autologous chondrocyte transplantation for hyaline cartilage defects in knees: a rapid and systematic review. *Health Technology Assessment*, 5(11).

Jones, J.R. et al., 2007. Extracellular matrix formation and mineralization on a phosphate-free porous bioactive glass scaffold using primary human osteoblast (HOB) cells. *Biomaterials*, 28(9), pp.1653–1663.

Jones, J.R., 2015. Reprint of: Review of bioactive glass: From Hench to hybrids. *Acta Biomaterialia*, 23, pp.S53–S82.

Jones, J.R., 2013. Review of bioactive glass: from Hench to hybrids. *Acta Biomaterialia*, 9(1), pp.4457–4486.

Jones, J.R., Ehrenfried, L.M. & Hench, L.L., 2006. Optimising bioactive glass scaffolds for bone tissue engineering. *Biomaterials*, 27(7), pp.964–973.

Justice, B.A., Badr, N.A. & Felder, R.A., 2009. 3D cell culture opens new dimensions in cell-based assays. *Drug Discovery Today*, 14(1–2), pp.102–107.

Kang, H., Zeng, Y. & Varghese, S., 2018. Functionally graded multilayer scaffolds for in vivo osteochondral tissue engineering. *Acta Biomaterialia*, 78, pp.365–377.

Karageorgiou, V. & Kaplan, D., 2005. Porosity of 3D biomaterial scaffolds and osteogenesis. *Biomaterials*, 26(27), pp.5474–5491.

Karimi, T. et al., 2015. A developmentally inspired combined mechanical and biochemical signaling approach on zonal lineage commitment of mesenchymal stem cells in articular cartilage regeneration. *Integrative Biology (United Kingdom)*, 7(1), pp.112–127.

Katagiri, H., Mendes, L.F. & Luyten, F.P., 2017. Definition of a Critical Size Osteochondral Knee Defect and its Negative Effect on the Surrounding Articular Cartilage in the Rat. *Osteoarthritis and Cartilage*, 25(9), pp.1531–1540.

Keaveny, T.M., Morgan, E.F. & Yeh, O.C., 2004. Bone Mechanics. *Standard Handbook of Biomedical Engineering and Design*, pp.8.1-8.23.

Kepa, K., Coleman, R. & Grøndahl, L., 2015. In vitro mineralization of functional polymers. *Biosurface and Biotribology*, 1(3), pp.214–227.

Keselowsky, B.G., Collard, D.M. & García, A.J., 2003. Surface chemistry modulates fibronectin conformation and directs integrin binding and specificity to control cell adhesion. *Journal of biomedical materials research. Part A*, 66(2), pp.247–259.

Kheir, E. & Shaw, D., 2009a. Hyaline articular cartilage. *Orthopaedics and Trauma*, 23(6), pp.450–455.

Kheir, E. & Shaw, D., 2009b. Management of articular cartilage defects. *Orthopaedics and Trauma*, 23(4), pp.266–273.

Khoryani, Z., Seyfi, J. & Nekoei, M., 2018. Investigating the effects of polymer molecular weight and non-solvent content on the phase separation, surface morphology and hydrophobicity of polyvinyl chloride films. *Applied Surface Science*, 428, pp.933–940.

Kirsch, T. et al., 2000. The roles of annexins and types II and X collagen in matrix vesicle-mediated mineralization of growth plate cartilage. *Journal of Biological Chemistry*, 275(45), pp.35577–35583.

Kokubo, T. & Takadama, H., 2006. How useful is SBF in predicting in vivo bone bioactivity? *Biomaterials*, 27(15), pp.2907–2915.

Kon, E. et al., 2014. Clinical results of multilayered biomaterials for osteochondral regeneration. *Journal of Experimental Orthopaedics*, 1(1), pp.10.

Koszyca, B., Fazzalari, N.L. & Vernon-Roberts, B., 1996. Quantitative analysis of the bone-cartilage interface within the knee. *Knee*, 3(1–2), pp.23–31.

Van der Kraan, P.M. et al., 2002. Interaction of chondrocytes, extracellular matrix and growth factors: Relevance for articular cartilage tissue engineering. *Osteoarthritis and Cartilage*, 10(8), pp.631–637.

Kurtz, S.M. & Devine, J.N., 2007. PEEK biomaterials in trauma, orthopedic, and spinal implants. *Biomaterials*, 28(32), pp.4845–4869.

Kwiatkowska, J., Suchanek, K. & Rajchel, B., 2012. Bioactive glass coatings synthesized by pulsed laser deposition technique. *Acta Physica Polonica A*, 121(2), pp.502–505.

Kwok, A.Y. et al., 2003. Synthetic hydrogels 2. Polymerization induced phase separation in acrylamide systems. *Polymer*, 44(24), pp.7335–7344.

Lanzalaco, S. & Armelin, E., 2017. Poly(N-isopropylacrylamide) and Copolymers: A Review on Recent Progresses in Biomedical Applications. *Gels*, 3(4), pp.36.

Laurencin, C.T. et al., 1999. Tissue Engineering: Orthopedic Applications. *Annual Review of Biomedical Engineering*, 1(1), pp.19–46.

Lavik, E. & Langer, R., 2004. Tissue engineering: Current state and perspectives. *Applied Microbiology and Biotechnology*, 65(1), pp.1–8.

Lee, S. et al., 2012. Potential Bone Replacement Materials Prepared by Two Methods. *MRS Proceedings*, 1418, pp.mrsf11-1418-mm06-02.

Yuan, Y. & Lee, T.R., 2013. Contact angle and wetting properties. In *Surface science techniques* (pp. 3-34). Springer, Berlin, Heidelberg..

Leferink, A.M., van Blitterswijk, C.A. & Moroni, L., 2016. Methods of Monitoring Cell Fate and Tissue Growth in Three-Dimensional Scaffold-Based Strategies for *In Vitro* Tissue Engineering. *Tissue Engineering Part B: Reviews*, 22(4), pp.265–283.

Leong, K.F. et al., 2008. Engineering functionally graded tissue engineering scaffolds. *Journal of the Mechanical Behavior of Biomedical Materials*, 1(2), pp.140–152.

Leong, K.F., Cheah, C.M. & Chua, C.K., 2003. Solid freeform fabrication of three-dimensional scaffolds for engineering replacement tissues and organs. *Biomaterials*, 24(13), pp.2363–78.

Levingstone, T.J. et al., 2014. A biomimetic multi-layered collagen-based scaffold for osteochondral repair. *Acta Biomaterialia*, 10(5), pp.1996–2004.

Li, L. et al., 2018. Natural hydrogels for cartilage regeneration: Modification, preparation and application.

Lien, S.M., Ko, L.Y. & Huang, T.J., 2009. Effect of pore size on ECM secretion and cell growth in gelatin scaffold for articular cartilage tissue engineering. *Acta Biomaterialia*, 5(2), pp.670–679.

Little, C.J., Bawolin, N.K. & Chen, X., 2011. Mechanical Properties of Natural Cartilage and Tissue-Engineered Constructs. *Tissue Engineering Part B: Reviews*, 17(4), pp.213–227.

Liu, C., Xia, Z. & Czernuszka, J.T., 2007. Design and Development of Three-Dimensional Scaffolds for Tissue Engineering. *Chemical Engineering Research and Design*, 85(7), pp.1051–1064.

Liu, M. et al., 2013. Tissue engineering stratified scaffolds for articular cartilage and subchondral bone defects repair. *Orthopedics*, 36(11), pp.868–73.

Liu, Y. et al., 2011. Study on the microstructure of human articular cartilage/bone interface. *Journal of Bionic Engineering*, 8(3), pp.251–262.

Lopes, D. et al., 2018. Bone physiology as inspiration for tissue regenerative therapies. *Biomaterials*, 185, pp.240–275.

Lord, M.S., Foss, M. & Besenbacher, F., 2010. Influence of nanoscale surface topography on protein adsorption and cellular response. *Nano Today*, 5(1), pp.66–78.

Lu, T., xin Li, R., Zhang, Y., xian Yan, Y., Guo, Y., Guan, J., min Wu, J., Ning, B., jie Huang, S. & zheng Zhang, X., 2011. Preparation, properties, and cell attachment/growth behavior of chitosan/acellular derm matrix composite materials. *Journal of Biomaterials and Nanobiotechnology*, *2*(02), p.124..

Lu, T., Li, Y. & Chen, T., 2013. Techniques for fabrication and construction of three-dimensional scaffolds for tissue engineering. *International Journal of Nanomedicine*, 8, pp.337–350.

Di Luca, A.,. et al., 2016. Gradients in pore size enhance the osteogenic differentiation of human mesenchymal stromal cells in three-dimensional scaffolds. *Scientific Reports*, 6(1), pp.22898.

Di Luca, A., et al., 2016. Influencing chondrogenic differentiation of human mesenchymal stromal cells in scaffolds displaying a structural gradient in pore size. *Acta Biomaterialia*, 36, pp.210–219.

Di Luca, A., Van Blitterswijk, C. & Moroni, L., 2015. The osteochondral interface as a gradient tissue: From development to the fabrication of gradient scaffolds for regenerative medicine. *Birth Defects Research Part C: Embryo Today: Reviews*, 105(1), pp.34–52.

Lynch, I. et al., 2005. Correlation of the Adhesive Properties of Cells to N - Isopropylacrylamide / N - tert -Butylacrylamide Copolymer Surfaces with Changes in Surface Structure Using Contact Angle Measurements , Molecular Simulations , and Raman Spectroscopy. *Chemistry of Materials*, 17(6), pp.3889–3898.

Lynn, A.K. et al., 2010. Design of a multiphase osteochondral scaffold. I. Control of chemical composition. *Journal of biomedical materials research. Part A*, 92(3), pp.1057–65.

Lyons, T.J. et al., 2006. The normal human chondro-osseous junctional region: Evidence for contact of uncalcified cartilage with subchondral bone and marrow spaces. *BMC Musculoskeletal Disorders*, 7, pp.1–8.

Ma, P.X., 2008. Biomimetic materials for tissue engineering. *Advanced Drug Delivery Reviews*, 60(2), pp.184–198.

Ma, P.X., 2004. Scaffolds for tissue fabrication. *Materials Today*, 7(5), pp.30–40.

Madry, H., 2010. The subchondral bone: a new frontier in articular cartilage repair. *Knee Surgery, Sports Traumatology, Arthroscopy*, 18(4), pp.417–418.

Madry, H., van Dijk, C.N. & Mueller-Gerbl, M., 2010. The basic science of the subchondral bone. *Knee Surgery, Sports Traumatology, Arthroscopy*, 18(4), pp.419–433.

Mai, T. et al., 2018. Anionic Polymer Brushes for Biomimetic Calcium Phosphate Mineralization—A Surface with Application Potential in Biomaterials. *Polymers*, 10(10), p.1165.

Mane, S., 2016. Effect of Porogens (Type and Amount) on Polymer Porosity: A Review. *Canadian Chemical Transactions Year*, 4(2), pp.210–225.

Mano, J.F., 2015. Designing biomaterials for tissue engineering based on the deconstruction of the native cellular environment. *Materials Letters*, 141(0), pp.198–202.

Marlovits, S. et al., 2005. Early postoperative adherence of matrix-induced autologous chondrocyte implantation for the treatment of full-thickness cartilage defects of the femoral condyle. *Knee Surgery, Sports Traumatology, Arthroscopy*, 13(6), pp.451–457.

Martin, I. et al., 2007. Osteochondral tissue engineering. *Journal of Biomechanics*, 40(4), pp.750–765.

Matyjaszewski, K., 2012. Atom Transfer Radical Polymerization (ATRP): Current Status and Future Perspectives. *Macromolecules*, 45(10), pp.4015–4039.

Matyjaszewski, K. et al., 2000. Gradient copolymers by atom transfer radical copolymerization. *Journal of Physical Organic Chemistry*, 13(12), pp.775–786.

Melero-Martin, J.M. & Al-Rubeai, M., 2007. In Vitro Expansion of Chondrocytes. In *Topics in Tissue Engineering*. pp. 1–37.

Miao, X. & Sun, D., 2010. Graded/gradient porous biomaterials. *Materials*, 3(1), pp.26–47.

Mithoefer, K. et al., 2009. Clinical efficacy of the microfracture technique for articular cartilage repair in the knee: An evidence-based systematic analysis. *American Journal of Sports Medicine*, 37(10), pp.2053–2063.

Mohan, Y.M. & Geckeler, K.E., 2007. Polyampholytic hydrogels: Poly(N-isopropylacrylamide)-based stimuli-responsive networks with poly(ethyleneimine). *Reactive and Functional Polymers*, 67(2), pp.144–155

Moriguchi, T. et al., 2003. Elucidation of adsorption mechanism of bone-staining agent alizarin red S on hydroxyapatite by FT-IR microspectroscopy. *Journal of Colloid and Interface Science*, 260(1), pp.19–25.

Morin, L.G., 1974. Direct colorimetric determination of serum calcium with o cresolphthalein complexion. *American Journal of Clinical Pathology*, 61(1), pp.114–117.

Mow VC, Huiskes R, Stokes IA, I.J., 2005. *Basic Orthopaedic Biomechanics and Mechano-Biology, 3rd ed.*, Lippincott Williams & Wilkins. Available at: https://www.barnesandnoble.com/w/basic-orthop

Müller-Gerbl, M., Schulte, E. & Putz, R., 1987. The thickness of the calcified layer of articular cartilage: a function of the load supported? *Journal of anatomy*, 154, pp.103–11.

Muramatsu K Wada T, Hirai H, Miyawaki F, S.Y., 2012. Poly(N-isopropylacrylamide-co-N-tert-butylacrylamide)- grafted hyaluronan as an injectable and self-assembling scaffold for cartilage tissue engineering. *Journal of Biomedical Science and Engineering*, 5(11), pp.639–646.

Murphy, C.M., Haugh, M.G. & O'Brien, F.J., 2010. The effect of mean pore size on cell attachment, proliferation and migration in collagen-glycosaminoglycan scaffolds for bone tissue engineering. *Biomaterials*, 31(3), pp.461–466.

Nam, Y.S. & Park, T.G., 1999. Porous biodegradable polymeric scaffolds prepared by thermally induced phase separation. *Journal of Biomedical Materials Research*, 47(1), pp.8–17.

NICE, 2017. *Autologous chondrocyte implantation for treating symptomatic articular cartilage defects of the knee | Guidance and guidelines | NICE*, NICE.

Norman, J.J. & Desai, T.A., 2006. Methods for fabrication of nanoscale topography for tissue engineering scaffolds. *Annals of Biomedical Engineering*, 34(1), pp.89–101.

Notingher, I. et al., 2002. Application of Raman microspectroscopy to the characterisation of bioactive materials. *Materials Characterization*, 49(3), pp.255–260.

Nukavarapu, S.P. & Dorcemus, D.L., 2013. Osteochondral tissue engineering: Current strategies and challenges. *Biotechnology Advances*, 31(5), pp.706–721.

O'Brien, F.J., 2011. Biomaterials & scaffolds for tissue engineering. *Materials Today*, 14(3), pp.88–95.

O'Shea, T.M. & Miao, X., 2008. Bilayered Scaffolds for Osteochondral Tissue Engineering. *Tissue Engineering Part B: Reviews*, 14(4), pp.447–464.

Osmekhina, E. et al., 2010. Sandwich ELISA for quantitative detection of human collagen prolyl 4-hydroxylase. *Microb Cell Fact*, 9, pp.48.

Othman, Z. et al., 2018. Understanding interactions between biomaterials and biological systems using proteomics. *Biomaterials*, 167, pp.191–204.

Pal, S., 2014. Design of artificial human joints & organs. In *Design of Artificial Human Joints & Organs*. pp. 1–419.

Pampaloni, F., Reynaud, E.G. & Stelzer, E.H.K., 2007. The third dimension bridges the gap between cell culture and live tissue. *Nature Reviews Molecular Cell Biology*, 8(10), pp.839–845.

Panseri, S. et al., 2012. Osteochondral tissue engineering approaches for articular cartilage and subchondral bone regeneration. *Knee Surgery, Sports Traumatology, Arthroscopy*, 20(6), pp.1182–1191.

Pape, D. et al., 2010. Disease-specific clinical problems associated with the subchondral bone. *Knee surgery, sports traumatology, arthroscopy : official journal of the ESSKA*, 18(4), pp.448–462.

Patel, N. & Buckland-Wright, C., 1999. Advancement in the zone of calcified cartilage in osteoarthritic hands of patients detected by high definition macroradiography. *Osteoarthritis and Cartilage*, 7(6), pp.520–525.

Patterson, J., Martino, M.M. & Hubbell, J.A., 2010. Biomimetic materials in tissue engineering. *Materials Today*, 13(1–2), pp.14–22.

Pelton, R., 2010. Poly(N-isopropylacrylamide) (PNIPAM) is never hydrophobic. *Journal of Colloid and Interface Science*, 348(2), pp.673–674.

Preethi Soundarya, S. et al., 2018. Bone tissue engineering: Scaffold preparation using chitosan and other biomaterials with different design and fabrication techniques. *International Journal of Biological Macromolecules*, 119, pp.1228–1239.

Promo Cell, 2016. *Osteoblasts : Instruction Manual*, Heidelberg, Germany: Promo Cell.

Puppi, D. et al., 2010. Polymeric materials for bone and cartilage repair. *Progress in Polymer Science*, 35(4), pp.403–440.

Qui, Y.S. et al., 2003. Observations of subchondral plate advancement during osteochondral repair: A histomorphometric and mechanical study in the rabbit femoral condyle. *Osteoarthritis and Cartilage*, 11(11), pp.810–820.

Redman, S., Oldfield, S. & Archer, C., 2005. Current strategies for articular cartilage repair. *European Cells and Materials*, 9(0), pp.23–32.

Rehfeldt, F. et al., 2007. Cell responses to the mechanochemical microenvironment-Implications for regenerative medicine and drug delivery. *Advanced Drug Delivery Reviews*, 59(13), pp.1329-1339.

Remanan, S. et al., 2018. Recent Advances in Preparation of Porous Polymeric Membranes by Unique Techniques and Mitigation of Fouling through Surface Modification. *ChemistrySelect*, 3(2), pp.609–633.

Roach, P. et al., 2010. Chemical Modification of Porous Scaffolds Using Plasma Polymers. *Design*, pp.1–20.

Roach, P. et al., 2007. Modern biomaterials: A review - Bulk properties and implications of surface modifications. *Journal of Materials Science: Materials in Medicine*, 18(7), pp.1263–1277.

Roberts, S. et al., 2003. Autologous chondrocyte implantation for cartilage repair: monitoring its success by magnetic resonance imaging and histology. *Arthritis research therapy*, 5(1), pp.R60–R73.

Sachlos, E. & Czernuszka, J.T., 2003. Making tissue engineering scaffolds work. Review: the application of solid freeform fabrication technology to the production of tissue engineering scaffolds. *European cells & materials*, 5, pp.29-39; discussion 39-40.

Sartori, M. et al., 2017. A new bi-layered scaffold for osteochondral tissue regeneration: In vitro and in vivo preclinical investigations. *Materials Science and Engineering C*, 70, pp.101–111.

Sato-Berrú, R.Y. et al., 2007. Application of principal component analysis and Raman spectroscopy in the analysis of polycrystalline BaTiO 3 at high pressure. *Spectrochimica Acta Part A*, 66, pp.557–560.

Schaefer, D. et al., 2002. Tissue-engineered composites for the repair of large osteochondral defects. *Arthritis and Rheumatism*, 46(9), pp.2524–2534.

Seidi, A. et al., 2011. Gradient biomaterials for soft-to-hard interface tissue engineering. *Acta Biomaterialia*, 7(4), pp.1441–1451.

Seo, S.-J. et al., 2014. Strategies for osteochondral repair: Focus on scaffolds. *Journal of Tissue Engineering*, 5,pp.2041731414541850.

Shahgaldi, B.F., 1998. Repair of large osteochondral defects: Load-bearing and structural properties of osteochondral repair tissue. *Knee*, 5(2), pp.111–117.

Shapiro, J.M. & Oyen, M.L., 2013. Hydrogel composite materials for tissue engineering scaffolds. *Jom*, 65(4), pp.505–516.

Sherwood, J.K. et al., 2002. A three-dimensional osteochondral composite scaffold for articular cartilage repair. *Biomaterials*, 23(24), pp.4739–4751.

Shi, J. et al., 2010. Nanotechnology in drug delivery and tissue engineering: From discovery to applications. *Nano Letters*, 10(9), pp.3223–3230.

Shin, H., Jo, S. & Mikos, A.G., 2003. Biomimetic materials for tissue engineering. *Biomaterials*, 24(24), pp.4353–64.

Shirtcliffe, N.J. et al., 2005. Porous materials show superhydrophobic to superhydrophilic switching. *Chemical communications (Cambridge, England)*, (25), pp.3135–3137.

Smith, G.D., 2005. A clinical review of cartilage repair techniques. *Journal of Bone and Joint Surgery - British Volume*, 87–B(4), pp.445–449.

Sobral, J.M. et al., 2011. Three-dimensional plotted scaffolds with controlled pore size gradients: Effect of scaffold geometry on mechanical performance and cell seeding efficiency. *Acta Biomaterialia*, 7(3), pp.1009–1018.

Sola, A., Bellucci, D. & Cannillo, V., 2016. Functionally graded materials for orthopedic applications – an update on design and manufacturing. *Biotechnology Advances*, 34(5), pp.504–531.

Solchaga, L.A. et al., 2005. Repair of osteochondral defects with hyaluronan- and polyester-based scaffolds. *Osteoarthritis and Cartilage*, 13(4), pp.297–309.

Sophia Fox, A.J., Bedi, A. & Rodeo, S.A., 2009. The basic science of articular cartilage: structure, composition, and function. *Sports health*, 1(6), pp.461–8.

Staiger, M.P. et al., 2006. Magnesium and its alloys as orthopedic biomaterials: A review. *Biomaterials*, 27(9), pp.1728–1734.

Steadman, J.R., Rodkey, W.G. & Briggs, K.K., 1997. Microfracture technique for full-thickness chondral defects: Technique and clinical results. *Op Tech Orthop*, 7(4), pp.300–304..

Steinwachs, M.R., Guggi, T. & Kreuz, P.C., 2008. Marrow stimulation techniques. *Injury*, 39(SUPPL.1), pp.26–31.

Steward, A.J., Liu, Y. & Wagner, D.R., 2011. Engineering cell attachments to scaffolds in cartilage tissue engineering. *Jom*, 63(4), pp.74–82.

Subia, B., Kundu, J. & C., S., 2010. Biomaterial Scaffold Fabrication Techniques for Potential Tissue Engineering Applications. In *Tissue Engineering*. Daniel Eberli, IntechOpen

Suh, J.K. et al., 1997. Injury and repair of articular cartilage: Related scientific issues. *Operative Techniques in Orthopaedics*, 7(4), pp.270–278.

Swann, A.C. & Seedhom, B.B., 1993. The Stiffness of Normal Articular-cartilage and the Predominant Acting Stress Levels - Implications For the Etiology of Osteoarthrosis. *British Journal of Rheumatology*, 32(1), pp.16–25.

Swieszkowski, W. et al., 2007. Repair and regeneration of osteochondral defects in the articular joints. *Biomolecular Engineering*, 24(5), pp.489–495.

Tampieri, A. et al., 2008. Design of graded biomimetic osteochondral composite scaffolds. *Biomaterials*, 29(26), pp.3539–3546.

Tan, J. et al., 2005. Improved cell adhesion and proliferation on synthetic phosphonic acid-containing hydrogels. *Biomaterials*, 26(17), pp.3663–3671.

Temenoff, J.S. & Mikos, a. G., 2000. Tissue Engineering for Regeneration of Articular Cartilage. *Biomaterials*, 21, pp.431–440.

Temenoff, J.S. & Mikos, A.G., 2000. Review: Tissue engineering for regeneration of articular cartilage. *Biomaterials*, 21(5), pp.431–440.

Thavarajah, R. et al., 2012. Chemical and physical basics of routine formaldehyde fixation. *Journal of oral and maxillofacial pathology : JOMFP*, 16(3), pp.400–5.

Thevenot, P., Hu, W. & Tang, L., 2008. Surface chemistry influences implant biocompatibility. *Current topics in medicinal chemistry*, 8(4), pp.270–280.

V Thomas, L., VG, R. & D Nair, P., 2017. Effect of stiffness of chitosan-hyaluronic acid dialdehyde hydrogels on the viability and growth of encapsulated chondrocytes. *International Journal of Biological Macromolecules*, 104, pp.1925–1935.

Tsou, Y.-H. et al., 2016. Hydrogel as a bioactive material to regulate stem cell fate. *Bioactive Materials*, 1(1), pp.39–55.

Turnbull, G. et al., 2018. 3D bioactive composite scaffolds for bone tissue engineering. *Bioactive Materials*, 3(3), pp.278–314.

Ueda, K. & Yoshimura, M., 2004. Fabrication of nanofigures by focused electron beam-induced deposition. *Thin Solid Films*, 464, pp.331–334.

Underwood, P. a & Bennett, F. a, 1989. A comparison of the biological activities of the cell-adhesive proteins vitronectin and fibronectin. *Journal of cell science*, 93 (Pt 4)(1984), pp.641–649.

Vahdati, A. & Wagner, D.R., 2013. Implant size and mechanical properties influence the failure of the adhesive bond between cartilage implants and native tissue in a finite element analysis. *Journal of Biomechanics*, 46(9), pp.1554–1560.

Vasita, R. & Katti, D.S., 2006. Nanofibers and their applications in tissue engineering. *International Journal of Nanomedicine*, 1(1), pp.15–30.

Vijayavenkataraman, S. et al., 2017. Design of Three-Dimensional Scaffolds with Tunable Matrix Stiffness for Directing Stem Cell Lineage Specification: An In Silico Study. *Bioengineering*, 4(3), p.66. Available at: http://www.mdpi.com/2306-5354/4/3/66.

Virtanen, P. & Isotupa, K., 1980. Staining properties of alizarin red S for growing bone in vitro. *Cells Tissues Organs*, 108(2), pp.202–207.

Vo, T.N. et al., 2015. In vitro and in vivo evaluation of self-mineralization and biocompatibility of injectable, dual-gelling hydrogels for bone tissue engineering. *Journal of controlled release : official journal of the Controlled Release Society*, 205, pp.25–34.

de Vries-van Melle, M.L. et al., 2014. Chondrogenic differentiation of human bone marrow-derived mesenchymal stem cells in a simulated osteochondral environment is hydrogel dependent. *European Cells and Materials*, 27, pp.112–123.

Wan, Y. et al., 2005. Adhesion and proliferation of OCT-1 osteoblast-like cells on micro- and nano-scale topography structured poly(L-lactide). *Biomaterials*, 26(21), pp.4453–4459.

Wang, T., Lai, J.H. & Yang, F., 2016. Effects of Hydrogel Stiffness and Extracellular Compositions on Modulating Cartilage Regeneration by Mixed Populations of Stem Cells and Chondrocytes *In Vivo*. *Tissue Engineering Part A*, 22(23–24), pp.1348–1356.

Weinbrandt, R.M. & Fatt, I., 1969. A Scanning Electron Microscope Study of the Pore Structure of Sandstone. *Journal of Petroleum Technology*, 21(05), pp.543–548.

Weiner, S. & Traub, W., 1992. Bone structure: from angstroms to microns. *The FASEB Journal*, 6(3), pp.879–885.

Weiner, S. & Wagner, H.D., 1998. THE MATERIAL BONE: Structure-Mechanical Function Relations. *Annual Review of Materials Science*, 28(1), pp.271–298.

Wells, R.G., 2008. The role of matrix stiffness in regulating cell behavior. *Hepatology*, 47(4), pp.1394–1400.

Williams, D.F., 2008. On the mechanisms of biocompatibility. *Biomaterials*, 29(20), pp.2941–2953.

Williams, D.F., 2009. On the nature of biomaterials. *Biomaterials*, 30(30), pp.5897–5909.

Wilson, J. et al., 1981. Toxicology and biocompatibility of bioglasses. *Journal of Biomedical Materials Research*, 15(6), pp.805–817.

Wojnar, R., 2010. Bone and Cartilage - its Structure and Physical Properties. In *Biomechanics of Hard Tissues*. Weinheim, Germany: Wiley-VCH Verlag GmbH & Co. KGaA, pp. 1–75.

Woo, R. et al., 2005. Biomaterials: historical overview and current direction. In *Nanoscale Technology in Biological Systems*. CRC Press, Boca Raton, FL, pp. 1–24.

Wu, C. & Xiao, Y., 2009. Evaluation of the In Vitro Bioactivity of Bioceramics. *Bone and Tissue Regeneration Insights*, 2009(2), pp.25–29.

Xiao, Y. et al., 2013. Mechanical Testing of Hydrogels in Cartilage Tissue Engineering: Beyond the Compressive Modulus. *Tissue Engineering Part B: Reviews*, 19(5), pp.403–412.

Yang, J. et al., 2009. A high-throughput assay of cell-surface interactions using topographical and chemical gradients. *Advanced Materials*, 21(3), pp.300–304.

Yang, J. et al., 2017. Cell-laden hydrogels for osteochondral and cartilage tissue engineering. *Acta Biomaterialia*, 57, pp.1–25.

Yang, R. et al., 2017. PTMAc-PEG-PTMAc hydrogel modified by RGDC and hyaluronic acid promotes neural stem cells' survival and differentiation: In vitro. *RSC Advances*, 7(65), pp.41098–41104.

Yeong, W.Y. et al., 2004. Rapid prototyping in tissue engineering: Challenges and potential. *Trends in Biotechnology*, 22(12), pp.643–652.

You, B. et al., 2018. Bilayered HA/CS/PEGDA hydrogel with good biocompatibility and self-healing property for potential application in osteochondral defect repair. *Journal of Materials Science and Technology*, 34(6), pp.1016–1025.

You, Y.-Z. et al., 2008. Temperature-Controlled Uptake and Release in PNIPAM-Modified Porous Silica Nanoparticles. *Chemistry of Materials*, 20(10), pp.3354–3359.

Yousefi, A.M. et al., 2015. Current strategies in multiphasic scaffold design for osteochondral tissue engineering: A review. *Journal of Biomedical Materials Research - Part A*, 103(7), pp.2460–2481.

Zengerink, M. et al., 2010. Treatment of osteochondral lesions of the talus: A systematic review. *Knee Surgery, Sports Traumatology, Arthroscopy*, 18(2), pp.238–246.

Ziats, N.P., Miller, K.M. & Anderson, J.M., 1988. In vitro and in vivo interactions of cells with biomaterials. *Biomaterials*, 9(1), pp.5–13.

Zizak, I. et al., 2003. Characteristics of mineral particles in the human bone/cartilage interface. *Journal of Structural Biology*, 141(3), pp.208–217.

Appendix 1. Standard curves

Alizarin quantification and calcium assay

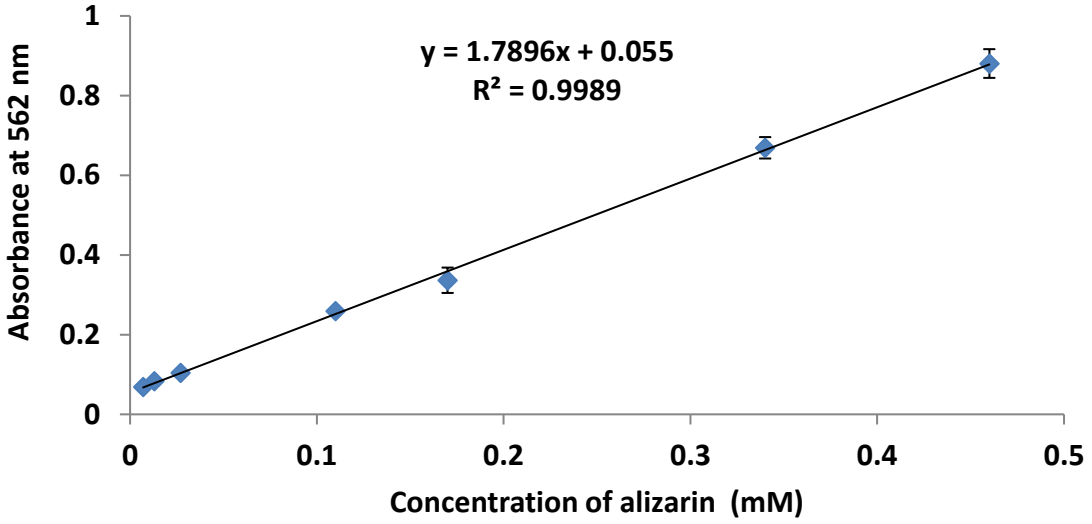

Best standard curve drawn for alizarin quantification using cetyl pyridenium chloride (CPC) test.

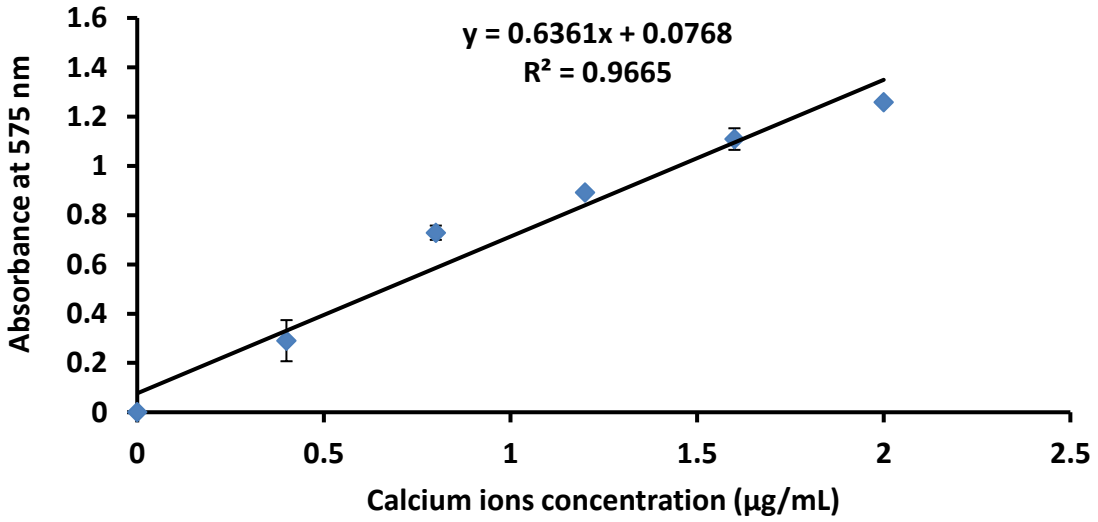

Best standard curve drawn for calcium assay (calcium ions standard solution is readily supplied with calcium assay kit).

DMMB assay for GAGs

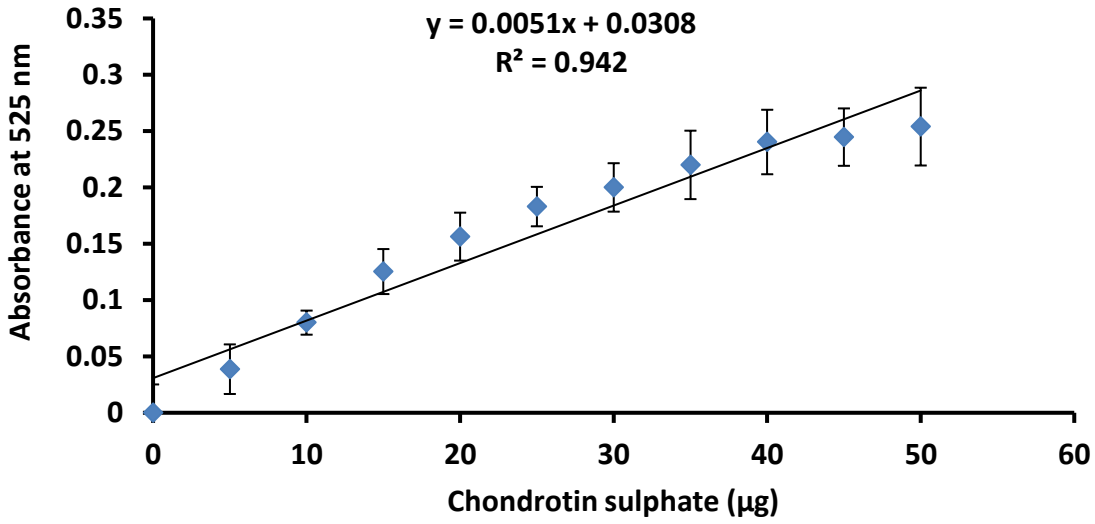

Best standard curve drawn for DMMB assay using serial dilutions of chondroitin sulphate measured at 525 nm wavelength

ELISA immunoassay

Collagen I

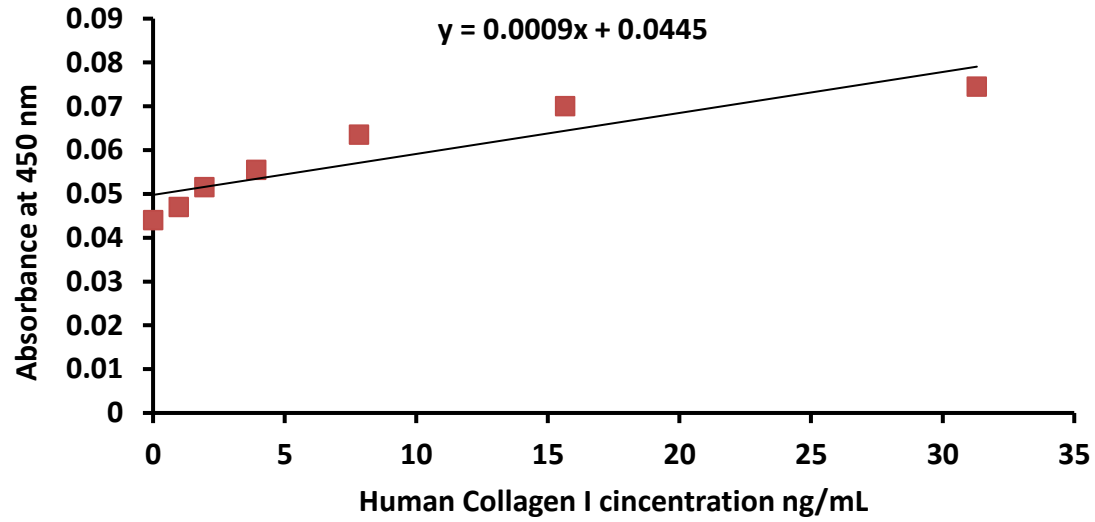

Best standard curve drawn for ELISA collagen I assay using serial delusion of collagen I standard solution (supplied with the assay kit).

Collagen II

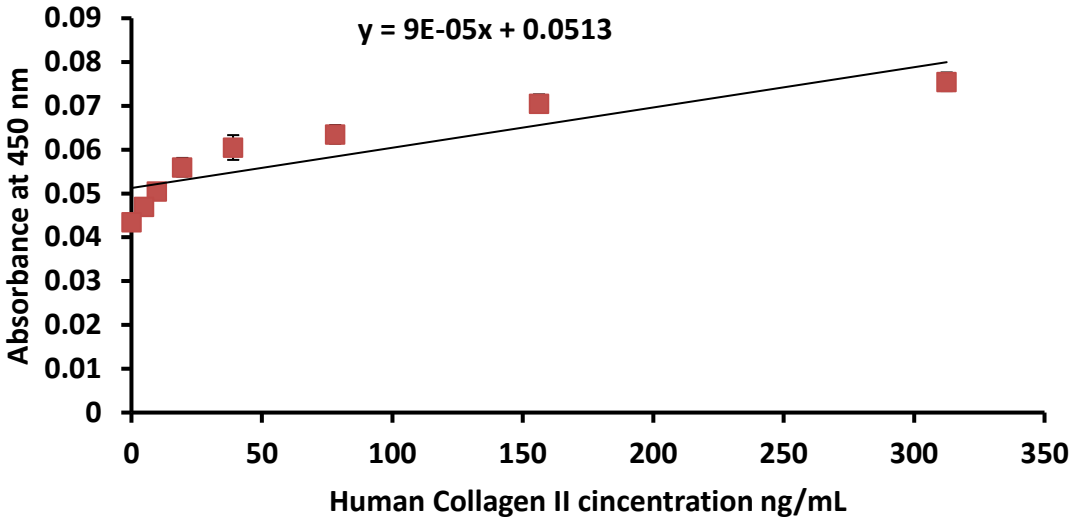

Best standard curve drawn for ELISA collagen II assay using serial delusion of collagen II standard solution (supplied with the assay kit).

Annexin A2

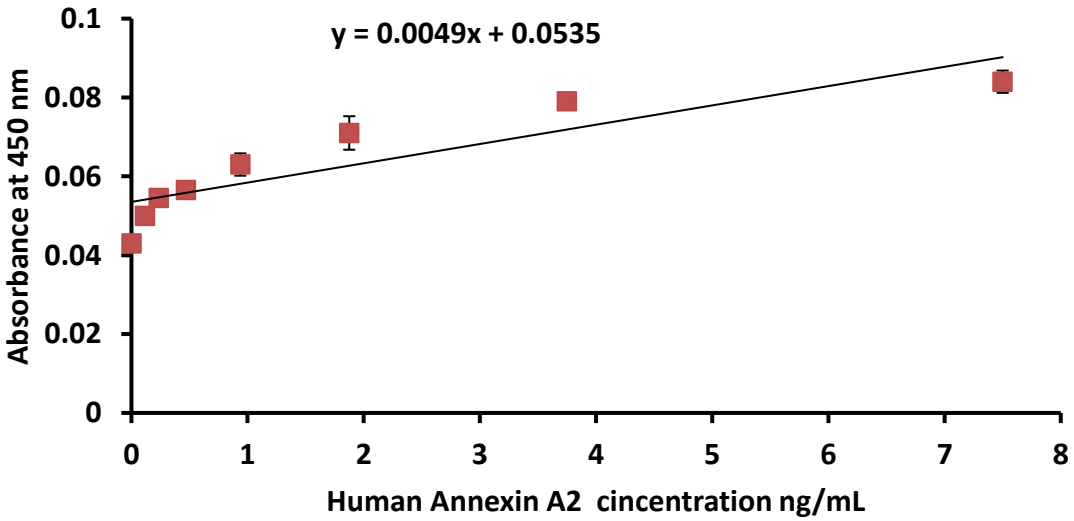

Best standard curve drawn for ELISA annexin A2 assay using serial delusion of annexin A2 standard solution (supplied with the assay kit).

Alkaline phosphatase

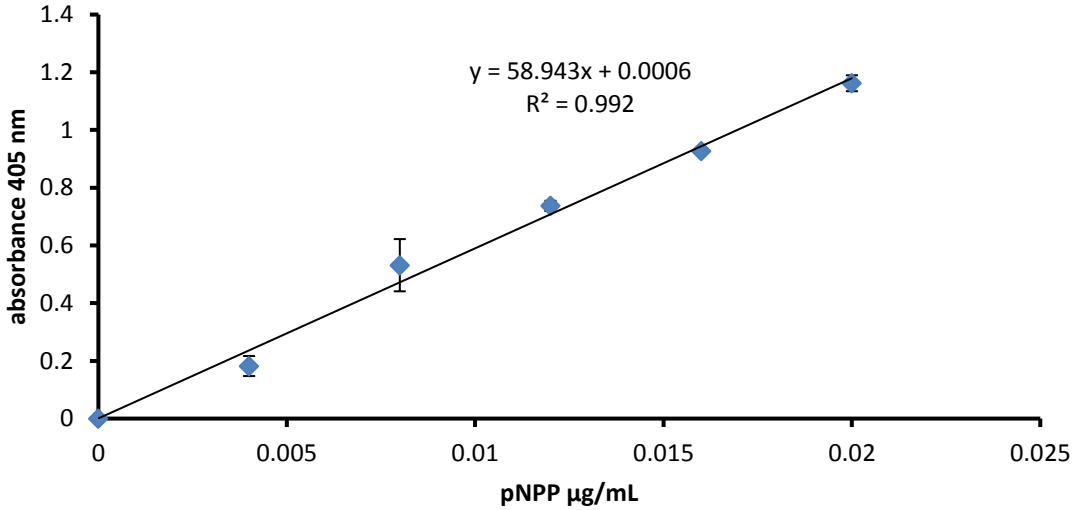

Best standard curve drawn for Alkaline phosphatase adjusted using serial concentrations of pNPP in µg/mL

Appendix 2. Protocol for preparing simulated body fluid (SBF)

The solution has ion concentrations nearly equal to those of human blood plasma and is buffered at pH 7.40 with 50 mM trishydroxymethylaminomethane and 45 mM hydrochloric acid at 36.5°C.

Department of Material Chemistry,
Graduate School of Engineering, Kyoto University

1. Wash all the bottles and wares with 1N-HCl solution, neutral detergent, and ion -exchanged and distilled water, and then dry them.
2. Put 500 ml of ion-exchanged and distilled water into one liter polyethylene bottle, and cover the bottle with a watch glass.
3. Stir the water in the bottle with a magnetic stirrer, and dissolve the reagents one by one in the order as given in Table 1 (One after the former reagent was completely dissolved).
4. Adjust the temperature of the solution in the bottle at 36.5℃ with a water bath, and adjust pH of the solution at pH 7.40 by stirring the solution and titrating 1N-HCl solution (When the pH electrode is removed from the solution, add the water used for washing the electrode to the solution).
5. Transfer the solution from the polyethylene bottle to a volumetric glass flask. Add the water used for washing the polyethylene bottle to thew solution in the flask.
6. Adjust the total volume of the solution to one liter by adding ion-exchanged and distilled water and shaking the flask at 20℃.
7. Transfer the solution from the flask to a polyethylene or polystyrene bottle, and store the bottle in a refrigerator at 5-10℃ (If some substance is precipitated in the solution during the storage, do not use this solution as SBF and its container again).

Table 1. Ion concentrations (mM) of SBF and juman blood plasma

Ion	Simulate Body Fluid	Blood plasma
Na^+	142.0	142.0
K^+	5.0	5.0
Mg^{2+}	1.5	1.5
Ca^{2+}	2.5	2.5
Cl^-	148.8	103.0
HCO^{3-}	4.2	27.0
HPO_4^{2-}	1.0	1.0
SO_4^{2-}	0.5	0.5

Table2. Regents for preparing SBF (pH7.40, 1L)

Order	Reagent	Amount
1	NaCl	7.996 g
2	$NaHCO_3$	0.350 g
3	KCl	0.224 g
4	$K_2HPO_4 \cdot 3H_2O$	0.228 g
5	$MgCl_2 \cdot 6H_2O$	0.305 g
6	1M-HCl	40 mL
(About 90 % of total amount of HCl to be added)		
7	$CaCl_2$	0.278 g
8	Na_2SO_4	0.071 g
9	$(CH_2OH)_3CNH_2$	6.057 g

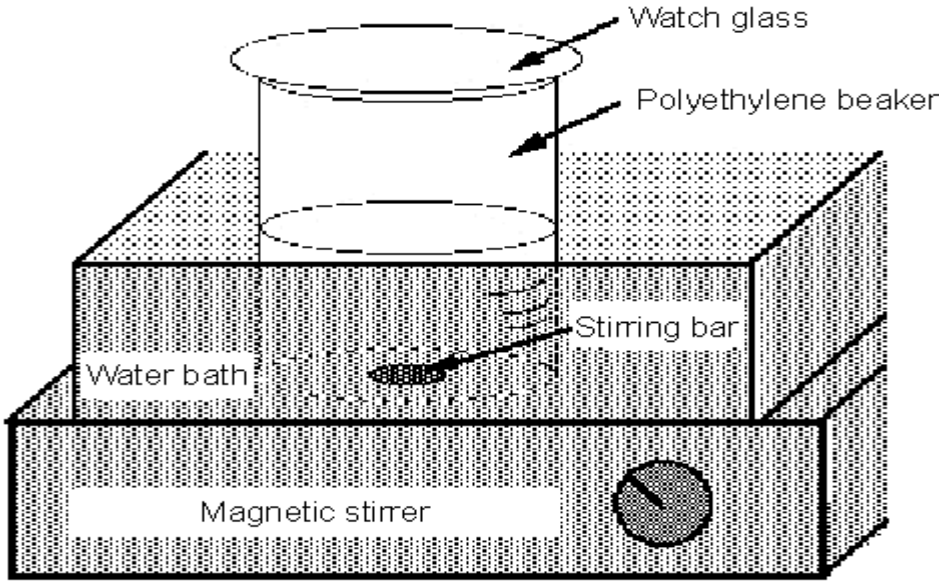

Figure 1. Preparation of SBF.

T. Kokubo, H. Kushitani, S. Sakka, T. Kitsugi and T. Yamamuro, "Solutions able to reproduce in vivo surface-structure changes in bioactive glass-ceramic A-W", ***J. Biomed. Mater. Res.*, 24**, 721-734 (1990).

Appendix 3. Supplementary figures

Positive control immunostaining for collagens I,II, and X

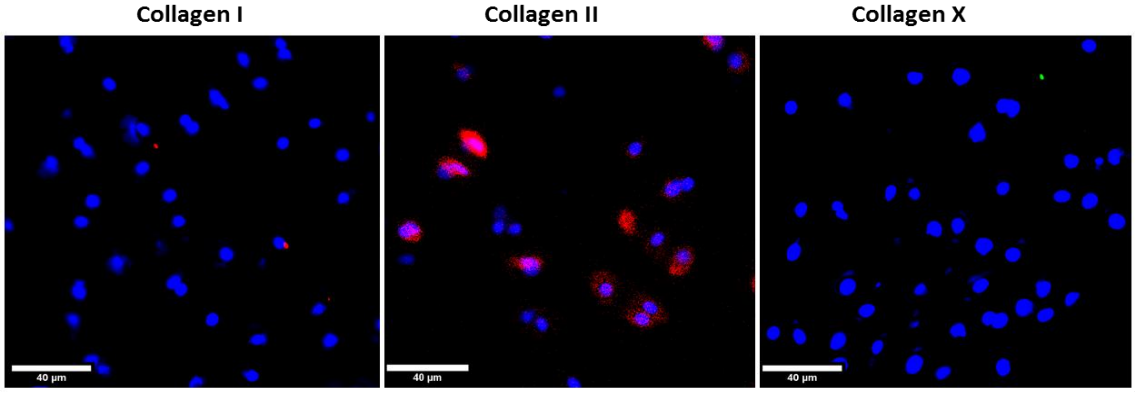

Immunostained frozen sections of bovine articular cartilage featuring the deep cartilage zone*. Collagen I and II represented by red colour (TRITC stain) while collagen X represented by green colour (FITC stain). Scale bar measure 40µm*

Appendic 4. Ethical standards for commercial primary human cells

Human Tissue Act (HT Act)

PromoCell

Informed Consent

"The HT Act makes consent the fundamental principle underpinning the lawful storage and use of body parts, organs and tissue from the living or the deceased for specified health-related purposes and public display."

see: www.hta.gov.uk/about_hta/human_tissue_act.cfm

PromoCell complies with this fundamental principle of the HT Act. All PromoCell cells are all isolated with the explicit informed consent of the patients or their relatives.

Other guidelines that focus on the informed consent:

- The Convention of Human Rights and Biomedicine:
  www.conventions.coe.int/treaty/en/Reports/Html/164.htm
- Declaration of Helsinki:
  www.wma.net/e/policy/b3.htm

Relevant material

"1. Specifically identified relevant material

This includes material like bodily organs and tissues, consisting largely or entirely of cells, and clearly identifiable and regarded as such. This category of relevant material includes human bodies, internal organs and tissues, skin and bone; and specifically the following:

- stem cells created inside the human body
- embryonic stem cells
- non blood derived stem cells
- umbilical cord blood stem cell
- bone marrow
- primary human cell cultures

but not:

- cultured cells which have divided outside the human body
- artificially created embryonic stem cells
- cell lines
- extracted DNA..."
- plasma extracted DNA...."

see: www.hta.gov.uk/guidance/licensing_guidance/definition_of_relevant_material.cfm

Most human cells from PromoCell have been cultured outside the human body after isolation (at least one passage). Certain blood cells ($CD34^+$ progenitor cells, mononuclear cells) and hepatocytes provided by PromoCell have been frozen immediately after isolation and therefore have not undergone any expansion process outside the body yet.

Licensing at HT Authority

Every researcher has to ensure on her/his own whether a licensing at the HT authority is necessary or not since the licence is not only dependent on the material used but also on the research purpose as well on local ethics committee approval.

For further information :

www.hta.gov.uk/_db/_documents/2006-06-28_Designed_Research_Compliance_Report_on_the_website_amended.pdf

as well as

www.hta.gov.uk/_db/_documents/2006-08-23_Application_guidance_research_v1_200612140314.pdf

or contact HT authority: enquiries@hta.gov.uk to check whether licensing is necessary or not.

Please do not hesitate to contact our technical support team if you need any further assistance concerning specifications and isolation details of PromoCell cell types.

Heidelberg, December, 2007

PromoCell GmbH
Dirk Hüttner
Managing Director

PromoCell GmbH
Sickingenstr. 63/65
69126 Heidelberg
Germany

North America 1 – 866 – 251 – 2860 (toll free)
Deutschland 0800 – 776 66 23 (gebührenfrei)
France 0800 90 93 32 (ligne verte)
United Kingdom 0800 – 96 03 33 (toll free)
Other Countries +49 6221 – 649 34 0

Email: info@promocell.com
www.promocell.com